UNE NOUVELLE APPROCHE POUR LA SYNTHESE DE POPULATIONS STELLAIRES DANS LES GALAXIES

Thèse présentée par
EDUARDO LUIZ DAMIANI BICA

pour l'obtention du Diplôme de Doctorat d'Etat ès-Sciences de l'Université Paris VII

Soutenue le 29 Septembre 1987 devant la commission

M. J. Heyvaerts Président
Mme. D. Alloin
M. R. Cayrel
M. M. Crézé
Mme. L. Gouguenheim
M. J. Lequeux
M. B. Pagel

à mes parents, frère et soeur

à Miriani Pastoriza et Horacio Dottori

Remerciements

Je voudrais remercier vivement mon directeur de thèse Danielle Alloin pour ses conseils et encouragements pendant toutes les étapes de ce travail. Je remercie Jean Heyvaerts d'avoir accepté la présidence du jury. James Lequeux et Laurent Vigroux d'etre rapporteurs et Roger Cayrel, Michel Crézé, Lucienne Gouguenheim et Bernard Pagel d'etre membres du jury. Je suis reconnaissant aussi à toutes les personnes qui, à un moment ou à un autre m'ont apporté leurs remarques, en particulier à Bernard Pagel, Giusa Cayrel de Strobel, Roger Cayrel, Chantal Balkowski, Nobuo Arimoto, Beatriz Barbuy, David Burstein, Hyron Spinrad, Jeremy Mould et Paul Hodge.

Je tiens à remercier les membres de l'Observatoire de Paris/Meudon et de l'Institut d'Astrophysique pour l'accueil, la gentillesse et les excellentes conditions de travail qu'ils m'ont offerts. En particulier, j'exprime ma reconnaissance au personnel du centre de calcul et au groupe qui a développé le système de commandes eVe, Michel Caillat, Didier Pelat et Jean Marc Sviga. Je suis redevable également à la direction et au personnel de l'ESO à Garching et à la Silla pour l'attribution de temps de télescope, pour l'assistance aux observations et pour l'aide à la réduction des données. Enfin, je dois toute ma gratitude à Erika Veia et à Jacqueline Plancy pour la dactylographie non seulement du présent texte, mais aussi de tous les articles résultant de ce travail. Que soit remerciée l'Institution Brésillienne CNPq pour la bourse de doctorat qu'elle m'a généreusement accordée.

Résumé:

On développe une nouvelle méthode pour la synthèse de populations stellaires dans les noyaux de galaxies,utilisant exclusivement une bibliothèque de spectres intégrés d'amas d'étoiles.Cette méthode présente l'avantage,par rapport aux méthodes traditionnelles basées sur des bibliothèques d'étoiles ou mixtes -étoiles plus amas-,d'être une analyse à deux paramètres: âge et métallicité. La fonction initiale de masses est implicite dans le cas des amas d'étoiles et l'évolution stellaire est automatiquement prise en compte dans cette méthode.Les observations consistent en 63 spectres d'amas d'étoiles et 164 spectres de noyaux de galaxies avec résolution de 12 Å dans le domaine visible,ainsi qu'un sous-ensemble de ces objets dans le domaine infrarouge,sous-ensemble qui couvre néanmoins la même varieté de types d'amas d'étoiles et de noyaux de galaxies.Une extension de cette méthode au domaine ultraviolet est aussi presentée.Une attention spéciale a été donnée aux différentes sources de rougissement interstellaire affectant les amas d'étoiles et les galaxies.En particulier on a développé une méthode pour la correction du rougissement interne dû à l'inclinaison du disque des galaxies spirales. Les différents types de noyaux ont été synthétisés à partir d'une grille de largeurs équivalentes en fonction de l'âge et de la métallicité construite au moyen des amas d'étoiles. Pour mener à bien cette synthèse, on a développé un algorithme capable de tester un très grand nombre de combinaisons d'amas d'étoiles le long de chemins évolutifs dans le plan âge-métallicité,qui représentent des scénarios possibles pour l'évolution chimique des noyaux de galaxies. Cette méthode a permis de dater les générations successives d'étoiles,de détecter d'éventuels sursauts de formation d'étoiles,ainsi que de déterminer l'enrichissement chimique dans les noyaux. Cette approche a donc permis de faire pour la première fois,une estimation directe de l'évolution chimique à partir du spectre en absorption des noyaux de galaxies.

Abstract:

A new approach for population synthesis in galaxy nuclei is developed. It makes use exclusively of a library of star cluster integrated spectra.This method presents the advantage,over those traditionally using libraries of stellar spectra or a mixture of stars and star clusters,of being a two parameter analysis: age and metallicity.The initial mass function is implicit in the case of star clusters and the stellar evolution is also automatically taken into account in the present method.The observations consist of 63 spectra of star clusters and 164 spectra of galaxy nuclei with 12 Å resolution in the visible range,as well as a subsample of the same objects in the near-infrared,which still spans the same variety of star clusters and galaxy types.An extension of the method to the ultraviolet is also provided.A special attention was given to the different sources of interstellar reddening affecting star clusters and galaxies; in particular a new method was developed to correct the reddening arising from inclination effects in spiral galaxies. The different types of nuclei were synthesized using a grid of equivalent widths as a function of age and metallicity, which was derived from the star cluster data. In order to compute the syntheses ,an algorithm was developed which tests an extremely large number of star cluster combinations along an evolutionary path in the plane age-metallicity. These paths represent several possible chemical evolution scenarios for the galaxy nuclei. This method has allowed to date the successive stellar generations,to detect eventual bursts of star formation,as well as to determine the chemical enrichment in the nuclei. Thus the present approach has provided ,for the first time, a direct estimate of the chemical evolution in galaxy nuclei using absorption spectra.

TABLE DES MATIERES

A) Bica, E. Dottori, H., Pastoriza, M.
Ages and metallicities of LMC and SMC red clusters through Hβ and Gband photometry
Astron. Astrophys. 156, 261–267, 1986

B) Bica, E., Alloin, D.
A base of star clusters for stellar population synthesis
Astron. Astrophys. 162, 21–31, 1986

C) Bica, E., Alloin, D.
A grid of star cluster properties for population synthesis
Astron. Astrophys. Suppl. Ser. 66, 171–179, 1986

D) Bica, E., Alloin, D.
The interstellar NaI strength versus reddening relationship : its incidence on stellar population synthesis
Astron. Astrophys. 166, 83–91, 1986

E) Bica, E., Alloin, D.
Analysis of absorption–line spectra in a sample of 164 Galactic Nuclei.
Astron. Astrophys. Suppl. Ser., 70, 281–301, 1987.

F) Bica, E., Alloin, D.
On the metallicity versus luminosity relationship for early type galaxies
Astron Astrophys. 181, 270–272, 1987.

G) Bica, E., Alloin, D.
Near–infrared spectral properties of star clusters and galactic nuclei
Astron. Astrophys., 186, 49–63, 1987

H) Bica, E.
Population synthesis in galaxy nuclei using a library of star clusters
Astron. Astrophys., 1987, in press
PUBLICADO EM 195, 76 (1988)

I) Bica, E., Alloin, D.
Constraints provided by star cluster spectra on the nature of the UV turn–up in giant elliptical galaxies.
Astron. Astrophys., 1987, in press
PUBLICADO EM 192, 98 (1988)

I – INTRODUCTION

La définition photométrique des composantes étendues des galaxies est assez précise. En particulier celle des disques, lesquels suivent une loi I(r) exponentielle, et celle des bulbes, lesquels suivent une loi en $r^{1/4}$ (de Vaucouleurs, 1979). Par contre l'étude détaillée des noyaux a toujours été difficile, par suite de l'existence de forts gradients d'intensité dans les régions centrales des galaxies et par suite de leurs dimensions angulaires réduites. Le développement récent de détecteurs linéaires à grande dynamique a considérablement amélioré la précision des études de profils de luminosité des noyaux. Cependant, pour les observations au sol, subsiste le problème de la dégradation des images par la turbulence atmosphérique. Le domaine prendra certainement plus d'essor lorsque s'ouvrira la possiblité d'observations systématiques depuis l'espace, dans les années à venir. Dans le présent travail, nous définissons le noyau en termes pratiques, comme étant le pic de luminosité, assez facile à repérer au télescope, vu à travers la fente du spectrographe. Pour l'échantillon de la présente étude, les dimensions angulaires typiques sont de 5" x 8". En adoptant H_o = 50 km s^{-1} Mpc^{-1}, la région observée pour chaque galaxie est donnée dans l'appendice E. La surface moyenne couverte est de 0.8(± 0.5) Kpc x 1.4(± 0.9) Kpc, les valeurs extrêmes étant pour NGC 692–(3 Kpc x 4.8 Kpc) et NGC 625, 5236, et 5253 (0.2 Kpc x 0.3 kpc). Il faut prendre en compte le fait que les observations spectroscopiques intègrent, le long de la ligne de visée des contributions de plusieurs sous-systèmes dans une galaxie. Ainsi on s'attend à la contribution de populations déficientes en métaux présentes dans les halos ; une contribution encore plus importante provient des parties internes des bulbes ; enfin, dans le cas particulier des galaxies spirales, la région interne du disque peut contribuer au flux. De même l'inclinaison du

disque a des effets supplémentaires en termes de rougissement et de raies interstellaires sur le spectre résultant observé (Appendices D et E).

L'objectif principal de ce travail est la détermination de l'age et de la métallicité du contenu stellaire des noyaux ordinaires de galaxies, autrement dit des noyaux non-actifs où la source d'énergie est constituée au premier ordre par le rayonnement des étoiles.

Le noyau et la partie interne du bulbe sont les régions où le taux de formation d'étoiles a été le plus élevé. Il est donc important de comprendre l'évolution de ce taux au cours du temps et sa relation avec les autres paramètres qui définissent la galaxie, tel que par exemple, le rapport bulbe/disque. Le noyau a une importance non seulement par l'information qu'il renferme sur l'histoire de la formation stellaire dans la galaxie en tant que système isolé, mais également parce qu'il constitue le puits gravitationnel d'une galaxie et pourrait ainsi garder trace de l'interaction d'une galaxie avec son environnement : accrétion directe d'autres systèmes stellaires ou accrétion de gaz ayant conduit à une éventuelle formation additionnelle d'étoiles. Le noyau est aussi la région où les plus fortes concentrations en éléments lourds sont observées dans le gaz interstellaire et dans l'atmosphère des étoiles.

En définitive, l'étude du spectre du noyau est un moyen d'analyser l'évolution d'une galaxie, non seulement comme système isolé mais aussi dans son rapport avec l'environnement, et d'analyser la synthèse des éléments lourds. L'objectif ultime de ce type d'étude est d'utiliser cette information conjointement avec des analyses de l'évolution dynamique du système dans l'espoir de comprendre comment eut lieu la formation des galaxies.

II – APPROCHES ANTERIEURES

Plusieurs articles de revue ont été écrits ces dernières années sur les populations stellaires dans les galaxies, et en particulier sur les méthodes de synthèse de populations (e.g. van den Bergh, 1975 ; Faber, 1977, Tinsley, 1980 ; Pagel and Edmunds, 1981 ; O'Connell, 1986).

La première étude tentant de déterminer les types d'étoiles présents dans une galaxie a été faite par Whipple (1935). Il a développé une méthode pour synthétiser l'intensité et le profil des raies d'absorption dans les galaxies au moyen de spectres d'étoiles de différents types spectraux et luminosités. Il a ainsi démontré que les spectres des galaxies étaient très composites. De Vaucouleurs et de Vaucouleurs (1959) ont appliqué cette méthode au spectre intégré de la barre du Grand Nuage de Magellan avec 16 raies dans le domaine spectral 3700 Å à 4900 Å et en ont déduit les contributions relatives des différents types spectraux. Stebbins et Whitford (1948) ont fait la synthèse de quelques galaxies en utilisant un système photométrique à six couleurs entre 3530 Å et 10300 Å. Ils ont conclu qu'un simple mélange d'étoiles naines G et de géantes M reproduisait le spectre des galaxies elliptiques. Cela montre en réalité que les couleurs, surtout à partir de photométrie à bandes larges, sont peu sensibles aux propriétés des populations et qu'il est indispensable de prendre en compte les raies d'absorption dans une synthèse de population stellaire.

Plus récemment, deux types d'approches ont été développés :

A) Synthèse de populations proprement dite. C'est la suite directe de ces travaux pionniers. A partir d'observations d'étoiles, on essaie de fabriquer un spectre synthétique reproduisant celui d'une galaxie (e.g. Spinrad et Taylor, 1971 ; Alloin et al., 1971 ; Faber, 1972 ; Joly et Andrillat, 1973 ; O'Connell, 1976 ; Turnrose, 1976 ; Pritchet, 1977 ; Pickles, 1985). Ces études diffèrent

entre elles par :

(i) le système d'acquisition des données. Certaines études reposent sur de la photométrie à bandes plus ou moins étroites tandis que d'autres ont utilisé la spectrophotométrie, laquelle a bénéficié, au cours des années, d'énormes progrès techniques.

(ii) le contenu de la bibliothèque d'étoiles par l'inclusion de types particuliers d'étoiles tels que des étoiles super-métalliques ou des étoiles de la branche horizontale bleue.

(iii) par l'algorithme de recherche de la solution et des contraintes astrophysiques imposées. En fait les travaux pionniers étaient très simples et non-contraints, les solutions étant cherchées par essais-et-erreurs. Les études plus récentes ont utilisé des algorithmes automatiques d'optimisation. Un certain nombre de contraintes sont généralement introduites afin de garantir l'obtention de solutions astrophysiquement plausibles.

B) Synthèse évolutive : Cette approche utilise en priorité la théorie de l'évolution stellaire pour calculer, à un age donné, la population issue d'un taux de formation d'étoiles, d'une fonction initiale de masse et d'une métallicité, adoptés. Le diagramme HR résultant est utilisé pour calculer un spectre ou bien des couleurs synthétiques, lesquels sont comparés à ceux observés pour les galaxies (e.g. Tinsley, 1972 ; Rocca-Volmerange et al., 1981 ; Bruzual, 1983 ; Arimoto et Yoshii, 1986). Ces auteurs analysent différents scénarios pour l'évolution des galaxies, selon les lois adoptées pour le taux de formation d'étoiles et la fonction initiale de masse. Les études diffèrent aussi par les tracés d'évolution stellaire utilisés. Le résultat, de la même façon que dans la méthode de synthèse de populations, est exprimé en fonction de la bibliothèque d'étoiles disponibles et du système photométrique ou spectrophotométrique employé.

Les principales limitations de ces deux approches de synthèse sont les

suivantes :

(i) On ne connait pas de façon exhaustive toutes les étapes de l'évolution stellaire, surtout certaines phases courtes qui, pourtant, peuvent contribuer beaucoup à la lumière intégrée à cause d'effets de luminosité ou de température : de même, certaines étapes avancées de l'évolution comme la branche asymptotique des géantes et sa suite, ou lors des étapes initiales telles que les "blue stragglers". La synthèse évolutive est particulièrement sensible à ces incertitudes. La synthèse de populations l'est aussi, quoique dans une moindre mesure, parce qu'elle fait souvent appel à des contraintes guidées par l'évolution stellaire.

(ii) Bibliothèques d'étoiles incomplètes : les bibliothèques possèdent un bon échantillon d'étoiles proches. Donc la métallicité est limitée à des valeurs voisines de l'abondance solaire. Ces bibliothèques n'incluent pas en général toutes les étapes de l'évolution stellaire et, même si cela était le cas, il serait difficile d'en tenir compte dans le calcul, par méconnaissance théorique de ces phases-là comme cela a déjà été mis en évidence ci-dessus pour la synthèse évolutive. Dans le cas de la synthèse de populations, leur non-inclusion peut entrainer l'algorithme à chercher des compensations internes avec les étoiles disponibles. Mais aussi, leur inclusion, en l'absence d'informations sur leur probabilité de présence par rapport à des populations associées peut aussi conduire à des résultats assez arbitraires (appendice I). Certaines études ont substitué aux types d'étoiles difficiles à observer des spectres synthétiques (e.g. Barbaro et Olivi, 1986). Malgré une dépendance supplémentaire en fonction des modèles d'atmosphères, c'est certainement une voie très prometteuse pour le futur.

(iii) Dépendance envers la fonction initiale de masse : la pente de la fonction initiale de masse est un paramètre inhérent à toutes les méthodes utilisant les bibliothèques d'étoiles. Parfois l'on adopte tout simplement une valeur plausible,

parfois l'on cherche le résultat au moyen de la synthèse. Face à cette inévitable dépendance on peut se demander si des simplifications souvent appliquées à d'autres paramètres, par exemple une métallicité constante, ne sont pas compensées aux dépens de la fonction initiale de masse. De plus, la fonction initiale de masse possède d'autres degrés de liberté en plus de sa pente : beaucoup d'analyses sont faites aussi en fonction des limites supérieure et inférieure de masse.

(iv) Interdépendance de l'âge et de la métallicité. Dans une atmosphère stellaire, au premier ordre, l'augmentation de l'opacité due à une forte abondance de métaux est à peu près équivalente à une diminution de la température moyenne du spectre émergent (O'Connell, 1986). Cette ressemblance de la distribution spectrale en fonction des variations de la température et de la métallicité résulte en ce que les couleurs obtenues à partir de photométrie à bandes larges ne sont pas assez sensibles pour séparer ces effets. Il est donc nécessaire d'avoir une résolution suffisante pour accéder aux raies métalliques, ce qui n'a pas toujours été le cas dans certaines études. Un autre point crucial est le fait que souvent les synthèses de populations et les synthèses évolutives ont explicitement compensé le manque de données à forte métallicité par des types spectraux plus tardifs, de métallicité solaire. La méthode idéale serait de disposer de tous les types spectraux, à toutes les gravités et pour toutes *les métallicités*. Même si cette bibliothèque idéale pouvait être rassemblée, il y aurait une énorme quantité de composantes à combiner. Il est clair qu'il faut trouver un moyen de grouper les étoiles en populations de différents âges et métallicités. Un premier pas dans ce sens a été l'inclusion d'amas globulaires pauvres en métaux pour tenir compte des effets de faibles métallicités dans les synthèses (Faber 1972 ; Cianni et al. 1984).

III – UNE NOUVELLE APPROCHE : SPECTRES INTEGRES D'AMAS D'ETOILES

On utilise exclusivement une bibliothèque de spectres intégrés d'amas d'étoiles couvrant de larges domaines d'âge et de métallicité. On suppose que chaque génération d'étoiles dans un noyau peut être représentée par un amas de métallicité Z et d'âge t. L'avantage de cette méthode est de réduire le nombre de variables à ajuster pour résoudre le problème. Une bibliothèque d'étoiles est décrite par la température, la gravité et la métallicité, tandis qu'une bibliothèque d'amas est fonction de l'âge et de la métallicité seulement. Le nombre de composantes fondamentales dans une bibliothèque d'amas est évidemment beaucoup plus petit. Du côté des faibles métallicités, les amas permettent de descendre d'un facteur 100 par rapport à l'abondance solaire, tandis qu'en pratique, il est très difficile d'obtenir des échantillons assez complets d'étoiles avec $[Z/Z_0] < -0.5$. Du côté des fortes métallicités, il est aussi difficile d'acquérir des données observationnelles pour les bibliothèques d'étoiles que pour celles d'amas. Néanmoins je souligne le fait que j'ai observé des amas globulaires Galactiques présentant des raies métalliques et des bandes moléculaires comparables à celles que l'on observe dans le noyau des galaxies elliptiques géantes. Ces amas de la partie centrale du bulbe, comme NGC 6440, 6528 and 6553, ont un spectre intégré nettement plus métallique que celui des amas globulaires généralement appelés "riches en métaux" dans la littérature, comme e.g. NGC 104(47Tuc), NGC 6637(M69) et NGC 6356 (voir figure 2 et les appendices B et G). Dans le passé c'étaient ces amas-ci qui étaient utilisés pour des comparaisons avec les galaxies en termes de spectres ou couleurs intégrés et à cause d'une quasi-absence de recouvrement des propriétés spectrales, s'était alors répandu dans la littérature le faux consensus que les amas globulaires Galactiques n'étaient pas utiles pour la synthèse de noyaux de galaxies

(voir appendice G). La valeur de la métallicité dans les amas globulaires à raies métalliques fortes (AGRMF) n'a pas encore été fermement établie au moyen de méthodes directes, i. e. en termes de spectres d'étoiles individuelles. Néanmoins, quelle que soit la valeur exacte de cette métallicité, ces amas sont fondamentaux pour la synthèse de populations, car leurs propriétés spectrales sont similaires à celles des galaxies. Il est regrettable que jusqu'à présent, si peu d'études leur aient été consacrées et il serait donc important d'explorer leurs propriétés en détail.

La présente méthode est également libre d'hypothèses sur la fonction initiale de masse et sur la théorie de l'évolution stellaire. En fait, les spectres intégrés d'amas d'étoiles possèdent implicitement les proportions relatives exactes, selon la Nature, des étoiles nées d'un nuage de gaz ayant la métallicité correspondante. Aussi les proportions relatives d'étoiles évoluées en fonction de l'âge et de la métallicité sont implicitement correctes.

Un autre avantage, en particulier par rapport aux modèles de synthèse évolutive, est la possibilité d'obtenir une information sur l'histoire de la formation stellaire dans une galaxie, d'une façon indépendante de scénarios établis à l'avance pour l'évolution du taux de formation d'étoiles. Cela est important, surtout pour les galaxies contenant d'éventuels sursauts stochastiques de formation stellaire.

Pour conclure sur ces avantages, soulignons enfin que cette nouvelle méthode garde une liberté de combinaison de composantes d'une bibliothèque, telle qu'on la trouve dans la méthode classique de synthèse de populations.

En même temps, la méthode incorpore implicitement deux principes de la synthèse évolutive, l'évolution stellaire et la fonction initiale de masse, tout en évitant les inconvénients liés aux incertitudes inhérentes aux modèles théoriques, par l'utilisation directe des amas réels d'étoiles, lesquels sont, après tout les meilleurs tests de laboratoire des théories de formation et d'évolution stellaires. En outre, la

méthode permet aussi d'étudier les effets de mélanges de populations ayant des métallicités différentes ; ce qui est innovateur par rapport aux études passées.

Les limitations de la méthode développée dans ce travail concernent toutes les sources possibles d'incertitudes surtout sur la fonction initiale de masse du fait que nous utilisons des amas Galactiques et des amas des Nuages de Magellan pour synthétiser les noyaux d'autres galaxies. On suppose que la fonction initiale de masse (IMF, d'après le sigle anglais usuel) dans un noyau de galaxie peut être reproduite à partir d'une combinaison de l'IMF dans les amas d'étoiles individuels. Les sources d'incertitudes possibles sont les dépendances de l'IMF en fonction de la métallicité et de la dynamique des nuages de gaz initiaux, ainsi que des changements ultérieurs de la fonction de luminosité du système stellaire résultant, induits par l'évolution dynamique. Néanmoins, comme cela est décrit en détail dans l'appendice H, il existe plusieurs arguments indiquant que la plupart de ces incertitudes ne sont pas importantes au premier ordre. Ainsi la dépendance de l'IMF avec la métallicité est prise en compte par le fait qu'on observe des amas de différentes métallicités. Dans la plupart des types de noyaux les résultats de la synthèse (appendice H) montrent que des populations similaires à celles des AGRMF comme NGC 6528 dominent. Ces amas globulaires appartenant à la partie centrale du bulbe de notre Galaxie, ont dû être formés dans un environnement physiquement et chimiquement similaire à celui d'un noyau typique de galaxie massive. Les effets de l'évolution dynamique des amas, de la relaxation et de la perte possible d'étoiles de faible masse par des effets de marée, seraient minimisés dans notre échantillon, puisqu'on observe les amas les plus massifs de notre Galaxie et des Nuages de Magellan.

Une limitation dans les données observationnelles vient du fait que nous n'avons pu observer des amas d'étoiles super-métalliques pour les âges intermédiaires et jeunes. En fait les amas observés dans le disque Galactique ont

au mieux la métallicité solaire. Cette lacune pourrait être comblée par l'observation future d'amas dans les bras internes de la galaxie M31. Dans la méthode de synthèse que nous proposons, ce défaut est compensé par la création d'une grille où l'on extrapole les largeurs équivalentes et la distribution du continu aux fortes métallicités. Ces propriétés pourront aussi être comparées à celles des spectres synthétiques d'amas super-métalliques. Pourtant, vers les âges jeunes, les effets de métallicité sont de moins en moins importants, surtout dans les domaines spectraux bleus.

Le domaine spectral de cette étude couvre le visible et l'infrarouge proche et, malgré cette limitation, de nombreuses informations ont pu être déduites de la synthèse (appendice H). Néanmoins la nécessité d'incorporer le domaine ultraviolet est évidente surtout pour l'obtention plus précise des contributions des composantes chaudes. Un premier pas dans ce sens a été réalisé par l'étude de la nature du flux ultraviolet des galaxies elliptiques géantes (appendice I).

Tout en étant conscient des limitations possibles et réelles de la présente méthode, nous considérons que les avantages dûs au nombre réduit de degrés de liberté dans l'analyse justifient son développement et son exploitation dans l'étude des populations stellaires et qu'elle représente un progrès.

IV - LE MATERIEL D'OBSERVATIONS

Le matériel consiste en des observations spectrales d'un grand nombre d'amas d'étoiles et de galaxies dans le visible et l'infrarouge proche (appendices B, E, G). Le domaine sera prochainement étendu à l'ultraviolet proche, dans le but de connecter l'optique à l'ultraviolet lointain disponible dans la bibliothèque IUE. Une étude préliminaire sur tout le domaine spectral ultraviolet lointain,

optique, infrarouge proche, est présentée dans l'appendice I.

Les spectres visibles ont été obtenus au télescope de 1.52m de l'ESO avec un détecteur IDS. Les spectres dans l'infrarouge proche ont été obtenus au télescope de 2.2m de l'ESO, avec un détecteur CCD. La résolution est de ~ 12 Å. En fait, il n'est pas nécessaire de rechercher une résolution plus élevée à cause de la grande dispersion de vitesse des étoiles dans les noyaux de galaxies.

Les observations CCD dans l'infrarouge proche sont affectées par le problème des franges d'interférence. J'ai développé une nouvelle méthode pour leur élimination, laquelle a donné d'excellents résultats (appendice G).

On présente dans la figure 1 les critères pour le tracé du continu pour des populations typiques bleue et rouge. La méthode consiste à mesurer les largeurs équivalentes W avec des limites de fenêtres fixes dans le système de référence au repos. Les limites de fenêtres sont données dans les appendices B et G respectivement pour le visible et l'infrarouge-proche. Des identifications de raies et molécules sont aussi données, mais en principe dans cette méthode, l'identification précise de l'absorbant est secondaire ; l'important est de suivre le comportement de l'absorption totale mesurée dans chaque fenêtre en fonction de l'âge et de la métallicité.

Les observations visibles ont porté sur 63 amas d'étoiles et 164 noyaux de galaxies. Ce sont des amas globulaires et ouverts Galactiques et des amas du Grand et du Petit Nuage de Magellan. Cela permet de couvrir un large domaine dans le plan âge versus métallicité (voir figure 1 de l'appendice B). Les galaxies recouvrent les types morphologiques E jusqu'à Sc et ont des magnitudes absolues $-23 < M_B < -16.5$ (appendice E). L'échantillon infrarouge-proche d'amas et de galaxies est un sous-ensemble de celui observé dans le visible, pourtant il couvre la même variété d'objets.

Pour tous les amas, des déterminations d'âge, métallicité et rougissement étaient disponibles dans la littérature. Il a donc été possible d'étudier les largeurs équivalentes W et la distribution intrinsèque du continu en fonction de l'âge et de la métallicité. Les principaux résultats de cette analyse sont les suivants : (i) il y a une séparation en groupes d'âges différents dans un diagramme W versus métallicité pour les absorbants métalliques dans le bleu, comme CaII K (voir figure 5a de l'appendice B). Cela est dû à la présence d'étoiles chaudes lumineuses dans les amas jeunes, lesquelles diluent les raies métalliques ou les absorptions moléculaires dans le bleu. Par contre les différents groupes d'âges ont une tendance à fusionner dans les domaines rouge et infrarouge proche, comme c'est le cas pour CaII 8542 Å (figure 7b dans l'appendice G). Donc la métallicité est le paramètre dominant vers les grandes longueurs d'onde, tandis que, outre la metallicité, l'âge est aussi un paramètre important pour les absorbants métalliques situés vers les longueurs d'onde courtes. La largeur équivalente W des raies de Balmer en fonction de l'âge présente un maximum vers 5×10^8 années, lorsque les étoiles A dominent le spectre intégré, tandis que la pente du continu croit fermement vers les âges jeunes (appendice B). Grâce à cette analyse il a été possible de construire puis d'interpoler une grille de propriétés spectrales d'amas d'étoiles à des pas convenables en âge et en métallicité (appendices C et G). Il a aussi été possible d'extrapoler les propriétés spectrales à des amas supermétalliques à $[Z/Z_\odot] = 0.6$. On souligne que cette extrapolation est raisonnable du fait que nous avons dans l'échantillon, des amas d'étoiles dont le spectre est très semblable à celui des galaxies (section III).

La figure 2 montre une séquence de spectres de groupes d'amas globulaires de différentes métallicités. La figure 3 montre une séquence d'âges intermédiaires et jeunes pour des amas du disque Galactique et du Grand Nuage de Magellan. Dans cette dernière figure on voit que pour certains amas très

jeunes l'infrarouge proche est dominé par des étoiles rouges. Dans le cas de NGC 2004 ($t \sim 10^7$ ans) ce sont des supergéantes rouges et dans le cas de NGC 1866 ($t \sim 10^8$ ans) ce sont probablement des étoiles (de type M) appartenant à la branche asymptotique des géantes (appendice G).

Initialement, on désirait obtenir un type moyen de noyau de galaxies pour chaque boîte déterminée par le type morphologique versus la classe de luminosité. Pourtant les observations ont montré que cela était impossible car chaque boîte contenait des spectres atypiques et que plus particulièrement les types morphologiques tardifs formaient une classe très hétérogène de noyaux (appendice E). Alors pour la synthèse nous avons tout d'abord groupé les spectres partageant les mêmes propriétés dans la limite des barres d'erreurs et seulement ensuite nous avons appliqué d'éventuelles séparations selon le type morphologique ou la classe de luminosité (appendice H). Neuf groupes de spectres ont été obtenus pour les galaxies E et S0 dont 8 sont montrés dans la figure 4. Les groupes E1 à E4 suivent la relation indicateur de métallicité versus magnitude totale (appendice F). Le groupe E1 possède des absorptions métalliques extrêmement fortes et contient des galaxies très massives, tandis que le groupe E4 renferme des galaxies de faible luminosité intrinsèque $M_B \simeq -18$. Les groupes plus clairsemés E5 à E8, signent la présence de composantes plus jeunes, par rapport aux groupes de E1 jusqu'à E4. Particulièrement le groupe E7 avec un excès de flux dans le bleu et la raie Hβ très intense en absorption, contient une importante composante d'âge intermédiaire (appendices E et H). Le groupe E8, qui correspond au cas particulier de NGC 5102, a eu un sursaut de formation d'étoiles à $t \simeq 4 \times 10^8$ ans (appendices E, H). Le groupe E9 est spectroscopiquement très similaire à E2, mais comporte des galaxies moins lumineuses. Beaucoup d'entre elles présentent des signes d'arrachage d'étoiles par effets de marée lors d'une interaction avec des compagnons plus massifs.

Il faut corriger les spectres de noyaux de spirales du rougissement provoqué par l'inclinaison de leur disque. Avant d'aborder ce sujet, rappelons comment les sources de rougissement sont traitées dans la présente méthode. Pour les amas nous avons adopté les rougissements extrinsèques indiqués dans la littérature (appendice B). Le rougissement extrinsèque pour les galaxies suit la loi en cosec avec les régions polaires Galactiques non-rougies (appendice E). Aucune correction de rougissement interne n'a été appliquée aux amas d'étoiles. Cela est un des principes de la méthode : le rougissement sera important pour les amas jeunes, encore associés à des régions de formation d'étoiles. Il doit par conséquent etre maintenu dans les données, parce que d'éventuelles régions de formation d'étoiles dans un noyau de galaxie, auront certainement une composante de poussière semblable, très localisée et n'affecteront pas nécessairement les populations plus agées environnantes. Donc le rougissement déduit dans la synthèse, par comparaison du modèle obtenu à partir des largeurs équivalentes, avec la galaxie observée, correspondra à de la poussière diffuse dans les bulbes ou les régions centrales pour tous les types morphologiques. On trouve que ce rougissement-ci, non associé directement aux régions de formation d'étoiles, est en fait très petit ($E(B-V) \simeq 0.04$) dans toutes les galaxies (appendice H).

Dans le cas des galaxies spirales, avant la synthèse, il a fallu développer une méthode pour corriger les spectres du rougissement dû à l'inclinaison du disque (appendice E). Le présent échantillon possède un grand nombre de galaxies spirales vues à différents angles d'inclinaison. Donc pour chaque galaxie inclinée, nous avons cherché une "référence" ayant la même population stellaire, parmi les spirales vues de face. Le critère pour décider si la même population stellaire est présente, est que W (raies métalliques) et W (bandes moléculaires) soient les mêmes sur tout le domaine de longueurs d'onde. Cela

repose sur les résultats de l'analyse du spectre intégré des amas d'étoiles de différents ages et métallicités (appendice B). Le rougissement résultant pour les galaxies vues par la tranche est typiquement $E(B-V) = 0.40 - 0.50$. On voit également dans ces objets de grands excès d'absorption dans la raie NaI D interstellaire, qui proviennent de la contribution du gaz dans le disque incliné (appendices D et E). On a aussi conclu que cette importante contamination interstellaire rend la raie NaI D inutilisable pour la synthèse de populations stellaires.

Nous avons obtenu sept types de spectres dans les noyaux de galaxies spirales (figure 5). En gros, le groupe S1 correspond au type K et le groupe S7 au type A dans la classification spectrale de galaxies de Humason et al., (1956). Les noyaux rouges, groupes S1 jusqu'à S4, sont très similaires aux groupes rouges E1 à E3. Les propriétés spectrales de ces groupes S1 à S4 sont associées à la luminosité du bulbe, mais il faut remarquer que S4 le groupe ayant les raies métalliques les plus faibles, a encore une métallicité très forte par rapport aux spectres d'amas globulaires pauvres en métaux (appendices H et E). Le rougissement interne associé aux régions de formation d'étoiles est lui-aussi déterminé dans cette méthode par les raies d'émission des régions HII pour les noyaux ayant une telle contribution. Le groupe S7, après décomposition spectrale selon les résultats de la synthèse, indique que $E(B-V) = 0.35$ à partir du rapport $H\alpha/H\beta$ (appendice H).

V – L'ALGORITHME DE SYNTHESE ET LES PRINCIPAUX RESULTATS

On utilise dans le calcul, les raies métalliques et les bandes moléculaires les plus intenses et ayant un comportement bien modélisé dans les grilles en

fonction de l'age et de la métallicité, pour les amas d'étoiles (appendices B et G). Ce sont : CaII K 3933 Å, CN 4200 Å, CH 4300 Å (bande G) ; MgI + MgH 5175 Å et CaII 8542, 8662 Å. Les raies de Balmer sont utilisées seulement quand elles ne sont pas affectées par l'émission. Il n'est pas nécessaire de tester tout le plan âge versus métallicité simultanément. Un argument de l'évolution chimique indique que le volume du noyau est assez petit pour que le gaz soit chimiquement homogène au cours du temps, et, par conséquent la solution décrit un chemin dans le plan âge versus métallicité. Une autre contrainte consiste en ce que le contenu en éléments lourds ne décroisse pas au cours du temps, donc vers les âges jeunes.

La méthode consiste à tester un nombre extrêmement grand de combinaisons de N points dans la grille (amas d'étoiles) avec un petit pas, le long d'un chemin donné (évolution chimique). Dans une première phase N = 8 avec un pas de 10%, et l'algorithme sélectionne toutes les solutions qui reproduisent les W de la galaxie dans la limite des barres d'erreurs. Dans une deuxième phase on utilise un plus grand nombre d'amas et un pas de 5% pour explorer l'espace des combinaisons autour du puits solution, déduit dans la première phase. Typiquement l'on teste 5 chemins différents dont les caractéristiques sont décrites dans l'appendice H. Les méthodes de synthèse de populations dans le passé ont en général utilisé des procédures de minimisation, lesquelles cherchaient une solution optimale. Il a toujours été difficile, voire impossible, d'estimer *l'unicité* de la solution trouvée, à cause du grand nombre de paramètres. Le présent algorithme permet d'obtenir une estimation de *l'unicité* au moyen du nombre de solutions obtenues par rapport au nombre de combinaisons testées. On obtient typiquement une famille extrêmement dégénérée de solutions qui correspond à 1 partie entre 10000 possibilités (appendice H).

Les résultats de la synthèse pour les 15 types de spectres de noyaux

reconnus sont présentés dans l'appendice H. La méthode permet donc de dater les générations successives d'étoiles, d'identifier et de dater d'éventuels sursauts de formation d'étoiles, ainsi que de déterminer l'enrichissement en métaux. La méthode est plus qu'une simple synthèse de populations, permettant pour la première fois, une estimation directe de l'évolution chimique dans ces noyaux.

Soulignons que les calculs de synthèse utilisent une grille couvrant tout l'espace nécessaire des propriétés spectrales des amas d'étoiles en fonction de l'âge et de la métallicité, interpolées à des pas convenables. Elle contient aussi une extrapolation raisonnable de ces propriétés jusqu'à $[Z/Z_{\odot}] = +0.6$. Les décompositions spectrales présentées dans l'appendice H sont, par contre, une simple visualisation de ces résultats, utilisant les spectres d'amas les plus proches possibles des résultats calculés. Dans cet article on a créé empiriquement le spectre intégré d'un amas globulaire supermétallique à $[Z/Z_{\odot}] = +0.6$, à partir des résultats de la synthèse et de la décomposition spectrale des galaxies les plus métalliques. Il serait extrêment intéressant de comparer ce spectre prédit avec des spectres synthétiques.

Pour les groupes E/S0 qui suivent la relation métallicité versus luminosité, la dernière génération d'étoiles a atteint une métallicité d'un facteur 4 supérieure à l'abondance solaire pour les galaxies ayant $M_B = -22$, et d'un facteur 0.5 à 0.3 pour $M_B = -18$. La majeure partie de la population est plus agée que 10 milliards d'années, mais ces galaxies ont formé des étoiles jusqu'à 5 milliards d'années. Une dispersion de métallicité est détectée dans le noyau : 10% du flux optique dans les galaxies E et S0 massives provient de populations sous-abondantes en métaux par rapport au soleil. Pour les groupes E et S0 plus bleus, quelques composantes d'âge plus jeune sont isolées et datées. Les groupes de spirales avec un spectre rouge formant une séquence de métallicité dépendante de la luminosité du bulbe, couvrent des métallicités jusqu'à 4 fois solaire. Finalement,

les groupes de noyaux de spirales plus bleus possèdent des composantes d'ages jeunes superposées à la vielle population, laquelle a atteint au moins la métallicité solaire. La méthode permet de déterminer l'importance d'un sursaut de formation d'étoile : pour le groupe le plus bleu, ayant NGC 5236 comme prototype, la population plus jeune que 3×10^8 ans contribue à 87% du flux à 4000 Å et 57% à 9000 Å.

VI – AUTRES ETUDES REALISEES

Une analyse préliminaire utilisant ensemble les domaines ultraviolet, visible, et infrarouge proche, est présentée dans l'appendice I. On étudie la nature de l'excès ultraviolet dans les galaxies elliptiques massives en supposant qu'il trouve son origine soit dans une formation récente d'étoiles soit dans une population pauvre en métaux mélangée au noyau. On montre qu'un amas d'age 10^7 ans explique bien l'excès sans affecter notablement le reste du domaine optique tandis qu'un amas globulaire pauvre en métaux ne l'explique pas. L'importance de cette analyse est de montrer les contraintes apportées par la fréquence d'apparition de types particuliers d'étoiles par rapport aux populations associées. Ainsi les étoiles de la branche horizontale bleue ont été habituellement considérées comme un groupe stellaire libre, en plus des groupes qui sont métalliques, dans les synthèse de populations. Par conséquent des contributions assez arbitraires ont été permises. Leur contribution est, en fait, liée à celle des géantes pauvres en métaux et seul le spectre intégré d'amas d'étoiles peut en indiquer les proportions correctes.

Dans l'appendice A est présentée une étude photométrique des amas des Nuages de Magellan. Le fait d'avoir utilisé des bandes étroites avec les mesures

directes d'une raie de Balmer et d'une absorption métallique a permis de séparer les effets d'âge et de métallicité. Ceci constitue un grand progrès par rapport aux photométries antérieures à bandes plus larges dans lesquelles les raies ne sont pas résolues. Cette conclusion est aussi valable pour la synthèse de populations basée sur des mesures de raies qui a été le sujet central de cette thèse. En effet la similitude des effets d'âge et de métallicité lorsqu'on utilise des couleurs obtenues à partir de bandes larges et les difficultés que cela a engendré lors de synthèses de populations basées seulement sur cette information(voir discussion dans O'Connell, 1986) sont bien connus. Il s'agissait d'éviter ces écueils.

VII – POURSUITE DE CE TRAVAIL ET PROSPECTIVE

a) Des galaxies *référence* non affectées par l'émission, ainsi que les spectres d'amas d'étoiles combinés selon les proportions indiquées par la synthèse des noyaux de galaxies (appendice H) sont utilisés pour isoler la composante en émission des noyaux de galaxies. Cette étude actuellement en cours portera donc sur le problème des LINERS (Keel, 1983) et de leur mécanisme d'ionisation.

b) Nous sommes en train d'étudier les spectres intégrés d'amas d'étoiles ainsi que le spectre de noyaux de galaxies, dans l'infrarouge proche en fonction de spectres individuels d'étoiles. Cette analyse porte sur les indicateurs de gravité, température et métallicité dans ce domaine spectral (Jones et al. 1984).

c) Nous étendons notre méthode au domaine ultraviolet avec la bibliothèque d'IUE ainsi que des nouvelles observations dans l'ultraviolet proche obtenues avec des CCD GEC pour faire la connection ultraviolet–optique. Cette extension est importante par les contraintes qu'elle apportera dans la

détermination précise de la contribution des composantes chaudes aux spectres intégrés des noyaux de galaxies (appendice I).

d) Il serait important d'obtenir de nouvelles observations d'amas d'étoiles surtout pour les âges intermédiaires et jeunes pour affiner la grille de propriétés spectrales en fonction de l'âge et de la métallicité. Les amas de M31, M33 et un plus grand nombre de ceux des Nuages de Magellan et du disque Galactique seront étudiés.

e) La synthèse des amas de la présente bibliothèque, en termes d'étoiles individuelles, réelles ou synthétiques serait également d'une grande importance.

f) La présente méthode sera certainement un outil important dans l'étude des galaxies distantes. Pour l'instant, nous envisageons son application aux galaxies à redshift intermédiaire (dans le sens où l'on a encore accès au type morphologique de l'objet). Du point de vue de l'évolution chimique, un volume plus grand sera alors inclus dans la fente du spectrographe, et les galaxies E et S0 pourront être directement comparées à des modèles d'évolution chimique globaux pour les sphéroïdes. Pour les spirales il sera intéressant d'explorer l'effet de la contribution des disques. Soulignons que dans ce dernier cas, la solution de la synthèse ne décrira pas nécessairement un chemin dans le plan âge versus $[Z/Z_{\odot}]$. Pour les galaxies à redshift intermédiaire il sera aussi possible de comparer directement le spectre intégré des galaxies spirales avec ceux de galaxies en interaction ou avec des sursauts de formation stellaire ce qui est fondamental pour comprendre ces objets plus distants pour lesquels nous n'avons pas accès à la morphologie. Dans notre échantillon de galaxies proches il y a plusieurs noyaux avec sursauts de formation d'étoiles.

Un autre problème intéressant qui peut être étudié avec les galaxies à redshift intermédiaire est l'effet de l'inclinaison des disques des galaxies spirales sur le spectre intégré *total*. Nos études précédentes (appendices D et E) ont

montré de grands effets de rougissement et de contamination par les raies interstellaires dans le spectre *nucléaire* des spirales, dus aux disques inclinés.

Dans l'attente de nouvelles observations on fera plusieurs modélisations de galaxies distantes avec la bibliothèque d'amas et de galaxies : (i) en suivant des modèles d'évolution chimique, l'effet de la contribution des régions extranucléaires pauvres en métaux peut être simulé avec des spectres de noyaux de galaxies E et d'amas globulaires pauvres en métaux ; (ii) des sursauts de formation d'étoiles jeunes et d'âges intermédiaires peuvent être empiriquement sommés avec différentes intensités par rapport à la population vieille. (iii) la présente méthode incorpore implicitement plusieurs principes de la synthèse évolutive, parce que les amas présentent une IMF et une évolution stellaire en accord avec la Nature. Alors les spectres intégrés d'amas peuvent également être combinés selon différents scénarios de l'évolution du taux de formation d'étoiles dans une galaxie. Ces modèles pourront être comparés avec le spectre intégré de galaxies distantes. Un avantage supplémentaire de cette méthode par rapport à la plupart des synthèses évolutives dans le passé tient en ce que les effets de métallicité peuvent être facilement inclus. Ces modèles pourront aider à mieux comprendre par exemple la nature des spectres des objets E + A (Dressler, 1986), tout en évitant beaucoup d'hypothèses simplificatrices ou l'utilisation de paramètres mal connus comme cela est de règle dans d'autres techniques de synthèse.

REFERENCES

Alloin, D., Andrillat, Y., Souffrin, S., 1971, Astron. Astrophys., 10, 401.

Arimoto, N., Yoshii, Y., 1986.

Barbaro, G., Olivi, F., 1986, In Spectral Evolution of Galaxies, eds. C. Chiosi and A. Renzini, Reidel, p. 283.

Bruzual, G., 1983, Astrophys. J., 273, 105.

Cianni, A., d'Odorico, S., Benvenuti, P., 1984, Astron. Astrophys., 137, 223.

Dressler, A., 1986, In Spectral Evolution of Galaxies, eds. C. Chiosi, A. Renzini, Reidel, p. 375.

Faber, S., 1972, Astron. Astrophys., 28, 109.

Fabers, 1977, In Evolution of Galaxies and Stellar Populations, eds. B. Tinsley, R. Larson (New Haven = Yale Univ. Obs.) p. 157.

Humason, M., Mayall, N., Sandage, A., 1956, Astron. J., 61, 97.

Jones, J., Alloin, D., Jones, B., 1984, Astrophys. J., 283, 457.

Joly, M., Andrillat, Y., 1973, Astron. Astrophys. 26, 95.

Keel, W., 1983, Astrophys. J., 269, 466.

O'Connell, R., 1976, Astrophys. J., 206, 370.

O'Connell, R., 1986, in Stellar Populations, eds. C. Norman, A. Renzini, M., Tosi, Cambridge Univ. Press, p. 167.

Pagel, B., Edmunds, M., 1981, Ann. Rev. Astron. Astrophys., 19, 77.

Pickles, A., 1985, Astrophys. J., 296, 340.

Pritchet, C., 1977, Astrophys. J. Suppl., 35, 397.

Rocca-Volmerange, B., Lequeux, J., Moucherat-Joubert, M., 1981, Astron. Astrophys., 104, 177.

Spinrad, H., Taylor, B., 1971, Astrophys. J. Suppl., 22, 445.

Stebins, J., Whitford, A., 1948, Astrophys. J., 108, 403.

Tinsley, B., 1972, Astron. Astrophys. 20, 383.

Tinsley, B., 1980, Fund of Cosmic Physics, 5, 287.

Turnrose, B., 1976, Astrophys. J., 210, 33.

Van der Bergh, S., 1975, Ann. Rev. Astron. Astrophys., 13, 217.

de Vaucouleurs, G., 1979, in Photometry, Kinematics and Dynamics of galaxies, Eds D. Evans, Univ. of Texas Austin, p. 1.

de Vaucouleurs, G., de Vaucouleurs, A., 1959, P.A.S.P., 71, 83.

Whipple, F., 1935, Harward College Obs. Circular 404.

Figure 1 : Tracé des continus dans le cas d'un noyau rouge et d'un noyau bleu. F_λ normalisé à F(5870 Å) = 10.

Figure 2 : Séquence d'amas globulaires en fonction de la metallicité (indiquée à droite). F_λ normalisé à F(5870 Å) = 10.

Figure 3 : Séquence d'amas ouverts en fonction de l'age (indiqué à droite). F_λ. normalisé à F(5870 Å) = 10.

Figure 4 : Groupes des galaxies elliptiques. F_λ normalisé à F(5870 Å) = 10.

Figure 5 : Groupes des galaxies spirales. F_λ normalisé à F(5870 Å) = 10.

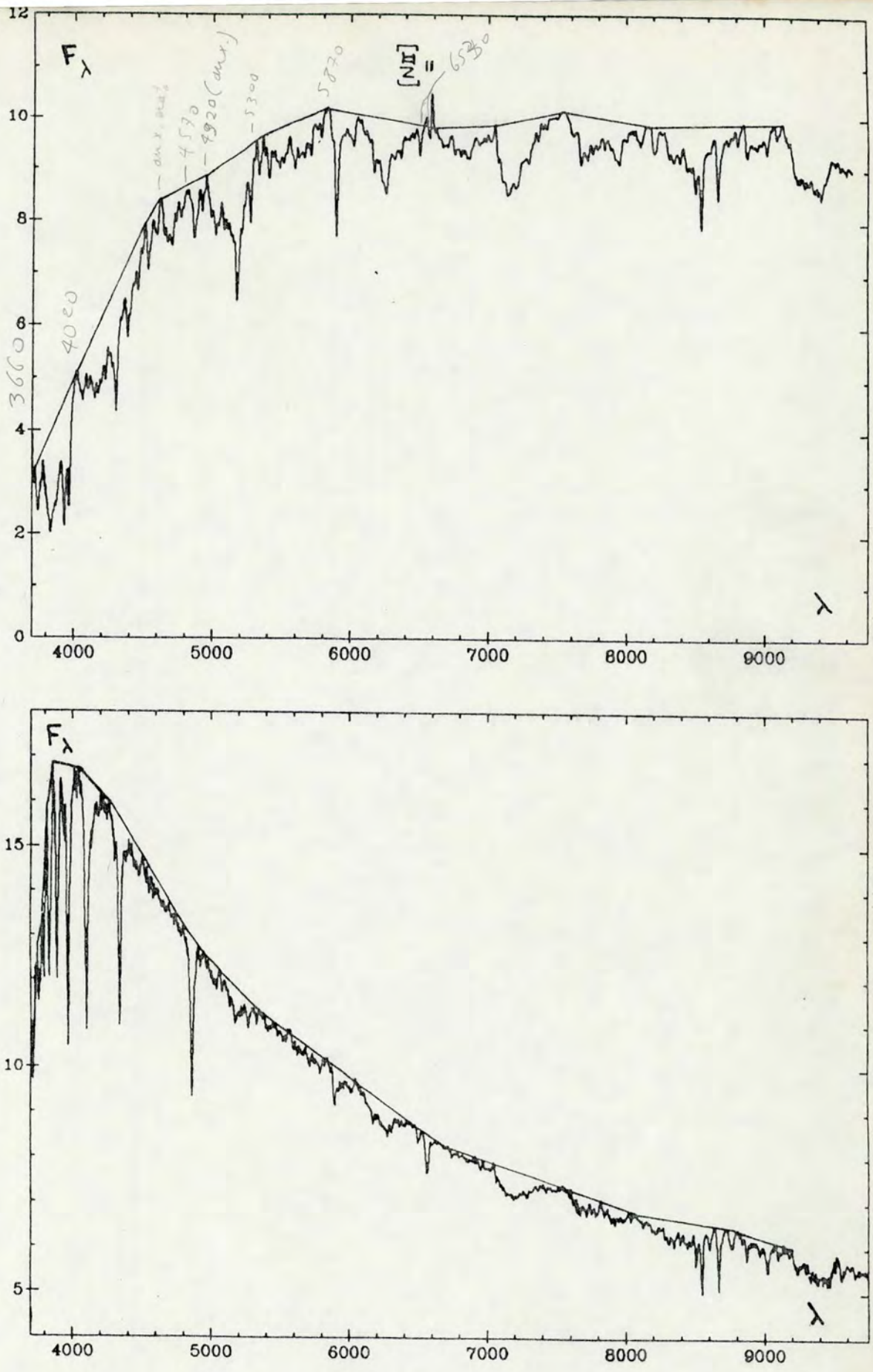

Figure 1

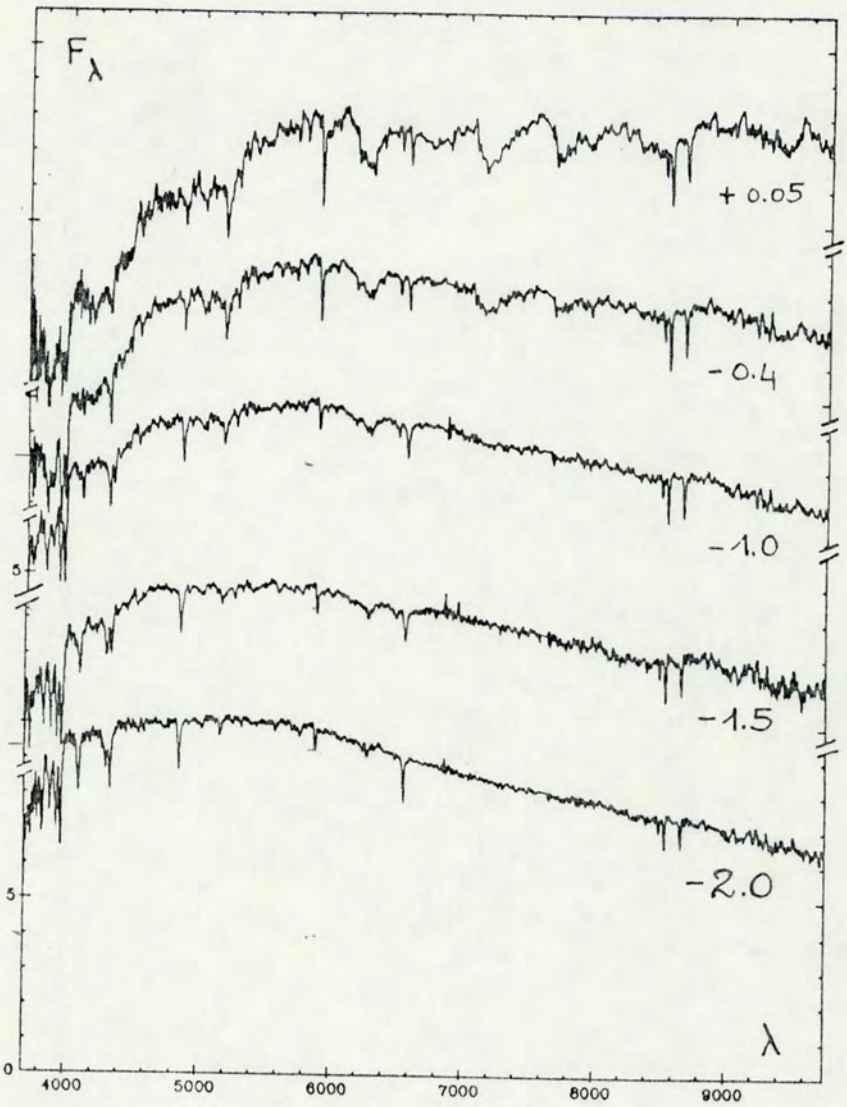

Figure 2

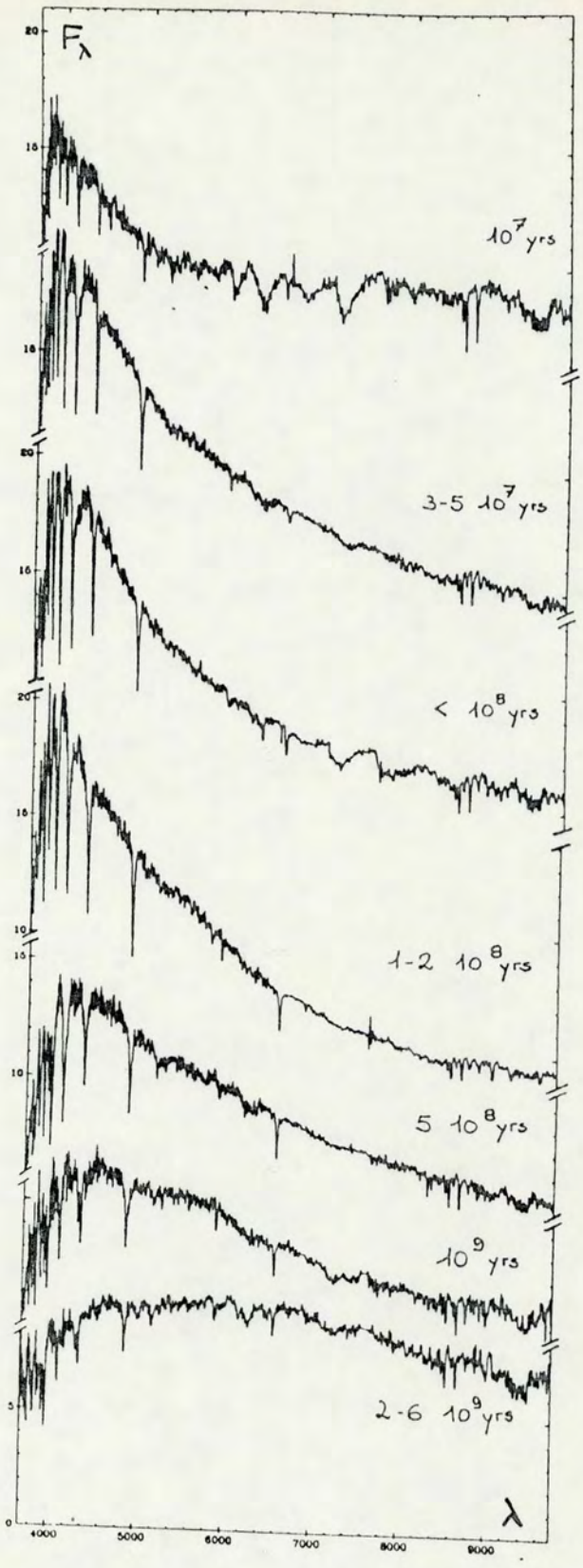
F_λ
10^7 yrs
3-5 10^7 yrs
< 10^8 yrs
1-2 10^8 yrs
5 10^8 yrs
10^9 yrs
2-6 10^9 yrs
λ
4000
5000
6000
7000
8000
9000

Figure 3

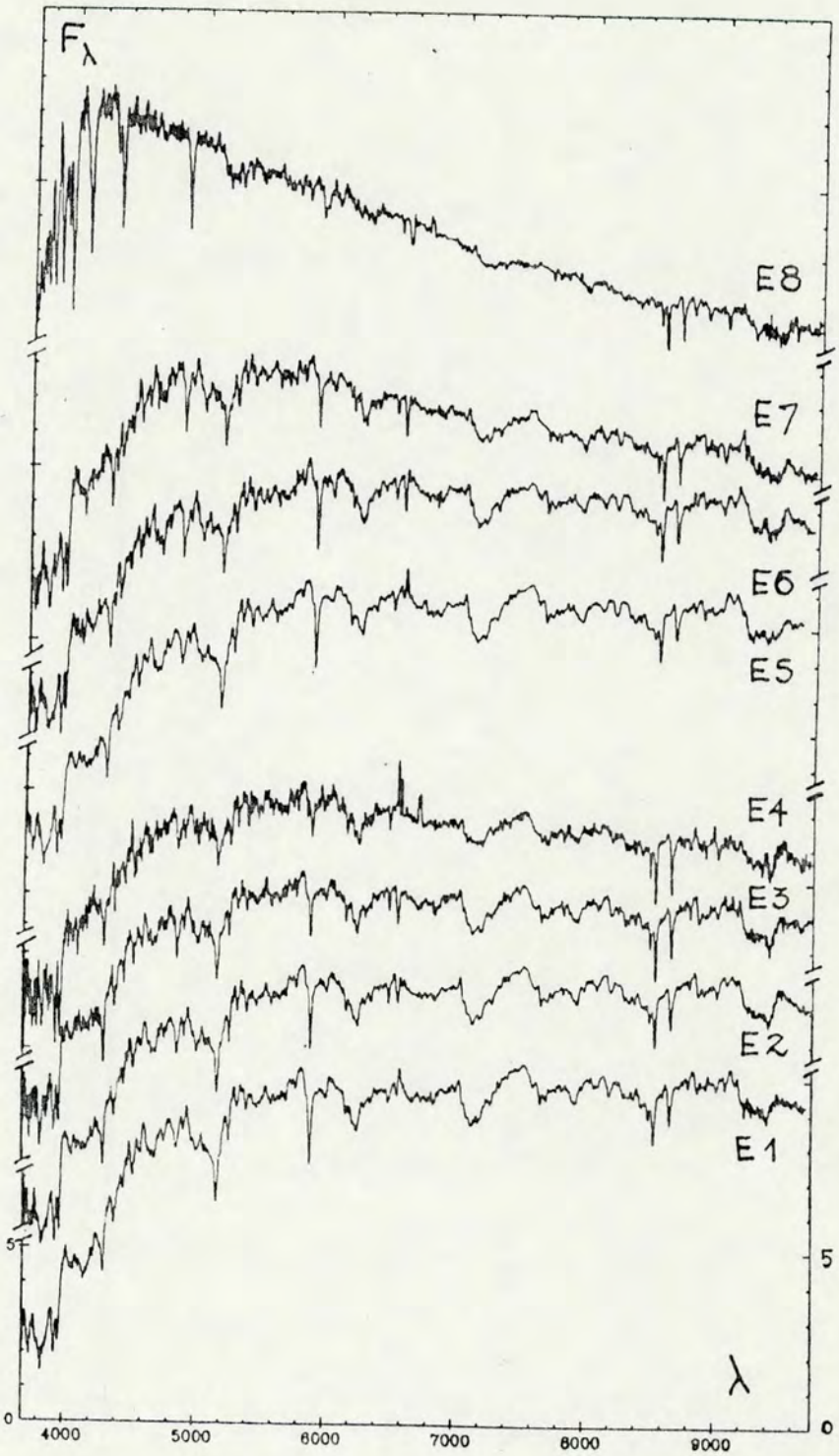

Figure 4

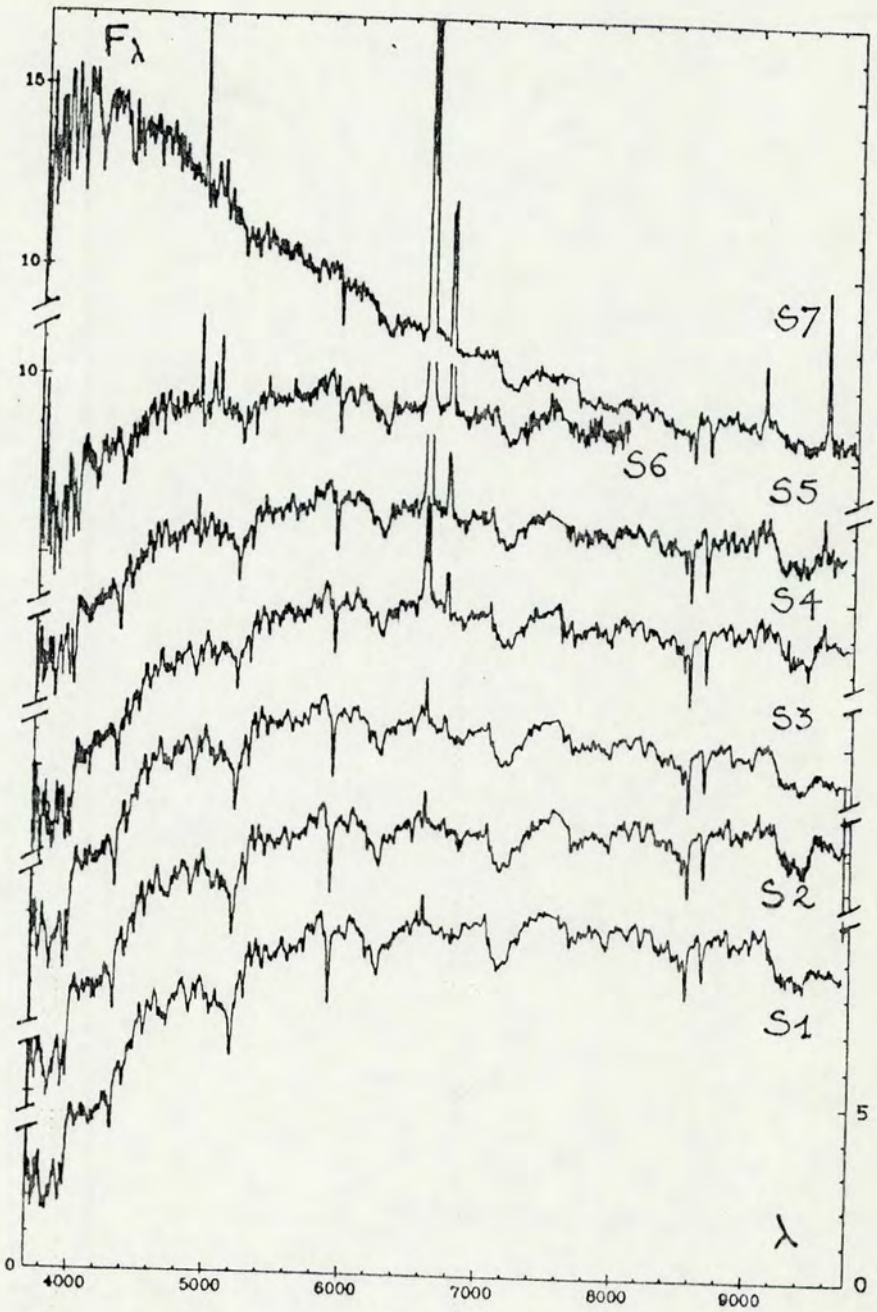
Fλ
15
10
10
S7
S6
S5
S4
S3
S2
S1
5
λ
0
0
4000
5000
6000
7000
8000
9000

Figure 5

Astron. Astrophys. 156, 261–267 (1986)

ASTRONOMY
AND
ASTROPHYSICS

Ages and metallicities of LMC and SMC red clusters through Hβ and G band photometry*

E. Bica[1] **, H. Dottori[2] ***, and M. Pastoriza[2]

[1] Observatoire de Meudon, F-92195 Meudon Principal Cedex, France
[2] Universidade Federal do Rio Grande do Sul, Instituto de Fisica, R. Luis Englert s/n°. 90000 Porto Alegre, RS, Brazil

Received June 13, accepted August 2, 1985

Summary. We present narrow band integrated photometry of the Hβ and G band absorption features for 41 LMC and 10 SMC red star clusters. An age-metallicity calibration is provided for the color-color diagram. We derive SWB types between IV and VII for 23 unclassified clusters and discuss their distribution in the age vs metallicity plane. We study the chemical evolution of the Magellanic Clouds (MC): the LMC presents a steeper chemical enrichment slope. An intrinsic metallicity dispersion is found in the LMC chemical evolution, indicating that the gas has been inhomogeneous at any time, prevailing a local enrichment over a global one. One zone models describe the evolution of both Clouds, being the efficiency of star cluster formation larger in the LMC. The LMC presents a burst of star cluster formation at $t = 4.5\,10^9$ yr. We also present new $B-V$ data for fainter SMC clusters, providing an essentially complete color histogram for clusters with globular cluster appearance.

Key words: Magellanic clouds – red star clusters – age-metallicity relationship

1. Introduction

The study of the evolution of star clusters through their integrated light is not simple owing to the difficulty of isolating spectral features sensitive either to age or metallicity. A two dimensional classification scheme for the MC clusters was provided by Searle, Wilkinson and Bagnuolo, 1980 (SWB) based on integrated photometry in the Gunn-Thuan system. Rabin (1982) compared measurements of equivalent widths (W) of Balmer lines and metallic features with synthetic spectra in order to estimate ages and metallicities. Searle (1984) showed that the SWB types IV to VII define a relationship in Rabin's diagram and provided a theoretical age-metallicity grid.

The DDO G band color index $C(42-45)$ is highly correlated with metallicity in the integrated light of old star clusters (McClure and Van den Bergh, 1968; Bica and Pastoriza, 1983; Dottori et al., 1983).

In this paper, we present narrow band photometry, carried out with filters 42 and 45 of the DDO System, as well as a narrow Hβ (FWHM = 27 Å) filter, for red clusters in the MC. This approach presents the advantage of photometric precision over the spectrophotometric equivalent widths, as well as resolution of spectral features with respect to the SWB's photometry.

We present the observations in Sect. 2. We derive an age-metallicity calibration of the reddening corrected $C(42-45)_0$ vs $C(45-H\beta)_0$ diagram and estimate SWB types for clusters not observed previously, as well as discuss the SWB's classification as a function of age and metallicity in Sect. 3. The chemical evolution of each Cloud is discussed in Sect. 4. Supplementary B and V observations for SMC faint clusters and concluding remarks of this paper are given in Sects. 5 and 6 respectively.

2. Observation

Integrated light photometry of 41 LMC and 10 SMC red clusters, as well as of 6 Galactic globular clusters, were carried out in January and November 1984 at the 1 m ESO Cassegrain telescope. The observations were made through the DDO 42 and 45 filters, measuring the G band and continuum respectively (McClure and Van den Bergh, 1968) and through a narrow Hβ (FWHI = 27 Å) interference filter. The integration time in each filter was such as to provide 1% in cluster plus sky count standard deviation, using a 2 s integration base; a sky integration was stopped when the precision level achieved 1% with respect to the cluster plus sky count. This combined precision level led to mean color errors $\epsilon(42-45) = 0.018$ and $\epsilon(45-H\beta) = 0.020$ as well as $\epsilon(m45) = 0.025$, for repeated measurements. For each cluster at least two sky areas at opposite position angles were observed; for clusters in crowded fields, several position angles were sampled. Each night 2 stars were monitored for extinction corrections and a set of 12 standard stars (including DDO's) was observed. For the color $C(45-H\beta)$ we defined the standard values which are listed in Table 1, together with DDO m45 and $C(42-45)$ values. In order to evaluate the errors in the standard system transformation, 15% of the object sample was observed on different nights, resulting in $\epsilon(m45) = \epsilon(42-45) = \epsilon(45-H\beta) = 0.007$. We have listed the results in Table 2: (1) name; (2) diaphragm size in arcsec; (3) m45; (4) $C(42-45)$ and (5) $C(45-H\beta)$.

3. The age-metallicity calibration

The color indexes $C(42-45)$ and $C(45-H\beta)$ have been corrected for reddening using the relations $E(42-45) = 0.23\ E(B-V)$

Send offprint requests to: E. Bica

* Partly based on observations collected at the European Southern Observatory, La Silla

** Fellowship from the Brazilian Institution CNPq
*** Humboldt Foundation Fellow

Table 1

Standard Star	m45	C(42-45)	C(45-Hβ)
HD 166	7.425	0.753	0.648
HD 4965	8.079	0.329	0.081
HD 6734	7.876	0.785	0.723
HD 6833	8.150*	1.302*	0.966
HD 8949	7.831	0.937	0.803
HD 13936	7.327	0.282	0.176
HD 21197	9.441	1.264	0.766
HD 48616	8.309	0.557	0.607
HD 51219	8.704	0.705	0.627
HD 52533	8.473	0.275	0.393
HD 224155	7.555	0.288	-0.001
AG 510	11.084	0.422	0.376
AG 513	10.463	0.920	0.800

* Values derived from the present photometry. The DDO original values are 8.476 and 0.912 respectively (Mc Clure, 1976). Variable star ?

and $E(45-H\beta) = E(45-48) = 0.31E(B-V)$(McClure, 1979). We adopted $E(B-V) = 0.06$ and $E(B-V) = 0.03$ respectively for the LMC and the SMC (Mould and Aaronson, 1980). For the Galactic globular clusters we used $E(B-V)$ from Bica and Pastoriza (1983). In Fig. 1a we present the reddening corrected diagram $C(42-45)_0$ vs $C(45-H\beta)_0$: the Galactic globular clusters show a linear relationship in this diagram. This behaviour is likewise observed for the W of Balmer lines vs W of metallic features (Rabin, 1982) and for the W of metallic features as a function of metallicity (Bica and Alloin, 1985). The globular cluster sequence essentially represents an isochrone for $1.65\,10^{10}$ yr (Vandenberg, 1983; Janes and Demarque, 1983). The MC clusters define a sequence similar to SWB's, as it can be seen in Fig. 1b, where we show the distribution of SWB types in the color-color diagram of the present photometry, for the 27 clusters in common between the two samples. A comparison of Figs. 1a and 1b allows the determination of SWB types for the 23 remaining unclassified clusters. The narrow band photometry provided a larger dynamical range which allowed a sharper separation of SWB types. Particularly, it has been possible to reassign types in some doubtful cases. The SWB types are listed in column 6 of Table 2.

The age-metallicity calibration of the $C(42-45)_0$ vs $C(45-H\beta)_0$ diagram consists of a grid which was built according to the following criteria:

a) The metallicity along the Galactic globular cluster isochrone was derived from Bica and Pastoriza, 1983.

(b) In order to constrain the grid at the lower age limit, we have used the blue-red transition object NGC 1868 as well as NGC 2209 (Van den Bergh, 1981; Hodge, 1982).

c) The definition of intermediate isochrones was made through the distribution of SWB types in the plane, together with their age calibration (Hodge, 1983).

d) As a constraint for the metal rich locus at $t \simeq 10^9$ yr, we have used spectrophotometric observations of the Galactic disk clusters NGC 2158 and NGC 2660 (Bica and Alloin, 1985). We have derived two equations, respectively for Hβ and G band, relating the spectrophotometric W and the reddening corrected color indexes, using the 11 clusters in common in both samples.

e) Finally, we took into account the distribution of clusters having age or metallicity determination through individual stars (Hodge, 1983; Mould and Aaronson, 1982; Cowley and Hartwick, 1982, Cohen, 1982).

The resulting grid is shown in Fig. 1. We derive new and homogeneous age and metallicity estimates for the whole cluster sample (Table 2).

The loci of SWB types VI and VII (Fig. 1b) with respect to the grid indicate that the type VI clusters are some billion yr younger than the Galactic globulars and present *only* intermediate metallicities. On the contrary, type VII clusters are, in general, indistinguishable from metal poor Galactic globular clusters. It is also possible that some type VII clusters present younger ages than Galactic Globulars. Thus they should be the metal poor counterparts of type VI. Two examples are NGC 2210 and 1466, which present partially blue horizontal branches (HB),

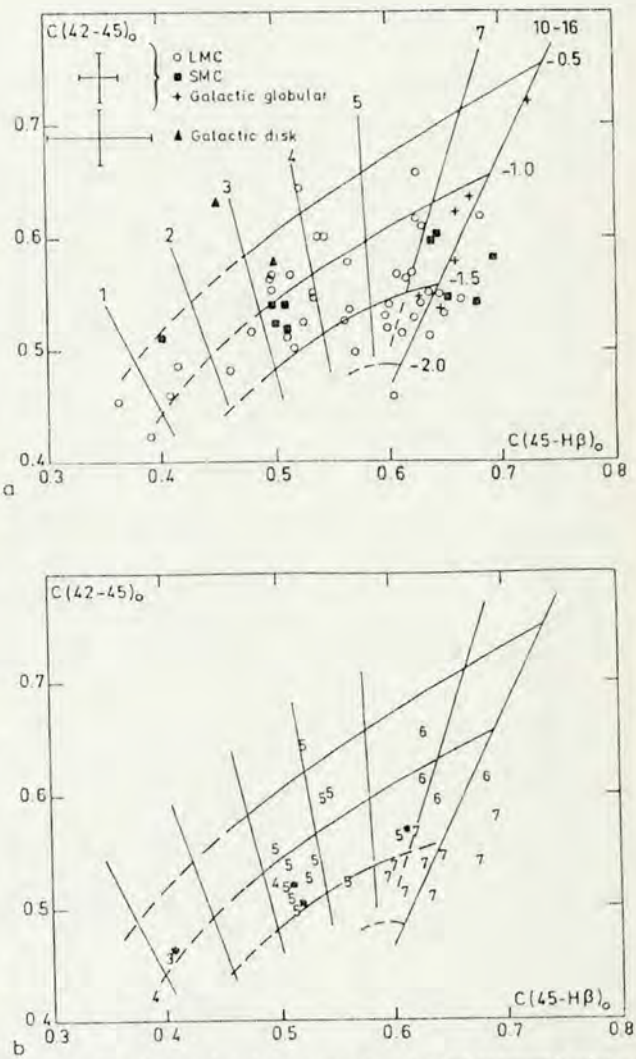

Fig. 1. a The cluster distribution in the reddening corrected color-color plane. Numbers along vertical and horizontal lines are respectively ages in units 10^9 yr and metallicities. **b** Numbers are SWB types, An asterisk denotes transition types as given by SWB (e.g. 5* means type V–VI). The grid is according to **a**.

Table 2

Object	Diaph(")	m_{45}	C(42-45)	C(45-HB)	SWB	Age (10^9 yrs)	(Z/Z_0)
SMC							
K3	61	13.580	.553	.662	VII*	≥10	-1.5 ±0.2
K5	61	14.737	.546	.507	V*	3.2±0.3	-1.1 ±0.2
NGC 121	61	12.788	.590	.701	VII	>10	-1.3 ±0.2
NGC 152	61	14.450	.530	.510	IV;V*	3.2±0.3	-1.25±0.25
NGC 339	61	14.350	.549	.686	VII	≥10	-1.5 ±0.2
NGC 361**	61	13.954	.609	.651	VI*	8±1.5	-1.25±0.2
NGC 411	61	13.616	.525	.520	V-VI,V*	3.4±0.3	-1.3 ±0.2
NGC 416	61	12.863	.605	.648	VI	8±1.5	-1.25±0.2
NGC 419	61	11.993	.545	.518	V	3.5±0.3	-1.2 ±0.2
NGC 643	61	14.538	.519	.410	IV*	1.5±0.3	-0.6 ±0.25
LMC							
NGC 1466	43	13.252	.553	.621	VII	6^{+2}_{-1}	-1.6 ±0.2
NGC 1644	43	14.371	.524	.530	V	3.4±0.4	-1.4 ±0.2
NGC 1651	61	14.079	.580	.532	V*	3.7±0.3	-0.9 ±0.3
NGC 1652	43	14.813	.622	.649	VI*	7^{+2}_{-1}	-1.2 ±0.2
NGC 1718	61	13.739	.577	.634	VII*	7^{+2}_{-1}	-1.4 ±0.2
NGC 1751	61	13.612	.658	.541	V	4±0.3	-0.4 ±0.2
NGC 1754	43	13.373	.546	.663	VII*	≥10	-1.6 ±0.2
NGC 1777	31	14.454	.500	.434	IV*	1.5±0.25	-0.8 ±0.3
NGC 1783	61	12.324	.567	.517	V	3.3±0.3	-0.9 ±0.4
NGC 1786**	43	12.268	.563	.654	VII*	≥10	-1.5 ±0.2
NGC 1795	61	14.168	.578	.516	V*	3.3±0.3	-0.9 ±0.4
NGC 1806	61	12.699	.615	.561	V	4.3±0.3	-0.7 ±0.35
NGC 1835	43	11.785	.563	.647	VII	≥10	-1.6 ±0.2
NGC 1841	61	14.027	.562	.662	VII	≥10	-1.6 ±0.2
NGC 1846	61	12.813	.615	.561	V	4.3±0.3	-0.7 ±0.35
NGC 1852	61	13.494	.561	.553	V*	4.0±0.3	-1.2 ±0.2
NGC 1868	61	12.309	.469	.380	IV*	0.5	-0.6 ±0.35
NGC 1898	43	13.240	.558	.683	VII*	>10	-1.6 ±0.2
NGC 1916	43	11.994	.553	.617	VII*	7^{+3}_{-2}	-1.75±0.2
SL 363	43	13.570	.550	.584	V*	4.6±0.4	-1.4 ±0.3
NGC 1917	61	13.569	.530	.498	IV*-V*	2.8±0.4	-1.1 ±0.2
NGC 1978	61	12.180	.625	.644	VI	$6.6^{+1.4}_{-0.9}$	-1.1 ±0.2
NGC 1987	61	13.387	.438	.408	IV	0.8±0.3	-1.0 ±0.3
SL 506	61	14.932	.538	.545	V*	3.8±0.4	-1.35±0.3
NGC 2005	43	12.685	.543	.642	VII*	>9	-1.7 ±0.2
NGC 2019	43	12.489	.582	.639	VII	7±2	-1.4 ±0.2
IC 2146	61	14.615	.472	.620	VII*	≥10	<-2.0
NGC 2108	61	13.605	.495	.479	IV*-V*	2.2±0.3	-1.2 ±0.2
NGC 2121	61	13.804	.672	.644	VI	6±0.5	-0.75±0.25
NGC 2154	61	13.552	.539	.580	V	4.5±0.5	-1.5 ±0.25
NGC 2155	61	14.102	.631	.700	VI	>10	-1.2 ±0.2
NGC 2162	61	14.091	.541	.546	V	3.8±0.4	-1.35±0.3
NGC 2173	61	13.818	.581	.626	V-VI;VI*	6.5±0.7	-1.4 ±0.2
NGC 2193	61	14.641	.512	.589	V*	4.6±0.5	-1.8 ±0.2
NGC 2203	61	13.511	.592	.584	V	4.7±0.3	-1.1 ±0.2
NGC 2209	61	14.462	.474	.426	III-IV;IV*	1.2±0.3	-0.9 ±0.3
NGC 2210	43	12.557	.543	.616	VII	6^{+3}_{-1}	-1.7 ±0.2
NGC 2213	61	13.863	.515	.536	V-VI;V*	3.5±0.4	-1.5 ±0.25
SL 868	61	12.557	.527	.655	VII	≥10	-1.75±0.2
NGC 2231	61	14.306	.562	.553	V	4.0±0.3	-1.2 ±0.2
NGC 2257	61	14.033	.528	.630	VII	≥10	-1.6 ±0.2
GGC							
NGC 104	61	7.860	.736	.749			
NGC 362	61	9.129	.648	.691			
NGC 1261	61	10.993	.621	.659			
NGC 1851	61	9.459	.598	.687			
NGC 1904	61	10.375	.546	.627			
NGC 7078	61	9.211	.554	.671			

* SWB types derived from the present photometry
** Magnitude and color corrected of foreground star

as well as RR Lyrae stars (Hodge, 1984). This suggests that, for metal poor clusters, RR Lyrae and blue HB stars may arise at younger ages than in classical globulars.

Along with NGC 1466 and 2210, the type VII clusters NGC 121, 1786, 1835, 1841 and 2257 contain RR Lyra stars, but none has been detected in the surveys of NGC 339, 2019 and SL 868 (Graham and Nemec, 1984). As well, no RR lyrae have been found in type VI (e.g. NGC 416, 1978 and 2155). Our results indicate that the LMC clusters NGC 1718, 1754, 1898, 1916, 2005 and IC 2146, as well as K3 in the SMC, are worth being surveyed for RR Lyrae.

4. The chemical evolution

We show in Figs. 2a and 2b the chemical evolution of the LMC and SMC respectively. We included in the figures the results for relative oxygen abundances for H II regions (Pagel et al., 1978 and references therein) as well as metal abundances for LMC blue clusters ($10^7 <$ ages $< 5\,10^8$ yr), as derived from spectra of individual stars (Cohen, 1982). A definite chemical enrichment occurs in both objects. For the LMC the scatter appears to be intrinsic, therefore suggesting that the gas has been inhomogeneous at any time. This result supports a local rather than global enrichment in the interstellar gas. On the contrary, in the SMC, there is a more homogeneous chemical enrichment. A scatter in the LMC metallicities is also visible in the LMC H II regions + blue clusters set. On the other hand the homogeneity of the chemical enrichment for the SMC older clusters is also present in the SMC H II region data set. We emphasize that although the SMC star cluster sample amounts to 25% of that of the LMC, it is about complete for populous clusters.

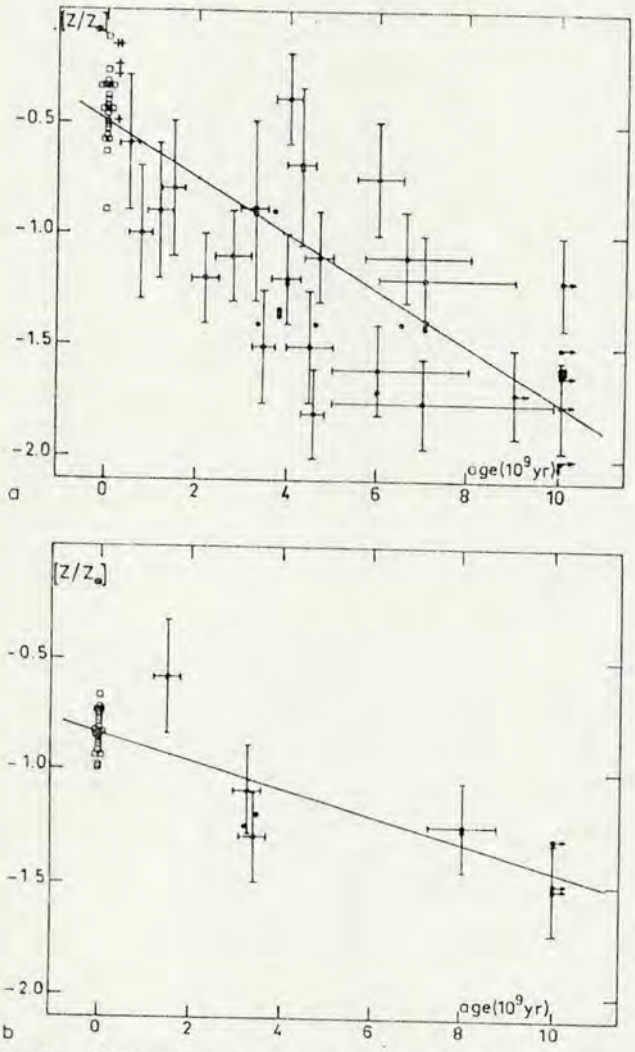

Fig. 2a and b The chemical evolution of the LMC and SMC respectively. For clarity some error bars were omitted. Squares are H II regions and crosses are blue star clusters

Linear regressions yield for the chemical enrichment of the Clouds (t in 10^9 yr units):

$$[Z/Z_\odot] = -0.123t - 0.52$$
$$[Z/Z_\odot] = -0.060t - 0.85$$

for the LMC and SMC respectively.

A steeper slope is found for the LMC, but it is rather ill-defined within the intrinsic dispersion.

The mean metal content for $t \geq 10^{10}$ yr is essentially the same within the error bars and intrinsic metallicity scatter. However, it is striking that the lowest metallicity in the SMC is $[Z/Z_\odot] = -1.5$.

The frequency distribution of ages for the LMC and SMC clusters are shown in Fig. 3. The LMC histogram presents two well-defined maxima, the one at $4.5\,10^9$ yr corresponding to a burst of star formation. The peak in the distribution tail results from the impossibility of separating ages for $t > 10^{10}$ yr. The redistribution of this accumulated peak, following the general trend of the histogram, suggests a primordial cluster formation in the LMC at $t \leq 14 \pm 2\,10^9$ yr. This cumulative effect in the tail of the distribution is also visible in the SMC histogram.

We show the metallicity histograms for the LMC and SMC in Fig. 4. Although the LMC metallicity spread at a given time cannot be described by a simple chemical evolution model which

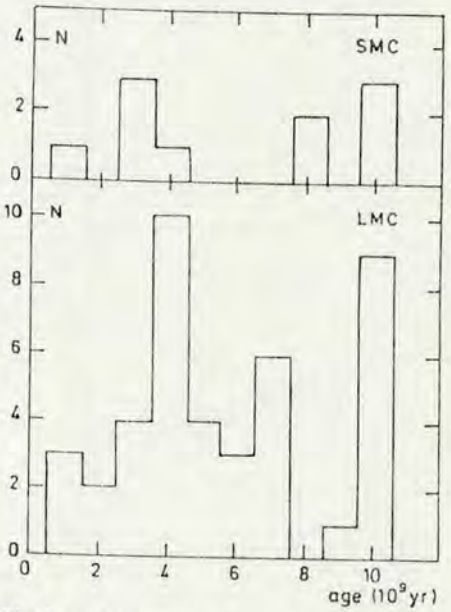

Fig. 3 Age histograms

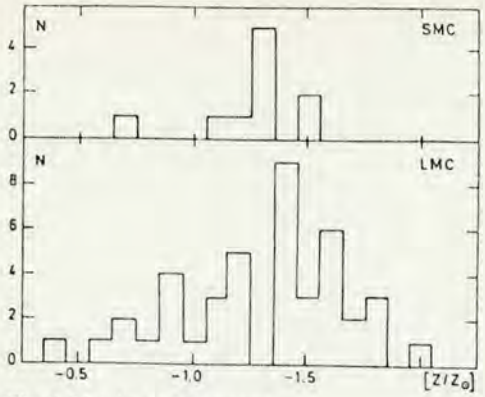

Fig. 4. Metallicity histograms

assumes a homogeneous metal content for the gas as a function of time, we have compared the LMC metallicity histogram with one-zone models (Hartwick, 1976). This is justified by considering that the gas local advances or delays with respect to the mean metal enrichment are implicitly taken into account in the Z histogram. As can be seen in Fig. 5, a model with $C = 10$ (the ratio of the mass ejection rate from star forming regions to the star formation rate) describes the star cluster formation in the LMC. This value confirms the result derived from a smaller sample in a previous paper (Dottori et al., 1983) and it is a factor 5 smaller than that derived for the LMC, from a sample of clusters with classical globular properties (Hartwick and Cowley, 1980). It is important to notice that the one-zone model describes quite well the chemical evolution of the LMC, but not that of the Galactic halo including metal rich globulars (Bica and Pastoriza, 1983). We also compare in Fig. 5 the SMC data with the one-zone

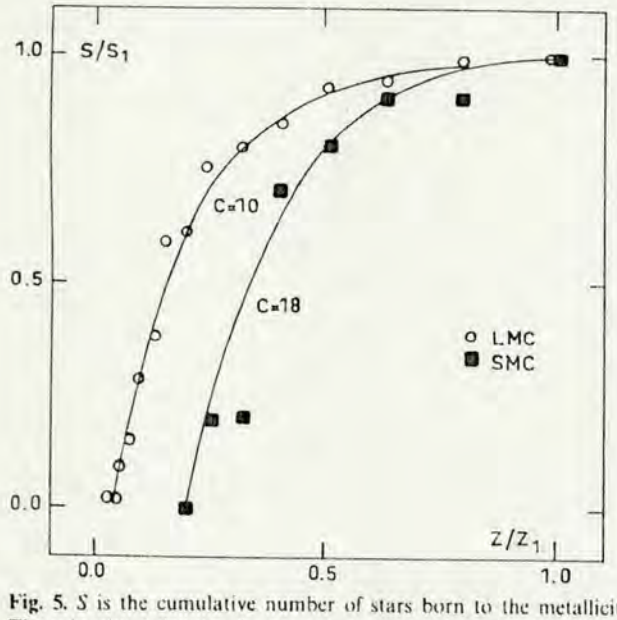

Fig. 5. S is the cumulative number of stars born to the metallicity Z. The subscript 1 denotes the present state of each Cloud. Lines are one-zone models with upper and lower $(Z/Z_\odot)$ limits $(-0.3, -2.0)$ and $(-0.9, -1.6)$ for the LMC and SMC respectively. Circles and squares are the cumulated metallicity histograms respectively for the LMC and the SMC

model. The best fit is obtained for $C = 18$. Owing to the scantiness of clusters, the metallicity limits to be used in the model are not well-defined. However different upper limits $(-0.7 \geq (Z/Z_\odot \geq -0.9)$ and lower limits $(-1.5 \geq [Z/Z_\odot] \geq -2.0)$ do not change much the value of C obtained for the best fit. Thus, the one-zone model also describes the star cluster formation in the SMC. The smaller value of C found for the LMC implies that star formation processes are more efficient in the LMC than in the SMC.

5. The $B - V$ photometry of SMC clusters

In view of studying the chemical evolution of the SMC through a larger sample of old star clusters, we discuss in this section the completeness of the present SMC red star cluster sample. Van den Bergh (1981) compiled and analyzed the UBV integrated photometry of the Magellanic Cloud clusters, being his SMC sample essentially complete to $V \simeq 13$. In this section we extend the photometry to $V \simeq 15$. The observations were carried out in 1982 at the Cassegrain focus of the 1.6 m telescope in Itajuba, Brazil. We observed 2 stars each night at different airmasses for extinction corrections and about 12 standard UBV stars from Landolt (1973) for the system transformation. The sky background was sampled at different position angles around the cluster, particularly for crowded fields. We list in Table 3 the name, diaphragm size, total number of 60 s integrations on the object, number of nights and the V and $B - V$ measurements with their respective errors. The table contains 27 new clusters with respect to Van den Bergh's list. The 13 clusters in common show a good agreement between the two data sets (Fig. 6) with rms = 0.03 for $B - V$ differences. Following Van den Bergh, we have built the integrated magnitude-color diagram: in our observations we excluded clusters associated with emission, so no new points are seen for $(B - V) < 0.1$. Thus our observations cover the plane for ages $> 10^7$ yr and $13 < V < 15$. From the $B - V$ histogram (Fig. 7), the new sample of blue clusters (not associated with emission) amounts to 40% of the previous one, 43% in the case of the new red star clusters sample $(B - V > 0.6)$ and 300% for the blue-red transition objects $(0.4 < (B - V) < 0.6)$. This confirms Van den Bergh's prediction that many intermediate color clusters would fade below his survey limit, as a result of the evolution and subsequent disappearance of the brightest cluster stars. Also the total number of objects in this class is intrinsically smaller than in the blue or red classes. This is obviously due to the fact that the intermediate color interval with respect to the red class corresponds to a rapid phase in the cluster color evolution, not exceeding 10^9 yr. Also unbounded blue clusters will have disintegrated before reaching the intermediate ages.

The present photometry makes essentially complete the $B - V$ color classification of clusters with globular cluster appearance in the SMC. Since the G Band-Hβ photometry for metallicity and age determinations is valid for $(B - V) > 0.4$, we conclude that the SMC clusters used for the chemical evolution study in Sect. 4 is one third complete and that the sample is 50% complete for clusters with $(B - V) > 0.6$.

6. Concluding remarks

a) The photometric system composed of DDO filters 42 and 45 and a narrow Hβ filter, allows the determination of age and metallicity through the integrated light of red clusters.

Table 3

Name	Diaph (")	n	N	V	B-V
*L1	50	9	3	13.39 ± .03	0.74 .08
K5, L7	44	7	2	13.51 ± .09	0.62 .02
*K3, L8	50	9	3	12.23 ± .17	0.72 .01
K6, L9	44	7	2	14.45 ± .08	0.63 .04
*NGC 121, K2, L10	50	8	3	11.44 ± .07	0.79 .01
*K7, L11	44	7	2	14.40 ± .10	0.74 .03
*NGC 152, K10, L15	50	9	3	13.15 ± .10	0.70 .10
K15, L21	44	3	1	14.55 ± .10	0.50 .07
*K21, L27	50	9	3	13.25 ± .23	0.73 .08
L28	44	3	1	13.58 ± .02	0.52 .02
K27, L36	20	7	2	14.00 ± .11	0.71 .10
L41	44	3	1	12.87 ± .02	0.15 .02
L52	20	3	1	14.58 ± .05	0.15 .06
*K37, L58	44	7	2	14.14 ± .07	0.56 .04
*NGC 339, K36, L59	50	9	3	13.01 ± .20	0.71 .04
K43, L64	44	3	1	14.24 ± .04	0.20 .09
L65	50	3	1	13.79 ± .03	0.24 .04
*K44, L68	50	7	2	13.79 ± .15	0.84 .06
K45, L69	44	3	1	14.65 ± .04	0.53 .05
IC1626, K53, L77	50	3	1	13.43 ± .02	0.34 .03
L80	44	3	1	13.66 ± .03	0.26 .04
K55, L81	44	4	1	14.39 ± .15	0.12 .08
*NGC 411, L60, L82	44	9	3	12.47 ± .07	0.66 .02
*NGC 416, L59, L83	44	8	3	11.62 ± .01	0.73 .01
*NGC 419, K58, L85	60	8	3	10.56 ± .08	0.64 .02
K57, L86	44	4	1	14.58 ± .12	0.40 .10
K61	44	3	1	14.18 ± .04	0.25 .03
K63, L88	44	3	1	14.29 ± .04	0.26 .05
L91	44	6	2	14.42 ± .15	0.64 .07
IC1662, L92	44	3	1	14.20 ± .03	0.12 .03
L95	44	3	1	14.70 ± .09	0.17 .09
K68, L98	44	4	1	15.25 ± .10	0.11 .09
L100	44	2	1	14.73 ± .03	0.61 .03
L102	44	6	2	14.63 ± .08	0.40 .03
L108	44	6	2	14.54 ± .05	0.49 .04
L109	44	7	2	14.77 ± .09	0.59 .03
L110	44	7	2	14.33 ± .14	0.77 .05
NGC 643, L111	44	9	3	13.47 ± .14	0.57 .04
*L113	50	9	3	13.73 ± .28	0.75 .02
L116	44	14	3	15.37 ± .17	0.45 .13

* Objects with previous photometry (Van den Bergh, 1981)

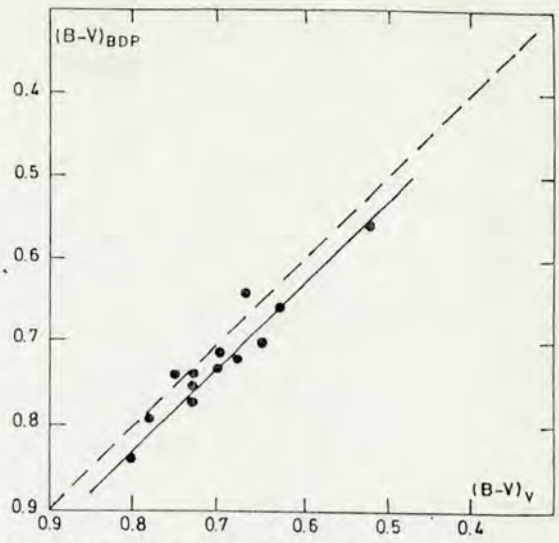

Fig. 6 Comparison of $(B-V)$ between the present photometry and that of Van den Bergh (1981) for the 13 clusters in common between the two data sets

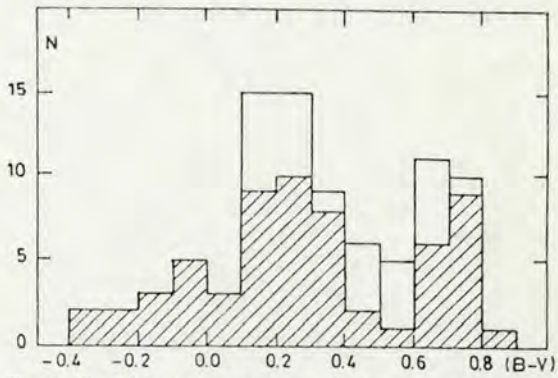

Fig. 7 The $B-V$ histogram: the dark area corresponds to Van den Bergh's (1981) sample; the other part is from the present photometry of clusters with $V \geq 13$

b) We derived an age metallicity calibration corresponding to the color-color diagram.

c) We have estimated SWB types for 23 new cluster. The SWB classification has a larger dynamical range in the present photometry, leading to a better understanding of types VI and VII as a function of age and metallicity.

d) We have obtained ages and metallicities for 41 LMC and 10 SMC red star clusters, which allow direct estimate of the chemical evolution in both Clouds.

e) An intrinsic metallicity scatter is observed along the chemical evolution of the LMC. The LMC presents a steeper chemical enrichment slope.

f) The LMC presents a burst of star cluster formation at $t = 4.5\,10^9$ yr.

g) One-zone models describe quite well the evolution of both Clouds, being the efficiency of star cluster formation in the LMC larger than in the SMC.

h) We present 27 new B and V observations for SMC clusters. These results make essentially complete the $B-V$ color classification of clusters with globular cluster appearance in the SMC.

Acknowledgments: We would like to thank the ESO staff at la Silla as well as Alex Schmidt for assistance during observations and/or reductions. We are indebted to D. Alloin for reading the manuscript and for the interesting suggestions. H. Dottori acknowledges the hospitality at the Astronomisches Institut der Ruhr Universität Bochum.

References

Bica, E., Alloin, D.: 1985, submitted to *Astron. Astrophys.*
Bica, E., Pastoriza, M.: 1983, *Astrophys. Space Sci.* **91**, 99

Cohen, J.G.: 1982, *Astrophys. J.* **258**, 143
Cowley, A.P., Hartwick, F.D.: 1982, *Astrophys. J.* **259**, 89
Dottori, H., Pastoriza, M., Bica, E.: 1983, *Astrophys. Space Sci.* **91**, 79
Graham, J.A., Nemec, J.M.: in Structure and Evolution of the Magellanic Clouds, ed. S. Van den Bergh and K.S. Boer, Dordrecht: Reidel, p. 37
Hartwick, F.D.: 1976, *Astrophys. J.* **209**, 418
Hartwick, F.D., Cowley, A.P.: 1980., in Star Clusters, IAU *Symp* 85, ed. J.E. Hesser, Dordrecht: Reidel. p. 335
Hodge, P.W.: 1982, *Astrophys. J.* **256**, 447
Hodge, P.W.: 1983, *Astrophys. J.* **264**, 470
Hodge, P.W.: 1984, in Structure and Evolution of the Magellanic Clouds. ed. S. Van den Bergh and K.S. Boer, Dordrecht: Reidel, p. 7
Janes, K.A., Demarque, P.: 1983, *Astrophys. J.* **264**, 206
Landolt, A.U.: 1973, *Astron. J.* **78**, 959
McClure, R.D.: 1976, *Astron. J.* **81**, 182
McClure, R.D.: 1979, *Dudley Observatory Report*, No. 14, p. 83
McClure, R.D., Van den Bergh, S.: 1968, *Astron. J.* **73**, 313
Mould, J., Aaronson, M.: 1980, *Astrophys. J.* **240**, 464
Mould, J., Aaronson, M.: 1982, *Astrophys. J.* **263**, 629
Pagel, B., Edmunds, M., Fosbury, R., Webster, B.: 1978, *Monthly Notices Roy. Astron. Soc.* **184**, 569
Rabin, D.: 1982, *Astrophys. J.* **261**, 85
Searle, L.: 1984, in Structure and Evolution of the Magellanic Clouds. ed. S. Van den Bergh and K.S. Boer, Dordrecht: Reidel, p. 13
Searle, L., Wilkinson, A., Bagnuolo, W.G.: 1980, *Astrophys. J.* **239**, 803
Vandenberg, D.A.: 1983, *Astrophys. J. Suppl.* **51**, 29
Van den Bergh, S.: 1981, *Astron. Astrophys. Suppl.* **46**, 79

Astron. Astrophys. 162, 21–31 (1986)

ASTRONOMY AND ASTROPHYSICS

A base of star clusters for stellar population synthesis*

E. Bica and D. Alloin

Observatoire de Paris, Section de Meudon LAM, F-92195 Meudon Principal Cedex, France

Received May 5, 1985; accepted January 16, 1986

Summary. Integrated spectra of 63 star clusters with 10^6 yr $\leqq$ age $\leqq 1.65\ 10^{10}$ yr and $-2.1 \leqq [Z/Z_\odot] \leqq 0.1$ are presented in this paper. The useful wavelength range 3780, 7690 Å was split into 70 consecutive windows, 24–190 Å wide. The main contributors to the absorption in each window were searched for: apart from the strong well-known absorption features, we detected a number of weaker absorptions quite often due to molecular bands arising from red stars. The equivalent widths W of the spectral features, as well as the continuous distribution are studied as a function of age and metallicity.

Metallic lines and molecular bands present essentially the same behaviour with metallicity. In particular, we show the influence of younger turn-off points on W, for features in the blue part of the spectrum. Indeed, the top main sequence stars then enhance the continuum, defining in the W vs. metallicity plots several loci depending on the age. On the contrary, the W vs. metallicity relationship in the red, tends to be single-valued, regardless of age.

For the windows containing Balmer lines from Hα to Hδ, the age dependence looks similar whatever the line, with a maximum W value for $t \sim 4\ 10^8$ yr. If any, the effect of different metallicities is weak in these windows. For a given age, $W(\mathrm{H}\alpha)$ is always smaller than $W(\mathrm{H}\beta)$, $W(\mathrm{H}\gamma)$ or $W(\mathrm{H}\delta)$, due to the fact that its underlying continuum is dominated by late-type stars which contribute very little to the line absorption. For Hε toH10 lines, strongly blended with metallic features, a metal-dominated behaviour is observed.

The continuous distribution of metal-poor globular clusters is strikingly different from that of young blue clusters of any age or metallicity, while their Balmer equivalent widths partly overlap.

These results form a base of star cluster properties which will be used for stellar population synthesis in galaxies. The comparison of W for metallic features in the star clusters and in a sample of 152 nuclei of normal galaxies having types from E to Sc and absolute luminosities M_B from -16.6 to -23.3, shows that around 50 % of the nuclei can be population synthesized with the present cluster base. An extrapolation of the base properties to a metallicity $[Z/Z_\odot] = 0.6$ is required to describe the entire galaxy sample.

Key words: star clusters – spectrophotometry – stellar population synthesis

Send offprint requests to: D. Alloin

* Based on observations collected at the European Southern Observatory, La Silla, Chile

1. Introduction

So far population synthesis in galaxies has been mostly based on spectra of individual stars (Van den Bergh, 1975; Pagel and Edmunds, 1981; Pickles, 1985 and references therein). Some authors used a composite base of stellar spectra and integrated spectra of globular clusters in order to account for possible low metallicity populations in the synthesis (e.g. Faber, 1972; Ciani et al., 1984). The large number of required stellar species and the need for three fundamental parameters (T, g, Z) make difficult the determination of unambiguous solutions, in spite of many plausible astrophysical constraints.

We intend to undertake a different approach to this problem, using *star cluster integrated spectra only*. Therefore a base of 63 star clusters with $-2.1 \leqq [Z/Z_\odot] \leqq 0.1$ and 10^6 yr $\leqq$ age $\leqq 1.65\ 10^{10}$ yr, and of known reddening has been studied. The data consist of low dispersion integrated spectra of Galactic globular clusters, intermediate age red globular clusters as well as blue globular clusters in the Magellanic Clouds (MC), rich and compact Galactic open clusters and H II regions. The main advantage of this method over conventional ones is to reduce the number of variables. A base of stars is essentially described by the temperature, gravity and metallicity. In the case of star clusters, this is reduced to age and metallicity only. Moreover, the number of fundamental species in the cluster base does not need to be as large. Star clusters allow a coverage in metallicity down to a hundreth of solar, while it is observationally difficult to get complete subsets of main sequence and evolved stars with $[Z/Z_\odot] < -0.5$. Finally, this approach is free of any assumption about the initial mass function (IMF) and the details of stellar evolution. Indeed, the integrated spectra of star clusters are built of Nature's exact relative proportions of stars of different masses born from a gas cloud of the corresponding metallicity. As well, the relative proportions of evolved stars as a function of age and metallicity are implicitly the right ones. No assumptions have to be made in that matter.

The choice of the clusters, their distribution in the age vs metallicity plane and the observations are described in the next section. In Sect. 3, we present the spectra in metallicity and age sequences and discuss their main characteristics. Section 4 deals with the selection of the windows, the identification of the contributing absorbers and the analysis of the W and continuum measurements. In view of the population synthesis in galaxies, we derive in Sect. 5 grids of star cluster properties as a function of age and metallicity, and summarize as well the conclusions of this study.

Table 1. Characteristics of the clusters' sample

NAME NGC	AGE 10^7 yrs	$[Z/Z_\odot]$	E(B-V)	AREA 'x'	EXP min	SOURCES
			Small Magellanic Cloud			
121	1200±300	-1.24±0.3	0.03[a]	1x1	60	[3], [5], [6], [10], [19]
330	1.5±0.6	-1.4 ±0.4	"	1x1	20	[3], [6], [7], [15], [19], [32]
419	200±100	-1.2 ±0.3	"	1x1	40	[1], [5], [6], [7], [10], [19]
N 88	<0.2[b]	-0.95[c]	"	0.08x0.22	10	[19], [30], [31]
			Large Magellanic Cloud			
*1466	1400±300	-1.6 ±0.3	0.06[a]	1x0.5	50	[3], [10], [11], [19]
*1714 N4A	0.25±0.05[b]	-0.4[c]	"	1x0.5	10	[19], [31]
1783	300^{+200}_{-100}	-1.0 ±0.5	"	1x1	70	[5], [6], [7], [10], [19], [20]
*1831	30±10	-1.0 ±0.5	"	1x1	30	[5], [6], [7], [19], [22]
*1847	2.5±1.0	-0.25±0.4	"	1x1	26	[6], [19], [25]
*1856	10±3	-0.1 ±0.3	"	1x1	16	[6], [7], [19], [23]
1866	8.6±0.5	-1.2 ±0.2	"	{1x1 / 1x0.5	{20 / 20	[6], [7], [15], [16], [19]
1868	50±20	-1.1 ±0.2	"	1x0.5	40	[6], [18], [19]
*1895 N33	0.55±0.05[b]	-0.3[c]	"	1x0.5	30	[19]
1978	200^{+200}_{-100}	-0.8 ±0.4	"	1x0.7	50	[2], [5], [6], [10], [11], [19]
2004	0.8±0.1	-0.25±0.25	"	1x1	20	[6], [19], [20]
2070 30Dor	0.20±0.05	-0.5[c]	"	comp[d]	24	[17], [19], [24], [31]
*2100	1.0±0.2	-0.5 ±0.1	"	1x1	20	[3], [6], [19], [20]
2157	3±2	-0.6 ±0.3	"	1x0.5	20	[6], [15], [19]
2214	4±1	-1.2 ±0.2	"	1x1	30	[6], [7], [15], [19]
			Galactic Globular Clusters			
104 47TUC	1650±150	-0.70±0.15	0.08±0.04	3x3	12	[8], [9], [12], [13], [21]
362	"	-1.25±0.15	0.06±0.02	{1.5x1.5 / 1x0.5	{20 / 15	[4], [8], [9], [12], [13], [20]
1851	"	-1.3 ±0.2	0.09±0.02	1x0.5	10	[4], [8], [9], [12], [13]
1904 M79	"	-1.55±0.15	0.00±0.02	{1x0.5 / 1x1	{20 / 20	[4], [8], [9], [12], [13]
2808	"	-1.25±0.20	0.21±0.02	2x2	20	[8], [9], [12], [13]
4590 M68	"	-2.00±0.15	0.04±0.02	2x1	40	[4], [8], [9], [12], [13]
4833	"	-1.7 ±0.2	0.31±0.03	1.5x1.5	30	[4], [8], [9], [12], [13]
5024 M53	"	-1.85±0.15	0.01±0.02	2x0.5	30	[4], [8], [9], [12], [13]
5824	"	-1.8 ±0.2	0.12±0.02	1x0.5	10	[8], [9], [12], [13]
5927	"	-0.15±0.15	0.47±0.05	1x0.5	20	[8], [9], [12], [13], [21]
*5946	"	-1.5 ±0.2	0.61±0.07	0.5x0.5	19	[8], [9], [12], [13]
*6093 M80	"	-1.6 ±0.2	0.17±0.03	1x0.5	10	[8], [9], [12], [13]
*6139	"	-1.5 ±0.2	0.70±0.07	1x0.5	16	[8], [9], [12], [13]
6171 M107	"	-0.90±0.15	0.37±0.04	2x2	50	[4], [8], [9], [12], [13], [21]
*6287	"	-1.6 ±0.5	0.5 ±0.1	1x0.5	30	[8], [9], [12], [13]
*6293	"	-1.8 ±0.2	0.36±0.02	1x0.5	16	[8], [9], [12], [13]
*6304	"	-0.2 ±0.4	0.50±0.07	1x0.5	16	[8], [9], [12], [13]
*6316	"	-0.1 ±0.4	0.6 ±0.1	1x0.5	20	[8], [9], [12], [13]
*6356	"	-0.25±0.35	0.27±0.03	1x0.5	30	[8], [9], [12], [13]
*6388	"	-0.6 ±0.2	0.37±0.02	1.5x0.5	10	[8], [9], [12], [13]
*6401	"	-1.1 ±0.2	0.81±0.03	0.5x0.5	32	[8] [12], [13]
6402 M14	"	-1.1 ±0.3	0.55±0.06	2x2	50	[4], [8], [9], [12], [13]
6440	"	0.04±0.3	1.11±0.02	1x05	40	[8], [9], [12], [13]
*6453	"	-1.4 ±0.2	0.61±0.02	0.5x0.5	20	[8], [9], [12], [13]
*6517	"	-1.75±0.4	1.06±0.02	0.5x0.5	20	[8], [9], [12], [13]
*6528	"	-0.05±0.2	0.66±0.09	0.5x0.5	20	[8], [9], [12], [13]
6541	"	-1.65±0.25	0.12±0.05	2x0.5	20	[8], [9], [12], [13]
*6544	"	-1.1 ±0.4	0.72±0.08	0.5x0.5	20	[8], [9], [12], [13]
*6553	1650±150	0.1 ±0.4	0.79±0.09	1x0.5	50	[8], [9], [12], [13]
*6558	"	-1.3 ±0.2	0.40±0.15	0.5x0.5	20	[8], [9], [12], [13]

Table 1 (continued)

NAME NGC	AGE 10^7 yrs	$[Z/Z_\odot]$	E(B-V)	AREA 'x'	EXP min	SOURCES
*6569	"	-0.8 ±0.1	0.59±0.04	1x0.5	30	[8], [9], [12], [13]
*6624	"	-0.3 ±0.2	0.29±0.05	1x0.5	10	[8], [9], [12], [13]
*6637 M69	"	-0.55±0.3	0.18±0.02	1x0.5	16	[8], [9], [12], [13], [21]
*6638	"	-0.95±0.2	0.40±0.02	1x0.5	16	[8], [9], [12], [13]
*6642	"	-1.35±0.2	0.38±0.02	0.5x0.5	14	[8], [9], [12], [13]
*6652	"	-0.6 ±0.3	0.09±0.02	0.5x0.5	18	[8], [9], [12], [13]
*6715 M54	"	-1.25±0.2	0.14±0.02	1x0.5	10	[4], [8], [9], [12], [13]
*6760	"	-0.4 ±0.2	0.85±0.09	1x0.5	28	[8], [9], [12], [13]
6864 M75	"	-1.25±0.15	0.16±0.02	1x0.5	20	[8], [9], [12], [13]
7006	"	-1.45±0.20	0.07±0.05	1x0.5	30	[8], [9], [12], [13]
7078 M15	"	-2.05±0.25	0.08±0.02	2x0.5	20	[4], [8], [9], [12], [13], [20]
			Galactic Open Clusters			
2158	120±50[e]	-0.65±0.25	0.43±0.05	1.5x1.5	90	[14], [27]
2660	120±30	-0.02±0.25	0.38±0.05	1x0.5 1.5x1.5	50 20	[14], [26]
6705 M11	17±5	0.11±0.09	0.42±0.05	2x2	30	[14], [28], [29]

Notes to Table 1

[a] We adopted for homogeneity, a Galactic reddening $E(B-V) = 0.03$ and 0.06 for all objects in the SMC and LMC respectively (Mould and Aaronson, 1980). However, there are indications that both H II regions and some blue star clusters may be reddened (e.g. Hodge and Lee, 1984)

[b] The age determination is based on the $W(H\beta)$ vs. age relationship in H II regions (Dottori, 1981), corresponding to the $5'' \times 13''$ entrance slit

[c] This value is deduced from the oxygen relative abundance

[d] Scans are made of three clumps in the stellar association and of the central emission filaments free of stellar contamination. The emission spectrum was adjusted with the sum of the stellar clumps' spectra so as to reproduce the integrated $H\beta$ equivalent width in a 10′ diaphragm (Dottori and Bica, 1981)

[e] Arp and Cuffey (1962) concluded that the age of NGC 2158 is intermediate between that of the Hyades and NGC 752. The value given here is the mean of recent age determinations for the latter clusters (McClure and Twarog, 1978)

References to Table 1

1 Durand et al. (1984)
2 Olszewski (1984)
3 Hodge (1984a)
4 Smith (1984)
5 Mould and Aaronson (1982)
6 Hodge (1983)
7 Searle et al. (1980)
8 Van den Berg (1983)
9 Bica and Pastoriza (1983)
10 Dottori et al. (1983)
11 Cowley and Hartwick (1982)
12 Janes and Demarque (1983)
13 Zinn and West (1984)
14 Janes (1979)
15 Richtler and Nelles (1983)
16 Becker and Mathews (1983)
17 Boeshaar et al. (1983)
18 Hodge (1982)
19 Mould and Aaronson (1980)
20 Cohen (1982)
21 Cohen (1983)
22 Hodge (1984b)
23 Hodge and Lee (1984)
24 Dottori and Bica (1981)
25 Nelson and Hodge (1983)
26 Hartwick and Hesser (1973)
27 Arp and Cuffey (1962)
28 Mermilliod (1981a)
29 Barbaro et al. (1969)
30 Dufour and Harlow (1977)
31 Pagel et al. (1978)
32 Carney et al. (1985)

2. Choice of the cluster base and observations

The main criterion in the selection of the star clusters was the knowledge of their age, metallicity and reddening. These quantities are listed respectively in columns 2–4 of Table 1, together with their uncertainties taking into account both individual error bars and the discrepancies among different sources which are given in column 7. The metal abundance determinations derived by a variety of methods were grouped under the symbol $[Z/Z_\odot]$, the logarithm of metal content relative to the Sun.

The distribution of the clusters in the plane age vs metallicity is shown in Fig. 1. Metallicities from solar down to $[Z/Z_\odot] \simeq -2$ fill in the plane for essentially all ages, from young clusters about 10^7 yr old to Galactic globular clusters with ages in the range 15 to 18 10^9 yr (Vandenberg, 1983; Janes and Demarque, 1983). The MC clusters allowed the coverage of the intermediate and low metallicity ranges for young and intermediate ages. The Galactic open clusters cover the metal rich young and intermediate ages in the plane. This base offers a wide range of possible chemical evolution models for subsystems in galaxies to be synthesized.

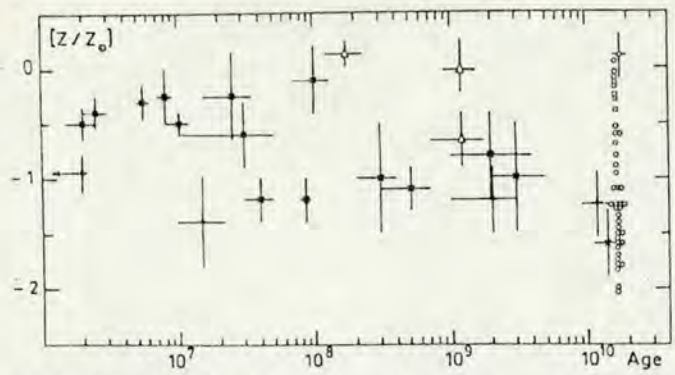

Fig. 1. Distribution of the cluster sample in the age, metallicity plane. For globular clusters, 1650 10^7 yr old, the typical error bar is indicated for one of the points only. Open triangles refer to Galactic open clusters (GOC); open circles to Galactic globular clusters (GGC); crosses and plus signs to the LMC and SMC clusters respectively

The observations were carried out with the IDS attached to the Boller and Chivens spectrograph at the ESO 1.52 m telescope (La Silla). We obtained in January, July and November 1984 and May 1985 integrated spectra of 3 clusters in the SMC, 12 in the LMC, 41 Galactic globular clusters and 3 rich compact Galactic open clusters, as well as of 4 H II regions.

The wide range of cluster angular sizes required different observing techniques in order to get integrated spectra. Larger angular size objects were scanned in declination with the slit height set along right ascension. Moreover several side by side successive exposures were made at different right ascensions. Small compact clusters in the MC demanded only restricted scanning. In column 5 of Table 1, we have listed the area of the cluster seen in our observations. The slit size was 5″ × 13″, except in the case of objects with an asterisk in column 1, for which the slit height had been set to 8″.

Low resolution spectra are particularly suitable for synthesizing stellar populations in galactic nuclei which, quite often, have large stellar velocity dispersions. Therefore, we used a 300 gr/mm grating in the first order providing a mean dispersion of 224 Å mm^{-1} over the range 3700, 8200 Å. A final resolution of 11 Å was achieved, as measured by the mean FWHM of the comparison lines. We provide in column 6 of Table 1, the total effective exposure on each object. These were such as to produce about the same signal to noise ratio for all spectra. Two or three standard stars were observed each night for flux calibration and estimate of the subsequent error-bars. The reductions were made in a convectional way, using the IHAP system at ESO (Garching) and IAP (Paris).

3. Metallicity and age sequences in the cluster base

All cluster spectra have been corrected for reddening using the $E(B-V)$ values from Table 1, a normal reddening law $A_\lambda = 0.65\, A_v(1/\lambda - 0.35)$ and the relation $A_v = 3\,E(B-V)$. They have been normalized relative to the continuum at 5870 Å. Apart from the strong well known absorptions, we detected a number of weaker features. Most of this widespread absorption, seen in clusters of all ages, is due to molecular bands arising in red stars (Sect. 4) and it tends to be underestimated in higher dispersion data, owing to the inclusion of fewer trustworthy maxima.

In Fig. 2, we present the Galactic globular clusters in a downward decreasing metallicity sequence. An obvious enhancement with metallicity appears for strong features such as Ca II K, the G-band, the Mg I triplet, Na I and TiO relative to the continuum height. Metal-rich globular clusters like NGC 5927 and 6528 exhibit lower blue to red continuum ratios. This arises from both the blanketing effect of numerous metallic absorptions towards the blue and the absence of blue horizontal branch stars (BHB). Conversely, the prominent BHB in metal poor clusters like NGC 7078 raises and flattens the blue end of the continuum, as well as strengthening the Balmer lines. The latter effect can easily be seen by comparing the blend Hε + Ca II H to Ca II K.

We have displayed in Fig. 3 a downward increasing age sequence for Magellanic clusters and one moderately metal rich Galactic open cluster. The properties of NGC 121 in the SMC are comparable to those of Galactic halo globular clusters with similar HR diagrams and having RR Lyrae stars (Van den Bergh, 1975 and references therein). The cluster NGC 1978 belongs to the red intermediate age clusters of the MC. The distribution of the integrated $(U-B)_0$ vs. $(B-V)_0$ colors of such clusters deviates from that of Galactic globular clusters (Van den Bergh, 1981), owing mostly to younger ages from 10^9 to 10^{10} yr, as derived from HR diagrams (Hodge, 1983). The integrated spectra of red star clusters from 3800 to 5200 Å have been analyzed by Rabin (1982); near the lower age limit of this class, we show the Galactic open cluster NGC 2158. The LMC cluster NGC 1868, with an integrated color $(B-V) = 0.45$ (Van den Bergh, 1981) is one of the rare objects intermediate between the so-called blue and red Magellanic globular clusters. In the upper part of Fig. 3, we show blue Magellanic clusters together with the giant LMC H II region NGC 2070: the increasing contribution from brighter and bluer turn-offs in younger clusters strengthens the blue part of the integrated continuum. The blue to red continuum ratios for star clusters younger than 10^9 yr (Fig. 3) are larger than those for old metal-poor objects like NGC 7078 (Fig. 2). Thus, the continuum distribution differences and not the Balmer line equivalent widths which partly overlap (Sect. 4) are important for distinguishing between young populations and old metal-poor ones in galaxies.

The effect of intrinsic reddening is easily observed in H II regions (NGC 2070). Together with internal reddening, the effect of rapid stellar evolution around 10^7 yr (NGC 2004) decreases the continuum slope by the development of an important red supergiant population. After this age, the clusters appear to be essentially dust free and as a consequence exhibit then a very blue continuum (Fig. 3).

4. Selected windows and results

Even in the case of individual stars, it is not a simple task to find out from low dispersion spectra, the nature of the numerous weak absorption features. This results obviously from blending effects and from a large number of atomic or molecular lines to be possibly assigned. The composite nature of a cluster spectrum is an additional difficulty in that matter.

The equivalent widths of selected wavelength ranges in the spectra of different clusters are intended to be used in a synthesis, for comparison with the same measurements in the spectra of galaxies. This approach does not require a detailed identification of the absorbers. Consequently the useful wavelength range 3780–7690 Å was split into consecutive windows, 24–190 Å wide. Such widths are suitable for avoiding problems due to possible

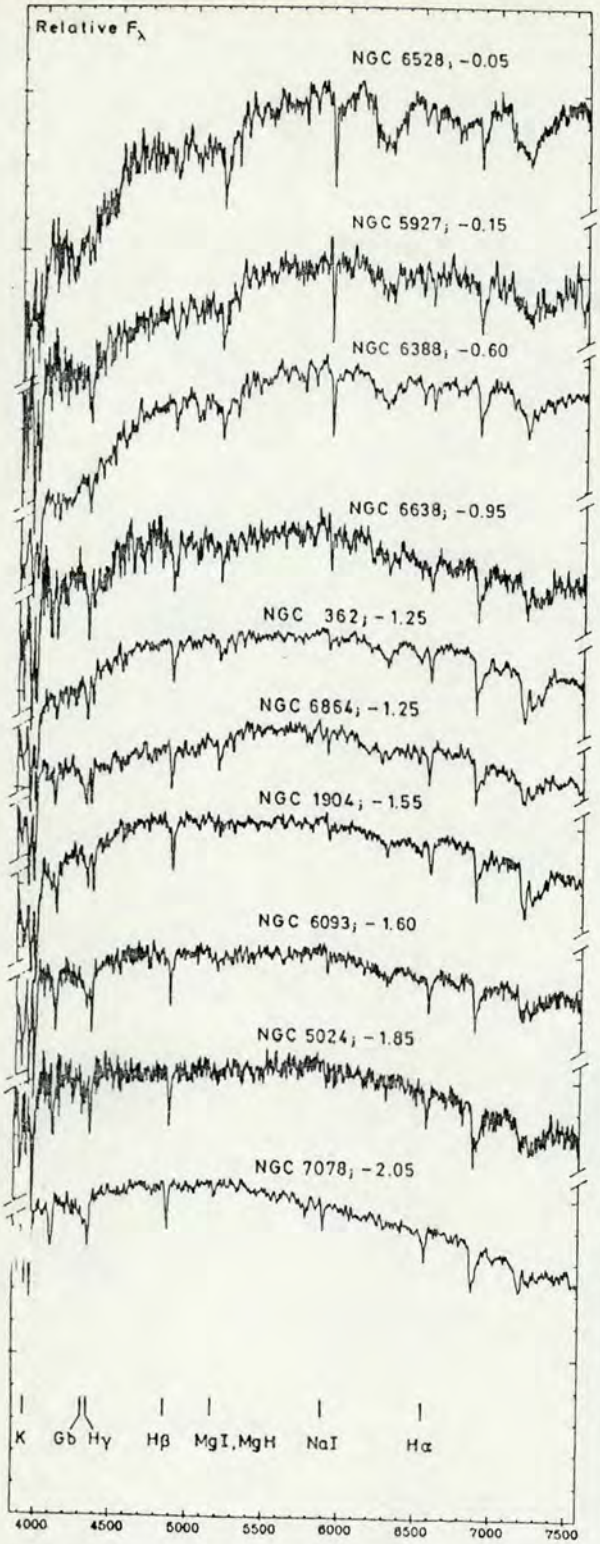

Fig. 2. The metallicity sequence for globular clusters. The spectra are corrected for foreground reddening and are normalized to $F_{5870} = 1$

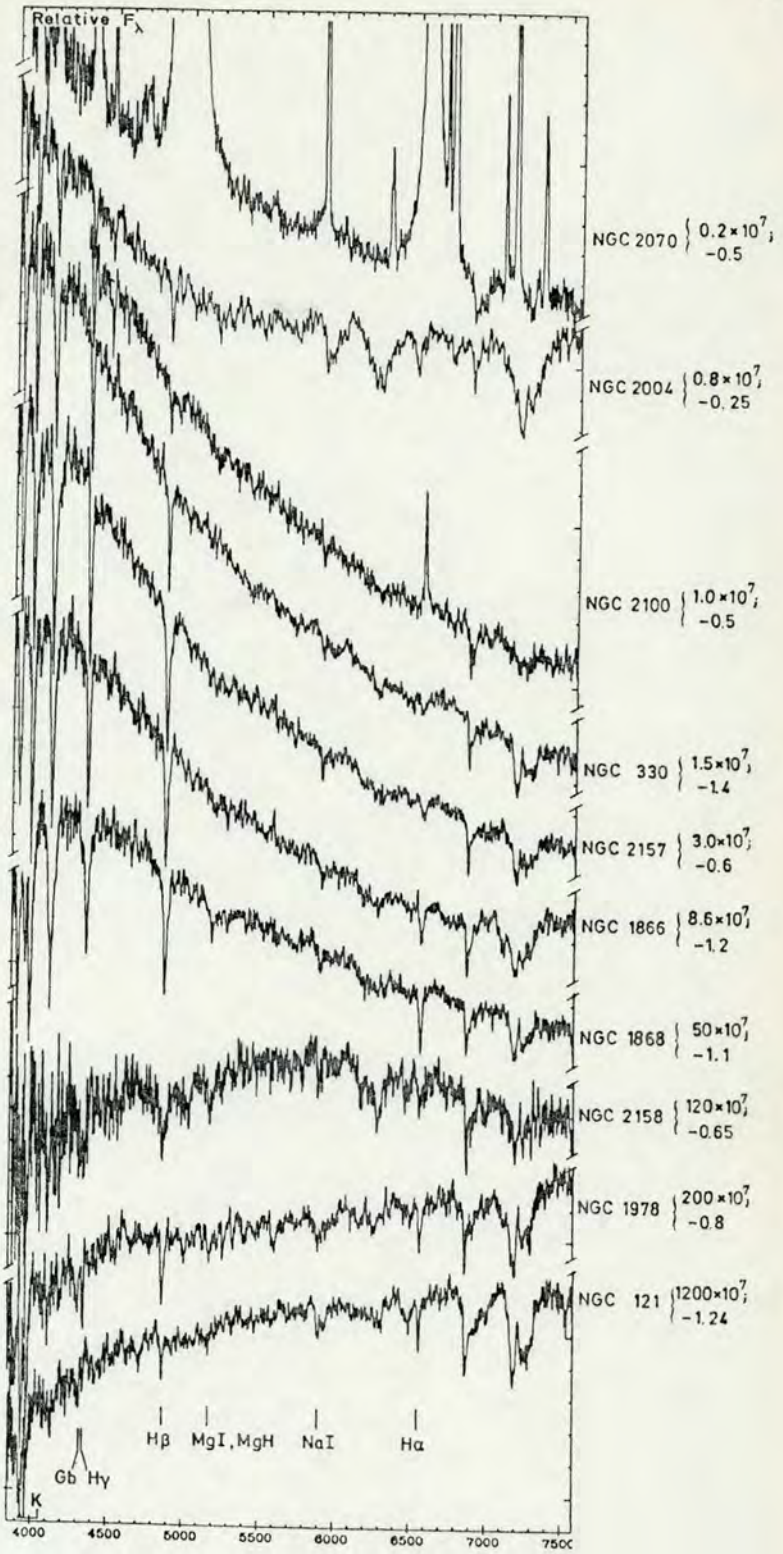

Fig. 3. The age sequence for young clusters. Reddening and normalization as in Fig. 2

Table 2. Window parameters

#	Δλ(Å)	W/Δλ	ABSORBERS
1	3780-3814	0.13	H10 ; CN Lband
2	3814-3862	0.19	H9 ; CN Lband ; FeI ; MgI ; HeI
3	3862-3908	0.18	H8 ; CN Lband ; FeI ; SiI ; HeI
4	3908-3952	0.20	CaII K
5	3952-3988	0.26	CaII H ; Hε
6	3988-4020	0.04	FeI ; HeI
7	4020-4058	0.03	FeI ; HeI
8	4058-4082	0.06	FeI ; SrII
9	4082-4124	0.13	Hδ
10	4124-4150	0.08	FeI
11	4150-4214	0.06	CN
12	4214-4244	0.06	CaI
13	4244-4284	0.07	FeI ; CrI
14	4284-4318	0.14	CH Gband ; FeI ; CrI
15	4318-4364	0.12	Hγ ; FeI ; FeII
16	4364-4420	0.06	FeI ; C_2 ; FeII ; TiII
17	4420-4450	0.06	FeI ; CaI
18	4450-4484	0.04	TiO ; MgII ; CaI ; HeI
19	4484-4510	0.01	CH ; CN
20	4510-4568	0.03	FeI ; BaII ; FeII ; TiII
21	4568-4622	0.02	FeI ; TiO ; CaI ; FeII ; TiII ; CN
22	4622-4668	0.02	FeI ; TiO
23	4668-4698	0.02	TiO ; C_2
24	4698-4750	0.02	FeI ; C_2 ; MgI ; TiI ; NiI ; HeI
25	4750-4802	0.03	MgH ; TiO ; FeI ; MnI ; NiI
26	4802-4846	0.03	TiO ; MgH ; CN ; MnI
27	4846-4884	0.11	Hβ ; TiO ; FeI
28	4884-4908	0.04	FeI
29	4908-4950	0.03	FeI ; FeII ; CN ; HeI
30	4950-4998	0.03	FeI ; TiO ; TiI
31	4998-5064	0.04	FeI ; TiO ; CN ; FeII ; TiI ; HeI
32	5064-5130	0.03	FeI ; C_2
33	5130-5156	0.05	MgH ; FeI ; C_2 ; CN
34	5156-5196	0.08	MgI+MgH ; C_2 ; TiO
35	5196-5244	0.04	MgH ; FeI ; CrI ; CN
36	5244-5314	0.03	FeI ; TiO ; CaI ; TiI
37	5314-5364	0.02	FeI ; TiO ; CN ; CaI
38	5364-5420	0.02	FeI ; MnI
39	5420-5460	0.02	TiO ; FeI ; MnI
40	5460-5516	0.02	MgH ; TiO ; C_2 ; MnI ; CN
41	5516-5562	0.01	MgH ; CaOH ; C_2 ; MgI ; MnI
42	5562-5630	0.01	MgH ; FeI ; CaI ; TiO ; C_2 ; CN
43	5630-5676	0.01	TiO ; C_2 ; FeI
44	5676-5726	0.02	TiO ; NaI ; MgI ; FeI
45	5726-5800	0.02	TiO ; CN ; FeI
46	5800-5848	0.00	TiO
47	5848-5880	0.01	TiO ; CN ; TiI ; HeI ; CaI
48	5880-5914	0.07	NaI ; TiO ; TiI
49	5914-5950	0.03	TiO ; C_2 ; TiI ; FeI
50	5950-6002	0.02	TiO ; CN ; C_2
51	6002-6056	0.01	TiO ; CaOH ; C_2 ; FeI
52	6056-6108	0.01	TiO ; MgH ; CaI ; FeI
53	6108-6156	0.03	CN ; C_2 ; FeI ; TiO
54	6156-6210	0.05	TiO ; CaI ; C_2 ; CN ; FeI
55	6210-6274	0.06	TiO ; FeI
56	6274-6322	0.06	TiO ; FeI ; CN

Table 2 (continued)

#	Δλ(Å)	W/Δλ	ABSORBERS
57	6322-6386	0.03	TiO ; CaH ; FeI ; CN
58	6386-6474	0.02	TiO ; CaI ; FeI ; CN
59	6474-6540	0.04	FeI ; BaII ; CaI ; TiO ; CN
60	6540-6586	0.06	Hα ; TiO ; FeI
61	6586-6670	0.02	TiO ; FeI ; CN
62	6670-6736	0.02	TiO ; CaI ; FeI
63	6736-6858	0.02	TiO ; CN ; FeI ; CaH
64	6858-6934	0.09	Atmospheric O_2
65	6934-7050	0.02	CaH ; CN ; FeI
66	7050-7158	0.03	TiO ; CN ; CaI ; FeI ; HeI ; NiI
67	7158-7274	0.09	TiO+Atmospheric H_2O
68	7274-7464	0.03	TiO ; VO ; CN ; FeI
69	7464-7580	0.01	CaH ; FeI
70	7580-7690	0.29	Atmospheric O_2

differences between the velocity dispersion of the clusters and that of the considered subsystems within the galaxies.

The choice of the windows was based on the following criteria:

(i) isolation of the strong, easily identifiable features,

(ii) use of absorption features in common among spectra from clusters in a broad range of age and metallicity,

(iii) cross comparison of features both present in various age-metallicity cluster groups and in nuclei of galaxies.

The latter spectra will be presented and population synthesized in a future paper.

We have listed in Table 2, the window limits and the most probable contributors, which, in some cases may become negligible due to age or metallicity differences. A search was made for all features so far used in stellar population synthesis based on spectral characteristics (de Vaucouleurs and de Vaucouleurs, 1959; Alloin et al., 1971; Joly and Andrillat, 1973; O'Connell, 1976; Williams, 1976; Turnrose, 1976; Pritchet, 1977). A number of features or blends, not included in previous studies, especially between 5000 and 7500 Å, were assigned an identification through stellar spectra analysis of different spectral types (Gahm, 1970; Strom et al., 1971; Fäy et al., 1974). The limits of the windows represent a compromise between the width of the absorption as seen on the spectra and the isolation of selected groupings of atomic lines and/or molecular bands. As can be seen in Table 2, most of the weak absorption features, mainly redward of 5000 Å, seen on spectra from clusters of all ages (Fig. 3) are molecular bands arising in low temperature stars (Fäy et al., 1974). Thus, red stars provide an important contribution to the optical light, not only in intermediate or old objects, but also in quite young clusters such as NGC 2004, via the presence of red supergiants.

In column 3 of Table 2, we provide the ratio between the mean equivalent width measured in all clusters for a particular window and the width of this window (excluding H II regions). This parameter represents the mean detection level of the absorption feature or blend. Windows with a 2% level or less, correspond in general, to flux maxima defining continuum points for clusters of any age or metallicity. Windows with a 3% or 4% level, include features which are definitely present in most spectra but cannot be measured accurately, owing to their weakness. The complete set of equivalent width measurements for all windows is presented elsewhere (Bica and Alloin, 1986a). We discuss below conspicuous results regarding some of the windows.

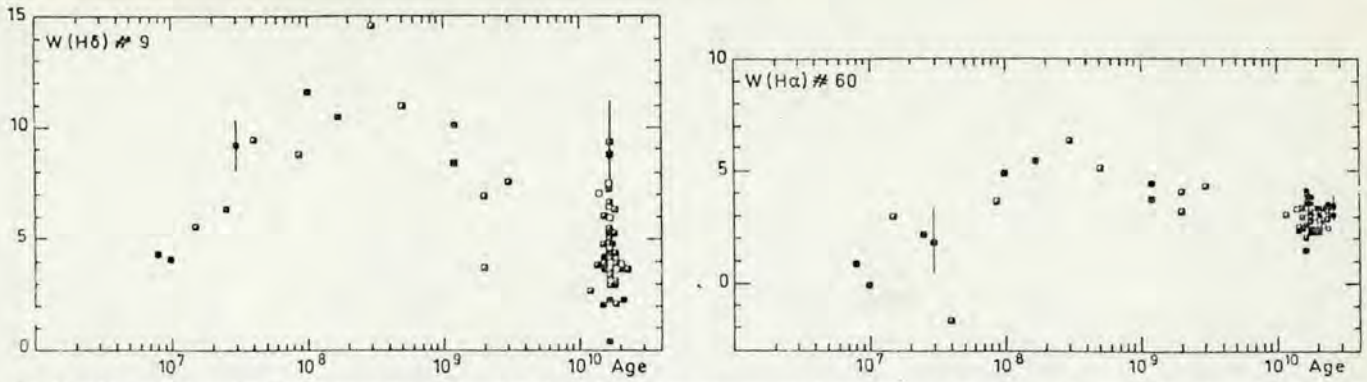

Fig. 4a and b. $W(H\delta)$ and $W(H\alpha)$ respectively, as a function of age. Empty squares correspond to a metallicity less than -1.5; semi-empty ones to the metallicity range $-1.5 \leqq [Z/Z_\odot] \leqq -0.75$; filled squares to a metallicity larger than -0.75

In Fig. 4a, we have plotted $W(H\delta)$ as a function of age. The larger values occur for ages around $4\ 10^8$ yr, where the turn-off point at A stars dominates the integrated spectrum of clusters like NGC 1831 and NGC 1868. The observed $W(H\delta)$ for old metal-poor clusters overlap with those measured in clusters younger than $5\ 10^7$ yr. The metallicity effects are weak or undetectable within the error bars. The lines $H\gamma$ and $H\beta$ present a similar behaviour. This holds true for $W(H\alpha)$ (Fig. 4b), in spite of the fact that the underlying continuum is dominated, then, by late type stars which essentially do not contribute to the line absorption. Due to the latter effect, the W values for $H\alpha$ are much smaller than those of other Balmer lines in the integrated spectrum of star clusters. We emphasize that emission plays no role in this matter because it is present or suspected only in very young clusters. Thus, an absorption Balmer decrement hypothesis for an underlying stellar population cannot be used to disentangle absorption from emission components in nuclei of galaxies.

We have plotted the equivalent widths of metallic lines or molecular bands as a function of metallicity in Figs. 5a through 5i, in an increasing wavelength order. The isochrone defined by the Galactic globular clusters in each plot shows a clear relationship between W of the feature and $[Z/Z_\odot]$. The same behaviour is observed for metallic lines and molecular bands, with the exception that the latter one is more often subject to departures from linearity (Sect. 5). The intermediate age clusters are, in some cases undistinguishable from the globular clusters and eventual drifts are systematically towards the sequence defined by the young blue clusters. The wavelength succession of the figures shows how younger turn-off points affect the equivalent width of metallic features. Indeed, the enhancement of the blue continuum, due to the upper main sequence stars, splits the W vs. $[Z/Z_\odot]$ plots into several loci dependent on the age. On the contrary, the W vs. metallicity relationship for features in the red tends to be more single-valued: in the Mg I + MgH plot, the isochrones defined by Galactic globular clusters and by young clusters are closer to each other and the sets of points even completely overlap for TiO bands.

The interstellar component of the Na I absorption, especially for highly reddened globular clusters, is responsible for most of the dispersion in Fig. 5h. A detailed study of the interstellar Na I as a function of $E(B-V)$ is given elsewhere (Bica and Alloin, 1986b).

In Fig. 6, we have displayed W (Ca II H + Hε) as a function of metallicity. A comparison with Ca II K (Fig. 5a) shows that the strength of this blend is ruled by metallicity, except for the blue clusters about $4\ 10^8$ yr old in which, obviously, Hε contributes much to W (Ca II H + Hε). The windows corresponding to H8, H9, and H10, also strongly blended with metallic features, are likewise metal dominated.

We show in Fig. 7, the continuum slope as measured by e.g. the ratio of the fluxes at λ4020 and λ6630 Å, as a function of age. On the contrary to the W vs. age relationship for $H\delta$ through $H\alpha$, the values for young blue clusters do not overlap with those of old metal poor globular clusters. The effects of metallicity differences are obvious in the globular cluster sample where metal rich objects present steeper spectra resulting from the blanketing effect and a lack of BHB stars. The shape of the curve around 10^8 yr represents an age effect as a result of rapid changes in the relative populations of evolved red stars and top main sequence stars. We checked this result by synthesizing the V flux ratio of red ($(B-V)_0 > 0.6$) to blue stars in composite HR diagrams for different age groups of star clusters in the Galactic disc (Mermilliod 1981a, b). These values have been displayed in an inset to Fig. 7. The flux contributions from magnitude intervals corresponding to the lowest main sequence part are negligible even before incompleteness starts to affect the HR diagrams. Not only is such a shape observed for the overall continuum slope, but also for normalized continuum points at various wavelengths (Bica and Alloin, 1986a). The minimum at $\sim 8\ 10^7$ yr in Fig. 7 coincides for C4020/C6630 and B/R, but a small age shift seems to be present towards 10^9 yr. We assign this difference to the difficulty of dating clusters as they approach the blue-red transition, while the determination of ages for blue clusters is quite precise from stellar evolution models (Renzini and Buzzoni, 1985).

The dispersion of the continuum slope in Fig. 7 for ages $t < 2\ 10^7$ yr is due to the combined effects of internal reddening and rapid integrated color variations as a consequence of the evolution of massive stars. Indeed a variable dust content among Magellanic Cloud H II regions is suggested by the observed spread of $H\alpha/H\beta$ ratios (Pagel et al., 1978 and references therein). The internal reddening of NGC 330 is negligible (Carney et al., 1985) and older clusters are expected to be dust free. The strong TiO bands in the integrated spectrum of NGC 2004 indicate an important flux contribution from red supergiants, contrarily to the slightly older clusters NGC 2100 and NGC 330. Also one should keep in mind that, although these clusters are among the most populous for their age range in the MC, their HR diagrams (references in Table 1) indicate that most of the integrated light comes from a small number of luminous stars subject to a rapid evolution.

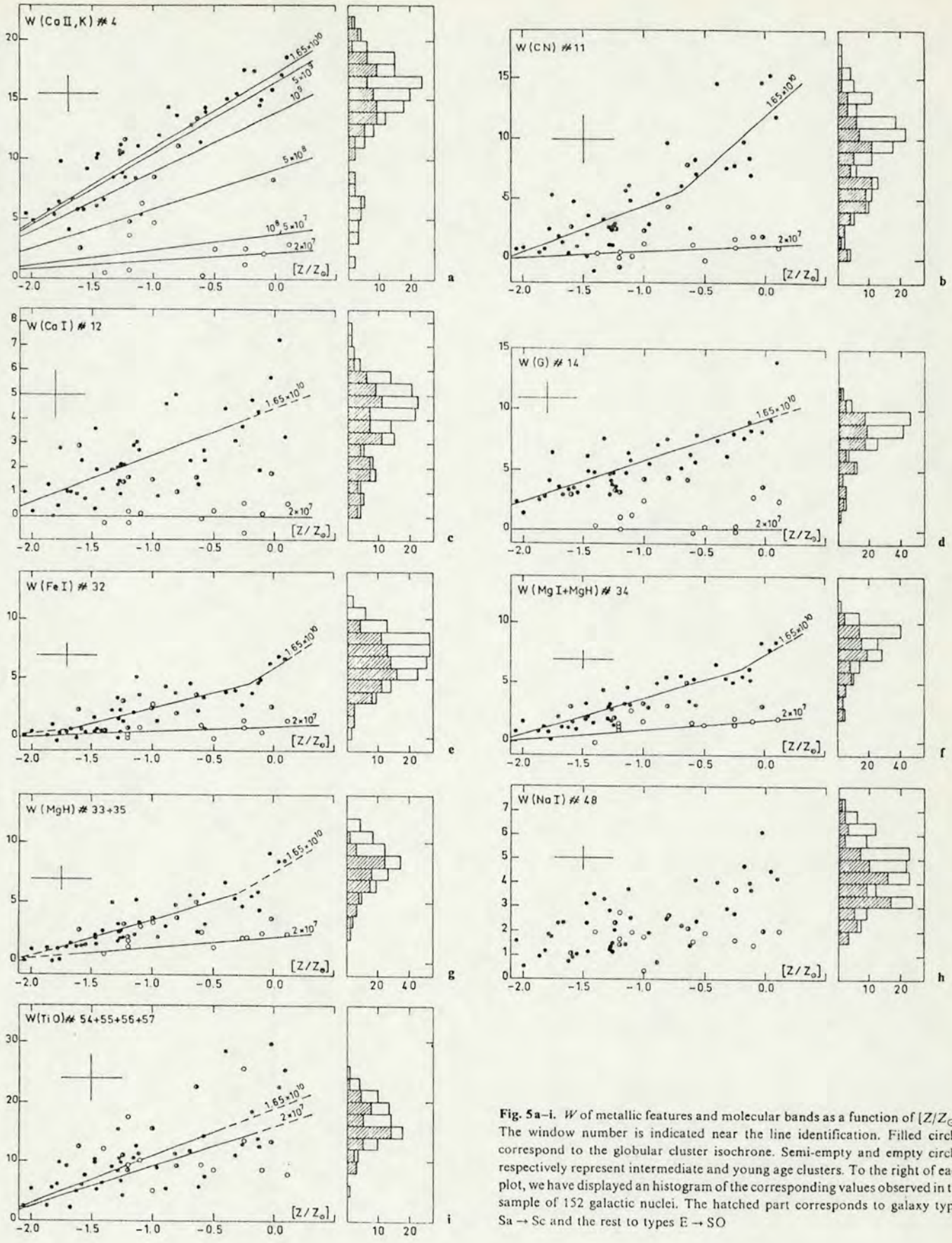

Fig. 5a–i. *W* of metallic features and molecular bands as a function of $[Z/Z_{\odot}]$. The window number is indicated near the line identification. Filled circles correspond to the globular cluster isochrone. Semi-empty and empty circles respectively represent intermediate and young age clusters. To the right of each plot, we have displayed an histogram of the corresponding values observed in the sample of 152 galactic nuclei. The hatched part corresponds to galaxy types Sa → Sc and the rest to types E → SO

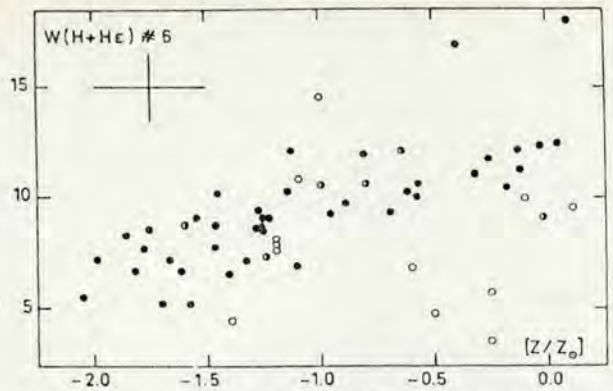

Fig. 6. W (Ca II H + Hε) as a function of $[Z/Z_\odot]$. The symbols are as in Fig. 5

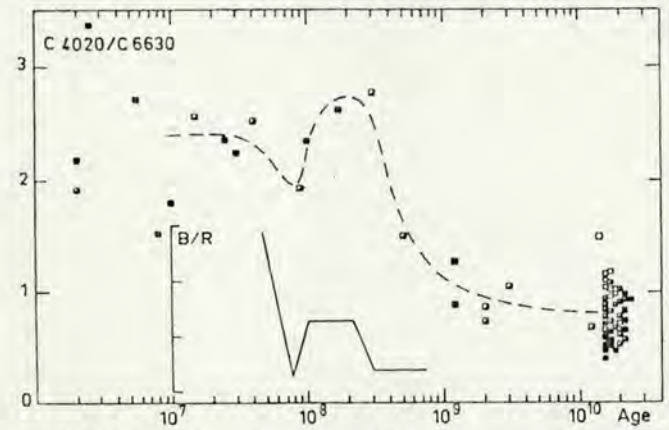

Fig. 7. Variation of the continuum slope with age. The same symbols as in Fig. 4 are used. The inset shows the V flux ratio from the blue to red stellar contributions synthesized from HR diagrams in clusters of different ages

5. Grids of star cluster integrated properties and concluding remarks

The fundamental questions regarding the population synthesis approach undertaken in this paper are as follows:

(i) What is the highest metal content of the stellar populations to be found in nuclear regions of galaxies?

(ii) What is the fraction of galaxies which can be described by the present base reaching up to the solar metallicity?

(iii) How far in $[Z/Z_\odot]$ is it necessary to extrapolate the base properties in order to synthesize populations in the most strong lined galaxies? How valid would such an extrapolation be?

In order to answer these questions, let us consider the results we have recently gathered on 152 normal nuclei in galaxies of morphological types E through Sc, in the luminosity interval $-23.3 < M_B < -16.6$. The spectra, which were obtained and reduced in conditions similar to those of the star clusters, will be presented in a forthcoming paper. They were rebinned to zero redshift, corrected for Galactic reddening, while continuum and equivalent width measurements were made through the same windows. For each metallic window in Fig. 5, we show an inset to the right, containing the histogram of the W values measured in galaxies. Giving more weight to metallic features in the red which are less biased regarding age effects (Sect. 4), no extrapolation at all is needed to describe 50% of the objects and an extrapolation to $[Z/Z_\odot] = 0.6$ is required to describe essentially the entire galaxy sample. Metallicity estimates in early-type galaxies lead to maximum $[Z/Z_\odot]$ values around 0.3 (e.g. Aaronson et al., 1978) and 0.3–0.5 (Pickles, 1985). Moreover, the present result, derived from absorption lines only, is in fair agreement with oxygen abundances in central H II regions of spiral galaxies (Pagel and Edmunds, 1984). The $[O/O_\odot]$ values for the gas imply that the present metal content in the most metal rich stellar generation in the nuclei of spiral galaxies is at most a factor 4 higher than solar. Moreover, 50% of galaxies in their sample (highly peaked at $-22 < M_B < -21$) could be population synthesized with a solar metallicity base. The required 0.6 dex extrapolation of the cluster base properties corresponds to 20% of the observed $[Z/Z_\odot]$ interval. It is important to note that the globular cluster scale has been recently calibrated up to the solar abundance through observations of individual stars in NGC 5927 (Cohen, 1983). Together with NGC 5927, we have also observed NGC 6528, NGC 6440 and NGC 6553, some of the most metal-rich globular clusters in the Galaxy, according to intermediate band photometry (Bica and Pastoriza, 1983; Zinn and West, 1984). Indeed, the integrated spectra of these three clusters are clearly more strong-lined than that of NGC 5927.

Metallicity indices in the optical (Faber, 1973; Burstein et al., 1984) as well as in the infrared (Frogel et al., 1978: Aaronson et al., 1978), indicated that the metal rich globular clusters were considerably more metal-poor than the major part of luminous galaxies. In fact, the most metal-rich clusters in the former optical and infrared samples (respectively NGC 6356 and NGC 6637) are a factor 4 to 6 more metal poor than the sun. In Fig. 8, the gap between NGC 6356 and, for example, one of the strongest-lined galaxies, the giant early-type Virgo member NGC 4649, is filled in the present sample by the very metal-rich globular cluster NGC 6440.

According to Fig. 5, the pure metallic features present a remarkable W vs. metallicity relationship, both for the well defined globular cluster isochrone and the young blue cluster sequence. A clear departure from linearity is present for the metal rich globular clusters in the CN band (#11). A similar effect has been observed in M 31 globulars (Burstein et al., 1984). The windows #32 to #35, which contain an important contribution from MgH and C_2, also present a slight departure from linearity. Possibly TiO does so.

In view of population synthesis, we wish to derive a grid of star cluster properties covering the whole age-metallicity plane with a suitable step. Therefore, we have for each feature, defined the extreme relations (W, metallicity) for the globular cluster and young cluster isochrones (taking into account only clusters younger than $5\ 10^7$ yr and excluding H II regions). These relations systematically converge at low metallicities: linear regressions for the 5 more significant features led to a zero-point $[Z/Z_\odot] = -2.45 \pm 0.35$ which was subsequently used as a reference point. The mean age within each group was assigned to the isochrone. The age interpolation has been weighted by the continuum slope vs. age relationship (Fig. 7). On top of Fig. 5, we have drawn the two extreme relations (globular and young clusters) and, in the case of Ca II K some intermediate ones as well. The grid predictions to be used in future stellar population synthesis is presented elsewhere (Bica and Alloin, 1986a). The mean properties of star clusters, having $-2.0 \leqq [Z/Z_\odot] \leqq 0$, with an 0.5 dex step as well as the extrapolated value at $[Z/Z_\odot] = 0.6$, and with ages $1.65\ 10^{10}$ yr, $5\ 10^9$ yr, 10^9 yr, $5\ 10^8$ yr, 10^8 yr, $5\ 10^7$ yr, 10^7 yr have been interpolated for this purpose.

The main conclusions of the present work are the following:

(i) Integrated spectra of 63 star clusters provide a useful base for population synthesis in galaxies.

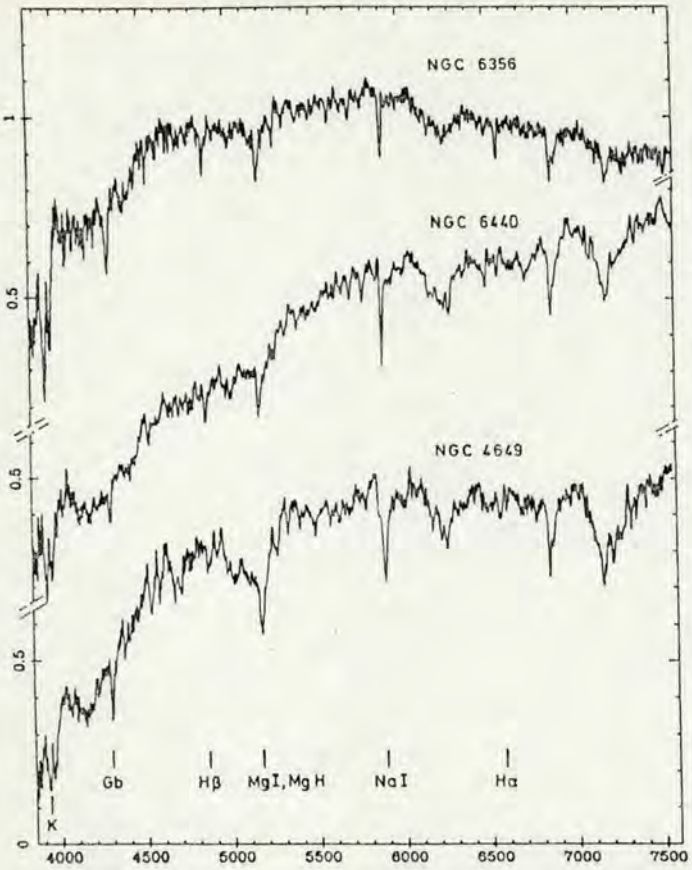

Fig. 8. Spectra of one of the most metal rich globular clusters in our sample (NGC 6440), a cluster (NGC 6356) considered metal-rich in previous comparisons with galaxies and NGC 4649, a very strong-lined early-type galaxy

(ii) A number of weak absorption features from 3780 to 7690, mostly arising from molecular bands in late-type star atmospheres, are present not only in red clusters but also in young ones via red supergiant stars.

(iii) As a consequence of the low dispersion we used, many trustworthy maxima led to a good estimation of the continuum level.

(iv) About 30 out of the 70 windows we defined present features at a significant level for being used in stellar population synthesis.

(v) We show the influence of younger turn-off points on W for metallic features and molecular bands. The enhancement of the blue continuum due to upper main sequence stars, defines, in the W vs. $[Z/Z_\odot]$ plots, several loci depending on the age. On the contrary, the W vs. $[Z/Z_\odot]$ relations in the case of red features tend to be single-valued, regardless of age.

(vi) Metallic lines and molecular bands present a similar behaviour as a function of $[Z/Z_\odot]$, the latter more often departing from linearity for large $[Z/Z_\odot]$.

(vii) The lines Hα to Hδ show the same dependence on age with maximum values at around $4\ 10^8$ yr. For a given age, $W(\mathrm{H}\alpha)$ is always smaller than the three next Balmer lines because the underlying continuum is dominated by late type stars which essentially do not contribute to the line absorption. Thus it is not possible to assume a Balmer absorption decrement in the underlying stellar populations for disentangling emission from absorption components in galaxies.

(viii) The lines Hε through H10, strongly blended with metallic features, present a metal-dominated behaviour.

(ix) The continuum distribution differences and not the Balmer line equivalent widths allow one to distinguish between young populations and old metal-poor ones in galaxies.

(x) The comparison of W for metallic features in 152 normal galactic nuclei and in the cluster base shows that around 50% of the galaxy sample can be population synthesized without extrapolation of the cluster base properties. An extrapolation to $[Z/Z_\odot] = 0.6$ is required to describe essentially the whole sample.

Acknowledgements. We are gratefully indebted to the ESO staff, both at La Silla and Garching as well as to the computer center groups in Meudon Observatory and at the Institut d'Astrophysique. We acknowledge interesting comments and suggestions from B. Pagel. Eduardo Bica thanks the Brazilian Institution CNPq, for a fellowship.

References

Aaronson, M., Cohen, J., Mould, J., Malkan, M.: 1978, *Astrophys. J.* **223**, 824
Aaronson, M., Frogel, J.A., Persson, S.: 1978, *Astrophys. J.* **220**, 442
Alloin, D., Andrillat, Y., Souffrin, S.: 1971, *Astron. Astrophys.* **10**, 401
Arp, H., Cuffey, J.: 1962, *Astrophys. J.* **136**, 51
Barbaro, G., Dallaporta, N., Fabri, G.: 1961, *Astrophys. Space Sci.* **3**, 123
Becker, S., Mathews, G.: 1983, *Astrophys. J.* **270**, 155
Bica, E., Alloin, D.: 1986a, *Astron. Astrophys. Suppl. Ser.* (in press)
Bica, E., Alloin, D.: 1986b, *Astron. Astrophys.* (in press)
Bica, E., Pastoriza, M.: 1983, *Astrophys. Space Sci.* **91**, 99
Boeshaar, G., Boeshaar, P., Czyzak, S., Aller, L., Lasker, B.: 1980, *Astrophys. Space Sci.* **68**, 335
Burstein, D., Faber, S.M., Gaskell, C.M., Krumm, N.: 1984, *Astrophys. J.* **287**, 586
Carney, B., Janes, K., Flower, P.: 1985, *Astron. J.* **90**, 1196
Christian, C., Heasley, J., Janes, K.: 1985, *Astrophys. J.* **299**, 683
Ciani, A., d'Odorico, S., Benvenuti, P.: 1984, *Astron. Astrophys.* **137**, 223
Cohen, J.G.: 1982, *Astrophys. J.* **258**, 143
Cohen, J.G.: 1983, *Astrophys. J.* **270**, 654
Cowley, A., Hartwick, F.: 1982, *Astrophys. J.* **259**, 89
de Vaucouleurs, G., de Vaucouleurs, A.: 1959, *Publ. Astron. Soc. Pacific* **71**, 83
Dottori, H.: 1981, *Astrophys. Space Sci.* **80**, 267
Dottori, H., Bica, E.: 1981, *Astron. Astrophys.* **102**, 245
Dottori, H., Pastoriza, M., Bica, E.: 1983, *Astrophys. Space Sci.* **91**, 79
Durand, D., Hardy, E., Melnick, J.: 1984, *Astrophys. J.* **283**, 552
Dufour, R., Harlow, W.V.: 1977, *Astrophys. J.* **216**, 706
Faber, S.M.: 1972, *Astron. Astrophys.* **20**, 361
Faber, S.M.: 1973, *Astrophys. J.* **179**, 731
Fäy, T.D., Stein, W.L., Warren, W.H.: 1974, *Publ. Astron. Soc. Pacific* **86**, 772
Frogel, J., Persson, S., Aaronson, M., Matthews, K.: 1978, *Astrophys. J.* **220**, 75
Gahm, G.F.: 1970, *Astron. Astrophys.* **4**, 268
Hartwick, F.D., Hesser, J.E.: 1973, *Astrophys. J.* **183**, 883
Hodge, P.W.: 1982, *Astrophys. J.* **256**, 447
Hodge, P.W.: 1983, *Astrophys. J.* **264**, 470
Hodge, P.W.: 1984a, IAU *Symp.* **108**, p. 7

Hodge, P.W.: 1984b, *Publ. Astron. Soc. Pacific* **96**, 947
Hodge, P.W., Lee, S.O.: 1984, *Astrophys. J.* **276**, 509
Janes, K.A.: 1979, *Astrophys. J. Suppl.* **39**, 135
Janes, K.A., Demarque, P.: 1983, *Astrophys. J.* **264**, 206
Joly, M., Andrillat, Y.: 1973, *Astron. Astrophys.* **26**, 95
Mermilliod, J.C.: 1981a, *Astron. Astrophys. Suppl.* **44**, 467
Mermilliod, J.C.: 1981b, *Astron. Astrophys.* **97**, 235
McClure, R.D., Twarog, B.A.: 1978, in *Chemical and Dynamical Evolution of the Galaxy*, eds. E. Basinska-Grezesik, M. Mayor, Torun
Mould, J., Aaronson, M.: 1980, *Astrophys. J.* **240**, 464
Mould, J., Aaronson, M.: 1982, *Astrophys. J.* **263**, 629
Nelson, M., Hodge, P.W.: 1983, *Publ. Astron. Soc. Pacific* **95**, 5
O'Connell, R.W.: 1976, *Astrophys. J.* **206**, 370
Olszewski, E.: 1984, *Astrophys. J.* **284**, 108
Pagel, B.E., Edmunds, M., Fosbury, R., Webster, B.: 1978, *Monthly Notices Roy. Astron. Soc.* **184**, 569
Pagel, B.E., Edmunds, M.G.: 1981, *Ann. Rev. Astron. Astrophys.* **19**, 77
Pagel, B.E., Edmunds, M.G.: 1984, *Monthly Notices Roy. Astron. Soc.* **211**, 507
Pickles A.J.: 1985, *Astrophys. J.* **296**, 340
Pritchet, C.: 1977, *Astrophys. J. Suppl.* **35**, 397
Rabin, D.: 1982, *Astrophys. J.* **261**, 85
Renzini, A., Buzzoni, A.: 1985, in *Spectral Evolution of Galaxies*, eds. C. Chiosi, A. Renzini, Reidel, Dordrecht
Richtler, T., Nelles, B.: 1983, *Astron. Astrophys.* **119**, 75
Searle, L., Wilkinson, A., Bagnuolo, W.G.: 1980, *Astrophys. J.* **239**, 803
Smith, H.: 1984, *Astrophys. J.* **281**, 148
Strom, S.E., Strom, K.M., Corbon, D.F.: 1971, *Astron. Astrophys.* **12**, 177
Turnrose, B.E.: 1976, *Astrophys. J.* **210**, 33
VandenBerg, D.A.: 1983, *Astrophys. J. Suppl.* **51**, 29
Van den Bergh, S.: 1975, *Ann. Rev. Astron. Astrophys.* **13**, 217
Van den Bergh, S.: 1981, *Astron. Astrophys. Suppl.* **46**, 79
Williams, T.B.: 1976, *Astrophys. J.* **209**, 716
Zinn, R., West, M.: 1984, *Astrophys. J. Suppl.* **55**, 45

Note added in proof: A very recent paper (Christian et al.) discusses in detail the Galactic open cluster NGC 2158. The best fit parameters found in that paper are compatible with our compilation in Table 1, except for a slightly older age (3 Gyr instead of 1.2 Gyr). Indeed, this new value is in better agreement with the locus of the cluster in our Figures.

ASTRONOMY & ASTROPHYSICS
SUPPLEMENT SERIES

NOVEMBER 1986, PAGE 171

Astron. Astrophys. Suppl. Ser. 66, 171-179 (1986)

A grid of star cluster properties for stellar population synthesis (*)

E. Bica and D. Alloin

Observatoire de Paris, Section de Meudon, Laboratoire d'Astrophysique, 92195 Meudon Principal Cedex, France

Received January 15, accepted January 23, 1986

Summary. — We present the measurements of equivalent widths in 70 windows as well as the normalized continuous distribution, from the integrated spectra of 63 star clusters with known age, metallicity and reddening. From this data we derive a grid of mean star cluster properties as a function of age and metallicity. We provide equivalent widths for the Balmer lines and for a selection of 13 metallic features, together with the continuum distribution, at ages 1.65×10^{10}, 5×10^{9}, 10^{9}, 5×10^{8}, 10^{8}, 5×10^{7}, 10^{7} yr and for metallicities $\left[Z/Z_{\odot}\right] = 0.6, 0.0, -0.5, -1.0, -1.5$ and -2.0.

Key words : star clusters — spectrophotometry — stellar population synthesis.

1. Introduction.

In view of synthesizing stellar populations in nuclei of galaxies, we have studied a sample of 63 clusters of known age, metallicity and reddening (Bica and Alloin, 1986a, hereafter BA). The complete set of measurements is presented here. From these, we have built a grid of star cluster properties, following the method described in BA. We provide this grid in the form of the equivalent-widths W of the selected spectral features, and relative continuum points as a function of age and metallicity. The mean properties of star clusters having $-2.0 \leq \left[Z/Z_{\odot}\right] \leq 0.0$ are given with a 0.5 dex step, as well as the extrapolated value at $\left[Z/Z_{\odot}\right] = 0.6$. The age interval spanned by the present sample goes from 10^{7} yr to 1.65×10^{10} yr. The star cluster properties have been interpolated at values 1.65×10^{10}, 5×10^{9}, 10^{9}, 5×10^{8}, 10^{8}, 5×10^{7} and 10^{7} yr.

2. Discussion.

We present in table I the measured equivalent widths in 70 windows from the integrated spectra of 63 clusters (Magellanic Clouds objects and Galactic open clusters in Tab. Ia, Galactic globulars in Tab. Ib). The definition of the windows and the respective contributors to the absorption are given in BA. We also give in table I the signal to noise ratios for the regions $3800\ \text{Å} < \lambda < 4500\ \text{Å}$, $(S/N)_b$, and $4500\ \text{Å} < \lambda < 7500\ \text{Å}$, $(S/N)_r$, which must be taken into account especially for faint lines. The higher S/N in the long wavelength range is due to the better response of the detector in the red. The wide spread of S/N values in the blue mostly results from reddening effects. Equivalent widths for the extremely young clusters NGC 1714, NGC 1895, NGC 2070 and N88 indicate which windows will be seriously affected by emission lines in nuclei of galaxies containing HII regions. These windows are # 3 ([NeIII] 3869, H9 and HeI 3889), # 15 (Hγ), # 27 (Hβ), # 29, 30, 31 ([OIII] 4959 and 5007), # 59, 60, 61 (Hα, [NII] 6548 and 6584) and # 66 (HeI 7065, [ArIII] 7136). Windows # 5 ([NeIII] 3967, Hε), # 9 (Hδ), # 47 (HeI 5876) and # 62 ([SII] 6717 and 6730) will also be contaminated to a lesser extent. We also give in table I a selection of normalized continuum points for the reddening corrected spectra (BA).

Applying the method described in BA we have built a grid of mean star cluster properties. We show in table II the grid predictions for the Balmer lines Hα to Hδ as a function of age. In tables II to V, we quote a standard deviation which corresponds to the difference between the measured value and that deduced from the grid for three age groups : globular, intermediate age and young clusters. In tables III and IV, we present the grid results for normalized continuum points. Contrarily to the equivalent widths of Balmer lines, the continuum points for globular clusters present a correlation with metallicity (e.g. Figs. 1a, 1b). Indeed such correlations for the continuous distribution are expected, owing to the fact that in more metal rich clusters, both the blanketing

(*) Based on observations collected at the European Southern Observatory (La Silla).

Send offprint requests to : D. Alloin.

effect and the absence of Blue Horizontal Branch stars (BHB), increase the slope of the spectrum. On the other hand, in the case of the Hα to Hδ windows, the weakening of Balmer lines in metal-rich clusters due to the absence of BHB stars, is compensated by the growing strength of underlying metallic features which are otherwise of second order in intermediate and metal poor clusters. We give in table III the metallicity dependence of the continuous distribution for globular clusters. In younger clusters, no obvious trends with metallicity being found for the continuum, we give in table IV the continuum points as a function of age only. Finally, we present in table V the resulting *W* for selected metallic features as a function of age and metallicity. Due to interstellar contamination, the NaI window # 48 is discussed in more detail (Bica and Alloin, 1986b). In some cases we added consecutive windows dominated by the same absorbers. In the CN window # 11, the *W vs.* $\left[Z/Z_{\odot}\right]$ relationship presents a strong departure from linearity for globular clusters with $\left[Z/Z_{\odot}\right] > -0.7$ (Fig. 5b in BA) ; the isochrones corresponding to younger ages were interpolated taking into account this non-linear effect. This is justified by the fact that for the same metallicity range in HII regions, both carbon and nitrogen abundances present a non-linear dependence on oxygen (Mathis *et al.*, 1985). We adopted the same procedure for the slight departures from linearity observed in windows # 31 to # 36, which cover a spectral interval contaminated by C_2 and possibly CN. As well window # 10 shows this effect which we assign to some blend with the CN heads in window # 11. The windows corresponding to H10, H9, H8 and Hε, in spite of their good detection level, were excluded from the present analysis since they are heavily blended with metallic features (BA).

The mean star cluster properties provided in tables II to V will be used for stellar population synthesis in galaxies.

References

BICA, E., ALLOIN, D. : 1986a, *Astron. Astrophys.* **162,** 21.
BICA, E., ALLOIN, D. : 1986b, *Astron. Astrophys.* in press.
MATHIS, J., CHU, PETERSON, D. : 1985, *Astrophys. J.* **292,** 155.

TABLE Ia. — *Measured equivalent-widths for the 70 windows defined in BA as well as continuum values at 6 wavelength points relative to the one at 5870 Å.*

Object	#	$(S/N)_b$	$(S/N)_r$	1	2	3	4	5	6	7	8	9	10	11	12	13	14	15	16	17	18
SMC																					
NGC	121	30	45	3.8	8.0	5.0	11.6	7.4	1.5	0.4	0.9	2.7	2.7	2.5	1.4	1.9	3.5	1.2	2.1	2.0	1.6
	330	40	50	1.8	2.9	3.8	0.5	4.5	0.1	0.3	0.7	5.5	0.8	0.4	-0.3	-0.2	0.5	4.1	1.2	0.6	1.2
	419	25	50	3.6	7.9	5.2	4.8	7.8	0.4	0.5	0.9	6.9	1.7	-0.7	1.6	1.3	3.3	7.1	2.6	1.1	0.7
N	88	10	15	-6.1	-30.1	-138.	-0.5	-85.4	-3.9	-3.8	-5.6	-77.1	-0.3	-2.3	-2.4	-0.9	-4.9	-214.	-38.1	-2.0	-20.5
LMC																					
NGC	1466	15	15	9.5	2.4	4.4	2.6	8.8	-1.3	0.0	5.4	7.0	1.7	2.7	2.9	2.3	3.1	6.5	2.3	-0.3	0.4
	1714	10	10	-1.4	-7.8	-43.8	-2.9	-26.7	-0.5	-4.2	-0.9	-28.2	-3.1	-1.1	-1.1	-2.0	-2.9	-78.3	-10.6	-4.1	-9.2
	1783	20	25	4.4	11.9	11.1	8.5	10.6	3.1	0.3	2.7	7.5	2.1	2.4	1.5	2.0	4.4	6.9	2.7	1.2	1.3
	1831	15	15	6.9	13.4	6.1	4.7	14.6	1.8	0.0	1.7	14.6	3.2	1.3	-0.7	-0.7	2.6	10.4	1.9	1.9	0.4
	1847	20	30	5.1	3.3	6.3	2.5	5.8	-0.3	0.4	1.3	6.3	1.5	0.9	-0.7	-0.8	0.5	5.6	1.6	0.4	1.9
	1856	30	35	5.9	7.8	4.6	2.1	10.0	0.4	0.8	1.1	11.6	3.2	1.9	0.1	0.4	2.9	10.0	2.4	1.7	0.7
	1866	40	35	3.1	4.2	7.0	0.8	8.1	1.0	0.6	0.1	8.8	1.4	0.6	-0.3	0.4	1.2	6.8	1.6	0.2	1.0
	1868	25	30	5.5	7.0	7.2	6.3	10.9	1.6	0.1	1.4	10.9	2.6	0.2	0.1	0.0	1.4	7.7	1.6	0.3	0.5
	1895	5	5	1.1	-3.3	-13.6	-3.6	-15.7	1.8	3.7	0.3	-13.0	-0.8	-5.8	-6.3	-3.0	-2.5	-43.0	-2.1	1.1	0.6
	1978	25	40	7.1	7.5	7.8	11.1	10.7	0.7	1.1	1.6	3.7	1.3	4.4	1.0	1.3	4.5	4.8	2.4	1.5	1.1
	2004	40	70	0.7	1.5	2.1	1.2	3.6	1.1	0.8	0.3	4.3	1.1	1.7	0.5	0.1	0.0	3.2	2.0	1.3	2.2
	2070	15	20	-3.2	-8.9	-42.7	-1.0	-24.1	-0.7	-3.2	-1.5	-30.0	-1.4	-1.8	-1.0	-1.5	-2.5	-75.6	-8.9	-0.9	-6.7
	2100	25	35	2.4	2.4	2.7	2.5	4.8	2.2	0.7	0.7	4.1	0.2	-0.1	0.2	0.8	0.4	3.5	3.1	1.0	2.6
	2157	35	40	2.6	5.5	5.6	0.3	6.9	2.2	1.7	1.1	9.2	2.3	1.2	-0.1	0.1	-0.1	6.2	1.8	0.2	0.4
	2214	25	35	1.8	5.9	5.7	3.7	7.9	0.2	0.7	0.9	9.4	2.2	0.1	0.2	1.0	0.2	6.4	0.9	0.3	1.0
GOC																					
NGC	2158	10	30	-2.8	10.4	6.5	13.4	12.1	0.0	5.8	1.2	10.1	3.8	7.9	1.6	3.1	4.4	8.3	3.4	1.7	2.8
	2660	25	30	7.3	9.2	7.5	8.4	9.2	1.5	2.4	1.8	8.4	1.0	1.9	1.8	1.6	3.8	7.8	4.2	1.3	2.1
	6705	30	30	3.0	6.7	7.3	2.9	9.6	0.3	0.3	1.6	10.5	1.5	1.5	0.5	1.6	2.6	10.1	1.8	0.8	0.9

Object	#	19	20	21	22	23	24	25	26	27	28	29	30	31	32	33	34	35	36	37	38
SMC																					
NGC	121	0.6	2.4	1.1	2.1	1.3	3.1	1.2	0.4	3.1	1.1	2.3	2.1	3.5	3.1	1.5	2.1	1.7	1.3	0.8	0.9
	330	0.1	1.6	0.7	0.5	0.8	0.6	0.9	0.6	4.6	0.6	1.1	1.1	1.4	0.6	0.6	0.0	0.1	0.9	0.8	1.6
	419	-0.3	0.5	1.8	1.5	0.6	0.9	1.5	1.9	6.3	1.7	1.9	2.0	2.6	0.8	0.6	1.1	1.4	1.2	0.1	0.8
N	88	0.1	-2.8	-0.9	-5.6	-1.3	-16.9	-13.6	-36.7	-543.	-38.5	-161.	-1640.	-4090.	-63.8	-7.4	-7.2	-6.5	-5.4	-2.9	-1.0
LMC																					
NGC	1466	0.0	0.2	1.3	-0.8	-0.2	-0.3	0.6	0.7	4.5	1.1	0.8	2.7	2.5	2.4	1.1	3.0	2.6	2.7	1.1	1.2
	1714	-1.0	0.2	0.8	-2.2	-0.2	-1.1	-2.1	-9.4	-229.	-12.1	-33.9	-409.	-1120.	-17.4	-1.4	-2.2	-1.7	-0.5	1.2	-0.1
	1783	-0.1	1.7	2.0	0.7	0.4	0.5	0.2	1.5	6.5	1.5	1.6	1.2	2.9	2.5	1.2	3.3	2.5	3.1	1.0	2.5
	1831	0.7	1.4	2.1	0.1	1.0	1.8	1.1	2.0	7.2	1.0	1.8	1.9	2.7	2.6	0.9	1.8	2.5	4.2	2.7	0.9
	1847	-0.1	1.6	0.8	0.6	0.4	-0.9	0.5	1.4	5.9	0.6	1.8	1.9	2.4	1.5	0.2	1.6	1.8	1.5	0.9	1.1
	1856	0.1	1.1	0.8	0.9	0.8	0.4	1.1	1.4	8.2	1.5	0.9	1.0	3.0	0.5	0.4	1.9	2.0	2.9	0.9	1.0
	1866	0.4	1.2	1.0	1.3	0.4	0.4	1.1	1.3	7.0	0.9	0.4	0.9	1.3	0.3	0.4	1.2	0.9	1.1	0.3	0.0
	1868	0.2	0.9	0.4	0.5	0.8	0.3	1.4	2.2	7.9	1.5	1.3	0.5	1.1	0.9	0.9	2.7	2.1	1.9	0.1	0.4
	1895	-1.0	-3.9	1.4	2.3	0.2	-1.9	0.3	-4.6	-115.	-4.9	-12.7	-127.	-374.	-5.4	-0.2	-1.5	-0.2	0.5	-0.7	-1.0
	1978	0.7	2.8	0.2	1.7	1.0	1.4	2.3	1.4	5.4	1.1	2.1	1.9	4.3	2.1	1.2	3.1	2.6	2.5	1.2	1.8
	2004	0.3	1.0	1.9	0.9	1.0	1.0	1.2	0.3	3.5	0.4	0.9	-0.1	2.0	0.9	0.5	2.0	1.5	1.8	-0.2	1.0
	2070	-0.5	-1.7	-0.7	-3.7	-4.2	-5.5	-4.7	-12.9	-224.	-15.9	-46.2	-476.	-1260.	-27.7	-4.3	-5.3	-2.9	-1.5	2.0	-0.6
	2100	0.5	1.3	0.3	0.0	0.0	-0.1	0.2	0.1	1.8	0.5	1.0	-0.3	-0.3	0.0	0.6	1.5	0.7	0.9	0.6	1.0
	2157	0.6	0.4	0.5	1.0	0.3	0.5	0.6	1.3	7.1	1.4	0.5	0.2	1.2	1.1	1.1	1.7	1.4	1.8	1.2	1.4
	2214	0.6	-0.2	0.5	1.8	0.6	0.4	1.2	1.5	6.7	1.3	0.4	0.5	1.7	-0.1	0.6	1.4	1.3	1.2	0.9	1.4
GOC																					
NGC	2158	1.9	4.3	3.3	1.3	0.7	3.4	3.9	5.0	7.4	3.2	4.1	4.9	7.7	3.6	1.8	5.0	3.2	3.9	2.5	1.3
	2660	0.4	1.4	1.1	2.1	1.1	1.6	2.1	3.7	8.2	2.6	3.0	2.3	3.4	2.7	1.5	3.1	2.2	3.4	1.4	2.1
	6705	0.2	1.1	1.2	0.3	-0.3	0.7	0.1	1.5	8.6	0.7	0.1	0.7	2.1	1.5	0.7	2.1	1.6	2.1	0.8	1.2

TABLE Ia (*continued*).

Object		39	40	41	42	43	44	45	46	47	48	49	50	51	52	53	54	55	56	57	58
SMC																					
NGC	121	0.8	1.6	0.8	1.7	-0.4	1.1	1.1	0.7	-0.1	2.3	2.1	1.0	0.7	0.9	1.7	1.9	3.1	3.2	1.5	1.5
	330	1.2	1.0	0.4	2.1	1.3	2.2	2.0	0.2	0.6	1.9	1.4	2.3	0.5	1.0	1.6	2.7	4.6	3.2	3.5	5.1
	419	0.8	1.3	0.6	2.0	1.0	0.4	1.9	-0.5	0.2	1.4	1.3	2.1	0.5	0.7	1.0	2.3	2.4	2.0	2.1	2.7
N	88	-0.8	-3.3	-6.2	-4.4	-2.4	-1.5	-3.2	-6.9	-66.1	-41.7	-5.0	-4.6	-5.1	-4.3	-3.3	-1.4	-2.0	-25.8	-13.4	-30.1
LMC																					
NGC	1466	1.0	0.4	0.2	0.6	1.3	1.0	1.8	0.0	0.2	1.0	0.5	0.3	1.9	2.1	3.0	2.8	3.9	3.1	2.7	5.4
	1714	1.3	0.5	-1.8	1.7	1.1	-0.8	-0.8	-1.3	-19.8	-29.6	-1.7	-0.1	-2.1	-3.4	-1.0	-0.6	-0.4	-11.7	-7.9	-18.9
	1783	1.5	2.4	0.9	1.7	1.1	1.8	0.7	-0.2	0.3	1.7	1.5	1.8	0.8	1.4	1.1	3.6	5.1	3.5	3.2	3.3
	1831	0.0	1.3	1.0	2.4	2.0	2.5	3.3	1.4	0.1	0.3	0.6	2.1	1.5	1.7	1.8	3.4	1.3	0.5	-0.2	2.4
	1847	-0.3	1.2	0.9	1.5	1.1	0.5	3.1	1.0	1.0	1.6	1.0	1.2	1.0	1.4	2.3	2.8	4.2	4.0	2.4	1.2
	1856	0.3	0.4	0.6	1.4	1.2	0.9	2.1	-0.1	-0.1	1.4	0.5	0.3	0.3	0.5	1.0	2.5	1.7	3.4	0.9	1.2
	1866	-0.1	0.8	0.5	0.8	1.0	0.8	1.1	-0.2	0.4	1.6	1.1	0.8	1.0	0.3	0.8	2.7	3.3	2.3	1.0	0.9
	1868	0.2	0.0	0.4	0.8	0.5	1.3	1.2	-0.5	0.3	1.9	0.9	1.2	0.3	0.6	0.9	2.7	3.5	2.3	1.6	1.7
	1895	4.6	0.6	0.8	-2.4	-2.1	-2.6	-3.8	0.1	-4.3	-11.8	0.2	-1.4	-0.2	0.4	1.0	-2.9	-1.3	-4.8	-1.8	-3.7
	1978	1.1	2.2	0.5	3.5	1.3	0.5	2.0	0.5	1.2	2.6	2.3	2.4	1.0	0.3	1.4	2.2	3.3	2.2	1.4	0.8
	2004	0.9	2.3	0.4	1.7	1.7	2.3	1.3	-0.3	0.7	3.7	3.5	2.8	1.0	0.0	2.1	5.3	10.1	5.7	4.0	2.7
	2070	-1.3	-0.9	-3.1	-0.3	-0.7	-0.8	-2.4	-4.9	-23.1	-29.3	-2.1	-3.1	-2.2	-1.9	-0.9	-0.5	-1.8	-11.3	-7.7	-21.0
	2100	0.8	0.5	0.9	0.8	1.3	1.5	1.3	0.5	0.1	1.9	0.1	0.7	1.6	0.9	0.8	2.1	2.9	2.0	1.4	1.5
	2157	0.3	0.9	0.5	0.6	0.5	1.0	0.2	0.0	0.2	1.5	0.4	0.5	-0.5	0.3	1.0	2.5	3.0	2.2	1.6	0.6
	2214	1.2	1.9	1.0	2.0	1.9	0.1	1.3	0.4	1.1	2.7	1.7	2.3	1.5	-0.3	0.6	3.6	6.4	4.0	3.4	2.3
GOC																					
NGC	2158	1.3	1.6	0.8	1.5	1.2	2.1	2.5	0.0	-0.7	2.1	0.6	1.6	1.3	0.2	1.9	5.0	6.6	7.3	3.5	4.6
	2660	1.4	0.7	0.7	1.8	0.8	1.1	1.2	0.4	0.1	2.0	0.2	1.2	1.7	1.6	2.2	2.8	3.9	3.1	3.5	3.8
	6705	0.8	0.1	1.1	0.4	0.5	0.6	2.9	1.1	0.2	2.0	0.8	1.3	0.8	0.9	1.9	2.4	2.8	0.9	1.8	2.5

Object		59	60	61	62	63	64	65	66	67	68	69	70	$C\frac{4020}{5870}$	$C\frac{4570}{5870}$	$C\frac{5340}{5870}$	$C\frac{6630}{5870}$	$C\frac{6990}{5870}$	$C\frac{7520}{5870}$
SMC																			
NGC	121	3.8	3.1	1.2	0.4	1.4	10.9	7.8	1.9	19.0	9.4	2.3	35.2	0.71	0.89	0.97	1.04	1.05	1.04
	330	3.9	3.0	1.2	0.1	1.5	7.3	4.4	3.6	18.3	9.8	0.6	32.0	2.07	1.67	1.17	0.81	0.74	0.64
	419	3.2	4.1	2.1	0.5	1.0	6.5	5.5	5.1	15.8	10.8	2.3	33.4	0.80	0.97	0.99	0.93	0.91	0.87
N	88	-116.	-2830.	-159.	-101.	-26.6	1.1	-11.3	-197.	1.3	-49.9	-3.2	34.8	1.88	1.39	1.10	0.98	0.98	1.00
LMC																			
NGC	1466	2.0	3.4	3.9	1.4	1.6	6.5	0.9	1.8	5.0	6.9	4.4	35.4	1.35	1.19	1.07	0.90	0.85	0.80
	1714	-52.2	-1720.	-147.	-79.8	-42.0	2.5	-13.5	-89.2	2.1	-21.9	-6.3	37.5	2.50	1.66	1.25	0.74	0.71	0.74
	1783	3.9	4.4	0.7	0.9	2.0	6.8	2.0	2.4	15.9	9.1	1.5	31.8	0.98	1.08	1.04	0.94	0.80	0.86
	1831	2.3	6.4	3.5	2.9	6.9	7.7	4.0	6.2	11.4	8.4	3.4	35.5	2.19	1.67	1.21	0.79	0.72	0.63
	1847	1.4	2.2	2.7	1.1	1.2	7.5	2.6	1.8	6.7	4.9	4.8	34.6	1.89	1.50	1.15	0.80	0.74	0.66
	1856	2.8	5.0	0.8	0.6	1.7	8.0	2.9	1.7	3.8	8.2	3.0	31.3	1.89	1.51	1.15	0.80	0.71	0.61
	1866	1.6	3.7	1.1	1.7	4.9	8.5	1.6	7.4	17.2	6.1	0.3	35.6	1.66	1.50	1.13	0.86	0.84	0.82
	1868	2.1	5.2	0.3	0.0	2.1	6.6	2.0	0.8	11.5	5.7	1.5	32.7	1.33	1.32	1.08	0.88	0.83	0.78
	1895	-24.5	-788.	-93.7	-61.8	-38.3	1.8	-11.0	-52.7	2.45	-22.10	0.75	60.9	2.11	1.66	1.21	0.78	0.70	0.61
	1978	2.3	3.3	2.0	0.7	2.7	8.5	5.3	6.6	17.8	9.2	-0.3	35.0	0.77	0.93	0.97	1.05	1.07	1.10
	2004	5.0	0.9	1.3	2.9	6.2	6.5	4.3	12.6	25.6	11.8	0.9	35.1	1.50	1.24	1.02	0.98	0.97	0.96
	2070	-66.9	-1670.	-158.	-95.7	-37.7	6.5	-6.1	-102.	-1.5	-31.3	2.0	31.6	1.82	1.45	1.17	0.83	0.76	0.73
	2100	1.5	-7.3	0.2	0.7	3.2	8.6	4.3	5.4	13.1	10.7	3.6	33.2	2.35	1.75	1.22	0.77	0.72	0.62
	2157	1.1	1.9	0.1	0.5	2.5	7.6	5.3	3.2	14.0	6.0	1.2	33.1	1.90	1.58	1.18	0.85	0.80	0.73
	2214	2.5	-1.6	0.6	2.9	6.9	9.9	1.8	11.3	19.0	10.0	0.8	38.8	2.12	1.68	1.17	0.84	0.82	0.78
GOC																			
NGC	2158	3.3	3.8	3.4	1.9	4.8	10.4	6.7	5.3	12.8	8.1	3.2	35.5	0.85	0.92	0.99	0.96	0.91	0.84
	2660	3.7	4.5	1.7	0.1	0.7	6.2	3.2	2.2	10.5	4.4	0.2	29.1	1.08	1.17	1.07	0.85	0.78	0.68
	6705	2.5	5.5	0.8	0.2	0.8	6.2	0.5	1.4	9.2	6.8	1.8	31.0	1.99	1.54	1.20	0.76	0.67	0.58

TABLE Ib. — *Same results as in table Ia, for Galactic Globular Clusters.*

object #	(S/N)b	(S/N)r	1	2	3	4	5	6	7	8	9	10	11	12	13	14	15	16	17	18
GGC																				
NGC 104	60	110	3.2	11.7	8.1	12.9	9.4	0.4	0.6	1.1	2.2	1.7	6.1	2.3	3.7	5.3	1.8	3.6	1.4	1.4
362	70	90	1.6	6.0	6.8	10.5	9.1	1.4	0.5	0.4	2.1	0.8	2.5	2.1	1.4	3.9	2.6	1.5	0.7	1.2
1851	50	90	2.7	8.5	6.9	10.5	9.4	0.4	0.7	1.1	4.1	0.8	1.2	1.3	0.9	3.1	3.6	2.7	1.2	1.7
1904	70	70	2.8	5.2	7.3	9.1	9.1	1.3	0.3	1.5	3.7	0.7	1.0	0.6	0.9	3.2	3.5	1.7	0.8	0.8
2808	40	60	-0.5	2.6	4.0	8.5	9.1	0.7	0.0	0.3	2.9	0.7	2.9	2.1	1.2	3.7	2.8	0.5	0.4	1.4
4590	30	45	1.5	2.1	2.1	4.9	7.2	1.1	1.0	1.6	3.6	0.4	0.9	0.2	0.0	1.5	3.4	0.5	0.2	0.1
4833	10	20	13.9	2.2	3.2	4.1	5.2	4.8	2.2	-0.2	6.4	1.4	1.9	1.0	3.8	3.7	4.6	1.0	1.8	0.6
5024	35	60	3.7	6.5	5.9	5.7	8.3	1.1	0.7	0.7	3.8	0.4	0.5	1.3	1.2	2.7	3.7	1.0	0.2	0.3
5824	40	65	0.3	4.1	4.1	5.3	6.7	-0.1	0.0	0.8	4.5	0.9	0.8	0.0	0.2	2.9	4.8	0.1	0.0	-0.1
5927	15	60	6.8	20.2	11.0	14.6	12.2	2.0	3.0	0.7	4.7	3.0	8.4	4.3	6.2	9.0	4.9	4.1	2.3	1.4
5946	15	30	-1.1	7.7	3.0	10.1	8.8	1.3	2.2	1.7	6.6	4.2	2.0	3.6	3.5	6.2	5.3	2.6	2.8	0.1
6093	35	50	1.2	3.2	6.5	5.8	6.7	-0.1	0.0	0.5	4.1	0.5	0.4	0.9	1.7	3.5	4.8	1.3	0.1	0.5
6139	15	45	1.6	8.3	11.7	6.1	7.8	0.5	-0.4	0.2	3.8	-0.3	0.2	0.3	1.6	3.8	5.4	1.6	0.7	0.5
6171	15	45	4.3	17.0	14.1	14.4	9.8	4.5	-0.5	1.9	3.8	2.3	5.4	4.6	5.8	7.2	5.8	6.5	2.3	-0.1
6287	10	25	8.3	-1.3	1.0	5.8	5.2	0.4	0.9	2.0	4.7	1.4	4.8	2.3	1.5	3.6	4.4	3.5	2.4	2.2
6293	20	45	1.0	4.1	3.9	6.4	7.7	0.4	0.9	1.6	5.9	2.6	2.5	0.4	1.5	4.2	5.8	1.8	0.5	0.7
6304	10	35	3.1	16.4	17.6	17.4	10.5	2.5	0.8	1.0	4.0	3.0	9.8	4.8	4.6	7.8	5.6	6.6	1.8	1.3
6316	15	40	1.4	15.0	13.1	15.0	11.3	2.1	0.5	2.2	2.0	0.7	7.0	1.9	4.5	8.4	5.8	5.6	1.9	2.1
6356	25	35	6.8	20.3	12.9	17.5	11.8	0.5	2.1	2.8	3.5	2.8	7.8	3.7	4.0	8.1	4.2	6.1	3.0	1.8
6388	30	60	4.9	16.6	11.2	14.3	10.1	0.7	0.5	2.1	4.3	2.6	8.3	2.7	3.0	5.8	4.1	4.2	2.0	1.7
6401	15	45	20.6	16.8	7.0	11.1	12.1	0.3	1.2	3.5	9.3	4.1	6.1	3.0	6.8	6.5	10.8	7.0	3.4	1.6
6402	30	60	4.1	8.7	6.7	5.4	7.0	1.0	0.9	2.6	6.0	1.5	4.9	2.7	5.0	5.9	6.7	4.5	3.0	1.7
6440	25	100	11.5	18.6	13.6	17.1	12.5	4.0	3.2	2.4	7.2	5.9	15.3	7.3	9.3	9.3	7.4	9.4	4.7	3.6
6453	15	40	-1.0	5.4	8.4	6.6	6.6	-0.2	1.5	0.8	4.3	1.8	-1.0	1.1	3.0	4.9	4.9	3.4	1.9	1.4
6517	10	30	-3.5	-0.3	10.6	9.8	8.6	0.5	3.4	1.5	7.4	3.0	5.3	2.8	4.2	6.5	6.6	6.4	3.4	2.3
6528	15	45	6.9	26.0	18.2	15.9	12.4	5.0	0.7	2.6	5.2	5.5	14.7	5.7	7.7	8.3	6.3	6.4	3.2	4.0
6541	45	60	2.2	3.9	3.6	6.7	7.2	1.3	0.5	0.8	3.8	0.1	1.4	1.0	0.6	3.1	2.6	0.7	0.9	0.8
6544	10	30	6.7	9.9	4.8	8.4	10.3	-0.3	3.7	-0.3	3.4	0.5	5.7	2.9	2.7	4.9	10.9	9.0	5.1	1.7
6553	5	20	0.5	22.0	20.0	18.6	18.0	1.7	6.3	-6.1	0.4	8.5	11.9	3.3	9.3	14.0	5.4	2.8	4.3	3.8
6558	10	20	5.7	16.7	13.1	10.5	8.7	0.1	0.3	4.4	6.3	1.7	2.6	2.0	5.0	4.8	4.1	7.9	3.7	-0.7
6569	10	25	10.0	17.5	7.6	13.7	12.0	0.4	-0.7	0.2	5.2	0.5	9.7	5.0	3.9	7.7	6.5	6.0	2.8	3.4
6624	20	45	6.1	16.4	10.4	15.5	11.1	0.3	-0.5	2.1	3.6	2.7	7.6	3.1	4.5	6.3	4.2	4.5	1.9	1.8
6637	20	45	6.8	14.6	12.8	14.0	10.7	-0.1	3.1	1.6	2.2	2.9	7.1	2.3	4.4	8.0	3.6	5.0	1.8	0.8
6638	15	40	0.2	8.4	9.3	12.0	9.3	-0.4	1.8	2.8	3.7	1.3	2.9	0.8	2.2	5.6	4.8	4.4	2.0	0.3
6642	15	40	2.2	6.3	5.6	8.5	7.2	1.2	0.0	2.0	5.4	2.1	3.2	1.9	3.6	7.7	5.7	5.6	2.2	1.6
6652	30	40	3.8	14.2	10.0	11.4	10.3	0.5	-0.1	1.6	2.9	1.5	2.6	1.3	3.4	6.4	3.6	3.5	1.1	0.5
6715	30	70	1.2	6.6	6.8	8.8	8.6	0.5	0.0	1.8	3.6	1.3	2.7	0.9	1.9	4.9	4.4	2.8	0.5	1.4
6760	5	30	19.0	-3.0	22.8	15.1	16.9	5.9	-0.3	10.7	6.8	2.8	14.6	4.4	10.7	7.6	4.4	9.7	3.8	3.2
6864	60	100	3.8	9.4	7.6	11.2	8.6	0.2	1.0	1.1	3.2	1.0	1.2	1.4	3.2	4.2	3.3	2.7	1.6	1.1
7006	30	30	5.4	9.0	10.1	10.4	10.2	0.3	1.0	2.2	5.0	0.5	3.6	1.9	2.6	5.0	4.8	1.9	0.7	0.9
7078	80	85	1.9	3.2	4.0	5.4	5.5	-0.2	0.3	0.3	3.2	-0.1	0.8	1.0	1.6	2.4	4.0	0.7	0.2	0.0

Object #	19	20	21	22	23	24	25	26	27	28	29	30	31	32	33	34	35	36	37	38
GGC																				
NGC 104	0.1	1.7	0.8	0.9	0.3	0.2	0.8	0.9	2.9	0.5	0.6	1.5	3.8	4.6	2.3	5.6	3.3	2.3	0.8	0.6
362	0.2	1.7	0.5	0.4	0.0	0.7	0.6	0.2	2.9	0.7	0.8	0.5	1.2	0.5	0.5	1.9	1.5	1.0	0.5	0.7
1851	0.4	1.7	1.1	0.6	0.0	0.1	1.0	1.1	3.5	1.0	1.4	1.1	1.5	0.0	0.5	2.0	1.3	1.9	0.3	0.8
1904	0.4	0.9	0.9	0.3	0.2	0.4	0.5	0.8	3.4	0.5	0.3	0.2	0.9	0.4	0.6	1.2	0.9	1.6	0.8	0.8
2808	0.0	2.8	0.8	-0.2	-0.2	-0.3	0.6	0.7	3.3	0.1	0.4	0.4	1.6	1.4	0.9	1.6	1.2	2.2	1.3	1.3
4590	0.1	0.9	1.0	1.0	0.3	1.3	1.4	1.0	3.8	0.9	0.9	0.7	0.3	0.5	0.1	1.8	1.0	1.5	0.6	0.8
4833	-0.2	2.4	0.3	1.1	0.3	0.7	0.0	0.7	3.8	0.7	1.3	0.6	2.1	0.5	0.1	2.2	1.2	2.3	1.2	1.7
5024	0.8	1.5	1.0	0.9	1.0	1.0	0.7	0.8	3.6	0.5	0.7	0.9	0.3	0.2	0.5	1.0	0.7	0.6	0.9	0.7
5824	0.1	0.7	0.5	0.3	0.3	1.4	0.8	0.0	2.7	0.3	0.6	0.1	1.7	1.1	0.4	1.3	-0.3	0.2	0.2	0.4
5927	1.4	3.0	1.8	1.0	0.7	2.2	1.7	1.2	4.1	0.9	2.3	2.0	4.7	4.7	2.2	6.2	3.7	2.7	1.0	1.4
5946	-0.4	1.8	1.5	1.3	0.7	0.6	1.2	0.2	3.4	0.7	1.0	1.2	3.1	1.7	0.9	2.1	1.2	1.1	0.7	0.8
6093	0.2	0.8	0.1	0.0	0.0	0.2	0.4	0.6	3.2	0.2	0.1	0.2	0.1	0.0	0.5	1.3	0.8	1.0	0.2	1.2
6139	-0.4	1.9	1.0	0.9	-0.9	1.4	1.0	0.2	3.9	0.4	0.1	0.9	1.3	0.5	0.8	3.3	1.2	1.4	0.1	0.1
6171	0.1	1.2	1.6	-0.1	0.3	0.5	1.1	0.6	2.7	1.3	1.4	1.5	2.9	4.3	1.5	5.0	1.5	1.7	0.6	0.8
6287	1.2	0.4	0.8	0.9	0.8	3.5	1.6	0.9	3.1	0.3	0.6	1.2	1.0	0.7	0.4	1.8	1.0	0.5	0.3	1.7
6293	0.4	0.2	0.6	0.4	-0.1	0.7	1.8	2.3	4.9	1.1	0.7	0.5	0.6	-0.2	0.6	0.9	0.5	1.4	1.3	0.2
6304	0.1	2.6	0.3	1.8	0.8	2.1	1.2	0.8	2.7	0.2	0.8	2.4	4.6	3.8	2.3	5.6	3.2	2.0	-0.1	0.8
6316	0.7	1.5	-0.1	0.2	0.3	1.5	3.6	1.5	2.9	0.9	1.4	2.3	4.9	4.8	2.3	5.3	2.1	1.3	0.6	0.9
6356	0.5	1.6	1.2	0.1	0.2	1.5	0.8	0.7	2.8	0.5	1.2	1.5	3.2	2.8	2.0	5.1	2.7	2.3	0.9	1.1
6388	0.4	2.7	1.7	0.5	0.9	0.7	1.1	0.3	2.5	0.6	0.7	0.7	4.9	3.4	2.1	5.3	3.6	3.9	1.0	1.4
6401	-0.5	3.5	-0.5	1.6	1.0	2.3	3.8	1.8	4.2	0.8	0.8	1.7	3.4	5.1	2.5	4.7	2.7	2.6	1.1	1.0
6402	1.0	2.4	1.8	0.9	0.4	1.4	0.9	0.8	3.9	0.9	1.3	2.2	3.1	3.6	1.3	3.2	2.0	1.8	0.5	1.6
6440	0.5	4.2	2.3	1.9	1.4	3.5	3.9	2.9	4.8	1.6	2.4	4.7	7.2	6.9	3.0	7.8	5.5	4.2	1.4	1.6
6453	0.1	0.9	0.5	0.7	-0.6	0.1	0.3	0.9	3.9	0.8	1.5	0.7	2.4	0.6	1.0	1.7	1.6	2.0	0.9	1.2
6517	0.8	2.5	1.2	0.8	0.4	0.9	0.5	1.6	3.5	0.6	0.7	-0.6	2.1	0.4	-0.2	0.3	0.4	0.0	1.1	0.1
6528	0.2	1.2	1.7	0.4	0.9	2.0	2.9	2.8	4.3	1.5	1.6	3.3	6.7	6.3	3.0	8.4	6.1	4.6	1.3	1.7
6541	0.5	1.2	1.5	1.4	1.0	2.1	1.7	1.4	4.0	1.0	0.9	0.9	1.1	0.7	0.6	1.4	0.9	0.8	0.5	0.5
6544	1.5	3.9	3.4	-0.4	0.2	1.5	2.5	1.3	4.1	1.8	0.9	1.1	0.4	2.1	0.1	3.3	2.2	2.6	1.4	1.4
6553	0.3	5.3	-0.1	0.7	-0.2	-0.7	2.7	1.8	6.2	1.4	2.3	4.3	7.0	6.7	3.2	8.5	5.3	4.5	-0.3	1.4
6558	-0.6	2.7	0.0	2.2	0.7	1.2	2.1	1.8	4.9	1.2	1.1	-0.1	2.7	3.3	1.0	3.0	2.2	3.0	2.1	1.7
6569	2.3	4.5	1.4	-1.8	2.0	0.3	1.5	1.8	2.3	0.7	0.6	2.7	2.3	3.8	2.7	5.5	2.1	2.0	0.1	0.9
6624	-0.6	2.6	1.3	-0.2	0.7	0.4	0.6	0.4	2.5	0.4	0.8	1.0	5.1	4.0	2.1	5.4	3.2	3.4	0.6	0.6
6637	-0.4	1.8	0.7	1.2	0.0	0.8	0.2	-0.2	1.8	-0.8	-0.2	0.6	2.2	0.8	0.9	3.2	2.3	1.8	0.3	0.6
6638	0.6	-0.3	0.5	1.2	0.0	-0.6	-0.4	0.7	4.2	0.5	0.9	0.6	2.0	1.4	0.8	3.0	1.3	1.5	0.6	1.1
6642	0.0	1.1	0.1	1.8	-0.3	0.1	1.1	1.2	4.3	-0.1	0.9	1.2	2.3	2.3	2.1	4.4	2.9	3.1	1.5	1.8
6652	-0.1	2.3	0.7	0.3	-0.6	1.1	0.8	0.2	2.7	0.0	0.5	0.8	3.2	2.3	1.6	3.5	0.9	1.5	0.2	0.5
6715	-0.2	1.8	1.1	0.2	0.9	1.1	1.1	0.0	3.0	0.8	1.2	0.9	3.2	2.3	1.4	2.8	1.2	1.5	0.6	0.6
6760	1.7	0.7	3.4	2.0	2.1	-0.4	2.3	1.7	3.0	1.6	1.1	4.6	7.5	3.9	2.6	6.6	4.1	4.0	1.2	1.0
6864	0.6	2.7	1.4	1.2	0.1	2.1	1.6	0.8	3.8	0.8	1.6	2.1	2.7	1.6	0.9	3.2	1.6	1.7	0.3	0.5
7006	0.5	2.7	1.0	0.6	0.2	0.7	0.9	1.0	3.0	0.2	1.2	0.9	1.8	0.6	0.6	2.2	0.9	1.3	0.0	1.9
7078	0.3	0.8	0.4	0.1	-0.1	0.5	0.8	0.4	2.5	0.0	0.3	0.5	0.9	0.2	0.1	0.9	0.0	0.3	0.2	0.6

TABLE Ib (*continued*).

Object	#	39	40	41	42	43	44	45	46	47	48	49	50	51	52	53	54	55	56	57	58
OGC																					
NGC	104	0.1	0.8	0.4	1.3	0.6	0.9	0.9	-0.5	0.1	2.2	1.2	0.9	0.3	0.6	0.9	2.5	4.5	2.8	1.8	0.5
	362	0.6	0.7	0.2	0.8	0.6	0.9	0.8	-0.1	-0.2	4.1	0.9	1.4	0.6	0.9	1.0	2.1	3.4	2.8	1.5	2.3
	1851	0.4	0.8	0.0	1.7	0.7	1.1	1.2	0.1	0.1	1.2	0.6	0.2	0.1	0.5	0.8	1.9	2.7	2.3	1.5	2.2
	1904	0.7	1.0	0.1	0.7	0.2	0.8	1.1	0.1	-0.2	1.0	0.8	1.0	0.7	0.9	1.0	1.1	2.3	2.3	1.9	2.0
	2808	1.2	0.9	0.5	1.3	0.5	1.3	2.3	0.1	0.1	2.0	0.5	0.9	0.8	0.0	0.5	1.0	1.4	1.5	0.3	0.2
	4590	0.4	1.8	1.4	2.0	0.9	1.0	2.6	0.2	-0.1	0.5	0.5	0.9	0.7	0.2	0.7	0.3	3.3	1.0	0.6	1.9
	4833	0.7	0.6	1.2	0.5	0.2	0.7	3.6	1.1	0.4	2.3	0.7	0.6	2.0	1.0	1.4	2.0	2.4	2.8	2.0	3.2
	5024	0.9	0.6	0.0	0.8	0.3	0.3	0.6	-0.1	-0.1	0.9	0.8	0.8	1.0	0.7	0.9	0.3	1.2	1.0	0.1	0.7
	5824	0.4	0.3	-0.1	0.5	-0.1	0.5	0.7	0.2	-0.1	1.1	0.5	0.4	-0.1	1.1	0.1	0.9	2.0	1.8	0.8	0.5
	5927	0.6	1.5	0.5	0.5	1.3	1.7	2.5	0.8	0.1	4.0	0.8	1.4	0.8	0.7	2.0	2.6	5.1	3.7	2.4	2.7
	5946	0.8	1.9	-0.1	0.1	-0.1	0.6	1.3	0.6	0.0	3.1	1.1	0.3	0.5	0.2	1.4	2.6	2.6	3.0	1.6	1.9
	6093	0.2	0.0	0.0	1.1	0.2	0.2	-0.3	-0.5	-0.3	0.7	0.2	0.0	0.1	0.2	0.6	0.9	1.8	1.9	0.3	0.9
	6139	0.5	-0.1	-0.7	0.1	-0.4	0.3	1.0	0.2	-0.1	2.3	0.8	0.7	0.5	0.5	0.9	2.6	3.3	2.7	1.5	1.8
	6171	0.0	0.0	1.5	1.1	0.2	0.4	1.2	0.3	-0.1	0.7	0.2	0.2	0.4	1.1	1.8	1.7	1.6	1.0	1.0	1.5
	6287	0.7	1.2	-0.1	-0.5	0.9	0.6	0.1	-0.3	0.2	0.9	0.8	-0.1	1.0	0.3	0.8	0.7	1.6	2.5	1.2	1.8
	6293	0.8	0.5	-0.1	-0.2	-0.1	-0.3	0.6	-0.2	-0.3	1.8	0.4	0.2	0.4	0.7	1.2	1.6	1.5	2.0	0.9	1.3
	6304	0.7	1.4	-1.0	0.6	0.5	0.7	-0.1	-0.3	1.2	4.7	1.8	0.9	1.1	-0.2	1.2	4.5	6.6	4.4	2.8	1.2
	6316	1.1	1.1	-0.2	0.6	0.5	0.5	0.7	0.1	-0.1	3.7	0.6	0.8	0.7	0.1	0.7	3.0	4.4	3.3	1.7	1.4
	6356	0.5	1.3	0.2	1.1	0.3	1.1	0.3	-1.0	-0.1	2.7	0.6	0.7	0.1	0.7	1.9	3.4	4.9	3.0	1.5	1.6
	6388	0.9	1.2	-0.7	0.4	0.5	1.7	0.6	-0.6	0.4	4.1	1.2	0.5	0.0	0.3	0.8	3.2	5.5	3.3	2.1	0.7
	6401	1.6	1.2	0.5	0.3	-0.1	0.3	0.6	-1.5	0.0	3.7	-0.1	0.3	0.0	0.7	2.8	3.3	3.9	3.1	2.1	3.4
	6402	1.0	1.1	0.8	1.1	-0.1	0.2	2.6	1.0	0.5	2.5	1.2	2.1	1.2	1.7	2.5	2.8	3.6	2.4	2.4	3.0
	6440	1.2	2.0	0.9	1.3	0.6	1.2	1.7	0.1	0.5	4.5	1.7	1.2	0.6	0.9	2.4	5.6	8.1	5.0	3.7	3.9
	6453	0.7	0.0	0.0	0.3	0.0	-0.1	-0.1	-0.2	-0.4	3.5	0.2	-0.2	0.5	-0.5	0.0	1.1	1.7	2.2	1.4	2.1
	6517	0.9	1.8	0.4	0.0	0.6	0.4	0.9	-0.2	0.2	2.7	0.7	0.4	-0.1	0.2	1.1	2.9	2.8	3.1	0.9	2.4
	6528	0.5	2.4	0.2	1.7	1.7	2.2	1.2	-0.2	0.9	6.1	2.6	2.5	1.3	0.3	1.9	7.1	10.4	6.8	5.3	2.5
	6541	0.3	0.3	0.4	0.2	0.3	0.6	1.8	0.7	0.7	2.3	1.1	0.3	0.7	0.8	0.7	1.0	0.8	0.7	-0.2	0.3
	6544	0.7	0.3	-0.6	-0.5	0.2	0.1	2.4	-0.1	-0.2	1.4	0.1	1.0	1.1	0.6	1.2	2.6	3.7	3.8	0.3	2.5
	6553	1.2	3.8	-0.8	0.8	0.5	0.7	0.7	0.7	0.5	4.2	1.0	1.7	1.4	-0.6	2.3	6.2	7.5	6.6	5.0	5.0
	6558	0.2	1.2	-0.7	0.2	0.2	1.6	2.4	0.7	0.0	2.8	1.1	0.3	2.9	1.6	1.1	2.7	4.5	4.5	3.6	3.7
	6569	0.5	1.4	-1.6	0.9	-0.3	1.3	0.0	-0.4	0.3	2.5	0.1	0.4	0.1	0.5	0.2	2.1	3.6	3.2	2.2	2.2
	6624	0.8	1.5	-0.6	0.3	0.6	1.9	0.9	-0.3	0.0	2.9	0.9	0.4	0.3	1.9	1.4	2.4	4.0	2.8	1.8	0.6
	6637	0.1	0.2	-1.1	0.7	0.5	0.2	0.6	-0.3	0.0	2.4	0.7	0.3	0.9	0.8	1.2	2.0	2.0	1.9	1.5	1.1
	6638	0.4	0.3	0.0	0.2	-0.2	0.6	0.5	-1.3	-0.2	1.9	0.3	0.8	1.5	-0.2	0.2	2.6	2.5	2.5	1.2	2.2
	6642	0.6	0.9	0.1	0.3	0.3	0.8	0.4	-1.2	0.0	3.3	0.0	0.0	-0.2	-0.1	0.1	2.1	3.2	2.6	1.1	1.1
	6652	0.5	1.5	0.0	1.9	0.0	1.0	0.1	0.3	-0.2	1.4	0.1	-0.3	0.2	0.5	1.1	1.0	2.5	2.0	0.2	0.0
	6715	0.5	1.2	-0.1	1.0	0.4	0.4	0.6	-0.1	0.0	1.4	0.4	0.1	0.3	0.5	0.8	1.5	2.7	1.6	0.8	0.4
	6760	2.4	4.4	0.7	1.9	1.6	1.4	1.1	0.0	1.0	4.0	1.9	2.8	1.4	1.4	2.2	7.5	10.3	6.5	4.1	3.0
	6864	0.5	0.2	0.7	0.7	0.4	0.2	2.0	0.0	0.6	1.3	0.6	0.4	0.8	1.3	2.3	2.3	3.5	2.6	2.1	2.6
	7006	1.3	0.8	0.6	1.6	1.0	1.5	2.0	0.6	0.0	1.1	0.6	0.0	1.1	1.0	1.5	0.5	1.7	2.2	0.8	-0.1
	7078	0.7	0.5	0.9	0.9	0.3	0.3	2.2	0.4	0.2	1.5	0.2	0.4	0.5	0.7	0.8	0.3	0.4	1.0	0.7	0.6

Object	#	59	60	61	62	63	64	65	66	67	68	69	70	$C_{\frac{4020}{5870}}$	$C_{\frac{4570}{5870}}$	$C_{\frac{5340}{5870}}$	$C_{\frac{6630}{5870}}$	$C_{\frac{6990}{5870}}$	$C_{\frac{7520}{5870}}$
OGC																			
NGC	104	1.2	1.6	-0.3	-0.2	-0.2	6.4	1.5	3.6	14.9	5.2	0.3	33.2	.53	.85	.96	1.02	1.02	1.02
	362	2.8	3.0	1.2	0.4	1.1	0.8	3.9	2.5	15.0	7.4	1.3	32.2	.76	.94	.99	.97	.94	.87
	1851	1.6	2.7	0.6	0.1	0.4	5.2	1.3	1.4	9.0	3.9	0.1	28.1	.76	.98	1.01	.90	.84	.77
	1904	2.5	3.1	0.4	-0.1	0.2	6.0	2.2	0.7	11.8	5.9	0.6	28.9	.83	.98	1.01	.95	.89	.82
	2808	0.7	2.1	0.7	0.4	1.4	7.3	4.3	1.5	12.8	5.7	0.8	30.8	.84	.99	1.00	1.01	1.01	.98
	4590	2.3	3.4	2.4	0.8	3.0	6.5	3.1	3.7	8.5	3.6	2.1	28.8	1.04	1.11	1.07	.90	.84	.76
	4833	1.9	3.0	0.3	-0.5	0.1	5.9	0.7	-0.5	3.7	1.4	1.8	34.5	.89	.96	1.00	.94	.91	.86
	5024	1.0	2.5	0.2	0.4	1.0	8.4	3.5	0.7	8.9	5.9	0.8	33.7	.94	.98	.99	.92	.87	.80
	5824	1.8	3.0	1.2	0.6	0.3	7.0	1.3	-0.2	8.2	3.5	1.1	31.2	.97	.98	1.00	.94	.89	.82
	5927	2.3	2.5	2.3	1.0	4.0	7.8	3.8	6.9	12.0	12.2	5.0	33.4	.69	.80	.94	.97	.95	.93
	5946	3.3	3.7	2.0	-0.2	-0.1	6.2	0.9	0.7	3.1	4.4	4.3	33.7	.86	.93	1.00	.92	.87	.79
	6093	1.5	2.9	0.6	0.4	0.8	6.0	2.0	0.9	8.3	4.1	1.0	29.8	.91	.98	1.00	.93	.91	.87
	6139	2.6	2.8	1.6	0.2	0.8	6.5	0.2	0.8	5.2	2.9	1.5	33.4	.72	.82	.95	.98	.96	.92
	6171	1.8	2.5	1.4	1.1	0.7	7.2	3.4	1.8	9.3	5.9	0.3	31.5	.86	.77	.93	1.00	.96	.90
	6287	2.3	4.0	1.4	0.7	1.6	7.5	1.5	1.3	4.2	4.0	4.4	31.7	.88	.92	.99	.99	.98	.92
	6293	1.7	2.6	0.9	-0.3	-0.3	4.9	0.5	-0.3	6.4	3.0	0.4	28.4	.98	.97	.99	.88	.84	.80
	6304	1.3	3.1	2.2	2.5	7.1	8.0	0.5	9.5	12.5	4.6	0.0	32.9	.57	.84	.96	.98	.97	.92
	6316	2.0	2.5	1.9	0.2	-0.1	6.3	1.7	2.7	8.1	6.8	1.6	31.3	.62	.81	.93	.97	.94	.90
	6356	1.8	2.3	1.3	0.6	1.7	5.1	0.1	1.8	6.0	2.9	0.6	29.6	.68	.89	.97	.93	.90	.84
	6388	2.6	2.4	1.4	0.9	1.2	6.5	0.0	4.7	11.2	5.4	-0.1	31.8	.55	.81	.96	.96	.95	.92
	6401	2.3	3.3	2.1	-0.5	1.4	5.7	1.2	0.6	6.7	4.0	-0.6	29.8	.58	.68	.86	1.01	1.00	1.03
	6402	3.8	3.4	2.5	1.6	1.7	7.4	4.2	4.3	12.0	9.6	2.6	32.3	.74	.83	.96	.96	.93	.88
	6440	4.0	2.3	5.1	4.8	6.4	8.1	1.2	6.7	14.2	6.6	1.0	34.8	.44	.64	.88	1.07	1.10	1.13
	6453	1.7	3.4	1.3	1.5	-0.4	5.6	3.3	1.3	8.5	3.4	0.6	30.3	.74	.86	.95	.95	.93	.89
	6517	2.0	3.2	2.2	-0.4	0.3	6.2	1.1	0.0	3.7	6.0	5.0	32.1	.70	.80	.97	.99	.99	.93
	6528	3.4	3.1	4.6	5.5	9.2	8.2	2.3	11.3	15.8	7.4	0.7	32.1	.50	.78	.94	.98	.96	.94
	6541	0.9	2.7	1.3	0.9	3.5	7.6	2.3	1.9	6.6	4.2	0.4	30.8	1.04	1.09	1.05	.88	.80	.71
	6544	2.9	3.4	2.4	0.4	0.3	5.9	1.7	2.9	6.1	6.4	1.7	33.1	.67	.80	.95	1.01	1.00	.97
	6553	3.9	4.2	3.5	3.9	1.8	7.1	2.4	8.6	16.2	6.4	-0.1	32.6	.48	.78	.95	.99	.99	.99
	6558	4.9	3.9	1.9	0.7	2.0	6.7	4.8	4.0	7.6	5.9	2.9	32.0	.90	.98	1.01	.90	.84	.77
	6569	2.7	3.6	1.2	1.0	-0.3	5.7	1.5	1.8	8.5	5.6	2.0	29.9	.59	.79	.95	.95	.93	.88
	6624	1.9	2.5	1.1	0.4	-0.5	5.6	0.3	1.7	8.0	4.4	0.7	29.7	.61	.90	.97	.93	.90	.85
	6637	1.5	2.3	1.0	0.2	1.1	6.1	2.3	1.4	8.0	4.0	1.6	32.6	.74	.97	1.01	.90	.86	.78
	6638	2.9	3.3	1.1	1.7	0.1	6.5	1.4	2.2	8.6	6.3	0.7	30.5	.83	.94	.98	.92	.88	.85
	6642	1.4	2.6	0.7	0.0	1.3	5.8	0.6	0.9	8.7	4.8	0.6	29.1	.53	.74	.89	1.00	1.00	1.00
	6652	1.2	3.5	1.2	0.2	0.2	6.1	1.1	0.5	6.8	5.2	1.9	29.8	.89	1.01	1.02	.91	.85	.79
	6715	1.8	2.9	0.6	-0.2	-0.8	5.9	1.1	1.0	7.2	2.1	-0.1	29.0	.86	.98	1.00	.93	.88	.82
	6760	4.2	3.5	6.8	6.2	10.7	9.3	-0.6	13.6	15.4	0.5	-0.2	37.7	.50	.68	.93	1.06	1.10	1.16
	6854	2.1	2.9	0.6	0.6	0.4	7.0	2.3	4.4	10.8	7.0	2.0	29.9	.86	.92	.99	.94	.91	.85
	7006	0.9	3.1	0.7	0.0	0.9	8.4	1.9	0.5	9.1	6.9	3.4	34.8	.97	1.05	1.05	.90	.84	.77
	7078	1.1	2.5	-0.4	0.1	-0.3	7.4	2.2	1.6	8.7	5.6	1.4	31.3	.96	1.04	1.06	.91	.85	.77

TABLE II. — *Balmer line mean equivalent widths from the grid, as a function of age.*

Age	Hα	Hβ	Hγ	Hδ
$1.65\ 10^{10}$	3.0 ± 0.5	3.5 ± 0.9	4.9 ± 1.8	4.4 ± 1.8
$5\ 10^{9}$	3.6 ± 0.5	4.9 ± 0.7	5.7 ± 1.8	5.0 ± 1.8
10^{9}	4.4 ± 0.5	7.5 ± 0.7	7.7 ± 1.0	9.7 ± 1.8
$5\ 10^{8}$	5.6 ± 0.5	7.9 ± 0.5	8.6 ± 0.8	11.9 ± 1.1
10^{8}	4.6 ± 0.8	7.9 ± 0.5	9.9 ± 0.3	10.5 ± 1.1
$5\ 10^{7}$	3.3 ± 1.6	6.2 ± 0.5	7.6 ± 0.3	8.9 ± 1.1
10^{7}	0.8 ± 1.6	3.9 ± 0.5	3.5 ± 0.3	4.5 ± 1.1

TABLE III. — *For galactic globular clusters, mean relative continuum points at different wavelengths from the grid, as a function of metallicity.*

$[Z/Z_{\odot}]$	C4020/C5870	C4570/C5870	C5340/C5870	C6630/C5870	C6990/C5870	C7520/C5870
0.6	0.39±. 10	0.71±.09	0.91±.04	1.01±.04	1.01±.06	1.02±.09
0.0	0.52±. 10	0.77±.09	0.93±.04	0.99±.04	0.98±.06	0.97±.09
-0.5	0.63±. 10	0.83±.09	0.95±.04	0.97±.04	0.96±.06	0.93±.09
-1.0	0.74±. 10	0.88±.09	0.97±.04	0.96±.04	0.93±.06	0.89±.09
-1.5	0.84±. 10	0.94±.09	0.99±.04	0.94±.04	0.90±.06	0.85±.09
-2.0	0.95±. 10	0.99±.09	1.01±.04	0.92±.04	0.88±.06	0.81±.09

TABLE IV. — *For intermediate and young clusters, mean relative continuum points at different wavelengths from the grid, as a function of age.*

age	C4020/C5870	C4570/C5870	C5340/C5870	C6630/C5870	C6990/C5870	C7520/C5870
$5\ 10^{9}$	0.82±0.18	0.95±0.11	0.99±0.04	0.95±0.05	0.91±0.10	0.90±0.10
10^{9}	1.04±0.18	1.08±0.08	1.03±0.03	0.92±0.05	0.87±0.06	0.80±0.08
$5\ 10^{8}$	1.41±0.15	1.33±0.08	1.08±0.03	0.86±0.04	0.79±0.04	0.72±0.06
10^{8}	1.84±0.10	1.52±0.05	1.15±0.01	0.82±0.02	0.77±0.04	0.68±0.06
$5\ 10^{7}$	1.87±0.10	1.54±0.05	1.16±0.01	0.85±0.02	0.82±0.04	0.77±0.07
10^{7}	2.00±0.26	1.55±0.15	1.16±0.06	0.84±0.08	0.80±0.10	0.75±0.13

Astron. Astrophys. 166, 83–91 (1986)

ASTRONOMY
AND
ASTROPHYSICS

The interstellar Na I strength versus reddening relationship: its incidence on stellar population synthesis*

E. Bica and D. Alloin

Observatoire de Paris, Section de Meudon, F-91195 Meudon Principal Cedex, France

Received March 24, accepted May 9, 1986

Summary. We study the equivalent width W of the Na I D lines in 41 globular clusters with reddening $0 \leqq E(B-V) \leqq 1.11$ and a wide spatial distribution in the Galaxy. Contributions to the line absorption from the stellar and interstellar components are separated via comparisons with the Ca II K and the Mg I b lines. The value W(Na I) is found to be enhanced for reddened clusters. The relationship between interstellar Na I and $E(B-V)$ presents a steeper slope for globular clusters than that derived for stars in the solar neighborhood.

In view of stellar population synthesis in galaxies, we study the age and metallicity effects in the W(Na I) vs W(Mg I) plane by means of 15 Magellanic Cloud and 3 Galactic open clusters. For solar and lower than solar metallicities a large excess E(Na I) can be produced only by interstellar line absorption.

We also analyze 154 normal and 11 active galactic nuclei. We find that the Na I line is enhanced with galaxy inclination in spirals. Very metallic early type galaxies deviate from a linear relationship in the W(Na I) vs W(Mg I) plane. This excess of the Na I absorption can be equally accounted for by, (i) an interstellar contribution from the central regions and/or an extended halo compatible with the existing H I detections in early type galaxies, and (ii) an enhancement of W(Na I) with respect to W(Mg I) in the atmospheres of very metal rich late type stars as suggested by synthetic spectra computations.

Key words: interstellar Na I – globular clusters – galactic inclination effects

1. Introduction

The existence of a correlation between the line strength of interstellar Na I and the continuous extinction of starlight by interstellar grains is an evidence that gas and dust are generally associated in the interstellar medium (Spitzer, 1948). Indeed, observations of stars at intermediate and high galactic latitudes indicate that the column density of interstellar Na I is correlated with $E(B-V)$ (Hobbs, 1974). However, spatial variations of this relationship are observed in the Galaxy. In nearby disc regions the equivalent width of interstellar Na I in spectra of stars situated behind or within dense clouds are smaller than those of more distant stars with the same amount of reddening, arising from a long pathlength through relatively diluted interstellar material. This is due to Na I depletion from the gas in dense clouds, where most of the heavy elements must be locked on grains (Cohen, 1973). The very strong Na I D lines with respect to Mg I b, observed in some galaxies indicate an interstellar line absorption much stronger than in Galactic stars having the same amount of reddening; this could be explained by a larger sodium abundance or a higher gas to dust ratio in the central regions of these galaxies (Véron-Cetty et al., 1982).

We study the interstellar Na I D line vs reddening relationship using Galactic globular clusters (GGC) which present over stars, the advantage of a wide spatial distribution in the Galaxy. Indeed the lines of sight to our sample of GGC probe the interstellar medium through the outer halo, the bulge as well as the disc. Thus, they could potentially provide an average relationship for the Galaxy. We also discuss the derived relation with respect to a set of 165 normal and active galaxies.

The observations are presented in Sect. 2. We discuss in Sect. 3 the method for separating the stellar from the interstellar Na I D absorption components, the construction of the interstellar line strength versus reddening relationship and its interpretation in terms of interstellar matter in the solar neigborhood. We also present in Sect. 4 the age and metallicity effects in the W(Na I) : W(Mg I) plane, on the stellar component. In Sect. 5 we apply these results to a set of normal and active galaxies, some of which showing a large Na I excess absorption with respect to that expected from the stellar population. Concluding remarks are given in Sect. 6.

2. The observational data set

The observations of 41 globular and 3 open Galactic clusters, as well as 15 Magellanic Cloud clusters and 165 galaxies are part of a program for population synthesis in galaxies using integrated spectra of star clusters. The observations were carried out in January, July, November 1984 and May 1985 with the IDS attached to the Boller and Chivens spectrograph at the European Southern Observatory (ESO), La Silla, 1.52 m telescope. For large angular size objects a scanning procedure was used. The dispersion was 224 Å/mm in the range 3700, 8200 Å, with 11 Å resolution. Reductions were made using the IHAP system at ESO (Garching)

Send offprints requests to: D. Alloin

* Based on observations collected at the European Southern Observatory, La Silla, Chile

Table 1

S1	Type	Galaxy			b/a*	Date	Exp (min)	Slit (kpc)	W(Mg I) (Å)	W(Na I) (Å)
		M_{BT}	A_B	V_R						
NGC3783	SBa(r)I	−20.81	0.21	2790	0.81	85 May 14	16	1.2×1.9	0.0	0.0
NGC7469	Sabpec	−23.10	0.05	4890	0.74	84 Nov 18	16	2.5×3.9	<0.2	0.1
IC4329A	S0/a	−21.70*	0.12	4815*	0.32	85 May 16	20	1.9×3.2	0.0	2.7

Observed parameters are from Sandage and Tammann (1981) except when denoted by an asterisk; then they are from de Vaucouleurs et al. (1976). For homogeneity, $H_0 = 50\,\mathrm{km\,s^{-1}\,Mpc^{-1}}$

and Institut d'Astrophysique de Paris. Exposure time, area covered by the observations, slit dimension as well as physical properties – age, metallicity, reddening – have been given previously for each cluster (Bica and Alloin, 1986a). The equivalent widths W(Ca II K), W(Mg I b) and W(Na I D), measured from windows respectively 44, 40 and 34 Å wide are to be found in Table 1 of Bica and Alloin (1986b). For 154 normal galaxies as well as 7 Seyfert 2, and 1 Seyfert 1 objects with spectrum around 6000 Å dominated by the stellar component, we give morphological and photometric parameters, details on the observational conditions and resulting measurements for W(Na I D) and W(Mg I b) in a paper to come (Bica and Alloin, 1986c). Finally, we provide in Table 1 observational results for 3 Seyfert 1 type galaxies with negligible stellar contribution.

For such a study, excellent sky cancellation is required, owing to the atmospheric Na I D emission lines. We tested our sky subtractions by searching for residuals at [O I] 5577 Å, which, in the night sky emission is about a factor two stronger than the total Na I D line and lies in a nearby spectral region very little disturbed by absorption lines. In 51 star cluster spectra, no [O I] residual could be distinguished against the noise or the eventual weak intrinsic absorptions. In four cases, detections are suspected (1 absorption and 3 emissions) but their weakness implies Na I residuals less than 0.1 Å. In three cases, NGC 1866, 4833 and 5024, an [O I] residual was found in emission from which we infer Na I residuals of 0.15, 0.20 and 0.25 Å respectively. These objects are marked with a colon in Figs. 2, 3 and 4. In one case NGC 6171, a strong residual was found and this object was then excluded from the analysis in Figs. 2a and 2b. Note that the galaxy spectra cannot be affected by sky emission as long as $V_R > 700\,\mathrm{km\,s^{-1}}$.

3. The interstellar W(Na I) versus reddening relationship for Galactic globular clusters

In addition to their wide spatial distribution in the Galaxy, globular clusters are useful in the study of the interstellar Na I vs reddening relation because they have equal ages within the precision of the determinations (Vandenberg, 1983; Janes and Demarque, 1983). Consequently, differences observed among integrated spectra of GGC are in first order due to metallicity. We compare in Fig. 1 the Na I and Mg I lines in 3 pairs of cluster spectra, with moderately rich, intermediate and poor metallicity downward. Within each pair the clusters differ by large amounts in reddening. To make the line strength comparison easier, the continuous distribution has been dereddened. The noticeable enhancement of Na I observed in the more reddened objects can only be explained in terms of interstellar gas Na I absorption. Equal cluster ages allow the comparison not only of metallic lines in the same wavelength range like Na I and Mg I, but also of lines further away to the blue like Ca II K. We have plotted W(Na I) as a function of W(Mg I) and W(Ca II K) respectively in Figs. 2a and 2b, classifying the clusters into three reddening groups: $0 \leqq E(B-V) \leqq 0.20$, $0.21 \leqq E(B-V) < 0.50$ and $0.51 \leqq E(B-V) \leqq 1.11$. In spite of the rather large spread, some separation among the points is observed; linear regressions and their attached r.m.s. deviations in the three groups confirm that these differences are significant. As a check, we have plotted W(Mg I) vs W(Ca II) in Fig. 2c. No trend for a separation is seen contrarily to what happens in the plots in Figs. 2a and 2b. Yet, an interstellar absorption is known to occur in the Ca II K line, its equivalent width being of the same order as that of Na I (e.g. Cohen, 1973). We do not detect it simply because in composite stellar populations W(Ca II K) is generally a factor 5 stronger than W(Na I). The Mg I triplet cannot be increased by an interstellar contribution since essentially all the interstellar lines arise from ground level transitions (Münch, 1968). Is is worth noticing that the group with negligible $E(B-V)$ in Fig. 2 does not contain any metal rich cluster. This is due to the fact that all metal rich GGC are concentrated towards the central regions of the Galaxy, at low Galactic latitudes and hence present a considerable reddening (Zinn, 1980; Bica and Pastoriza, 1983).

In order to somehow quantify the interstellar Na I vs reddening relationship, we define in Figs. 2a and 2b the pure stellar population relations for W(Na I) vs W(Mg I) and W(Na I) vs W(Ca II). For this we use the regressions deduced for the group with negligible reddening, a small slope correction being introduced from the reddened groups which cover a wider range in metallicity. An average excess E(Na I) with respect to W(Mg I) and W(Ca II) has been derived for each cluster; they are plotted against $E(B-V)$ in Fig. 3. The slope and dispersion of this relation can be understood in terms of a combination of different interstellar matter properties, as derived from interstellar line equivalent widths and reddening in solar neighborhood stars (Cohen, 1973, 1974, 1975; Cohen and Meloy, 1975). In order to compare those observations to ours, obtained with a lower dispersion, we selected stars having both D_1 and D_2 Na I measurements. Although the original conclusions of their papers were mostly based upon the less saturated D_1 component, they remain unchanged using $D_1 + D_2$ for the present star group. We also use data from Hobbs (1969, 1974). We show in Fig. 3 various zones filled in by stars from the Galactic plane: (i) within or behind dense dark clouds, (ii) more distant stars for which the line of sight goes through the low density intercloud medium, as well as, (iii) intermediate and high latitude stars (some of them might even be Halo members). Cloud stars exhibit weaker E(Na I) than do the more distant ones with the same

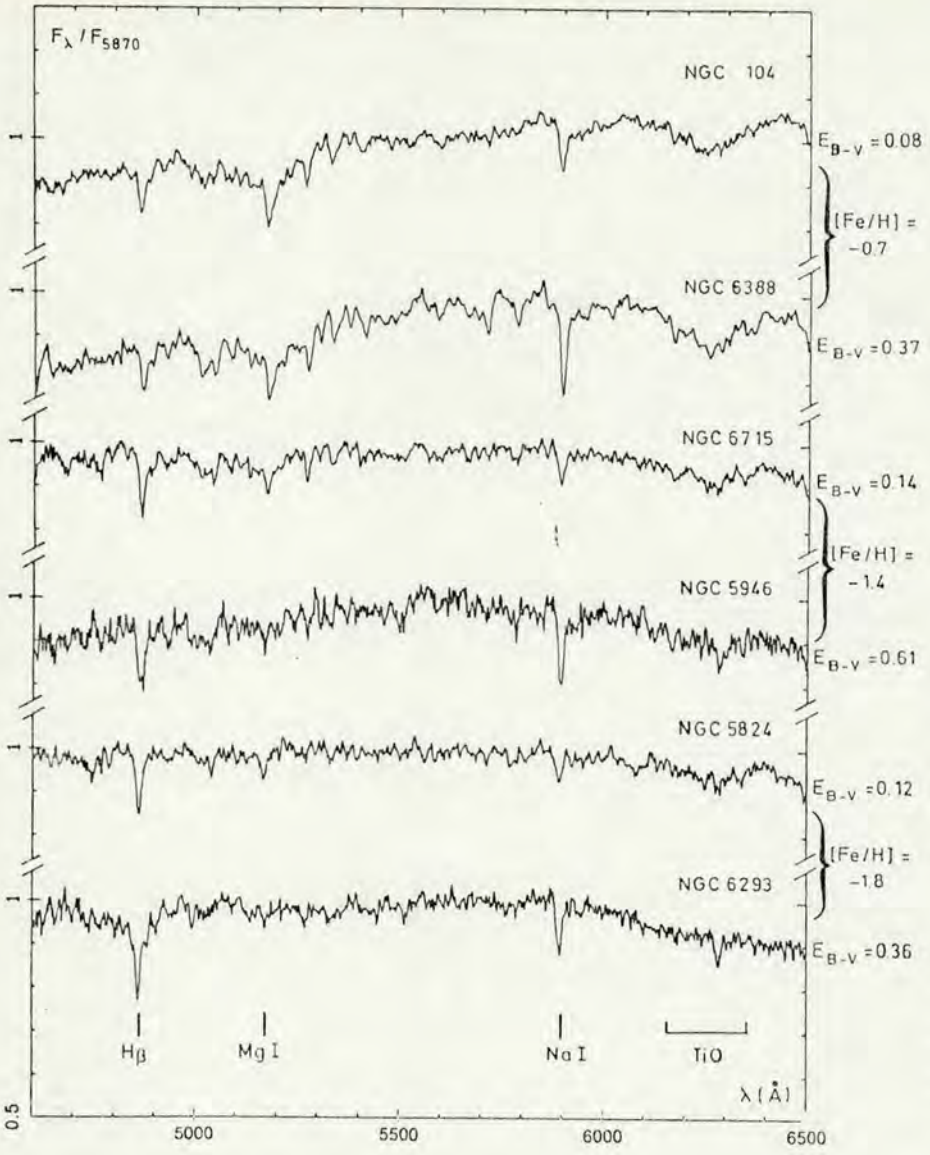

Fig. 1. Comparison of the relative strengths of the Na I and Mg I lines in pairs of GGC of similar metallicity, which differ by their amount of reddening. The Na I enhancement can only result from interstellar gas contribution

amount of reddening. This results from Na I depletion in the gas cloud where most of the heavy elements must be locked in dust grains (Cohen, 1973). The reddening for intermediate and high latitude stars arises most probably from a disc layer with half-thickness 100 pc. The line-strengths indicate that gas must be present as far as 1 kpc or more above the plane (Cohen, 1974; Cohen and Meloy, 1975).

With respect to stars, the GGC relation presents a steeper slope although a similar scatter. For our three reddening groups, we provide in Table 2 the mean solar distance $\langle d_\odot \rangle$ and the mean distance above the Galactic plane $\langle Z \rangle$, derived from Bica and Pastoriza (1983). The steeper global slope for the GGC is explained by their much longer pathlengths through the interstellar medium. As a matter of fact, most stars in this subset are within 1 kpc from the Sun, none exceeding 2.5 kpc, while the nearest GGC lies at $d_\odot \simeq 4$ kpc and the smallest mean distance in our reddened groups is $\langle d_\odot \rangle = 7.3$ kpc. Saturation effects in the lines, although certainly present do not affect this conclusion. Indeed, different systematic velocities and velocity dispersions of the gas clouds and the low density intercloud medium through various subsystems in the Galaxy are to be found along the lines of sight to GGC. The spread in the relation can be assigned, at least in part, to the different amount and physical conditions of the interstellar material intercepted towards each particular cluster. A typical globular cluster in the low reddening group is a distant outer halo object at high Galactic latitude with E(Na I) and $E(B-V)$ similar to the ones associated with intermediate and high latitude stars. The values of E(Na I) for these clusters, whose pathlength crosses both the local dust patches and the gaseous disc layer, indicate that the upper limit for Galactic gas contamination in the Na I window for galaxies having $V_R < 1000\,\mathrm{km\,s^{-1}}$, is 1 Å. In most cases however, this contribution should not exceed 0.5 Å. The group of clusters with $0.21 \leqq E(B-V) \leqq 0.50$ corresponds to typical low latitude bulge objects. They show a stronger E(Na I) than the local stars with the same $E(B-V)$, this being probably the result of a longer pathlength through the interstellar matter above the plane. Clusters from the last group, with $0.51 \leqq E(B-V) \leqq 1.11$, lie at smaller values of $\langle Z \rangle$ and $\langle d_\odot \rangle$ than the previous

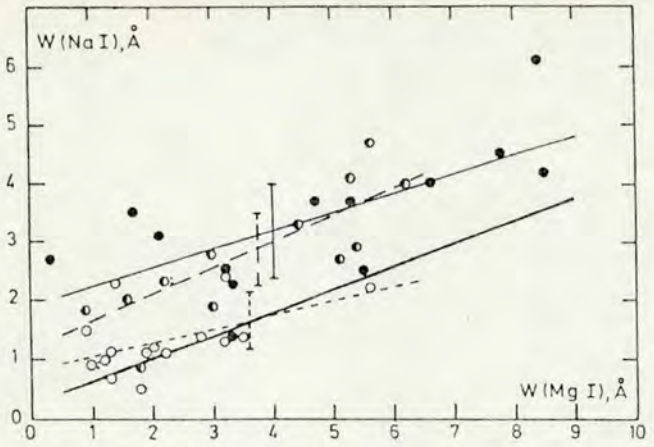

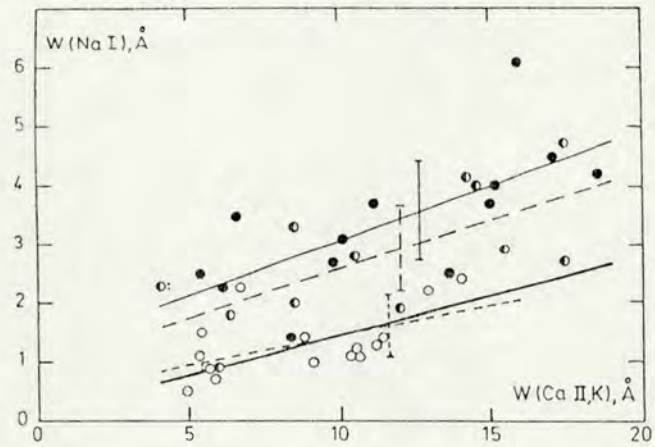

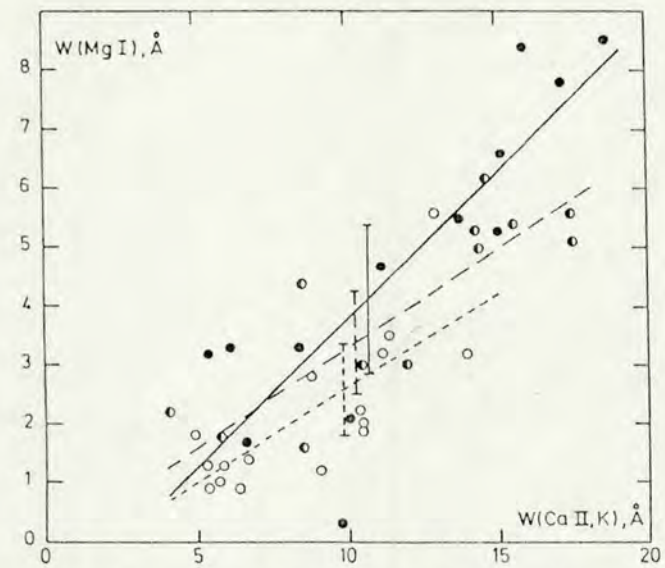

Fig. 2a–c. Comparison of metallic lines in GGC for three reddening groups: open circles, $0 \leqq E(B-V) \leqq 0.20$, semi-filled dots, $0.21 \leqq E(B-V) \leqq 0.50$, and black dots, $0.51 \leqq E(B-V) \leqq 1.11$. The corresponding linear regressions and r.m.s. deviations are represented respectively by a dotted line, an interrupted line and a thin solid line. The thick solid line in Figs. 2a and 2b is the adopted relationship, free from gas contamination

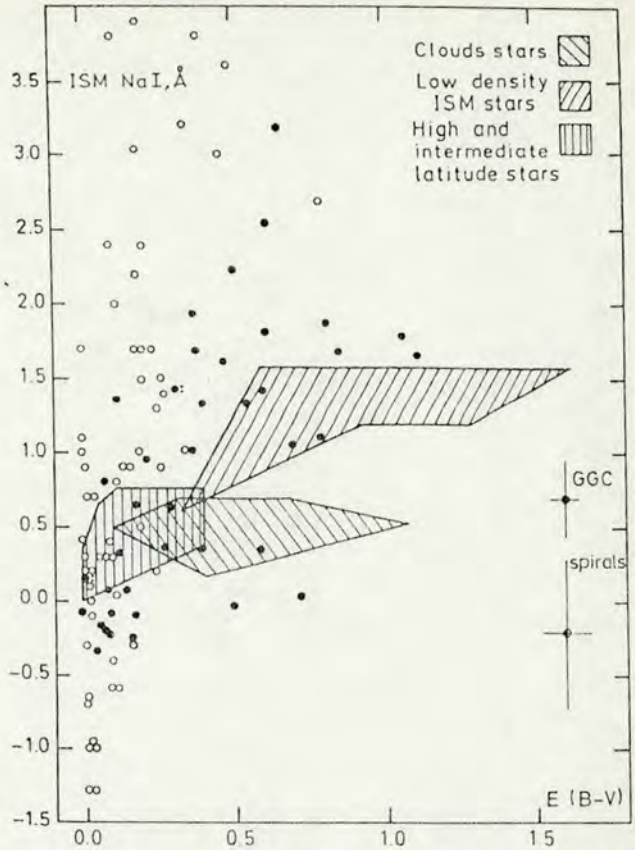

Fig. 3. The interstellar gas component of Na I vs reddening for GGC (black dots) as compared to Galactic stars with various line of sight properties. Open circles present inclined spirals ($b/a \leqq 0.75$) where the excess $\mathscr{E}$(Na I) and $\mathscr{E}(B-V)$ are given with respect to nearly face-on spiral templates of similar stellar population (Sect. 5)

Table 2

Group No.	$E(B-V)$	N	$\langle d_\odot \rangle$ (kpc)	$\langle Z \rangle$ (kpc)	$\langle E(\mathrm{Na\,I}) \rangle$ (Å)
1	0–0.20	15	14.6 ± 8.6	6.3 ± 4.4	0.13 ± 0.47
2	0.21–0.50	13	8.5 ± 3.4	1.3 ± 0.7	1.13 ± 0.70
3	0.51–1.11	13	7.3 ± 2.3	0.8 ± 0.7	1.52 ± 0.82

ones, a result in agreement with their large reddening. The line of sight to these clusters at very low Galactic latitude crosses on average a larger number of dense clouds so that their reddening grows much faster than does E(Na I). This explains why the two groups of intermediate and high reddening are almost undistinguishable in Figs. 2a and 2b.

4. Age and metallicity effects in the W(Na I) vs. W(Mg I) plane

In view of stellar population synthesis in galaxies, we study the effects of age and metallicity in the W(Na I) vs W(Mg I) plane using the pure stellar population relationship derived in Fig. 2a and the results from the integrated spectra of intermediate age and blue Magellanic Cloud clusters, as well as Galactic open clusters from

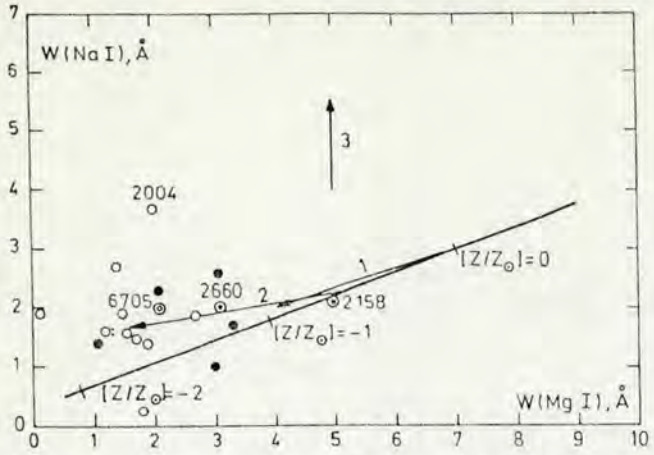

Fig. 4. Age and metallicity effects on W(Na I) and W(Mg I). The gas-free relation for GGC from Fig. 2a is labelled with metallicity. Black dots and open circles are for red and blue Magellanic Cloud clusters respectively. Encircled black dots and encircled empty dots are for red and blue Galactic open clusters. Vector 1 illustrates an age shift of $1.5\ 10^{10}$ yr at constant $[Z/Z_\odot]=0$. Vector 2 illustrates an age shift of $1.65\ 10^{10}$ yr at constant $[Z/Z_\odot]=-0.5$. Vector 3 shows the direction of interstellar gas contamination

Bica and Alloin (1986a, 1986b). In Fig. 4, the pure stellar population relation for the globular cluster isochrone is labelled with $[Z/Z_\odot]$. This demonstrates the effect of metallicity variations within the old clusters: as expected, both metallic lines Mg I and Na I become weaker for low metallicities. The vector labelled 1 corresponds to an age variation from a GGC to a red GOC about 10^9 yr, both with solar metallicity. The two 10^9 yr old GOC, NGC 2158 and 2660 present considerable reddening ($E(B-V)\simeq 0.40$), so that W(Na I) certainly contains some interstellar contribution. These considerations make it still more difficult to interpret the W(Na I) enhancement in terms of age variation. The vector labelled 2 corresponds to an age change from a GGC to the mean locus of blue LMC clusters, for a constant $[Z/Z_\odot]=-0.5$. The W(Na I) measurements for LMC clusters may also contain some interstellar contribution around 0.5 Å due to the Galactic and MC gas clouds (York, 1982). So, the intrinsic vector is more probably parallel to the GGC sequence. This is due to the fact that the blue turn-off points for these clusters contribute similarly to the underlying continuum owing to the wavelength proximity of these lines, while not to the line absorption. This is also supported by the position in Fig. 5, of NGC 5102, an S0 galaxy with a spectrum dominated by a population younger than in other early type galaxies. The abnormal position of the LMC blue cluster NGC 2004 in Fig. 4 results from a large TiO contribution to the Na I window as expected for an enhanced supergiant population in this cluster, 10^7 yr old (Bica and Alloin, 1986a). An age variation at constant solar metallicity from a GGC to the blue Galactic open cluster NGC 6705 is also essentially parallel to the GGC sequence. We conclude that for solar or lower than solar metallicity a strong enhancement of Na I D can only be produced by interstellar gas absorption.

5. Position of galaxies in the plane W(Na I) vs W(Mg I)

Measurements of W(Na I) and W(Mg I) for our sample galaxies (Bica and Alloin, 1986c) are plotted in Figs. 5a through 5d, corresponding respectively to types E-S0, S0/Sa-Sa, Sab-Sb and Sbc-Sc. We also recall in these figures the gas-free relation derived in Sect. 3 for GGC. The strong-lined early type galaxies (Fig. 5a) depart from the linear extrapolation of the GGC relationship, in the sense that for large W(Mg I) values, a 2 Å excess is observed in Na I. It can also be noticed that this effect tends to be stronger for higher luminosities. We also checked the presence of other contributors to the absorption in the Mg I and Na I windows. Using local continua, we estimated that for E and S0 galaxies, 50 % of the absorption in the Mg I window is due to MgH, while TiO is responsible for 25 % of the absorption in the Na I window. This implies even stronger relative excess of Na I with respect to Mg I. Such an excess might be explained by a larger interstellar gas content in the more massive galaxies or by an intrinsic population effect.

A stellar population effect could result from a variable giants to dwarfs ratio among galaxies. Another possible explanation is a larger increase rate of W(Na I) with respect to W(Mg I) for metallicities higher than solar, which could be associated with the different mechanisms responsible for the absorption in the wings of these lines. According to this latter hypothesis, for massive galaxies which are metal enriched (Faber, 1973), W(Na I) might increase more rapidly than W(Mg I) with metallicity in the stars contributing most to the galaxy light, an alternative to be explored. On the other hand, variations in the dwarfs to giants ratio seemed to be a promising assumption because dwarf stars show larger W(Na I) values than giants of the same spectral type (Spinrad, 1962). However, detailed population synthesis using solar metallicity stars, in some cases SMR stars, and fitting spectral features over a wide wavelength interval, do not allow a huge dwarfs contribution. Indeed, large Na I residuals remain in the best fit models for strong-lined galaxies like M 31 and M 81 (Spinrad and Taylor, 1971; Faber, 1972; Pritchet, 1977).

We can investigate the explanation of the 2 Å excess in W(Na I) with respect to W(Mg I) in terms of the relative increase rates of W(Na I) and W(Mg I) with metallicity. We compare our galactic observations to synthetic spectra of K0 giant and dwarf stars representing best the stellar groups which dominate the 5000–6000 Å flux in early type galaxies (Pickles, 1985). The models consist of computed profiles of the Mg I triplet and Na I doublet lines for a grid of values: $T_{\text{eff}}=4710$ °K, $\log g=2.2$ and 4.5, and $[Z/Z_\odot]=0.6$, 0, −1 and −2 (Cayrel de Strobel and Cayrel, 1986). Atmosphere models are from Gustafsson et al. (1975), Bell et al. (1976) and Gustafsson (1982). A description of the actual profile computation is given in Cayrel et al. (1985). Results are displayed in Fig. 6 where we compare W(Na I) and W(Mg I) computed from model atmospheres to those of GGC and for galaxies as derived from the mean relation in Fig. 5a assuming $[Z/Z_\odot]=0.6$ in strong-lined galaxies (Bica and Alloin, 1986a). In the dwarf models, we observe a trend for W(Na I) increasing more rapidly than W(Mg I) in the interval $0.0\leqq[Z/Z_\odot]\leqq 0.6$. The increase of W per metallicity interval is presented in percentage, in the upper part of Fig. 6: giant stars present a W(Na I) increase rate which is consistent with that observed for galaxies, although the amplitude variation is less for giants. We conclude from this study that W(Na I) grows faster than W(Mg I) for metallicities above solar, both in dwarfs and giants. This is probably due to the fact that the damping in the Mg I triplet wings is essentially collisional while that in the Na I doublet wings is radiative.

Following Spinrad (1962) we can estimate the amount of interstellar gas required to produce an equivalent width of the Na I D lines: $W_\lambda=\pi l N\lambda^2 e^2 f/mc^2$, where l is the pathlength, N the number density of neutral Na atoms, $\lambda=5893$ Å and $f=1$. Typical values for the gas density in the Galaxy are $N_{\text{H}}=0.1\ \text{cm}^{-3}$ and

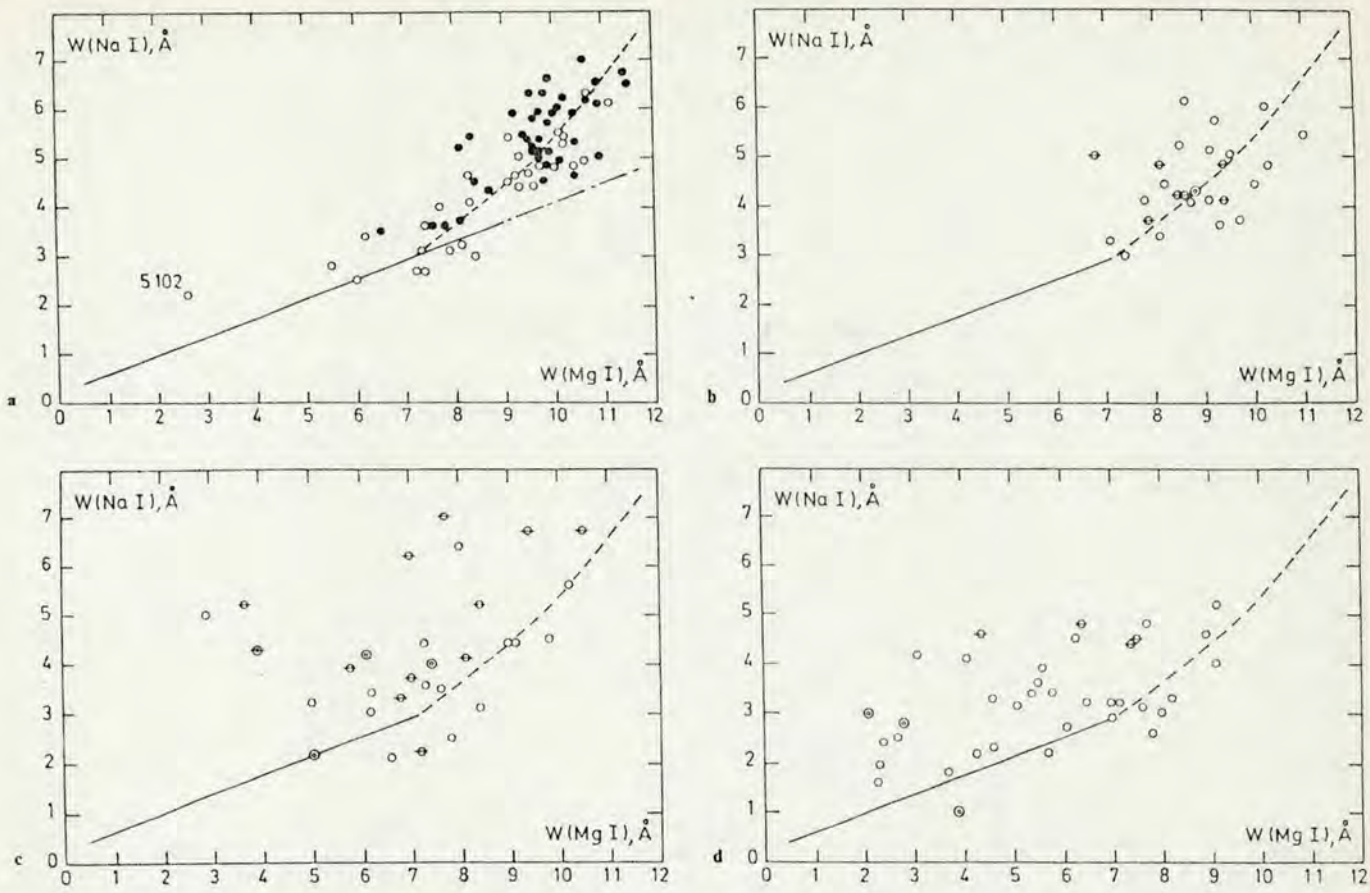

Fig. 5a–d. Line-strength comparisons for respectively E-S0 (**a**), S0 /Sa-Sa (**b**), Sab-Sb (**c**), and Sbc-Sc (**d**) galaxies. In **a**, black dots and open circles are respectively for galaxies with $M_v \leqq -21$ and $M_v > -21$. In Figs. **b** through **d**, open circles and barred circles denote respectively little and highly inclined ($b/a \leqq 0.50$) spirals. Encircled symbols are for Seyfert galaxies whose spectrum is dominated in the visible range by the stellar population component. We have recalled with a solid line the gas free GGC relationship from Fig. 2a, while the dashed-line is the mean relation for early type galaxies from Fig. 5a

$N_H = 8\,cm^{-3}$ respectively for the intercloud medium and the clouds (Allen, 1973). Assuming $N_H = 1\,cm^{-3}$ for a line of sight intercepting both kinds of medium, a solar sodium abundance $Na/H = 1.8\ 10^{-6}$ (Allen, 1973) and the ionization degree of Na in an H I region to be $N_i/N_0 = 1500$ (Spinrad, 1962), we obtain $N = 1.2\ 10^{-9}\,cm^{-3}$. In order to reproduce the observed 2 Å excess in early type galaxies, the pathlength should then be of 1.8 kpc. Under simple assumptions for the gas distribution, a 1.8 kpc pathlength results in a total gaseous mass of about $6\ 10^7\ M_\odot$. This value is in agreement with the H I content detected in some massive E and S0 galaxies; it is also compatibele with most of the upper limits for the undetected ones, although in some cases the upper limits are only $M_{HI} \leqq 5\ 10^9\ M_\odot$ (Knapp et al. 1985; Wardle and Knapp, 1986). We recall however that $M_{HI} \sim 10^9\ M_\odot$ is the typical H I content found in dwarf early type galaxies in the Local Group, such as NGC 185 and NGC 205. This simple estimate suggests that, if the gas is to be responsible for the 2 Å excess in W(Na I), it has to be most probably extended. Indeed, extended H I gas is observed in the elliptical NGC 1052 (Van Gorkom et al., 1986). On the other hand, would the gas be confined to a small volume, its density should be around that found in Galactic clouds; very high density gas is likely to be associated with dust and then Na would probably be depleted (Sect. 3). In this extreme case, a strong E(Na I) is not expected anymore. The presence of high density gas clouds in the nuclear regions of some early type galaxies is suggested by the detection of dust lanes or complexes (Sparks et al., 1985).

Galaxies of later types (Figs. 5d to 5d) show three effects as follows: (i) the increasing contribution from hot stars in the spectra shifts the points in the W(Na I) vs W(Mg I) plots towards smaller values, as does also a nonstellar continuum in active galaxies, (ii) the cases of strong W(Na I) enhancement in the two last groups (Figs. 5c and 5d) are preferentially associated with inclined galaxies, (iii) last, the lower envelope for W(Na I) coincides roughly with that for early type galaxies and that for GGC from Figs. 5a and 2a.

The shifts described in (i) are consistent with the age effects in the plane W(Na I) vs W(Mg I), as derived for young star clusters in Sect. 3. This is also the case of the blue S0 galaxy NGC 5102 in Fig. 2a. Such age effects are not expected to produce significant enhancement of W(Na I) with respect to W(Mg I), as shown in Sect. 3.

In order to study the effects of inclination on W(Na I) in spirals, we have applied a template method for deriving the internal reddening due to galaxy inclination (Bica and Alloin, 1986c). For a given inclined spiral, it consists in selecting from the nearly face-on galaxies ($b/a \geqq 0.75$), templates showing a similar stellar population. The selection criterion is the minimization of differences in

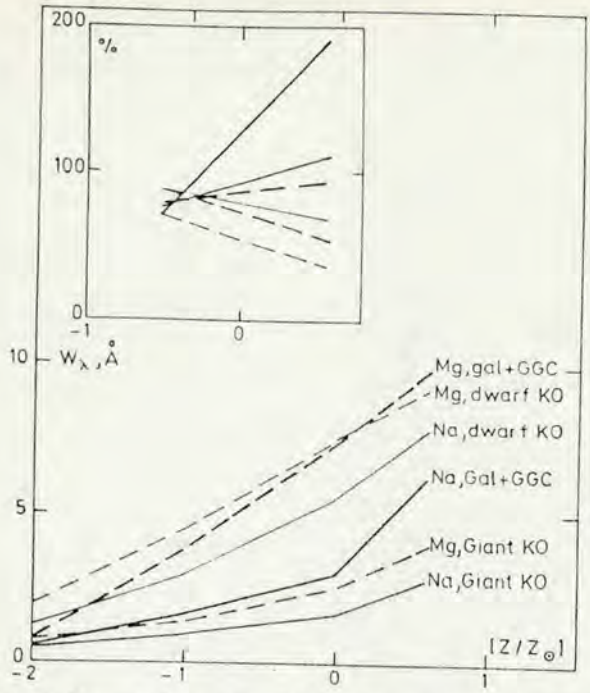

Fig. 6. The equivalent widths of Na I (solid line) and Mg I (dashed-line) as a function of metallicity. Thick lines correspond to GGC plus early type galaxies, thin lines to the synthetic spectrum of a K0 giant star and very thin lines to that of a K0 dwarf star. In the upper inset, we show the percentage increase of equivalent width per metallicity interval, with the same conventions

W(Ca II K), $W(Gb)$, W(Mg I) and W(TiO). Metallic features in the blue insure a same content in younger age components, those in the red a same metallicity (Bica and Alloin, 1986a). Due to a possible emission, Balmer lines are not suitable for this analysis. The method is described extensively and the templates found for each inclined galaxy are given in Bica and Alloin (1986c). Although rather similar populations may, in some cases, exist in early or late spiral types, we have restricted our search to templates within 1.5 morphological class intervals. We also include in the present analysis the three Seyfert 1 galaxies with negligible stellar content (Table 1). Then, NGC 3783 was adopted as the nearly face-on template. As an illustration of the method applied to a Seyfert and a normal galaxy, we provide in Fig. 7 the reddened and dereddened spectra of a very inclined galaxy, together with the respective templates. By comparing each galaxy to the face-on template in its group, we derive the internal reddening $\mathscr{E}(B-V)$ required to produce a continuous distribution similar to that of the template, and we estimate the Na I and Mg I excess $\mathscr{E}$(Na I) and $\mathscr{E}$(Mg I) as $W_{gal} - W_{templ}$.

Galactic nuclear regions, as seen through the spectrograph slit, are however a spatial average over zones possibly composite with respect to the population content and reddening distribution. A population effect is not expected to affect much the averaged observations, due to strong luminosity gradients which are as a rule present in the nuclear regions of massive galaxies of all morphological types. On the other hand, the situation is different in the case of an inhomogeneous reddening. A mixture of highly reddened to reddening-free regions produces a composite reddening law which departs from the normal one, even if the individual regions along the line of sight themselves obey a normal reddenning law. For the sake of simplicity we have assumed in the present study that a normal reddening law was still valid. When applied to the reddened nuclei in our sample, it allows to reproduce the continuum distribution of the respective templates, at least over the 4000 Å wavelength range considered (Fig. 7). This indicates that an eventual composite law does not depart significantly from the normal one, in turn suggesting highly peaked distributions around the best fit value of $E(B-V)$.

Results for the whole sample of inclined spirals are shown in Fig. 8. One observes that $\mathscr{E}$(Na I) increases with inclination, due to the gas component in the disc. As a test we have displayed $\mathscr{E}$(Mg I) which is null as mean. We also show $\mathscr{E}(B-V)$ resulting from inclination, which tends to be larger for low values of b/a, although this effect is not as conspicuous as that occuring for $\mathscr{E}$(Na I). This is in agreement with observations of the Milky Way revealing that dust and gas are mostly contained in layers with halfthickness 100 pc and 1 kpc respectively (Cohen, 1974; Cohen and Meloy, 1975). We compare the excess in Na I and the reddening due to inclination in galaxies, with GGC and stars in Fig. 3. This confirms the result that some galaxies have a strong $\mathscr{E}$(Na I) with respect to Galactic stars of the same $E(B-V)$ (Véron-Cetty et al., 1982). However, the template method used in our study as well as the results for GGC in Sect. 3 suggest that the Na I excess results from long paths through inclined discs rather than from metal rich gas in the central regions of galaxies.

We can look for galaxies with a large amount of gas not located in a disc, by plotting the residuals of W(Na I) with respect to the mean relation in Fig. 5, for the elliptical and S0 galaxies, as well as the nearly face-on spirals having $b/a \geqq 0.75$ (Fig. 9). Large positive residuals would be an indication of atypical gas content, either in the central regions or in an extended halo. This seems to be the case for the spiral NGC 986, and to as lesser extent for NGC 1316 and 2442. As already noticed by Véron-Cetty et al. (1982), NGC 986 shows dust lanes associated with the nucleus; NGC 1316 also presents dust lanes (Baade and Minkowski, 1954), as well as NGC 2442, but in this case the galaxy seems to be more inclined than suggested by the axial ratio which is large owing to asymmetric arms (Sersic, 1968).

Finally, we observe that the lower enveloppe for spirals (Figs. 5b to 5d) coincides with that for E and S0 galaxies (Fig. 5a). This suggests a common origin in all galaxies, for the linearity departure of W(Na I) at large W(Mg I) values.

6. Concluding remarks

The main conclusions of this study are as follows:

1. The absorption Na I D line is enhanced in reddened Galactic globular clusters.

2. The stellar and interstellar components of the Na I D lines are separated via comparisons with Mg I b and Ca II K lines.

3. The derived interstellar W(Na I) versus reddening relationship for GGC shows a stronger slope than that for Galactic stars. This arises essentially from longer pathlengths through the interstellar medium outside the Galactic plane. The characteristics of the lines of sight to GGC are interpreted in terms of the various properties of the interstellar gas along the lines of sight to stars in the solar neighborhod.

4. A comparison of GGC with Magellanic Cloud and Galactic open clusters in the plane W(Na I) : W(Mg I) indicates that age and metallicity effects cannot produce a relative enhancement of Na I with respect to Mg I for solar and lower than solar metallicities.

5. The Na I line is enhanced with inclination in spirals.

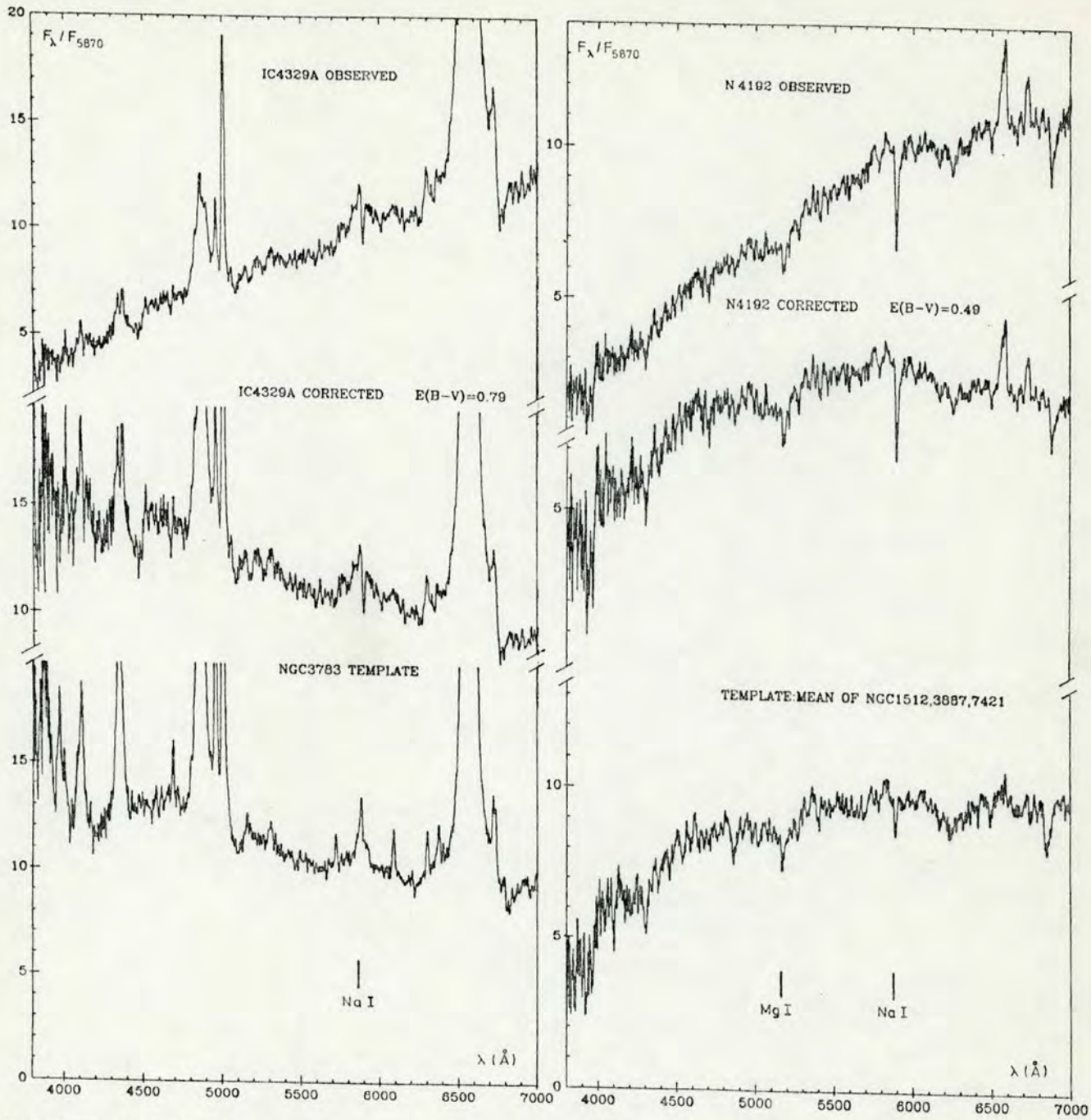

Fig. 7. Spectra of inclined spirals with their respective nearly face-on templates. Left: Seyfert 1 with negligible stellar population contamination; Right: normal galaxy. Dereddened spectra are also shown. Notice the strong NaI excess in the inclined galaxies. The spectra are normalized to $F_\lambda = 10$ at $\lambda = 5870$ Å

6. Very metallic early type galaxies deviate from a linear relationship in the W(Na I) : W(Mg I) plane. This excess in the Na I absorption could be accounted for in different ways:

(i) An interstellar contribution from the central regions and/or from an extended halo compatible with some existing H I detections in early type galaxies,

(ii) An enhancement of W(Na I) with respect to W(Mg I) in the atmospheres of very metal rich late type stars as suggested by synthetic spectra computations.

7. We conclude that the Na I D lines are not of a straightforward use in stellar population synthesis, owing to their contamination by the interstellar contribution. This contribution

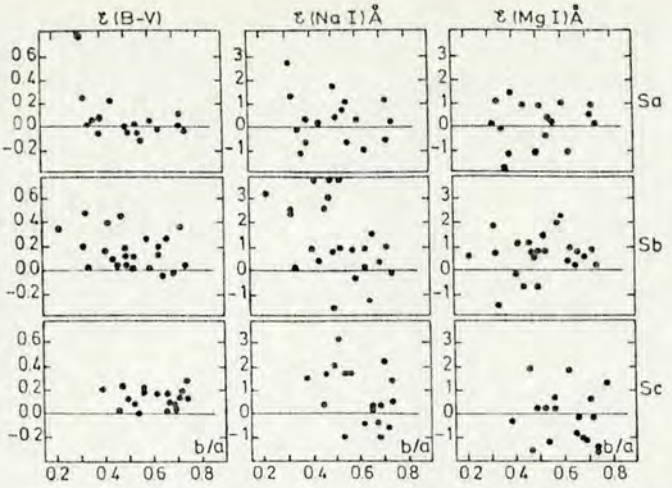

Fig. 8. The Na I excess found for inclined spirals ($b/a \leqq 0.75$), with respect to nearly face-on spiral templates of similar stellar population, as a function of the inclination

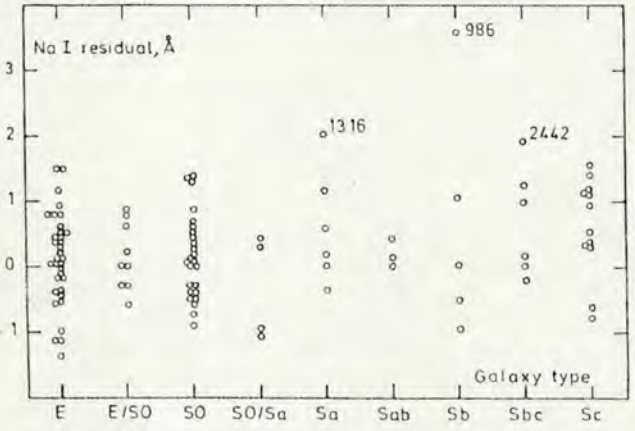

Fig. 9. Residuals in the Na I line, with respect to the GGC plus early type galaxies relationship (Figs. 5a through 5d), for early type galaxies and nearly face-on spirals ($b/a > 0.75$) in our sample

can be substantial, even larger than the stellar one, in spiral galaxies highly inclined.

Acknowledgements. We are gratefully indebted to G. Cayrel de Strobel, R. Cayrel, J. Mould and C. Balkowski for helpful discussions. We wish to thank C. Bentolila who computed the theoretical spectra for dwarf and giant K0 stars with various metallicities. Finally, we acknowledge an efficient assistance from the ESO staff at La Silla and Garching, from the Paris Institute of Astrophysics and from the staff at the Computer Centre in Paris/Meudon Observatory, especially the group who developed the new command system eVe. E.B. thanks the Brazilian Institution CNPq for a fellowship.

References

Allen, C.: 1973, in Astrophysical Quantities, University of London
Baade, W., Minkowski, R.: 1954, *Observatory* **74**, 130
Bell, R., Eriksson, K., Gustafsson, B., Nordlund, Å.: 1976, *Astron. Astrophys. Suppl.* **23**, 37
Bica, E., Alloin, D.: 1986a, *Astron. Astrophys.* **162**, 21
Bica, E., Alloin, D.: 1986b, *Astron. Astrophys. Suppl. Ser.* (in press)
Bica, E., Alloin, D.: 1986c, in preparation
Bica, E., Pastoriza, M.: 1983, *Astrophys. Space Sci.* **91**, 99
Cayrel, R., Cayrel de Strobel, G., Campbell, B.: 1985, *Astron. Astrophys.* **146**, 249
Cayrel de Strobel, G., Cayrel, R.: 1986, private communication.
Cohen, J.: 1973, *Astrophys. J.* **186**, 149
Cohen, J.: 1974, *Astrophys. J.* **194**, 37
Cohen, J.: 1975, *Astrophys. J.* **197**, 117
Cohen, J., Meloy, D.: 1975, *Astrophys. J.* **198**, 545
Faber, S.: 1972, *Astron. Astrophys.* **20**, 361
Faber, S.: 1973, *Astrophys. J.* **179**, 731
Gustafsson, B.: 1982, private communication to G. Cayrel de Strobel
Gustafsson, B., Bell, R., Eriksson, K., Nordlund, Å.: 1975, *Astron. Astrophys.* **42**, 407
Hobbs, L.: 1969, *Astrophys. J.* **157**, 135
Hobbs, L.: 1974, *Astrophys. J.* **191**, 381
Janes, K., Demarque, P.: 1983, *Astrophys. J.* **264**, 206
Knapp, G., Turner, E., Cunniffee, P.: 1985, *Astron. J.* **90**, 454
Münch, G.: 1968, in Nebula and Interstellar matter, Ed. B. Middlehurst and L. Aller, University of Chicago Press, Chap. 7
Pickles, A.: 1985, *Astrophys. J.* **296**, 340
Pritchet, C.: 1977, *Astrophys. J. Suppl.* **35**, 397
Sandage, A., Tammann, G.: 1981, A revised Shapley-Ames Catalogue of Bright Galaxies, Carnegie Institution of Washington
Sersic, J.L.: 1968, Atlas de Galaxias Australes, Observatorio Astronomico de Cordoba
Sparks, W., Wall, J., Thorne, D., Jorden, P., Van Breda, I., Rudd, P., Jorgensen, H.: 1985, *Monthly Notice Roy. Astron. Soc.* **217**, 87
Spinrad, H.: 1962, *Astrophys. J.* **135**, 715
Spinrad, H., Taylor, B.: 1971, *Astrophys. J. Suppl. 22*, 445
Spitzer, L.: 1948, *Astrophys. J.* **108**, 276
Vandenberg, D.: 1983, *Astrophys. J. Suppl.* **51**, 29
Van Gorkom, J., Knapp, G., Raimond, E., Faber, S., Gallagher, D.: 1986, *Astron. J.* **91**, 791
de Vaucouleurs, G., de Vaucouleurs, A., Corwin, H.: 1976, Second Reference Catalogue of Bright Galaxies, the University of Texas
Véron-Cetty, M., Véron, P., Tarenghi, M.: 1982, *Astron. Astrophys.* **113**, 46
Wardle, M., Knapp, G.: 1986, *Astron. J.* **91**, 23
Zinn, R.: 1980, *Astrophys. J.* **241**, 602

ASTRONOMY & ASTROPHYSICS
SUPPLEMENT SERIES

AUGUST 1987, PAGE 281

Astron. Astrophys. Suppl. Ser. 70, 281-301 (1987)

Analysis of absorption-line spectra in a sample of 164 galactic nuclei (*)

E. Bica and D. Alloin ([1])

([1]) Observatoire de Paris, Section de Meudon, 92195 Meudon-Principal Cedex, France

Received October 7, 1986 ; accepted February 23, 1987

Summary. — We present in this paper spectral observations in the range 3700 Å $< \lambda <$ 8000 Å, of 154 normal galactic nuclei, 2 amorphous galaxies, as well as of 8 intrinsically faint active nuclei with their visible spectrum dominated by the stellar component. This sample of galaxies covers a range in luminosity $-23.3 \leq M_B \leq -16.6$ and spans morphological types from E to Sc. We provide measurements of the continuous distribution and equivalent widths W for 14 metallic features, Balmer lines Hα through Hδ, metallic and Balmer line blends Hε through H9. We derive the internal reddening due to inclination in spiral galaxies through comparison with nearly face-on spirals having a similar nuclear stellar population. We analyse the intrinsic scatter of the stellar population content within each group of galaxies around a given absolute luminosity and morphological type. In each group from E to Sb *versus* $-23.2 < M_B < -19.0$, as well as for the very luminous Sbc and Sc galaxies, it is possible to recognize a typical spectrum which is, as a rule in all groups, red and strong-lined. The few atypical nuclei exhibit variable contents of bluer stellar components. Also exceptions are galaxies showing different degrees of activity in their nuclei. For Sbc and Sc galaxies in the range $-21.9 < M_B < -19.0$ however, no prototype can be assigned ; the spectra of these nuclei form a quasi-continuous sequence from red strong-lined to very blue ones, the latter being clearly dominated by a young star formation burst. Analysis of the W measurements indicates that CN λλ4216-4250 is the feature with largest dynamical range as a function of metallicity. As an example of the potential use for stellar population synthesis, of the present set of galaxy templates as well as of star clusters from papers I and II, we analyse empirically the spectra of the blueish early-type galaxies NGC 2865, 4382 and 5102. We conclude that young stars are responsible for the blue colors and find strong evidence that metal-poor stars do not contribute significantly. If the star formation burst is time-peaked, it is $4 \pm 1 \times 10^8$ yr old in NGC 5102 and $12 \pm 3 \times 10^8$ yr old in NGC 2865 and NGC 4382.

Key words : galaxies : stellar content of — galaxies : nuclei of — galaxies : evolution of — stars : formation of.

1. Introduction.

The blue-violet spectral classification of galactic nuclei has revealed that spectral classes do not closely correlate with morphological types (Humason *et al.*, 1956 ; Morgan and Mayall, 1957). In particular late spirals exhibit spectral types from A5 to G5 covering almost the entire range observed in galactic nuclei.

Early type galaxies exhibit both a strengthening of absorption lines and a reddening of colours when their absolute luminosity increases. This is thought to result mainly from metallicity differences ; however some scatter is present which has led to various interpretations (Faber, 1977 ; Sandage and Visvanathan, 1978).

The interpretation of spectral characteristics in nuclear regions of spiral galaxies is more controversial. For example, blue nuclei in late spiral galaxies have been interpreted in terms of a low metallicity, on the basis of their line-strengths in the blue spectral range being similar to those observed in metal-poor globular clusters (McClure *et al.*, 1980 ; Cowley *et al.*, 1982). However, *UBV* colours of Sc nuclei cannot be reproduced from a mixture of globular clusters only (O'Connell, 1982). Balmer line profiles in the blueish nucleus of NGC 7793 indicate that this object is light-dominated by A and early F main sequence stars rather than blue horizontal branch stars like in metal-poor globular clusters (Diaz *et al.*, 1982). Furthermore, the extension of the visible photometry to the infrared has demonstrated that no significant contribution from metal-poor stars is allowed, at any wavelength, in Sc nuclei (Frogel, 1985).

In this paper, we present spectral observations in the wavelength range 3700-8000 Å of a sample of galaxies with absolute luminosities M_B from − 16.6 to − 23.3 and

Send offprint requests to : D. Alloin.

(*) Based upon observational data collected at the European Southern Observatory.

morphological types from E to Sc. The sample includes 154 normal galaxies, 2 HII region nuclei in amorphous galaxies and 8 Seyfert galaxies having an active nucleus intrinsically faint enough so as to exhibit a spectrum dominated by the stellar component in the visible. The spectra will be population-synthesized in a forthcoming paper, using a base of star clusters defined by two parameters, age and metallicity. In that aim, we have built a grid of star cluster spectral properties, obtained from integrated spectra (Bica and Alloin, 1986a, 1986b, hereafter Papers I and II). The main purpose of the present study is to outline the different stellar populations which can be found within a given interval of galaxy luminosity *versus* morphological type. In view of the population synthesis, we group objects with similar spectral properties which might be described by the same model, and hence define templates. We also give some results concerning age and metallicity effects, which can be readily drawn from our galaxy sample, although straightforward conclusions will possibly be stated in a quantitative form only from the simultaneous synthesis of many spectral features and continuous distribution in the visible and near infrared, in a paper to come.

The definition of the sample and the observational data are reported in section 2. The set of equivalent widths, W, and continuum measurements are given in section 3. A specific method to determine the intrinsic reddening in spiral galaxies, resulting from galactic inclination, is described in section 4. In section 5 we present a set of prototypes corresponding to different type-luminosity groups, and we mention the atypical spectra. The dependences of W and continuum measurements on the morphological type and luminosity are discussed in section 6. Finally, examples of empirical population synthesis using template galaxies and star clusters are given in section 7, together with the conclusions of this study.

2. Definition of the galaxy sample and observational conditions.

2.1. CHOICE OF THE SAMPLE. — The primary objective of this program was to collect spectra of southern galaxies, as far as possible free from emission lines, spanning ranges in absolute magnitude, $-23 < M_B < -17$, and in morphological type, E to Sc. Being interested in synthesizing absorption spectra, at first we selected only objects without emission lines, as reported in redshift surveys mostly based upon blue spectral data. From our observations however, many of these galaxies turned out to show emission lines in the red, Hα6562, [NII]6548-84 and [SII]6717-31. Hence we decided to extend our sample as to include other normal galaxies known to contain emitting gas, as well as some liner prototypes, in view of a future analysis of the emission component. We also observed a few northern galaxies, especially Virgo members, in order to have some overlap with earlier spectral analysis. The objects originally selected under the absorption line criterion represent 55 % of the total sample of 154 normal galaxies. In addition, we observed the HII region nucleus of two amorphous galaxies, NGC 625 and 5253 (in the former, the brightest knot lying slightly off-center). This class consists of structurally normal low-luminosity early type galaxies, whose appearance has been altered by recent star formation (Véron and Véron-Cetty, 1985 and Refs. therein). Last, we included eight Seyfert or Seyfert-to-liner transition galaxies with their optical spectrum dominated by the stellar component.

Global properties and observational data for these galaxies are summarized in table I. Galaxy parameters are from Sandage and Tammann (1981), with the exception of a few (see the Tabl. notes). Throughout the paper we adopted $H_0 = 50\ \mathrm{km\ s^{-1}\ Mpc^{-1}}$. Following the columns order, we provide (1) the NGC or IC number, (2) the radial velocity, (3) the absolute blue magnitude, (4) the morphological type, (5) the extrinsic reddening $E(B\text{-}V) = 0.25\,A_B$ where the Galactic absorption A_B is from the cosec law with absorption-free polar caps (Sandage and Tammann, 1981), and (6) the axial ratio b/a derived from log R_{25} (de Vaucouleurs *et al.*, 1976). In the case of NGC 692, a bright southern galaxy so far lacking published parameters, we derived them from our data and the ESO B survey as described in the table notes.

The sample distribution, in terms of absolute magnitude and morphological type is shown in table II. The galaxy NGC 4039, classified by de Vaucouleurs *et al.* (1976) as Sm pec was grouped here with Sc galaxies. Indeed it has a small nucleus, like an Sc, and its irregular appearance results from its interaction with NGC 4038. Seyfert galaxies are given separately (+ sign). The sample is well represented in all morphological types from E to Sc, for galaxies brighter than $M_v = -20$. We recall there is evidence that spiral galaxies from Sa to Sc, fainter than $M_B \sim -17$ do not exist (Sandage *et al.*, 1985).

2.2 OBSERVATIONAL CONDITIONS. — The observations were carried out with the IDS attached to the Boller and Chivens spectrograph at the ESO 1.52 m telescope (La Silla) during three runs : July and November 1984 and May 1985. The slit size was set to 5″ × 8″, except in a few cases specified in the notes to table I. The slit length was always set E-W, but for NGC 4594 where it had been aligned with the minor axis of the galaxy. We provide in column (7) of table I, the corresponding slit size in kpc. The mean area covered by our observations of galactic nuclei is 0.8 (± 0.5) kpc × 1.4 (± 0.9) kpc, the extreme values being for NGC 692 (3 kpc × 4.8 kpc) and NGC 625, 5236, 5253 (0.2 kpc × 0.3 kpc).

Low resolution spectra are particularly suitable for synthesizing stellar populations in galactic nuclei which, quite often, display large velocity dispersions. Therefore, we used a 300 gr/mm grating over the range 3700-

8200 Å. A final resolution of 11 Å was achieved with 5″ slit width, as measured by the mean FWHM of the comparison lines. We give in column (8) in table I, the total exposure for each object. Two or three standard stars were observed each night for flux calibration. A classical reduction procedure was applied, using the IHAP system at ESO (Garching) and at the IAP (Paris). The present set of galactic spectra and the set of integrated star cluster spectra from papers I and II, have been reduced in a similar way, many objects in the two samples having been observed on common nights.

3. The data set : results.

The galactic spectra have been corrected for external reddening, using $E(B\text{-}V)$ values from table I and a normal reddening law, $A_\lambda = 0.65\, A_v(1/\lambda - 0.35)$ where $A_v = 3\, E(B\text{-}V)$. Then, they have been rebinned to zero redshift from the velocities in table I and normalized to the continuum at 5870 Å. The useful wavelength range from 3780 to 7690 Å was split into 70 consecutive windows, as defined previously for the star cluster spectra in paper I. The widths of these windows, from 24 to 190 Å, are suitable for avoiding problems due to possible differences in velocity dispersion among the galaxies and/or with respect to the star clusters. We provide in table III, columns (2) and (3), the signal to noise ratios respectively for the blue region $3800 < \text{Å} < \lambda < 4500$ Å, $(S/N)_B$, and for the red one $4500 \text{ Å} < \lambda < 7500$ Å, $(S/N)_R$.

To make easier the comparison of W and of the continuum distributions among normal galactic nuclei, we present the measurements in table III, classified in groups of morphological types *vs.* luminosity. In each group, the galaxies have been ordered by decreasing luminosity. The results for amorphous and Seyfert galaxies are given separately at the end of the table. Some galaxies in the latter group are rather transition objects between Seyferts and liners. We kept them apart from the rest of the sample because a nonstellar contribution might be present in their continuum.

Taking into account our previous analysis of measurement accuracy and feature strength for star cluster spectra in paper I, we give in table III only the most significant window measurements for the galaxy set. In some strong-lined galaxies observed with a high signal to noise ratio however, other features could be accurately estimated and many weaker ones are definitely present. The main absorbers in each window are indicated in table III headings, and a detailed compilation of all possible contributors can be found in paper I (Tab. II).

The set of selected windows for galaxies consists of the 13 metallic features and 4 Balmer lines for which a grid W (age, $[Z/Z_\odot]$) has been built from the star cluster sample (paper II). We have also considered the blends CaII + Hε, H8 + CN Lband + Fe, and H9 + CN Lband + Fe, which, in general, appear as very strong features in galaxy spectra. We provide too W(NaID), which, owing to the contamination by the interstellar component, is discussed elsewhere (Bica and Alloin, 1986c). Last, we present results for window # 62, which contains a rather weak absorption — even in strong-lined ellipticals — but encloses the [SII]6717, 31 lines and hence, is a good indicator of the emission line contamination in galaxy spectra.

Emissions in table III, distinguished by a negative sign, are not to be taken at face value since no attempt was made to disentangle them from the underlying absorption features, nor to deblend them from other nearby emission lines (e.g. Hα + [NII]). A more careful analysis of these emission features will be presented in a paper to come, using synthetic absorption line spectrum subtractions. In addition to the Hα through Hδ lines, also the following windows are possibly contaminated by emission in some galaxy spectra : # 3([NeIII]3869, H9 and HeI3889), # 31 ([OIII]5007) and, to a lesser extent, # 5([NeIII]3967, Hε). The relative importance of the emission contamination for a given normal galaxy, as seen in our windows defined for absorption feature purposes, can be estimated through a comparison with the HII region nuclei of the amorphous galaxies and with the Seyfert nuclei in table III, or even with the HII regions presented in paper II. A straightforward emission correction for [OI]6300 and in some cases [FeX]6374, was applied to the values W(TiO) denoted by the letter a in table III.

Continuum points F_λ, normalized to the continuum at 5870 Å, C(5870), from spectra corrected for external reddening, are also shown in table III.

4. Internal reddening due to the inclination in spiral galaxies.

The large number of spiral galaxies in our sample with different inclination angles, together with the 4000 Å range of continuum covered by our observations allow us to estimate the internal reddening. We compare the observed continuous distribution of a given inclined spiral to that of a nearly face-on template ($b/a \geq 0.75$) *with a similar population content.* The criterion used to search for similar populations is the minimization of W_{gal}-W_{templ} for metallic features distributed over this wide wavelength interval. We considered the strongest metallic features which are free from emission line contamination, i.e., CaIIK, Gband, Mg + MgH and TiO. The latter was corrected for a possible contribution from [OI]6300, 6364 and [FeX]6374 (Sect. 3). These emission lines can be detected down to the 0.5 Å level, and, if weaker, their contribution is negligible with respect to W(TiO).

The equivalent widths W of metallic features towards the blue are sensitive to the younger age components,

while those in the red provide an estimate for the metallicity, as can be seen in the integrated spectra of star clusters in papers I and II. Balmer lines are not suitable for population comparison, due to their possible contamination by emission components. On the other hand, their presence with a variable strength in galactic nuclei, does not necessarily imply a subtantial population difference among nuclei of otherwise similar metallic feature strengths. Indeed if nuclear emission lines arise from HII regions, their observed weak intensities in galactic nuclei imply a negligible optical continuum from the gas and ionizing star cluster with respect to the underlying older stellar population. The nonstellar continuum in liners is expected to be negligible (Keel, 1983). This is generally not the case for Seyfert nuclei (e.g. Alloin *et al.*, 1985). For the stronger Seyfert nuclei in our sample however, the nonstellar continuum should not exceed 25 % in the blue and 10 % in the red. Thus, we also applied this method for deriving the internal reddening in inclined Seyferts ; we assumed that a small contribution from the nonstellar continuum mimics a slightly bluer population.

Although rather similar populations may exist in early or late spiral types, we have restricted our search for templates within 1.5 morphological class intervals. Results are shown in table IV, where we give for each inclined spiral, the nearly face-on templates considered, the internal reddening $\varepsilon(B\text{-}V)$ due to inclination and the corrected continuum points. We show in figure 1, two examples, respectively for a red and a blue nucleus, where we compare the observed and the reddening corrected spectra to those of the templates. Note the stronger W(NaID) in the inclined spirals, enhanced by the interstellar contribution from gas in the discs (Bica and Alloin, 1986c).

A thorough discussion on the internal reddening $\varepsilon(B\text{-}V)$ and NaID excess, ε(NaI), as a function of inclination is presented in Bica and Alloin (1986c). We emphasize that the behaviour of $\varepsilon(B\text{-}V)$ and ε(NaI) as a function of spiral type (Fig. 8 in Bica and Alloin, 1986c) is consistent with the expected higher dust and gas content towards later morphological types, although our sample lacks highly inclined Sc galaxies owing to the intrinsic faintness of the nucleus in this morphological type.

Such an analysis allowed us, not only to identify spirals with similar population to be later described by the same model, but also to eliminate a free parameter from the synthesis, that is the internal reddening due to inclination which can be very important in some cases like NGC 5746 (Fig. 1).

5. The population content within each type/luminosity group.

A simple comparison of W and continuous distributions for galaxies within a particular type/luminosity group (Tabs. III and IV), provides an estimate of the degree of inhomogeneity of populations in that group. We have displayed in figure 2 a selection of typical and atypical nuclear spectra found in different groups. Every galaxy is labelled with the external and internal reddening corrections which were applied to the continuum, according to sections 3 and 4. For the sake of simplicity, we shall assign to luminosity groups in table III the following notation, I′, II′, III′ and IV′, inspired by luminosity classes for late spirals.

For very luminous ellipticals, the E I′ group, a prototype spectrum is that of IC4296, with a red continuous distribution and very strong absorption lines. The only peculiar spectrum in our sample, for this group, is that of NGC 4486 (M87). Although weak emission lines are present in most of our early type galaxies with $M_B < -20$, in none of them are they as strong as in NGC 4486. Whatever the nature of the associated continuum, either nonstellar or from a burst of star formation, it is negligible in the optical range. Indeed, the continuous distribution as well as the strength of metallic features in NGC 4486 are indistinguishable from those of other strong-lined ellipticals.

The E II′ group prototype, illustrated by NGC 1399, is much like the E I′ one. One exception in this group is NGC 2865, where a bump centred at about 4600 Å and associated with a strengthening of the Balmer lines, is quite obvious. As shown in section 7 this bump arises neither from a very young residual star formation nor from old metal-poor stars, but rather from an intermediate age burst of star formation. The galaxy NGC 5061 represents an intermediate case between the group prototype and NGC 2865. This interpretation of the bump would imply that elliptical galaxies suffer occasional bursts of star formation, which are more or less conspicuous according to their age and strength. If they are older than 2×10^9 yr, no bump would be seen any more, although strong Balmer absorption lines should remain, as is the case in intermediate age Galactic open clusters and Magellanic Cloud clusters. Only a detailed synthesis will give precise information on the relative importance of such intermediate age bursts with respect to the underlying population, as well as on their age distribution. On the other hand, the optical signature of recent residual star formation in giant early type galaxies will be difficult to detect if it is related to the ultraviolet upturn observed in some of these galaxies.

A similar picture is observed for the E III′ group, with NGC 3379 as a prototype and NGC 4742 its bluer exception. In the low luminosity group, E IV′, the sample is small and possibly atypical. Two kinds of spectra can be seen ; firstly, NGC 4387, which resembles the strong-lined prototypes of the previous groups. This galaxy, together with NGC 4486B (Tab. III) are faint high surface brightness objects in the centre of the Virgo cluster, possibly tidally stripped by close encounters with

giant neighbours (Faber, 1973 ; Sandage and Binggeli, 1984). For the second type of spectrum, NGC 4476 exhibits a continuous distribution like that of NGC 5061, the intermediate case in the E II′ group. A fundamental difference, however, is that metallic features are systematically weaker in NGC 4476, both in the blue and red ranges, suggesting a lower metal content. Indeed, its spectrum looks like that of globular clusters in the range $-1.0 \leqslant [Z/Z_{\odot}] \leqslant -0.5$ (Paper I). Again, a detailed synthesis is necessary to test this assumption or to check whether such a spectrum could be reproduced from mixtures of clusters covering a wider range in metallicity or even age.

The S0 groups are very similar to the E ones : we show in figure 2(b), successively a typical S0 I′ NGC 5419, then NGC 7744 and 4382, respectively a red prototype of the S0 II′ group and the counterpart of the elliptical NGC 2865 presenting a bump around 4600 Å. For the S0 III′ group, we display NGC 3115, all other objects in that group being also red and strong-lined. From the low luminosity group, S0 IV′, we show NGC 3056 having a moderately weak-lined spectrum. Finally, we present NGC 5102 whose spectrum resembles that of blue star clusters in paper I. In this case, obviously a recent burst of star formation has occurred in the nucleus, prevailing over the older underlying population (Sect. 7).

The various Sa luminosity groups are the most homogeneous in our sample, both internally and one with respect to the others. They all show red strong-lined spectra like the prototypes in the E and S0 groups and we show in figure 2(c) only the prototype for the Sa II′ group, IC5267. One exception is NGC 7213, which presents emission lines much stronger than the other Sa galaxies although the underlying stellar population remains similar.

The prototype for the Sb I′ group, NGC 1398, does not differ much from those in the earlier groups of the same luminosity class (Fig. 2(c)). An atypical case is that of the blue nucleus in NGC 4569 (Tab. III) which is due to contamination from a young stellar component, a common phenomenon in later morphological types (Sect. 6). Prototypes for the Sb II′ and Sb III′ groups, respectively NGC 3521 (Fig. 2(c)) and NGC 4462, also have red spectra although not as strong-lined as those for the earlier groups. Examples of atypical nuclei are the blueish object NGC 3351, as well as the red nuclei NGC 4438 and 6300 hosting a liner and a Seyfert nucleus respectively. They will be discussed in detail in a paper to come.

Finally we come to the Sc groups which are less homogeneous. Luminous Sc I′ can be represented by NGC 692 with a red strong-lined spectrum (Fig. 2(c)), except for NGC 4536 which shows signs of a bluer component. No prototype could be found for the Sc II′ group : it is more like a sequence from the red case of NGC 6923 through moderately blue objects like NGC 6215 (Fig. 2(c)) to the very blue objects shown in figure 1(b) containing obviously a young stellar component. The less luminous Sc III′ group is likewise extremely heterogeneous and it is not possible to define any prototype.

6. Discussion.

6.1 ANALYSIS OF THE MEASUREMENTS AS A FUNCTION OF MORPHOLOGICAL TYPES. EFFECTS OF AGE CONTAMINATION ON W FOR METALLIC FEATURES. — We plot in figures 3(a), through 3(e) the equivalent width W for the strongest metallic features as a function of morphological type, in a sequence of increasing wavelength. Part of the late type spiral galaxies present very low W values for metallic features in the blue spectral range. On the other hand, for TiO a metallic feature in the red, W values are large for the whole spiral sample, suggesting that spiral nuclei are not metal-poor (Fig. 3(e)). Indeed, in the integrated spectra of star clusters, W for metallic features in the red tend to be univalued functions of metallicity, regardless of age, while those in the blue present also an age dependence, owing to dilution by blue stars in young clusters (Paper I).

Continuum slopes of the spectra also corroborate the interpretation in terms of young age contamination rather than of low metallicity, as the source of low W values in many spiral galaxies. This is shown in figure 4 where we give the spectral slope expressed as the F_{λ} ratio C (4020/7520 Å), as a function of morphological type. We also recall in this figure the values for metal poor Galactic globular clusters (MPGGC) having $[Z/Z_{\odot}] = -2$ and $[Z/Z_{\odot}] = -1$ (Papers I and II). Spiral galaxies showing small W values for metallic features in the blue are those with continuum slopes much steeper than that of MPGGC, resembling rather the continuum slopes observed in young blue clusters as recalled in figure 4 (Papers I and II). Compare also these blue spiral galaxies with two amorphous galaxies in the upper left corner of figure 4, which are HII region nuclei with essentially no contribution from the underlying old population. Measurements displayed in figure 4 correspond to continua corrected for the instrinsic reddening $\varepsilon(B\text{-}V)$ due to inclination in spiral galaxies (Tab. IV). Non-corrected values for the blue galaxies, indicated by arrows in figure 4, do not alter the above interpretation because face-on galaxies remain unchanged and inclined ones, which enter the MPGGC zone, still differ from the latter by their stronger W(TiO) values.

We show in figure 5, W *vs.* W plots for two metallic features in the blue, CaIIK and G-band (Figs. 5(a) through 5(c)), and for one metallic feature in the blue CaIIK against one in the red, TiO (Figs. 5(d) through 5(f)). Groups of morphological types E + S0, Sa + Sb, Sc have been considered. Following Burstein (1979) and Heckmann (1980) we attempt to identify the direction of

age and metallicity effects. We provide in figures 5(c) and 5(f) corresponding to the Sc type, the loci of star cluster values (Papers I and II). We indicate two youth vectors for solar metallicity clusters : Y_1 from a Galactic globular cluster (1.65×10^{10} yr) to a cluster 10^9 yr old, and Y_2 from the latter cluster to a very young one, 10^7 yr old. We also show two metallicity vectors for Galactic globular clusters : M_1 from a solar metallicity cluster to one with $[Z/Z_\odot] = -1$, and M_2 from the latter to a cluster having $[Z/Z_\odot] = -2$. Young age and low metallicity directions merge in the W(CaIIK) *vs.* W (G-band) diagram, while a separation exists for the W(CaIIK) *vs.* W(TiO) one. In this graph, Sc galaxies with small W(CaIIK) follow the young age sequence rather than the metallicity one. This is a further evidence, in addition to those quoted by O'Connell (1982), Diaz *et al.* (1982) and Frogel (1985), that the spectral indices defined by McClure *et al.* (1980) and Cowley *et al.* (1982) are not measuring metallicity differences in spiral galaxies. Indeed, all the metallic features in their spectral indices are situated in the blue-green part of the spectrum and are thus subject to dilution effects in nuclei with important young age contributions. McClure *et al.* (1980) argued that, for a composite population with a range in $[Z/Z_\odot]$, one sees light predominantly from the metal-poor population in the ultraviolet and from a more metal-rich one in the red. However, we point out that, in the range covered by our observations and over which the spectral indices used by McClure *et al.* (1980) are defined, a metal-poor population mixed to a metal-rich one would dilute metallic features as much in the blue as in the red since its continuum distribution is flat (a combination of almost featureless cool metal-poor giants in the red and blue horizontal branch stars in the blue).

Comparisons of galaxies with star clusters in a W *vs.* W diagram are useful to follow the direction of age and metallicity effects. They cannot be used straightfordwardly to assign mean metallicities or ages to individual galaxies because in general, the resulting point for a mixture of two star clusters in a W *vs.* W plot does not necessarily lie on a straight line joining them, owing to their respective underlying continua. The best approach is rather to reproduce the galaxy spectrum empirically, as described in section 7, or to calculate a synthetic spectrum using a large number of features and continuum points over a wide range, as will be presented in a forthcoming paper.

It is interesting to note that in our sample, containing mostly luminous galaxies, the range in W(TiO) values for spiral galaxies is essentially the same as that found for early type galaxies (Fig. 3(e)). This result suggests that the range in metallicities in spiral bulges is comparable to that in the central regions of luminous E and S0 galaxies. Only the lenticular galaxy NGC 5102 which presents an important young age component (Sect. 7) exhibits a very small W(TiO) value, possibly tracing out a genuine metal deficiency compatible with its low luminosity too. However, TiO shows a rather complex behaviour as a function of age amoung young star clusters. Rapid red phases occur, due to asymptotic giant branch stars with massive progenitors and to red supergiants, which can be seen more clearly through molecular bands in the near infrared (Bica and Alloin, 1987a). Examples of this phenomenon are the star clusters NGC 2004, 10^7 yr old with strong TiO from red supergiants, NGC 2157, slightly older with weak TiO owing to the absence of such luminous cool stars, and NGC 1866, 10^8 yr old with massive AGB stars producing strong TiO absorption. Such a variable content in young massive red stars does not affect our conclusions about blue spirals derived from figure 5(f). On the contrary, the fact that TiO is quite strong indicates that red supergiants contribute to the flux in blue spiral nuclei and thus confirms the presence of a young age component rather than that of an old metal-poor one.

We also call attention in figure 3(b), to the fact that CN can reach relatively smaller W values than the neighbouring features CaII K and G-band. This cannot be assigned to different dilution factors by blue stellar components because of the wavelength proximity of the three features. Furthermore, this effect is particularly prominent in early type galaxies where the continuum is reddish. We can explain this effect by the stronger CN dependence on metallicity, according to our results for GGC in paper I, where the slope $\Delta W(\mathrm{CN})/\Delta[Z/Z_\odot]$ becomes remarkably steep for $[Z/Z_\odot] > -0.5$, the metallicity range expected for galaxies brighter than $M_v = -18$. This result suggests than CN λλ4150-4216 is the metallicity indicator with largest dynamical range in the visible. Indeed, CN is in general the feature showing the strongest radial gradients in individual galaxies and was used alone as a probe of metallicity gradient (Spinrad *et al.*, 1971 ; Joly and Andrillat, 1973 ; Spinrad and Stone, 1975 ; Burstein, 1979).

The behaviour of Balmer lines *vs.* morphological type is quite complex. First, their W is not an univalued function of age in the integrated spectra of star clusters and for very metal rich red clusters, underlying metallic features become important, especially in the Hγ window (Paper I and II). Moreover, in galactic nuclei, emission is an additional complication. In the Hδ window emission is generally negligible, in the Hγ one the age, metallicity and emission effects are of the same order and for Hβ the emission may be prominent in a few cases. For Hα however, the emission dominates in most nuclei : in those nuclei where Hα appears in absorption, W for the higher Balmer lines can be safely used in population synthesis.

In figure 6 we show W histograms for 17 metallic features, only E and S0 galaxies being considered since they are expected to be less affected by age effects. We have excluded from this subsample, the objects NGC 2865, 4382 and 5102 in which we know that age

effects are important (Sect. 7). We have computed W normalized to its maximum value in the considered window. We have examined not only purely metallic features but also a few windows in which Balmer lines are blended with metallic absorptions (windows # 2, # 3 and # 5). The assumption that age effects are negligible on the metallic-Balmer blends for this subsample can be tested by comparing the CaII K and CaII H + Hε W distributions which are not very different one from the other. The large dynamical range of CN # 11 is remarkable. The two adjacent windows, FeI # 10 and CaI # 12 share the same property, probably because of some CN contamination. The flat distribution of the W/W_{max}(CN) histogram is confirmed to result indeed from a high sensitivity to metallicity rather than to be due to error bars or continuum dilution, from figure 7 where we compare CN as well as the neighbouring features CaII K and G-band, to MgI + MgH which is considered to be a good metallicity indicator (e.g. Terlevich *et al.*, 1981). The two histograms in figure 6 which correspond to the CN Lband, show a dynamical range intermediate between those of CN # 11 and of the other metallic windows. We assign this to strong iron lines in windows # 2 and # 3 which must contribute significantly to the absorption (Paper I). The absorption line of NaI (window # 48) in elliptical and S0 galaxies in possibly enhanced by an interstellar gas component. The latter should behave however like the stellar NaI component due to the expected larger gas content in more massive galaxies (Bica and Alloin, 1986c).

6.2 ANALYSIS OF THE MEASUREMENTS AS A FUNCTION OF ABSOLUTE MAGNITUDE. — As seen in figure 7(b), W(CN) and W(Mg + MgH) are the most sensitive metallic features. Thus, we use them jointly to analyse the relationship between metallicity and absolute magnitude among early type galaxies. The scatter present in this relation (Faber, 1977 ; Sandage and Visvanathan, 1978) deserves a careful analysis and a complete discussion is given in Bica and Alloin (1987b). For our galaxy sample we find that the scatter observed in the W(CN) + W(Mg + MgH) *vs.* M_B diagram reflects genuine population differences among the objects.

Regarding the spiral galaxy sample the occurrence of strong age effects, especially in late types, precludes any concluding remark to be derived from the analysis of their line strength *vs.* absolute magnitude diagrams. The important dilution of metallic lines in the blue requires a detailed population synthesis to be carried out. This will be done in a forthcoming paper for the relevant objects in our sample.

7. Empirical population synthesis for blueish E and S0 galaxies and concluding remarks.

We demonstrate the potential use of the present set of galactic templates and star clusters from papers I and II for extracting information about the star formation history in galaxies, by applying an empirical synthesis to the spectra of the blueish early type objects NGC 2865, 4382 and 5102. Because they show a very similar spectrum, we synthesize a mean of NGC 2865 and 4382. In order to estimate the contribution from the redder underlying population, we have built high signal to noise ratio templates in each case. For NGC 5102, it has been derived from 10 emission-free E and S0 galaxies with $-19.3 \leq M_B \leq -18.0$ so as to consider objects with a comparable metal content. For NGC 2865 and 4382, the template has been built from 17 emission-free E and S0 galaxies with $-21.9 \leq M_B \leq -21.0$. We define R(5870) as the flux ratio, at 5870 Å, of the template to the studied object and find out the best R value so as to reproduce a real star cluster spectrum. The best fit we find for NGC 5102 is $R(5870) = 0.30 \pm 0.10$ and for the mean spectrum of NGC 2865 and 4382, $R(5870) = 0.50 \pm 0.05$. In figure 8(a), we have displayed the following downward sequence : NGC 5102, its template a, the difference [NGC 5102 – (0.30 × template a)], the mean of NGC 2865 and 4382, the corresponding template b and the difference [NGC 2865, 4382 – (0.50 × template b)]. These differences are compared to integrated spectra of star clusters of various ages in figure 8(b) : this allows to identify the age of the burst. In the case of NGC 5102, the residual spectrum is intermediate in shape, between those of NGC 1831 and NGC 1868, suggesting a burst age of $4 \pm 1 \times 10^8$ yr. Although these two clusters belong to the Magellanic Clouds, metallicity effects are expected to be negligible because of their young age and because NGC 5102 itself has a total luminosity comparable to that of the LMC. Regarding NGC 2865, 4382, the difference spectrum matches that of the solar content Galactic cluster NGC 2660, leading to an age of $12 \pm 3 \times 10^8$ yr ; for $R(5870) \neq 0.50$ none of the residual continuum distributions provides a satisfactory fit to real cluster spectra. A detailed comparison of NGC 2660 with the difference spectrum for NGC 2865, 4382 shows that the latter has stronger metallic lines and in its short wavelength region suffers from a large line blanketing. This effect can be attributed to a metal content larger than solar as expected for a moderately young stellar generation in massive E or S0 galaxies. An attempt to cancel the metallic lines, that is $R \geq 0.70$, produces a steep spectrum with negligible flux in the red, very different from that observed in the metal poor globular cluster NGC 7078 (Fig. 8(b)). This result suggests that blue horizontal branch stars are not responsible for the blue colours of NGC 2865 and 4382 unless they are present without metal poor giants, an implausible picture. The burst ages empirically derived above, assume a time-peaked burst duration. Different combinations of clusters in the range $10^8 - 3 \times 10^9$ yr like the Galactic open clusters NGC 6705 and 2158 (Fig. 8(b)), or even younger, may give similar results. Information on the duration of the bursts will possibly be derived by

considering a wider wavelength range, that is, near infrared spectra of star clusters and galaxies (Bica and Alloin, 1987a). A burst of star formation occurring 1 Gyr ago in the S0 NGC 4382, a Virgo member, might at first sight contradict the conclusion reached in section 6 that cluster giant galaxies stopped forming stars before field galaxies. However, NGC 4382 forms a close pair with the spiral NGC 4394 and the burst could be related to this interaction.

The fact that a simple decomposition into a burst and an old underlying population is possible for the blueish E and S0 galaxies above, is perhaps not fortuitous. Similar attempts in the case of spiral nuclei were not successful, more complicated combinations being required. This result points towards a more continuous character of the star formation in spiral nuclei.

Conclusions of the present work are as follows :

(1) We present results for 164 spectra of galactic nuclei in the luminosity range $-23.3 \leq M_B \leq -16.6$, from E to Sc morphological types.

(2) Measurements are provided both for the continuum distribution and the equivalent widths of 22 features.

(3) We derive the internal reddening due to inclination in spiral galaxies through comparison with nearly face-on templates having a similar nuclear stellar population. The knowledge of the internal reddening removes one free parameter for the future population synthesis.

(4) It is possible to find spectral prototypes for galaxies E to Sb with $-23.3 \leq M_B \leq -19.0$, as well as for luminous Sbc and Sc galaxies. These prototypes are, as a rule, red and strong-lined. Less luminous Sbc and Sc's are distributed along a quasi-continuous sequence from red strong-lined to very blue objects, the latter being clearly dominated by young stars.

(5) The CN absorption band λλ4216-4250 is the metallicity indicator with largest dynamical range.

(6) A tentative population synthesis using galaxy templates and star clusters indicates that for time-peaked bursts of star formation, they occurred $4 \pm 1 \times 10^8$ yr ago in NGC 5102 and $12 \pm 3 \times 10^8$ yr ago in NGC 2865 and 4382. We exclude the possibility that blue horizontal branch stars contribute significantly to the integrated light in these galaxies.

Acknowledgements.

We are gratefully indebted to the ESO staff at La Silla and Garching, to the Paris Institute of Astrophysics and to the staff at the Computer Centre in Paris/Meudon Observatory, especially the group who developed the new command system eVe. We thank Pr. B. Pagel for interesting comments and suggestions. E. B. thanks the Brazilian Institution CNPq for a fellowship.

References

ALLOIN, D., PELAT, D., PHILLIPS, M., WHITTLE, M. : 1985, *Astrophys. J.* **288**, 205.
BICA, E., ALLOIN, D. : 1986a, *Astron. Astrophys.* **162**, 21 (Paper I).
BICA, E., ALLOIN, D. : 1986b, *Astron. Astrophys. Suppl. Ser.* **66**, 171 (Paper II).
BICA, E., ALLOIN, D. : 1986c, *Astron. Astrophys.* **166**, 83.
BICA, E., ALLOIN, D. : 1987a, *Astron. Astrophys.*, in press.
BICA, E., ALLOIN, D. : 1987b, *Astron. Astrophys.*, in press.
BURSTEIN, D. : 1979, *Astrophys. J.* **232**, 74.
COWLEY, A., CRAMPTON, D., MCCLURE, R. : 1982, *Astrophys. J.* **263**, 1.
DIAZ, A., PAGEL, B., EDMUNDS, M., PHILLIPS, M. : 1982, *Mon. Not. R. Astron. Soc.* **201**, 49P.
EASTWOOD, T., ABELL, G. : 1978, *Publ. Astron. Soc. Pac.* **90**, 367.
FABER, S. : 1973, *Astrophys. J.* **179**, 731.
FABER, S. : 1977, in *Evolution of Galaxies and Stellar Populations*, B. Tinsley and R. Larson (Eds) (New Haven : Yale University Observatory) p. 157.
FROGEL, J. : 1985, *Astrophys.* **298**, 528.
HECKMANN, T. : 1980, *Astron. Astrophys.* **87**, 142.
HUMASON, M., MAYALL, N., SANDAGE, A. : 1956, *Astron. J.* **61**, 97.
JOLY, M., ANDRILLAT, Y. : 1973, *Astron. Astrophys.* **26**, 95.
KEEL, W. : 1983, *Astrophys. J.* **269**, 466.
LAUBERTS, A. : 1980, The ESO/Uppsala Survey of the *ESO (B) Atlas*.
MCCLURE, R., COWLEY, A., CRAMPTON, D. : 1980, *Astrophys. J.* **236**, 112.
MORGAN, W., MAYALL, N. : 1957, *Publ. Astron. Soc. Pac.* **69**, 291.
O'CONNELL, R. : 1982, *Astrophys. J.* **257**, 89.
SANDAGE, A., TAMMANN, G. : 1981, *A revised Shapley-Ames Catalogue of Bright Galaxies* (Carnegie Institution of Washington).
SANDAGE, A., BINGGELI, B. : 1984, *Astron. J.* **89**, 919.

SANDAGE, A., BINGGELI, B., TAMMANN, G. : 1985, *Astron. J.* **90,** 395.
SANDAGE, A., VISVANATHAN, N. : 1978, *Astrophys. J.* **225,** 742.
SPINRAD, H., GUNN, J., TAYLOR, B., MCCLURE, R., YOUNG, J. : 1971, *Astrophys. J.* **164,** 11.
SPINRAD, H., STONE, R. : 1975, *Astrophys. J.* **201,** 563.
TERLEVICH, R., DAVIES, R., FABER, S., BURSTEIN, D. : 1981, *Mon. Not. R. Astron. Soc.* **196,** 381.
DE VAUCOULEURS, G., DE VAUCOULEURS, A., CORWIN, H. : 1976, *Second Reference Catalogue of Bright Galaxies,* the University of Texas.
VÉRON, P., VÉRON-CETTY, M. P. : 1985, *Astron. Astrophys.* **145,** 433.

TABLE I. — *Data for the sample.*

NGC/IC	v Km/s	MB	Type	E(B-V)	b/a	Slit (kpc)	Expos. (min)	Notes
289	1618	-21.41	SBbcI-II	0	.72	89x1.42	40	
488	2268	-22.86	SabI	0	.78	1.18x1.89	36	
524	2377	-21.93	S0/Sa	0	.98	1.24x1.99	30	
584	1875	-21.80	S0(3.5)	0	.63	97x1.54	20	
625	403	-17.35	Am/IaIII	0	.44	.17x .27	20	#1
692	6281	-23.96	Sc	0	.91	3.00x4.79	30	#2,#3,#4
772	2443	-23.29	SbI	.02	.83	1.28x2.05	45	
779	1587	-21.67	SbI-II	0	.34	72x1.16	36	
908	1542	-22.15	ScI-II	0	.50	61x .61	50	#5
986	2073	-21.81	SBbI-II	0	.76	.97x1.56	40	
1084	1410	-21.62	ScII	0	.54	.72x1.15	40	
1201	1722	-21.09	S0(8)	0	.63	.82x1.31	20	
1232	1782	-22.57	ScI	0	.89	86x1.38	60	
1302	1703	-21.25	Sa	0	.95	.81x1.29	18	
1316	1801	-23.08	Sa pec	0	.78	.73x1.17	10	Merger?,Fornax
1339	1287	-19.56	E4	0	.83	.47x .47	20	#5
1350	1940	-21.38	Sa	0	.56	.73x1.17	20	
1353	1545	-20.75	SbcII	0	.48	.74x1.18	40	
1366	891	-18.27	S0(8)	0	.46	.40x .64	26	
1371	1462	-20.78	Sa	0	.74	.69x1.10	40	
1379	1457	-20.53	E0	0	.95	.73x1.17	20	Fornax
1380	1861	-21.30	S0(7)/Sa	0	.39	.73x1.17	24	Fornax
1381	1871	-20.06	S0(10)	0	.29	.73x1.17	26	Fornax
1387	1274	-20.57	S80 pec	0	.93	.73x1.17	20	Fornax
1396	1702	-21.43	E2	0	.78	.73x1.17	20	
1398	1524	-22.80	SBabI	0	.79	.71x1.14	10,18	
1399	1468	-21.61	E1	0	.95	.73x1.17	16	Fornax
1400	624	-17.94	E1/S0(1)	0	.89	.20x .20	20	#5
1404	1994	-21.34	E2	0	.93	.73x1.17	16,12	Fornax
1411	1058	-19.46	S0(4)	0	.81	.45x .73	18	
1425	1510	-21.53	SbII	0	.50	.70x1.12	40	
1427	1681	-20.40	E5	0	.72	.73x1.17	20	Fornax
1512	898	-20.14	SBbI pec	.01	.79	.87x .59	20	
1533	740	-18.59	SB0(2)SBa	.01	.87	.22x .22	20	#5
1537	1353	-20.43	E6	.01	.65	.61x .97	30	#4
1543	1400	-20.49	SB0(0)/a	.01	.55	.51x .94	20	
1553	1236	-21.26	S0(5) pec	.01	.68	.51x .82	18	
1574	890	-19.60	SB0(3)	.01	.95	.34x .54	20	
1596	1479	-20.10	S0(7)	.01	.51	.63x1.00	20	
1600	4738	-22.87	E4	.03	.74	2.29x3.67	30	
1617	1040	-21.68	Sa	.02	.51	.41x .66	10	
1637	717	-19.72	SBcII	.03	.87	.35x .56	32	
2484	1388	-19.68	E0	.06	1.00	.54x .87	20	
2442	1427	-21.20	SBbcII	.06	.91	.66x .90	20	
2781	2195	-20.75	Sa	.06	.50	.95x1.52	16	
2811	2514	-21.75	Sa	.06	.89	1.10x1.77	20	
2868	2714	-21.37	E4	.07	.76	1.10x1.91	20	
2903	550	-20.96	ScI-II	.01	.52	.23x .37	20	
2997	1081	-21.40	ScI	.08	.79	.89x .62	40	
3064	2194	-21.46	SBbcI	.06	.66	.94x1.50	30	
3066	1047	-18.36	S0(5)	.06	.69	.38x .60	20	
3115	656	-19.82	S0(7)	.02	.38	.21x .34	10	
3223	2911	-22.69	SbI-II	.07	.63	1.27x2.04	28	
3351	779	-20.66	SBbII	0	.69	.31x .50	20	M95
3368	2910	-21.69	SaI	.06	.60	1.27x2.03	26	
3368	896	-21.41	SabII	0	.72	.37x .59	16	M96
3379	893	-20.59	E0	0	.89	.37x .59	14	M105
3521	818	-21.66	SbII-III	0	.52	.30x .49	10	
3567	3151	-22.56	E3	.06	.68	1.38x2.21	16	
3588	1491	-21.11	E7/S0(7)	.03	.56	.69x .94	14	
3623	806	-21.48	SaII	0	.33	.33x .52	18	M65
3627	723	-21.48	SbII	0	.60	.29x .46	18	M66
3818	1498	-19.26	E5	0	.68	62x1.00	24	
3887	1163	-20.32	SbI-II	.01	.81	.44x .71	50	
3904	1613	-20.30	E2	.03	.74	.65x1.03	20	
3923	1788	-21.61	E4/S0(4)	.03	.65	.73x1.17	26	
4027	1672	-21.06	ScIII	.02	.79	.69x1.10	30	
4033	1821	-19.62	E6/S0(6)	.01	.44	.62x .99	20	
4038	1642	-21.40	Sc pec	.01	.69	.67x1.08	50	#15
4039	1641	-19.43	Sm pec	.01	.69	.67x1.08	30	#8,#12,#13,#15
4192	-140	-21.85	SbII:	0	.33	.53x .85	26	M98,Virgo
4254	2415	-21.59	ScI	0	.89	.53x .85	26	M99,Virgo
4303	1561	-21.84	ScI	0	.91	.53x .85	20	M61,Virgo
4321	1568	-21.91	ScI	0	.89	.53x .85	24	M100,Virgo
4374	982	-21.47	E1	0	.97	.53x .85	14	M84,Virgo
4382	739	-21.60	S0(3) pec	0	.74	.53x .85	16	M85,Virgo
4387	511	-18.76	E5	0	.62	.53x .85	32	Virgo,#8,#9,#12
4406	-250	-21.68	S0(3)/E3	0	.74	.53x .85	14	M86,Virgo
4435	869	-19.99	SB0(7)	0	.66	.53x .85	20	Virgo
4438	1	-21.73	Sb tides	0	.42	.53x .85	30	Virgo
4440	707	-19.04	SBa	0	.85	.53x .85	20	Virgo,#9,#10,#12
4482	1868	-20.97	SBabI-II	.02	.44	.78x1.25	30	
4472	961	-22.38	E1/S0(1)	0	.93	.53x1.25	14	M49,Virgo
4476	1978	-18.62	E5 pec	0	.68	.53x .85	30	Virgo
4478	1482	-19.56	E2	0	.87	.53x .85	18	Virgo
4479	822	-18.25	SB0(0)	0	.81	.53x .85	42	Virgo,#8,#9,#11
4486	1254	-22.08	E0	0	.93	.53x .85	16	M87,Virgo
4486B	1486	-16.59	E1	0	.93	.53x .85	26	Virgo,#8,#9,#11
4501	2269	-21.93	SbcII	0	.56	.53x .85	30	M88,Virgo
4507	3513	-21.98	SBabI	.06	.87	1.67x2.60	20	Seyf.2
4535	1953	-21.58	SBcI	0	.74	.53x .85	40	Virgo
4536	1809	-22.15	ScI	0	.47	.80x1.29	26	
4548	472	-21.27	SBbI-II	0	.91	.53x .85	30	Virgo
4552	319	-20.90	S0(0)	0	1.00	.53x .85	12	M89,Virgo
4569	-261	-22.31	SabI-II	0	.49	.53x .85	16	M90,Virgo
4579	1805	-21.69	SabII	0	.81	.53x .85	18	M58,Virgo
4594	1089	-22.81	Sa*/Sb-	0	.46	.42x .68	16	M104
4621	438	-21.05	E5	0	.66	.53x .85	14	M59,Virgo
4649	1259	-21.87	S0(2)	0	.85	.53x .85	10	M60,Virgo
4697	1224	-21.47	E6	0	.63	.50x .80	14	
4742	1321	-19.63	E4	0	.86	.54x .86	18	
4767	3075	-21.29	S0/a	.06	.54	1.36x2.17	20	
4866	1251	-20.22	S0(6)/Sa	.01	.35	.50x .80	16	
4938	3309	-21.66	E2	.03	1.00	1.48x2.37	20	
4941	1081	-20.07	SabII	0	.52	.43x .68	24	Seyf.2
4958	1615	-20.63	S0(7)	0	.84	.64x1.03	18	
4976	1369	-20.95	S0(4)	.11	.60	.55x .84	22	
4981	1678	-20.91	SBbcII	0	.79	.72x1.16	26	
5018	2897	-21.99	E4	.01	.79	1.50x2.07	18	
5061	2066	-21.54	E0	.02	.91	.88x1.41	16	
5084	2982	-22.27	Sa	.10	.44	1.31x2.09	80	
5090	3067	-21.37	E2	.07	.95	1.36x2.16	30	
5101	1857	-21.06	SBa	.02	.89	.78x1.25	22	
5102	420	-18.73	S0(5)	.04	.57	.16x .44	20	#6
5121	1532	-19.80	S0(4)/Sa	.04	.87	.62x .98	24	
5156	2950	-21.49	SBbcI	.11	.96	1.30x2.07	60	
5236	520	-21.12	SBcII	.03	.91	.17x .27	16	M83
5248	1154	-21.19	SbcI-II	0	.76	.51x .81	28	
5253	396	-19.2	Amorph.	.03	.44	.17x .27	20	#1
5266	3110	-21.92	S0(5)pec	.10	.65	1.58x2.20	24	Prolate
5419	4254	-22.5	S0(2)	.04	.90	1.93x3.08	30	#4
5612	2764	-21.65	SbII	.08	.41	1.22x1.94	26	
5643	1194	-21.20	SBcII-III	.09	.89	.46x .74	34	Seyf.2
5746	1731	-22.34	Sb	0	.22	.80x1.27	28	
6215	1663	-21.33	ScII	.17	.79	.66x1.06	30	
6221	1478	-21.66	SbcII-III	.16	.74	.62x .98	28	Seyf.2
6300	1107	-21.32	SBbII pec	.10	.66	.44x .70	42	Seyf.2
6684	896	-19.91	SBa	.06	.72	.32x .89	30	#6
6699	3509	-21.91	SbcI	.06	.95	1.62x2.60	40	
6744	833	-21.98	SbcII	.04	.66	.32x .61	40	
6758	3367	-21.62	E2	.04	.89	1.44x4.07	30	#6
6776	5488	-22.59	E1 pec	.04	.81	2.69x4.14	28	Merger?
6782	3903	-22.57	SBab	.04	.59	1.82x2.92	22	
6861	2859	-21.77	S0(6)	.03	.54	1.34x2.15	20	
6868	2764	-21.92	E3/S0(3)	.03	.83	1.30x3.37	30	#7
6923	2948	-21.61	SBbcII	.02	.56	1.43x2.29	34	
6925	2775	-22.37	SbcI	.02	.39	1.08x1.08	30	#5
6942	3204	-20.94	SBa	.02	.72	1.50x2.40	20	#14
7041	1920	-20.86	S0(7)/E7	.01	.39	.72x .72	20	#5
7049	2193	-21.57	S0(4)/Sa	.01	.78	.83x .83	20	#5
7079	2819	-21.23	SBa	.01	.63	1.34x3.60	20	#7
7083	3089	-22.81	SbI-II	.02	.65	1.43x2.28	40	
7144	2113	-21.32	E0	.01	1.00	1.00x1.60	20	
7145	1921	-20.73	E0	.01	.93	.91x1.45	20	
7184	2617	-23.10	SbII	0	.32	1.51x2.10	30	
7206	1482	-21.48	SbII	.01	.52	.67x1.07	40	
7213	1770	-21.96	Sa	0	.96	.83x1.33	20	Seyf.1
7329	3189	-22.08	SBbcI-II	.01	.68	1.18x1.18	40	#5
7392	2941	-21.73	SbcI-II	0	.62	1.47x2.36	40	
7410	1731	-22.40	SBa	0	.37	.66x .66	30	#5
7421	1833	-20.45	SBbcII-III	0	.83	.89x1.43	40	
7496	1472	-20.89	SBcII	0	.79	.70x1.12	28	Seyf.2
7507	1548	-21.10	E0	0	1.00	.72x2.02	30	#8
7552	1589	-21.49	SBbcI-II	0	.71	.76x1.22	18	
7592	1493	-21.75	SBab	0	.48	.72x1.15	20	Seyf.2
7744	2990	-21.51	SB0(3)	0	.78	1.43x3.73	40	#7
1459*	1628	-21.61	E4	0	.70	.70x1.27	18	#4
4296*	3633	-22.72	E0	.04	1.00	1.61x4.26	40	#4,#6
4329*	4266	-22.10	S0(5)	.03	.49	2.00x3.20	28	
4797*	2632	-22.41	E5/S0(5)	.05	.48	1.21x1.94	20	
4889*	2631	-21.36	S0(5)	.03	.65	1.17x1.87	20	
5105*	5363	-22.53	E5	.01	.43	2.38x6.72	30	#6
5267*	1719	-21.53	Sa	0	.81	.82x1.31	26	
5328*	1477	-20.30	ScII-III	0	1.00	.71x1.13	60	

Notes to table I

- # 1 HII region nucleus in amorphous galaxy.
- # 2 NGC 692 : velocity from our spectrum using CaII K, MgI b, NaI D and [NII] 6548, 84, resulting $V = 6281 \pm 354$ km/s. B from a PDS measurement on the ESO B Plate in Garching. The galaxy E197-GO9 on the same plate with $B = 14.0$ (Lauberts, 1982) was used as a standard, resulting for NGC 692 in $B = 12.54$.
- # 3 Morphological type from Lauberts (1982).
- # 4 Axial ratio estimated on ESO plate.
- # 5 Slit 4" × 4" ; # 6 : 4.6" × 13" ; # 7 : 5" × 13".
- # 8 Velocity from de Vaucouleurs *et al.* (1976).
- # 9 Computed with Virgo (m-M) = 31.7 and B from Sandage and Binggeli (1984) or de Vaucouleurs *et al.* (1976).
- # 10 Velocity from Eastwood and Abell (1978).
- # 11 Morphological type from Sandage and Binggeli (1984).
- # 12 Morphological type from de Vaucouleurs *et al.* (1976).
- # 13 Computed with apparent magnitude from de Vaucouleurs *et al.* (1976).
- # 14 The velocity for NGC 6942 is from our spectrum using CaII K, Hβ, MgI b and NaI D, resulting $V = 3204 + 200$ km/s. The value from Sandage and Tammann (1981) is too high. Indeed in the reference therein, the measurement was classified as uncertain. The absolute magnitude was computed with our velocity.
- # 15 NGC 4038 and NGC 4039 form an interacting pair.

TABLE II. — *The sample properties.*

M_V \ Type	A_m	E	E/SØ	SØ	SØ/Sa	Sa	Sab	Sb	Sbc	Sc	Σ
-23						1		2			3
-22		6	1	2		2	5	3	2	4	25
-21		15	5	9	4	8+1	2+2	10+1	11+1	10+1	74+6
-20		6	1	6	2	4	1+1	3	3	2+1	28+2
-19		5	1	4	1	2				2	15
-18	1	2		4	1						8
-17	1		1			non - existent					2
-16		1									1
Σ	2	35	9	25	8	17+1	8+3	18+1	16.1	18+2	164

TABLE III. — *Equivalent widths* (Å) *and continuum measurements* F_λ *relative to* F_λ (5870 Å).

NGC / IC*	(B/N) B	(B/N) R	#2 L+NO	#3 L+KB	#4 K	#5 K+HC	#6 HÕ	#10 Fe	#11 CN	#12 Ca
E I'			-22.9 < M < -22.0							
1600	15	40	21.8	18.3	13.9	13.0	3.4	3.1	11.4	1.8
4296*	45	80	21.2	16.5	15.0	11.6	2.1	3.6	9.0	3.9
3557	30	60	19.8	15.0	15.3	12.6	3.9	4.8	13.1	5.0
5105*	20	45	20.4	14.2	16.8	12.8	3.7	3.1	10.8	4.2
6776	25	50	21.8	15.2	14.7	10.2	3.8	4.0	9.2	4.9
4486	25	55	19.7	12.0	16.7	12.4	2.5	4.9	14.8	5.3
E II'			-21.9 < M < -21.0							
5018	40	70	18.6	15.0	14.8	9.6	4.3	2.4	6.5	5.0
4936	20	55	12.3	11.1	16.3	14.1	4.2	5.3	12.5	5.2
6758	25	80	21.5	16.5	17.2	13.7	4.4	4.4	12.4	4.8
1459*	35	80	20.5	15.8	16.1	11.4	5.0	4.9	14.5	4.9
1399	20	60	20.0	11.0	14.9	9.3	7.3	5.5	13.6	5.6
5061	35	80	18.4	13.9	13.5	9.4	3.5	2.3	9.2	3.5
4697	55	80	15.3	16.7	14.4	8.9	4.3	3.6	11.6	4.0
4374	40	70	18.6	15.3	15.7	10.6	3.0	4.2	10.1	3.2
1395	25	55	25.0	13.7	16.4	12.8	4.9	4.3	10.8	4.4
5090	20	60	23.1	14.7	12.0	13.3	3.3	5.0	15.0	6.4
2865	25	70	17.6	11.4	13.2	10.0	4.1	1.2	4.1	1.9
1404	30	70	23.8	14.9	17.6	11.1	5.8	4.4	11.0	4.8
7144	20	40	28.5	17.9	19.9	12.7	6.0	5.8	13.4	6.1
7507	25	60	20.4	16.9	15.9	11.9	1.6	3.9	10.0	4.0
4621	30	80	19.3	13.6	16.2	11.4	5.0	5.1	16.9	5.4
E III'			-20.9 < M < -19.0							
7145	20	40	22.8	14.1	21.2	10.6	6.1	3.0	9.1	4.9
5379	40	80	20.1	17.3	18.5	12.6	5.2	5.3	11.4	4.7
1427	25	60	15.8	12.8	16.4	9.2	.5	3.2	9.1	5.8
1537	25	60	22.0	13.0	14.2	10.3	5.5	5.6	10.7	5.7
1379	25	60	20.6	13.6	17.3	12.5	3.9	5.1	9.5	4.0
3904	35	45	24.0	12.1	15.2	10.2	3.8	3.1	10.4	4.3
2434	15	40	19.9	16.8	15.2	12.6	6.6	4.8	9.6	4.4
4742	55	90	9.0	6.5	11.2	10.0	6.6	1.8	5.6	1.7
1339	25	60	21.3	12.6	17.1	9.2	1.9	3.5	10.1	6.4
4478	25	60	15.1	13.6	17.1	11.4	5.4	4.8	11.1	4.6
3818	25	70	20.9	15.8	17.4	13.5	4.4	3.8	11.8	5.4
E IV'			-18.9 < M < -16.5							
4387	20	60	21.7	19.7	20.7	14.4	6.4	4.8	11.3	5.5
4476	25	60	6.8	9.4	11.6	11.0	2.5	1.6	2.4	1.2
4486B	30	70	21.0	14.0	15.8	13.9	2.9	3.6	10.7	4.4

NGC / IC*	#13 Fe	#14 G	#15 HγF	#16 Fe	#27 Hβ	#31 Fe	#32 Fe	#34 Mg+MgH	#35+36 MgH	#36 Fe
E I'			-22.9 < M < -22.0							
1600	4.6	9.6	5.6	6.5	3.7	7.7	10.6	10.9	10.3	5.8
4296*	4.3	7.2	2.1	6.0	2.8	6.8	9.2	10.9	10.3	5.3
3557	7.4	9.5	4.8	7.0	3.9	6.4	7.8	9.9	9.6	3.6
5105*	5.0	7.9	3.6	7.4	2.8	8.5	8.6	10.4	10.1	3.2
6776	5.1	7.4	4.1	6.4	3.5	4.1	7.0	8.7	8.8	3.3
4486	7.2	8.9	5.2	5.9	2.1	6.9	10.6	10.4	10.2	3.2
E II'			-21.9 < M < -21.0							
5018	4.7	8.2	6.0	6.2	4.7	5.6	6.1	8.5	8.9	3.1
4936	7.4	9.0	3.9	8.3	2.7	7.6	8.2	8.1	7.9	3.2
6758	5.9	8.8	4.1	8.7	2.4	6.0	9.2	10.1	9.9	3.8
1459*	6.7	9.6	4.2	7.5	2.0	6.2	9.9	9.8	10.4	3.6
1399	7.3	9.6	5.2	7.6	3.5	7.7	10.7	11.4	11.1	3.7
5061	4.4	8.3	3.8	4.4	4.0	6.5	7.5	8.3	9.3	3.5
4697	6.7	9.4	4.9	8.5	3.5	6.5	7.4	9.5	9.7	3.2
4374	6.4	8.5	2.1	5.2	3.1	6.9	9.1	9.7	8.8	3.4
1395	5.6	7.1	2.8	5.5	4.1	7.4	9.1	10.0	9.6	4.4
5090	5.9	8.5	5.1	8.5	2.5	7.4	8.1	9.7	10.0	5.0
2865	1.9	5.8	5.5	6.4	4.4	6.3	6.6	7.5	7.6	4.3
1404	6.6	8.8	4.3	6.5	3.6	7.3	9.4	9.9	9.8	3.4
7144	7.2	9.7	8.0	9.6	3.5	6.7	8.6	9.8	10.2	4.9
7507	5.6	7.6	2.3	5.4	2.6	7.2	8.8	10.1	11.3	5.3
4621	7.6	8.9	3.8	5.3	3.9	8.5	10.3	10.9	10.6	3.6
EIII'			-20.9 < M < -19.0							
7145	5.8	9.5	7.3	6.6	4.5	7.7	7.0	9.1	9.8	4.7
5379	6.1	8.0	4.9	6.2	2.7	8.0	9.5	10.2	10.7	5.9
1427	5.6	8.5	2.9	5.9	3.1	4.4	4.2	7.3	7.4	2.1
1537	7.0	8.5	3.5	4.3	3.8	7.0	7.7	9.3	9.2	4.0
1379	5.5	9.5	5.2	6.0	2.4	6.5	7.1	9.2	8.1	4.8
3904	7.0	9.8	5.7	7.5	4.2	7.9	6.7	9.1	10.4	4.9
2434	6.9	9.5	4.1	8.1	3.8	4.9	5.5	8.3	8.4	3.1
4742	2.5	6.4	5.7	4.8	5.0	5.5	4.9	6.2	6.9	3.4
1339	6.4	9.4	5.7	7.7	4.0	7.0	8.9	10.6	9.8	3.6
4478	6.4	8.9	5.6	7.9	3.1	7.9	7.9	9.6	10.3	4.6
3818	7.3	9.7	3.9	6.6	2.4	6.6	7.5	9.6	10.1	4.2
E IV'			-18.9 < M < -16.5							
4387	7.8	9.6	7.4	8.6	2.7	6.1	5.0	7.3	7.1	2.9
4476	2.4	6.2	4.6	5.4	3.1	4.1	4.3	5.5	6.5	3.9
4486B	6.7	9.1	6.2	6.6	3.4	7.0	8.5	9.4	10.0	3.3

NGC / IC*	#48 Na	#54-57 Ti0	#60 HK	#62 [SII]	4020 5870	4570 5870	5340 5870	6650 5870	6990 5870	7520 5870
E I'			-22.9 < M < -22.0							
1600	6.1	19.2	1.8	3.2	.55	.88	.97	.97	.97	.97
4296*	5.0	12.8	.3	2.9	.47	.78	.95	1.01	.99	.99
3557	5.1	17.8	1.7	4.1	.49	.82	.96	1.00	.99	.98
5105*	4.7	13.2	.4	3.0	.50	.79	.94	.82	.98	.99
6776	4.3	16.1	-.6	.9	.55	.85	.95	.98	.96	.95
4486	5.9	10.0a	-11.4	-8.0	.49	.78	.96	.95	.98	.97
E II'			-21.9 < M < -21.0							
5018	5.5	12.1	.8	1.4	.55	.81	.94	1.00	1.00	.99
4936	5.2	14.4	-6.7	-1.7	.42	.70	.89	1.05	1.07	1.11
6758	4.9	12.7	-1.4	.9	.47	.78	.97	1.00	.92	.93
1459*	6.3	17.3a	-4.7	.4	.45	.81	.95	.93	.96	.98
1399	6.7	22.6	2.0	3.6	.51	.85	.94	.93	.99	1.00
5061	5.4	17.5	2.6	3.4	.58	.90	.99	.96	.94	.93
4697	5.3	17.4	1.4	3.2	.43	.76	.93	.99	.99	1.00
4374	5.1	18.5	-1.6	1.4	.47	.81	.97	.97	.97	.93
1395	5.9	22.4	2.0	3.3	.62	.80	.95	1.01	1.02	1.01
5090	5.3	15.5	-1.6	.5	.43	.76	.94	1.01	1.01	1.01
2865	3.6	10.7	1.5	.8	.74	.98	1.03	.93	.85	.81
1404	5.7	22.5	2.2	3.8	.58	.84	.96	1.00	1.00	1.00
7144	4.5	17.5	1.5	2.7	.57	.83	.94	1.00	1.00	1.00
7507	6.0	17.8	2.6	4.6	.48	.75	.93	1.03	1.03	1.06
4621	6.5	17.4	2.1	1.2	.50	.89	.96	.93	.93	.94
E III'			-20.9 < M < -19.0							
7145	4.0	19.7	2.6	1.4	.63	.82	.92	1.00	1.00	.99
5379	5.4	15.7	1.6	3.0	.40	.75	.93	1.01	1.01	1.02
1427	5.1	15.7	3.4	2.8	.60	.84	.95	1.01	1.02	1.02
1537	5.0	19.6	1.6	3.4	.62	.89	.98	1.00	.96	.94
1379	4.6	21.7	2.4	4.7	.66	.92	1.00	.97	.96	.93
3904	5.4	17.9	1.6	2.9	.47	.75	.95	1.00	1.01	1.01
2434	4.6	21.2	1.2	2.1	.55	.75	.93	1.04	1.08	1.08
4742	3.4	11.1	2.5	1.1	.62	.90	.99	.93	.91	.89
1339	4.9	20.0	2.2	2.1	.45	.78	.94	.99	1.00	1.00
4478	4.4	14.7	1.7	2.4	.55	.85	.99	.96	.96	.95
3818	4.7	16.8	2.2	3.3	.49	.82	.97	.98	.98	.97
E IV'			-18.9 < M < -16.5							
4387	2.7	17.0	2.0	4.2	.61	.81	.94	1.01	1.01	1.01
4476	2.8	14.7	-.4	1.5	.62	.89	.98	.95	.93	.89
4486B	4.7	19.5	3.2	4.1	.58	.89	1.01	.97	.96	.95

TABLE III *(continued).*

NGC	(B/H)	(S/N)	#2	#3	#4	#5	#9	#10	#11	#12
IC*	B	K	L+H9	L+H8	K	H+K8	HδA	Fe	CN	Ca
	So I'		-22.3 < M < -22.0							
4472	40	80	22.5	16.7	17.9	14.5	7.2	6.3	15.2	5.5
5419	25	70	22.1	17.4	16.1	11.6	3.9	5.4	12.5	7.5
4329	25	70	23.5	14.4	16.8	11.9	4.9	4.8	8.9	4.0
	So II'		-21.9 < M < -21.0							
6868	40	100	21.4	15.6	16.4	10.0	2.5	4.5	13.0	5.3
5266	25	70	17.1	12.0	16.5	11.0	3.4	7.3	7.3	3.2
4649	35	80	23.1	13.1	19.4	11.6	6.9	6.4	15.5	5.8
584	25	60	23.2	14.6	16.6	9.7	2.1	1.7	10.3	4.6
6861	20	50	28.2	15.3	14.9	9.5	6.8	5.1	11.5	5.0
4406	25	60	23.8	18.0	19.2	10.8	5.7	6.0	13.3	4.9
5923	40	70	20.9	14.3	16.2	11.2	4.4	5.6	13.8	5.9
4382	30	70	20.2	13.1	12.9	8.9	6.1	3.7	9.0	5.1
7744	60	100	21.1	15.3	15.1	11.4	3.5	5.3	11.5	4.7
4707+	25	70	20.7	16.4	16.5	12.4	3.4	2.8	11.4	4.3
4889+	30	70	22.9	13.7	18.1	10.6	4.5	2.8	8.7	3.9
1553	30	70	14.2	9.2	12.2	9.0	2.1	3.6	7.9	5.6
5585	30	90	17.4	14.9	14.5	10.3	5.0	4.5	11.2	5.1
1201	25	80	22.4	12.9	15.5	12.2	3.5	3.6	10.4	4.9
	So III'		-20.9 < M < -19.0							
4976	30	70	14.9	11.3	16.1	10.7	4.0	2.0	8.4	4.4
4552	30	70	24.1	17.6	17.8	12.6	7.0	5.0	14.8	6.5
7041	25	60	20.9	15.5	18.0	12.2	5.1	4.7	13.0	5.2
4958	40	90	20.2	12.6	16.6	12.6	4.5	3.9	9.8	3.8
1387	25	60	21.3	16.1	17.3	10.5	6.2	4.6	11.9	5.5
1596	25	60	16.5	16.5	19.4	11.4	5.0	4.1	11.7	5.2
1381	25	60	20.3	11.8	15.3	10.7	.5	3.0	5.3	4.2
4435	50	65	19.0	16.6	16.4	10.8	6.8	6.6	10.9	4.1
3115	40	90	20.0	15.2	16.4	10.7	3.6	4.3	12.2	5.4
1411	25	60	24.8	14.6	19.2	12.3	4.5	4.3	11.5	4.2
4033	30	70	14.5	9.1	14.5	11.5	3.1	2.0	6.2	2.7
1574	25	60	20.7	14.0	15.8	11.3	5.2	4.3	10.9	5.5
	So IV'		-18.9 < M < -17.9							
5102	40	40	6.6	8.0	8.4	10.4	9.2	.6	.3	.1
3068	25	60	13.9	9.9	16.8	12.6	5.0	2.4	4.3	2.3
1366	25	60	22.4	16.1	16.2	10.5	4.4	5.2	10.6	4.4
4479	15	40	14.2	9.6	14.1	6.6	1.7	3.1	8.5	3.8
1400	20	45	21.8	15.3	13.6	9.6	5.1	4.4	16.7	5.5

NGC	#13	#14	#15	#16	#27	#31	#32	#34	#33+35	#36
IC*	Fe	G	HγA	Fe	Hβ	Fe	Fe	Mg+MgH	MgH	Fe
	So I'		-22.3 < M < -22.0							
4472	6.1	8.6	5.0	7.3	2.5	8.2	10.0	10.7	11.4	5.3
5419	6.0	9.1	4.3	6.2	3.9	7.1	8.3	10.4	10.4	3.7
4329	6.4	9.6	6.0	8.0	3.8	8.2	8.6	9.6	9.8	4.5
	So II'		-21.9 < M < -21.0							
6868	6.7	8.2	5.1	7.4	3.2	7.1	8.9	9.6	9.9	3.8
5266	4.4	9.2	5.2	8.0	3.1	5.6	7.8	9.2	9.6	4.2
4649	6.3	9.8	4.9	7.2	2.4	9.0	10.7	11.5	10.6	3.4
584	4.3	9.2	3.3	5.6	3.0	7.0	6.8	8.4	8.6	3.2
6861	4.9	9.0	3.3	6.6	3.3	7.6	9.6	9.9	11.1	3.3
4406	6.9	9.1	2.5	5.8	3.6	7.0	8.3	9.7	9.1	3.5
5923	6.3	10.5	4.8	7.3	3.8	8.5	8.8	9.7	11.7	4.0
4382	4.4	7.4	3.5	5.7	4.8	6.0	6.6	7.8	7.6	3.5
7744	5.5	8.3	2.8	5.9	3.4	7.5	8.8	10.2	10.3	4.1
4707+	4.9	9.0	5.4	8.6	2.5	7.7	9.2	9.6	10.0	5.0
4889+	6.3	9.6	4.3	6.4	3.5	6.4	7.6	8.1	7.2	4.3
1553	6.0	8.3	3.6	7.9	3.7	6.5	7.0	9.4	8.8	3.6
5585	6.4	9.6	4.3	7.8	3.3	7.2	8.3	9.8	10.1	4.1
1201	7.2	10.5	4.6	9.3	4.7	6.7	8.5	9.6	8.8	3.9
	So III'		-20.9 < M < -19.0							
4976	5.2	9.6	6.7	7.0	5.4	7.5	6.8	7.5	8.3	3.8
4552	7.5	8.9	4.0	8.4	3.6	9.0	10.6	10.6	10.7	3.4
7041	8.1	9.3	6.3	7.7	3.8	7.4	8.9	9.8	8.5	3.9
4958	4.9	8.6	3.5	6.7	2.9	8.0	8.6	9.3	10.2	5.1
1387	7.6	8.0	4.3	8.2	4.7	8.5	10.5	10.7	12.1	3.5
1596	8.2	9.9	8.3	8.7	3.6	7.4	8.6	10.0	10.0	3.4
1381	6.4	8.1	1.5	4.8	2.6	5.6	6.4	8.4	7.2	3.4
4435	6.6	8.5	4.5	8.2	4.3	6.0	7.8	8.3	8.4	4.4
3115	7.8	9.9	6.6	8.0	4.2	8.2	8.4	10.1	10.5	4.9
1411	5.3	8.9	3.0	5.5	3.3	5.1	7.2	8.1	7.1	2.9
4033	4.9	8.0	3.9	4.2	2.5	6.5	5.5	7.7	8.1	2.9
1574	6.3	10.4	5.1	6.9	3.9	7.2	8.4	10.2	10.2	4.5
	So IV'		-18.9 < M < -17.9							
5102	-.5	2.5	6.6	1.0	5.5	-.1	.5	2.6	3.8	2.6
3068	5.9	7.4	4.6	6.3	2.7	3.8	5.0	6.0	7.2	3.8
1366	5.4	8.4	2.9	5.9	3.2	4.1	5.7	7.3	7.4	4.1
4479	3.7	7.3	4.0	4.0	2.6	6.9	5.9	7.9	9.3	2.7
1400	6.2	8.9	4.0	5.6	4.1	7.6	10.9	11.1	11.1	3.7

NGC	#48	#54-57	#60	#62	4020	4570	5340	6830	6990	7620
IC*	Na	TiO	HCI	[SII]	4870	4870	4870	4870	4870	4870
	So I'		-22.3 < M < -22.0							
4472	6.2	17.5	2.4	3.5	.45	.75	.96	.99	.99	1.00
5419	5.3	18.3	2.3	3.6	.49	.85	.96	1.01	1.01	1.01
4329	6.3	18.2	1.9	4.5	.47	.78	.93	1.02	1.02	1.03
	So II'		-21.9 < M < -21.0							
6868	5.2	12.4	-3.9	.9	.44	.72	.93	1.03	1.06	1.07
5266	5.9	15.7	-4.1	-.5	.27	.69	.91	1.03	1.03	1.05
4649	6.5	18.9	2.2	3.0	.41	.78	.94	.99	.98	1.00
584	4.5	21.7	1.1	1.9	.84	.83	.96	.97	.97	.96
6861	6.6	23.0	.2	4.0	.62	.80	.94	1.05	1.08	1.09
4406	5.0	18.1	2.2	3.5	.52	.88	1.00	.97	.96	.96
5923	5.9	21.1	2.4	3.6	.44	.75	.96	1.02	1.02	1.03
4382	3.6	13.4	1.7	1.2	.65	.98	1.03	.91	.90	.89
7744	5.2	16.2	.1	2.1	.46	.74	.95	1.03	1.04	1.06
4707+	5.8	14.3	1.0	2.6	.48	.80	.97	.97	.98	.95
4889+	3.7	13.9	-1.0	1.8	.56	.84	.95	.97	.96	.95
1553	5.4	17.3	-1.4	-1.0	.47	.81	.92	.99	.98	.97
5585	4.8	18.7	2.2	3.6	.50	.84	.96	.98	.97	.95
1201	5.1	19.4	2.7	1.2	.48	.81	.91	.99	.97	.99
	So III'		-20.9 < M < -19.0							
4976	3.6	15.6	2.5	3.0	.56	.85	.98	.98	.99	.99
4552	7.0	20.0	.1	1.2	.51	.86	.98	.93	.93	.94
7041	4.6	20.7	2.8	2.8	.45	.74	.92	1.02	1.03	1.05
4958	4.4	12.6	-.2	1.5	.60	.90	.98	.95	.94	.95
1387	5.3	20.1	-1.8	.1	.60	.79	.90	1.04	1.05	1.07
1596	4.8	17.9	.9	.5	.56	.84	.95	.99	.99	.98
1381	3.0	20.5	1.6	3.1	.62	.89	.98	.96	.95	.94
4435	4.1	18.3	.3	2.5	.59	.88	1.00	.98	.97	.95
3115	5.5	20.2	2.2	2.8	.45	.77	.95	1.01	1.01	1.02
1411	3.2	19.6	.6	2.4	.65	.86	.98	.99	.99	.99
4033	4.0	13.7	2.8	3.9	.60	.81	.98	.98	.97	.96
1574	5.3	19.6	.3	1.9	.49	.82	.93	1.01	1.03	1.01
	So IV'		-18.9 < M < -17.9							
5102	2.2	5.2	2.3	-.2	1.21	1.19	1.07	.99	.83	.78
3068	2.5	16.0	-1.4	-.4	.60	.87	.98	.96	.94	.94
1366	2.7	17.6	.5	1.9	.61	.84	.96	1.00	1.00	.99
4479	3.1	14.5	2.9	2.5	.66	.89	.99	.98	.97	.94
1400	6.1	21.3	0	2.7	.39	.71	.92	1.02	1.03	1.06

NGC	(B/H)	(S/N)	#2	#3	#4	#5	#9	#10	#11	#12
IC*	B	K	L+H9	L+H8	K	H+K8	HδA	Fe	CN	Ca
	Ba I'		-23.1 < M < -22.0							
1316	30	70	17.2	13.8	14.9	9.3	3.5	5.3	9.0	4.5
7410	20	40	26.2	17.5	21.6	16.9	1.6	5.6	14.1	5.4
5064	25	50	14.4	6.2	14.3	10.9	4.2	4.2	6.4	3.3
	Ba II'		-21.9 < M < -21.0							
524	20	40	27.1	17.4	16.4	12.7	5.7	8.1	9.8	4.3
2811	25	60	21.8	11.9	13.5	8.2	4.3	5.0	10.1	5.1
3358	25	50	19.8	13.1	15.6	8.0	1.4	3.4	6.3	4.5
5267+	25	60	15.7	11.7	17.7	9.8	5.3	2.4	9.1	3.9
7049	20	40	24.0	12.5	19.7	9.4	4.2	4.0	12.4	7.2
3623	25	60	16.4	16.2	13.3	8.9	4.5	4.3	11.8	5.8
1350	25	50	22.1	16.2	17.5	9.2	3.3	1.3	11.8	4.5
1380	30	70	21.9	13.1	20.8	10.8	5.8	5.2	13.1	5.6
4767	30	70	20.8	19.3	18.8	11.9	5.3	5.0	11.9	5.6
1302	20	40	16.8	11.6	15.9	9.3	.5	2.8	5.9	3.0
7079	40	80	12.2	13.5	16.5	10.6	2.9	2.0	8.7	4.6
6101	25	60	19.5	16.3	12.0	9.4	4.3	5.1	13.1	5.7
	Ba III'		-20.9 < M < -18.6							
6942	20	45	15.8	17.9	14.0	9.6	1.6	1.0	9.1	5.1
1371	25	50	27.1	18.3	17.1	12.7	2.5	2.7	9.1	4.0
2781	25	50	16.7	14.3	15.8	11.7	3.7	3.6	7.4	3.4
1617	30	70	25.7	15.2	18.2	10.8	2.9	4.3	11.0	4.5
1643	25	50	19.0	12.4	16.9	9.2	3.2	3.1	10.2	4.4
4856	30	60	20.9	16.1	18.8	12.1	2.3	3.4	8.3	3.5
6684	35	80	18.4	16.1	17.1	11.6	2.9	1.8	6.6	3.7
5121	35	50	21.1	12.1	15.4	9.9	4.6	3.1	11.2	4.9
4440	25	50	21.6	13.6	17.1	10.7	4.5	3.9	10.6	3.4
1553	20	40	22.0	14.5	19.1	11.9	4.4	3.9	14.1	6.4

NGC	#13	#14	#15	#16	#27	#31	#32	#34	#33+35	#36
IC*	Fe	G	HγA	Fe	Hβ	Fe	Fe	Mg+MgH	MgH	Fe
	Ba I'		-23.1 < M < -22.0							
1316	6.1	7.9	3.4	6.2	4.7	6.5	7.2	8.6	9.3	3.8
7410	8.8	11.5	7.2	9.9	2.6	3.5	7.9	8.6	7.2	3.2
5064	5.6	7.9	4.0	5.9	3.3	6.5	6.3	7.9	8.8	3.4
	Ba II'		-21.9 < M < -21.0							
524	6.5	9.5	5.0	8.5	3.3	8.3	8.9	10.0	10.6	5.0
2811	7.5	9.4	3.4	7.1	3.0	6.6	8.4	9.4	9.2	3.5
3358	6.4	9.0	5.3	4.0	3.4	5.7	6.3	9.1	8.8	2.7
5267+	6.3	8.7	4.5	6.2	3.2	6.2	7.9	8.5	8.7	4.1
7049	7.3	10.3	6.0	6.0	3.3	7.6	9.7	10.2	10.2	4.0
3623	8.2	9.1	4.9	8.2	2.3	6.7	6.5	9.1	9.1	4.3
1350	6.9	9.3	5.3	7.5	3.6	6.8	6.8	9.7	9.7	2.8
1380	7.1	9.1	5.6	9.8	3.7	6.5	8.8	9.4	9.5	5.9
4767	6.1	10.1	4.9	6.6	4.0	8.8	8.1	9.1	9.5	4.2
1302	5.9	8.4	5.5	6.6	4.0	6.2	6.1	8.1	9.2	4.3
7079	5.2	8.3	4.0	5.5	3.6	4.3	5.6	7.4	7.0	2.9
6101	6.6	9.7	3.6	7.6	3.0	6.6	8.1	9.5	10.1	4.3
	Ba III'		-20.9 < M < -18.6							
6942	6.6	9.1	3.8	7.0	2.7	5.2	6.1	9.3	8.8	3.3
1371	5.9	7.9	5.0	5.5	2.6	6.1	7.3	8.7	7.5	3.8
2781	6.3	8.6	5.6	7.3	4.1	5.7	6.2	6.9	7.8	3.9
1617	6.2	9.0	5.3	8.2	4.0	6.8	8.7	10.3	10.2	4.0
1643	5.0	7.9	1.8	4.9	4.2	7.3	8.7	9.2	9.1	5.2
4856	6.4	9.1	3.7	6.5	2.2	7.2	8.2	8.5	8.2	2.9
6684	3.9	7.2	2.7	4.9	3.1	4.6	6.3	8.2	9.2	4.8
5121	7.8	9.7	7.3	7.8	4.8	7.5	5.7	7.1	8.5	5.4
4440	5.3	8.2	3.2	6.9	3.8	7.1	7.3	7.8	7.5	3.1
1553	7.8	10.9	7.8	9.5	3.6	7.4	9.5	11.0	11.2	3.7

NGC	#48	#54-57	#60	#62	4020	4570	5340	6830	6990	7620
IC*	Na	TiO	HCI	[SII]	4870	4870	4870	4870	4870	4870
	Ba I'		-23.1 < M < -22.0							
1316	6.1	18.1	-1.2	-.2	.67	.78	.90	1.01	.99	.96
7410	4.2	19.0	-2.9	-.1	.42	.68	1.00	1.07	1.10	1.10
5064	3.7	14.5	-1.6	1.5	.41	.73	.91	1.04	1.05	1.07
	Ba II'		-21.9 < M < -21.0							
524	4.4	19.6	.2	2.4	.59	.70	.91	1.08	1.11	1.16
2811	4.1	16.4	.9	2.4	.49	.85	.96	.98	.97	.97
3358	4.1	15.7	.6	2.1	.61	.81	.98	.99	.98	.99
5267+	5.2	15.3	-2.8	.6	.47	.74	.95	1.00	1.00	.99
7049	6.0	23.8	-.9	3.0	.40	.71	.90	1.04	1.05	1.07
3623	4.8	14.5	-1.8	0	.57	.71	.91	1.02	1.02	1.03
1350	3.7	20.3	1.5	2.4	.60	.83	.96	.97	.97	.97
1380	4.8	22.4	.7	3.3	.56	.84	.93	1.00	1.00	1.00
4767	5.1	16.7	1.7	2.6	.47	.74	.91	1.01	1.01	1.03
1302	3.4	15.1	1.8	.6	.56	.87	.94	.99	.97	.94
7079	3.0	10.6	-.1	1.1	.58	.80	.95	1.01	1.01	1.02
6101	5.0	20.4	-2.0	2.1	.42	.76	.92	1.01	1.01	1.02
	Ba III'		-20.9 < M < -18.6							
6942	3.6	17.4	.2	1.5	.44	.77	.92	1.00	1.00	1.02
1371	4.1	21.0	-.2	2.0	.60	.81	.96	1.01	1.02	1.01
2781	5.0	18.2	1.2	2.1	.61	.83	.97	.98	.97	.96
1617	4.8	19.6	-.2	2.6	.53	.84	.93	1.00	1.00	1.02
1643	5.7	19.9	2.2	1.3	.54	.82	.97	.99	.99	.99
4856	4.2	14.7	-1.3	1.6	.62	.80	.93	.99	.98	.99
6684	4.4	13.0	2.0	2.6	.51	.84	.97	.94	.99	.95
5121	3.3	14.2	.6	2.7	.51	.82	.97	1.01	1.01	1.02
4440	4.1	15.3	2.6	3.2	.62	.89	.96	.98	.97	.95
1553	5.4	22.6	1.1	2.2	.47	.78	.92	1.00	1.00	1.00

TABLE III *(continued)*.

NGC / IC*	(S/N) B	(S/N) R	#2 L+Hδ	#3 L+Hε	#4 K	#5 K+Hε	#9 Hδ	#10 Fe	#11 CH	#12 Ca
Sb I'			**-23.3 < M < -22.0**							
772	20	40	17.5	8.9	11.5	5.0	1.9	6.3	3.6	3.1
7184	25	60	20.8	10.4	14.5	10.1	1.9	2.8	8.9	4.2
488	20	40	11.5	1.8	17.7	13.4	6.4	3.1	11.3	6.3
4594	60	90	23.5	17.2	17.5	15.3	6.8	6.0	15.4	5.7
7083	15	30	17.4	6.5	12.7	14.9	1.8	1.3	4.8	1.7
5225	25	40	15.3	8.7	13.0	10.7	1.0	2.6	7.8	1.9
6782	25	50	13.5	7.8	6.7	6.3	.7	1.8	4.1	.7
5746	25	60	14.2	13.0	11.8	12.8	4.8	3.9	10.7	5.3
4569	40	60	2.3	6.2	5.4	7.2	7.3	1.9	1.5	.3
1398	25	60	20.3	14.2	19.0	10.5	5.0	3.7	13.0	6.0
Sb II'			**-21.9 < M < -21.0**							
4192	15	40	8.9	12.0	18.6	10.1	5.6	3.7	9.5	3.8
986	20	30	-1.5	1.0	2.3	1.4	1.4	.6	2.0	1.7
4438	15	40	14.7	17.9	14.3	8.3	5.5	3.7	10.2	5.3
4579	35	70	21.0	15.2	18.1	11.2	4.6	3.5	8.6	4.4
3521	55	80	17.5	12.5	16.0	10.2	6.1	3.9	8.2	3.6
5612	25	50	10.0	14.8	13.1	13.3	2.1	2.7	9.4	5.0
779	20	40	17.3	15.9	16.1	9.9	3.9	3.8	10.0	5.0
1426	20	40	13.9	11.7	18.8	8.8	6.6	1.0	5.2	2.6
3627	35	80	15.0	14.3	13.0	12.5	7.0	1.3	6.3	2.7
7205	15	30	21.1	12.5	13.1	9.7	5.5	3.1	6.5	4.7
5368	25	60	18.1	10.7	14.8	8.7	4.2	1.9	6.8	3.1
4548	50	70	24.0	14.8	18.1	9.5	8.9	4.1	11.3	4.8
Sb III'			**-20.9 < M < -20.0**							
4402	25	50	18.0	14.6	14.2	11.9	1.2	2.4	8.0	4.2
3351	25	60	7.1	5.8	9.5	6.1	4.2	1.2	4.8	2.5
3887	20	40	19.0	10.2	16.4	9.3	6.7	2.2	5.4	2.1
1512	20	40	18.5	16.3	16.1	9.0	1.2	1.2	9.3	4.5

NGC / IC*	#13 Fe	#14 G	#15 Hγ	#16 Fe	#27 Hβ	#31 Fe	#32 Fe	#34 Mg+MgH	#33+35 MgH	#36 Fe
Sb I'			**-23.3 < M < -23.0**							
772	4.0	5.0	4.5	4.8	2.3	6.7	5.3	6.2	6.5	2.8
7184	7.8	8.4	4.4	6.2	5.9	6.0	7.7	8.4	7.1	2.8
488	5.5	8.1	4.2	7.2	5.2	6.6	9.3	9.8	9.8	3.7
4594	7.8	10.0	4.9	7.5	2.5	7.1	9.7	10.5	10.8	4.5
7083	4.8	7.7	5.4	6.2	4.8	5.1	5.3	6.6	8.2	4.9
5225	4.7	10.1	5.6	4.3	4.2	5.9	7.4	9.1	8.9	4.2
6782	1.6	7.0	-.3	4.7	2.7	5.5	7.6	8.4	8.7	3.3
5746	7.1	10.2	5.7	7.6	3.3	6.3	6.7	9.4	8.7	3.2
4569	.8	2.8	6.1	.3	3.6	1.5	2.8	3.7	4.4	2.1
1398	7.6	9.3	4.8	7.3	3.5	7.3	8.2	10.2	10.0	3.2
Sb II'			**-21.9 < M < -21.0**							
4192	6.3	8.7	4.5	6.3	2.5	6.1	6.3	7.0	7.5	3.9
986	1.4	2.8	1.2	4.1	-6.3	-.2	2.7	2.9	2.7	2.7
4438	4.5	7.7	4.4	5.8	1.8	2.7	7.5	7.7	7.8	4.5
4579	6.2	8.6	5.1	5.2	.6	1.9	6.1	7.3	6.7	2.8
3521	4.6	7.5	4.5	6.2	4.3	5.9	7.0	8.0	8.4	3.7
5612	5.6	8.5	6.1	9.4	4.2	6.8	5.2	8.1	8.6	4.7
779	3.5	7.6	3.4	4.5	3.4	3.4	5.3	6.9	7.9	3.9
1426	5.3	7.4	4.7	6.1	3.6	5.0	5.6	7.2	7.1	4.2
3627	4.1	6.9	5.2	3.3	4.6	3.9	3.4	5.8	5.4	3.2
7205	8.8	9.3	5.8	6.2	3.2	5.2	5.0	7.6	9.4	5.5
5368	4.5	8.2	4.1	4.5	3.6	4.5	4.8	7.3	8.1	4.2
4548	5.0	8.8	3.9	6.8	3.0	5.7	7.4	9.0	9.8	3.7
Sb III'			**-20.9 < M < -20.0**							
4402	6.6	9.5	4.2	6.6	4.1	4.9	5.9	7.1	7.3	3.1
3351	2.9	7.0	3.5	4.7	-.1	3.0	4.2	6.2	6.5	3.1
3887	5.0	8.9	6.1	7.0	4.6	5.4	4.9	5.0	6.4	4.5
1512	7.1	8.3	4.0	5.1	4.3	5.2	6.2	7.8	9.0	4.6

NGC / IC*	#48 Na	#54-57 TiO	#60 Hα	#62 [SII]	4020 5870	4670 5870	5340 5870	6830 5870	6990 5870	7520 5870
Sb I'			**-23.3 < M < -22.0**							
772	5.0	20.4	-1.2	2.6	.38	.65	.87	1.08	1.12	1.11
7184	5.2	11.5	-.9	2.2	.44	.72	.89	1.02	1.04	1.06
488	4.5	20.4	.2	1.5	.47	.76	.94	1.02	1.03	1.04
4594	6.7	17.5	-3.8	-.4	.45	.77	.95	.95	.93	.92
7083	2.1	17.9	-2.3	2.0	.67	.87	.96	1.01	1.00	1.00
5225	4.6	15.4	.7	4.2	.48	.80	.95	1.00	1.00	1.00
6782	3.1	13.0	-7.3	-.3	.55	.86	.96	.98	.96	.94
5746	6.7	19.4	1.1	2.4	.33	.62	.84	1.09	1.14	1.23
4569	5.2	10.1a	-12.1	-5.8	.91	1.02	1.02	.92	.88	.84
1398	5.8	19.4	.5	1.9	.51	.82	.93	1.00	1.01	1.00
Sb II'			**-21.9 < M < -21.0**							
4192	6.2	13.1	-6.8	-1.9	.30	.65	.84	1.11	1.16	1.25
986	5.0	13.7a	-89	-15	1.14	1.08	.98	.95	.92	.87
4438	7.0	14.6a	-21	-8.2	.33	.62	.89	1.08	1.13	1.19
4579	5.5	12.6a	-16	-6.9	.51	.81	.95	.95	.92	.89
3521	6.4	18.4	3.6	2.4	.45	.76	.93	.97	.96	.97
5612	4.1	15.3	-1.7	1.4	.43	.73	.92	1.02	1.03	1.03
779	5.3	20.0	1.2	1.9	.57	.81	.95	1.00	.99	.99
1426	2.2	13.8	.9	0	.64	.84	.94	1.01	.99	.97
3627	5.9	12.7	-1.4	-1.8	.49	.73	.92	1.00	.99	.97
7205	5.5	15.9	-1.1	3.4	.64	.80	.93	1.01	1.01	1.02
5368	4.4	12.5	-1.1	0	.35	.62	.89	1.05	1.08	1.15
4548	4.4	16.8	-1.0	.1	.39	.74	.93	.99	.97	.97
Sb III'			**-20.9 < M < -20.0**							
4402	3.7	16.8	1.6	2.4	.60	.80	.95	.99	.99	.98
3351	3.6	15.6a	-16	.2	.79	.90	.96	1.00	.99	1.01
3887	3.2	16.0	-5.2	-.6	.65	.85	.98	.99	.99	.99
1512	2.5	18.2	.1	1.8	.63	.89	.98	.98	.97	.96

NGC / IC*	(S/N) B	(S/N) R	#2 L+Hδ	#3 L+Hε	#4 K	#5 K+Hε	#9 Hδ	#10 Fe	#11 CH	#12 Ca
Sc I'			**-23.0 < M < -22.0**							
692	20	40	21.6	12.3	12.8	9.1	1.9	4.3	5.8	2.4
1232	15	30	15.2	7.6	16.8	14.5	2.6	5.9	8.9	2.0
6925	20	40	18.5	12.4	13.9	10.7	4.5	4.8	12.1	3.3
4536	30	60	9.6	8.3	7.5	7.2	3.9	1.1	5.2	1.3
908	15	30	11.2	11.8	15.9	9.3	8.0	4.1	7.7	4.5
7329	25	50	21.9	22.6	20.1	10.7	7.3	6.1	12.8	5.6
Sc II'			**-21.9 < M < -21.0**							
6744	20	40	25.5	18.5	15.1	9.5	5.3	1.9	9.2	4.9
4501	30	70	19.1	11.0	14.2	7.9	3.0	3.2	12.2	5.3
4321	25	50	10.3	5.2	5.0	6.4	3.8	1.3	4.7	2.0
6099	20	40	10.1	5.1	4.0	5.4	.4	1.9	4.6	3.2
4303	35	80	7.5	5.6	5.0	6.0	4.7	1.8	5.1	2.0
7392	20	40	6.8	5.6	7.0	8.8	1.7	1.1	4.0	3.2
1084	20	35	18.1	10.5	3.9	8.5	9.5	1.8	5.1	1.1
6923	25	50	16.8	12.6	13.9	9.8	2.7	2.3	7.5	5.1
4254	25	50	15.1	10.8	14.6	7.9	5.4	2.7	6.1	1.7
4535	20	40	2.9	-1.1	1.8	.5	3.8	1.0	3.1	1.2
5156	20	40	11.9	8.5	10.8	12.5	1.7	2.4	4.6	3.0
7552	35	35	4.9	5.5	4.8	6.7	6.1	1.4	.3	.2
3084	15	35	17.2	7.7	20.2	11.7	2.8	2.9	9.4	3.9
289	15	35	15.6	8.3	17.3	11.9	1.0	.7	8.3	3.7
2997	25	50	8.7	4.7	8.4	7.9	4.8	2.7	6.5	2.0
4038	13	25	4.3	-3.4	6.6	1.0	1.7	1.5	4.8	2.4
6215	15	35	6.8	1.4	3.7	7.8	3.1	-.6	2.0	.5
2442	15	35	17.4	6.3	16.1	12.5	4.5	1.8	6.2	1.6
5248	25	50	3.6	8.7	5.8	9.0	6.3	2.7	7.7	1.8
5236	50	50	5.0	5.4	1.7	3.8	4.3	.9	.8	.3
4027	20	25	1.4	2.9	3.7	8.3	4.9	-.5	.3	.6
Sc III'			**-20.9 < M < -19.4**							
2903	20	35	7.0	5.2	5.0	5.2	4.5	2.6	1.5	.9
4981	30	35	10.6	6.9	12.2	10.0	3.4	.5	5.6	2.5
1353	15	35	12.9	4.3	8.4	9.9	4.9	5.1	5.2	1.9
7421	10	20	10.0	10.5	15.2	11.0	7.2	0	4.7	4.0
5325+	13	20	17.4	8.9	6.1	9.0	6.3	2.2	5.6	1.7
1637	15	35	16.5	15.2	10.8	14.9	8.9	2.2	9.2	4.9
4039	10	13	6.8	4.6	8.3	3.0	-1.1	.5	5.9	3.8

NGC / IC*	#13 Fe	#14 G	#15 Hγ	#16 Fe	#27 Hβ	#31 Fe	#32 Fe	#34 Mg+MgH	#33+35 MgH	#36 Fe
Sc I'			**-23.0 < M < -22.0**							
692	3.7	8.9	4.7	6.3	4.3	6.5	8.6	9.1	9.4	5.5
1232	4.6	7.9	2.3	5.6	4.8	5.5	6.6	8.0	7.4	3.1
6925	6.6	9.6	5.9	7.9	4.1	5.3	4.9	7.4	7.8	3.7
4536	3.6	5.3	1.6	3.1	-3.9	.8	3.3	4.4	4.7	2.4
908	5.5	7.1	7.4	7.9	3.7	4.8	7.1	6.4	7.2	2.5
7329	8.6	9.2	5.5	9.5	5.1	7.0	9.0	8.9	8.8	3.0
Sc II'			**-21.9 < M < -21.0**							
6744	7.5	9.7	4.4	8.4	3.0	8.7	6.4	8.2	8.6	5.9
4501	5.5	8.0	1.4	6.6	2.5	5.8	8.2	9.1	8.9	5.8
4321	4.7	5.5	4.2	4.5	2.6	3.7	4.7	7.0	8.1	3.7
6099	2.7	5.9	5.7	3.5	2.8	4.0	5.7	5.8	6.8	4.5
4303	2.4	5.7	4.5	3.8	1.0	1.9	4.3	5.4	5.6	3.2
7392	1.4	5.2	4.7	5.5	2.6	6.1	6.4	7.6	9.5	3.0
1084	1.3	5.0	6.0	3.5	2.5	2.6	3.5	5.7	5.9	3.3
6923	6.9	8.9	6.5	7.0	3.8	5.8	7.3	7.7	7.9	4.1
4254	2.1	6.9	5.1	3.5	1.5	3.3	3.5	5.1	5.0	3.0
4535	.7	3.1	1.8	2.8	-3.6	2.6	3.9	4.3	4.4	2.7
5156	3.7	7.1	4.9	3.8	3.7	4.7	5.2	6.1	7.7	3.5
7552	-.1	1.5	4.0	2.4	-2.0	2.1	2.9	3.1	3.9	2.7
3084	6.2	9.8	4.2	4.1	3.1	6.1	5.7	7.1	8.2	4.5
289	4.7	8.2	4.0	7.6	3.4	3.8	5.9	7.8	9.1	2.9
2997	4.0	4.0	3.3	5.2	.9	3.8	4.2	6.5	6.5	3.4
4038	5.3	4.6	-2.9	2.2	-11.0	-.2	3.7	4.8	7.6	3.4
6215	1.0	3.8	3.5	2.1	-4.8	0	1.3	2.4	4.0	2.9
2442	5.1	7.1	5.9	5.7	4.9	5.1	4.9	6.3	7.4	3.4
5248	3.8	5.3	5.4	3.8	4.7	5.5	5.1	5.5	5.9	3.1
5236	.3	2.3	2.5	2.0	-4.4	-.1	1.6	2.7	2.5	1.3
4027	.9	3.0	6.7	-.5	.4	.2	.7	2.3	2.9	1.6
Sc III'			**-20.9 < M < -19.4**							
2903	1.8	2.1	.7	.1	-1.0	3.2	5.0	4.1	4.6	2.4
4981	2.3	6.8	3.8	5.8	2.2	5.4	5.8	7.0	7.7	4.4
1353	1.9	5.5	3.9	5.4	3.1	5.5	5.8	7.5	8.6	4.3
7421	1.8	7.1	3.9	1.1	3.6	4.0	4.0	5.7	7.3	4.1
5325+	1.7	3.6	2.8	2.6	3.5	3.9	4.0	4.6	4.6	2.1
1637	3.8	6.4	-.5	6.0	.5	2.3	5.1	5.6	7.2	3.8
4039	.8	5.1	-2.7	.5	-21	-18	1.2	2.3	.7	1.9

NGC / IC*	#48 Na	#54-57 TiO	#60 Hα	#62 [SII]	4020 5870	4670 5870	5340 5870	6830 5870	6990 5870	7520 5870
Sc I'			**-23.0 < M < -22.0**							
692	4.0	18.6	-6.8	2.0	.56	.87	.98	.99	.98	.97
1232	3.0	18.4	2.8	1.8	.56	.84	.95	1.00	.99	.99
6925	4.4	16.2	-1.7	.7	.42	.69	.89	1.03	1.04	1.05
4536	4.8	16.9a	-54	-9.1	.60	.70	.89	1.05	1.07	1.12
908	4.8	18.7	-16	.7	.55	.70	.88	1.07	1.10	1.14
7329	4.8	20.6	-.6	1.1	.42	.70	.90	1.03	1.03	1.04
Sc II'			**-21.9 < M < -21.0**							
6744	3.3	16.8	-1.1	.4	.46	.72	.89	1.04	1.05	1.08
4501	5.2	14.6	-8.2	-1.5	.37	.73	.93	.98	.96	.95
4321	3.2	13.9	-13	-1.1	.61	.81	.94	1.00	1.01	1.06
6099	3.4	14.4	-6.9	.8	.64	.90	.96	.97	.95	.94
4303	3.4	10.8a	-26	-4.5	.72	.92	.97	.93	.92	.93
7392	5.1	16.0a	-8.2	-1.4	.51	.78	.93	1.04	1.06	1.08
1084	1.8	14.7	-24	-4.8	.87	.95	.98	1.00	.99	.99
6923	4.8	16.2	-1.5	1.9	.44	.69	.92	1.04	1.06	1.06
4254	5.1	15.3a	-8.4	1.2	.64	.81	.93	1.01	1.02	1.03
4535	2.2	11.3a	-53	-9.0	1.00	1.07	1.03	.93	.90	.85
5156	2.7	13.1	-2.5	1.3	.42	.67	.87	1.06	1.08	1.12
7552	4.2	9.9a	-80	-13	1.12	1.09	1.05	.92	.88	.87
3084	3.2	15.5	.6	2.0	.64	.82	.96	.99	.99	.99
289	2.6	16.3	-12	-.8	.55	.80	.92	1.03	1.06	1.09
2997	3.2	16.2a	-14	.9	.69	.88	.95	.98	.97	.97
4038	3.3	14.9a	-85	-17	.67	.91	.94	1.03	1.05	1.07
6215	2.4	13.3	-74	-11	.94	1.00	.99	.96	.95	.94
2442	4.5	18.6a	-8.5	-2.0	.37	.60	.87	1.10	1.15	1.19
5248	3.6	15.0	-6.7	1.6	.68	.86	.94	.99	.98	1.00
5236	2.5	12.3a	-70	-9.5	1.60	1.36	1.09	.83	.78	.74
4027	1.6	14.1	-29	-5.7	1.36	1.30	1.13	.88	.82	.77
Sc III'			**-20.9 < M < -19.4**							
2903	4.1	15.7	-44	-7.2	.97	1.02	1.03	.93	.92	.92
4981	2.9	9.1	-11	-1.4	.40	.69	.92	1.06	1.07	1.10
1353	4.6	18.9	-4.6	1.1	.57	.81	.95	1.00	1.01	1.01
7421	2.2	19.0	1.5	3.0	.61	.84	.96	.99	.99	.99
5326+	2.3	10.8a	-11	-1.3	.91	.97	.99	.98	.96	.93
1637	3.9	19.3a	-51	-9.2	.64	.77	.91	1.05	1.07	1.11
4039	1.9	11.6a	-135	-38	.80	.89	.95	1.00	1.00	.99

TABLE III *(continued)*.

NGC IC*	(B/V) B	(U/B) B	#2 L+K9	#3 L+K8	#4 K	#5 K+H	#9 Hδ	#10 Fe	#11 CN	#12 Ca
Seyferts -22.0 < M < -20.0										
7213	20	40	16.8	8.8	15.3	8.2	3.9	5.6	12.6	4.0
4507	15	30	2.7	-8.4	13.0	-.2	-1.3	.8	2.7	1.3
7582	15	30	2.8	-.1	1.7	3.6	2.9	.4	5.0	.6
6221	35	50	7.6	.8	6.1	3.2	1.8	.3	.8	.1
6300	20	40	14.5	9.8	18.1	10.8	5.7	3.3	6.1	2.7
5643	25	40	1.1	-9.8	12.6	2.9	3.0	1.4	4.5	1.5
7496	15	15	8.6	2.9	4.3	7.9	4.9	3.1	2.2	1.1
4941	30	40	16.5	5.2	8.9	4.1	1.8	2.6	6.9	5.1
Amorpheus -18.3 < M < -17.3										
5253	20	30	-5.5	-28	.6	-15	-14	-.5	-.2	-.3
626	5	5	-11	-52	-4	-42	-36	-8	-6	2

NGC IC*	#18 Fe	#14 G	#15 Hγ	#16 Fe	#27 Hβ	#31 Fe	#32 Fe	#34 Mg+MgH	#33+35 MgH	#36 Fe
Seyferts -22.0 < M < -20.0										
7213	4.7	7.5	.6	4.2	-.6	.8	6.6	8.8	8.2	4.1
4507	4.5	4.5	-10	-.9	-20	-131	2.1	5.0	3.1	.1
7582	.7	2.9	-2.1	4.8	-11	-52	2.6	5.9	5.6	2.5
6221	1.1	3.5	-3.5	2.7	-14	-6.1	1.3	2.1	2.7	1.6
6300	4.2	7.1	4.2	5.8	5.3	-6.0	6.2	6.1	6.7	4.7
5643	2.5	7.3	3.4	3.1	-1.7	-74	2.5	2.8	3.6	2.3
7496	2.2	1.2	-2.1	3.3	-13	-4.8	4.0	3.9	3.2	1.9
4941	7.1	7.8	1.0	6.3	-1.5	-39	3.3	7.4	7.8	4.0
Amorpheus -18.3 < M < -17.3										
5253	-1.1	1.3	-40	-1.8	-116	-665	-8.5	-.4	-1.9	.1
626	-12	-5	-113	-10	-266	-1310	-10	-3	-5	-3

NGC IC*	#48 Na	#54-57 TiO	#60 Hα	#62 [SII]	4020/5870	4570/5870	5340/5870	6630/5870	6990/5870	7520/5870
Seyferts -22.0 < M < -20.0										
7213	4.8	14.1a	-25	-4.2	.54	.82	.98	1.00	1.00	.99
4507	2.2	11.8a	-91	-20	.56	.77	.92	1.00	1.01	1.01
7582	4.3	13.1a	-115	-19	.64	.90	.93	1.02	1.03	1.04
6221	3.0	10.6a	-141	-19	.70	.90	.96	1.00	1.01	1.01
6300	4.2	17.6a	-12.5	-2.1	.42	.67	.91	1.06	1.09	1.13
5643	2.8	18.2a	-66	-20	.59	.77	.93	1.05	1.06	1.01
7496	1.0	15.9a	-107	-16	1.80	1.22	1.10	.92	.89	.85
4941	4.0	16.1a	-33	-7.8	.83	.89	.89	1.00	1.02	1.07
Amorpheus -18.3 < M < -17.3										
5253	-4.9	0a	-790	-80	1.89	1.44	1.16	.85	.78	.73
626	-8.4	0a	-1470	-126	2.64	1.62	1.14	.88	.83	.76

TABLE IV. — *The internal reddening, the corrected continuum and the respective face-on templates.*

NGC	E(B-V)	C4020/C5870	C4570/C5870	C5340/C5870	C6630/C5870	C6990/C5870	C7520/C5870	Nearly face-on template NGC or IC*
289	.10	.63	.87	.96	.99	1.01	1.02	1232,1302,1512,4440
772	.10±.15	.50	.77	.92	1.01	1.02	.98	1637,5156,7421
779	.02±.05	.69	.82	.96	.99	.99	.98	692,1232,1302,1512
908	.11±.05	.64	.77	.91	1.03	1.04	1.06	1232,4254,7421
1084	0 ±.05	same as table 3						4303,5325*
1350	-.12±.13	same as table 3						488,,524,1398,1411
1353	.02	.59	.82	.96	.99	1.00	1.00	1637
1371	-.03±.10	same as table 3						488,1411,1512,5267*
1380	-.06	same as table 3						1398,1553
1425	.04±.03	.69	.87	.96	1.00	.97	.94	1302,4440
1543	-.06±.09	same as table 3						488,4440,5101,5267*
1617	-.05±.13	same as table 3						488,524,1398,1411
2781	0 ±.03	same as table 3						1302,1512,4440
2811	.07±.07	.54	.88	.97	.96	.94	.92	1302,1512,4440,5267*
2903	.18	1.25	1.19	1.09	.87	.84	.81	7496
3064	.02	.56	.83	.96	.98	.98	.98	1232
3223	.14±.03	.56	.90	.99	.96	.93	.91	692,1302,1512,4440
3351	-.02±.09	same as table 3						2997,5248,5325*,6099
3358	.06±.08	.56	.85	1.00	.97	.95	.93	1302,1512,4440,5267*
3368	.26±.02	.58	.85	.98	.92	.90	.90	1302,3887,4254,4440
3521	.11±.04	.56	.84	.97	.93	.91	.90	1232,1512,7421
3625	.25±.06	.53	.88	.98	.94	.90	.87	1302,3887,4440,5121
3627	.11±.02	.57	.80	.95	.96	.94	.90	3887,4254
4038	.08±.10	.75	.87	.96	1.00	1.01	1.01	2997,4303,4321,5325*
4039	.04±.06	.85	.92	.96	.99	.98	.96	4303,6215
4192	.49±.02	.60	.84	.98	.93	.91	.92	1512,3887,7421
4438	.39±.02	.57	.87	1.00	.93	.93	.93	1302,3887,4440,7421
4482	.09±.03	.57	.87	.96	.96	.96	.92	1232,1302,1512,4440
4501	.18±.01	.48	.85	.98	.92	.88	.84	692,1232
4535	.19±.06	1.31	1.26	1.09	.87	.82	.75	4027,5236,7496
4536	.23±.03	.69	.86	.94	.97	.95	.96	2997,4321,5325*
4569	.19±.03	1.19	1.21	1.08	.86	.80	.74	4027,7496
4594	.04±.09	.48	.80	.96	.94	.91	.90	488,1398,1411
4767	.02±.13	.48	.75	.92	1.00	1.00	1.02	488,524,1398,1411
4856	.01±.09	.53	.81	.93	.99	.98	.98	488,1302,4440,5267*
4941	.26±.03	.56	.87	.96	.92	.90	.90	1637,3887,7421
5064	.22±.06	.56	.89	.97	.96	.94	.92	1302,3887,4440,5121
5612	.17±.03	.55	.85	.97	.96	.95	.92	692,1232,1302,1512
5746	.34±.09	.53	.84	.93	.97	.96	.98	488,1512
6221	.27±.15	1.15	1.14	1.03	.91	.88	.84	4027,5325*,7496
6300	.26±.02	.61	.84	.99	.97	.96	.95	3887,7421
6694	0 ±.06	same as table 3						1302,1512,4440,5121
6744	.11±.04	.54	.79	.91	1.00	.99	1.00	692,1232,1512
6782	.01±.05	.56	.87	.96	.98	.96	.93	1637,2997,4321,6099
6923	.20±.04	.58	.82	.98	.97	.96	.93	692,1232,1512,3887
6925	.20±.03	.56	.82	.95	.96	.94	.92	692,1232,1512,7421
6942	.11±.12	.51	.85	.96	.96	.95	.95	1512,4440,5101,5267*
7079	-.01±.12	same as table 3						1411,1512,5101,5267*
7083	-.04±.03	same as table 3						1637,4440,7421
7184	.20±.02	.58	.86	.95	.95	.94	.93	1302,1512,3887,7421
7205	.01±.02	.65	.81	.93	1.01	1.00	1.01	1512,3887,7421
7329	.09±.03	.48	.76	.93	1.00	.98	.98	488,1398
7392	.16±.04	.64	.90	.98	.98	.98	.97	1637,2997,5248,6099
7410	.05±.09	.46	.71	1.01	1.05	1.07	1.06	524,1398,1553,7049
7552	.18±.04	1.44	1.28	1.09	.86	.81	.77	4027,5236
7582	.45±.04	1.24	1.19	1.07	.87	.82	.77	4027,7496

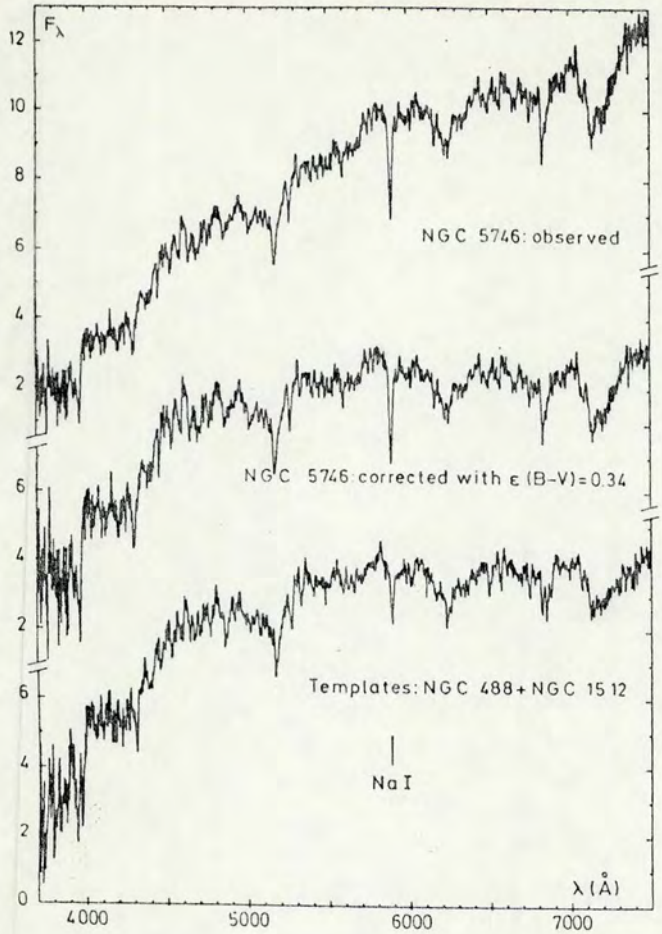

(a)

FIGURE 1. — Examples of the method used to derive the internal reddening, respectively for red (left) and blue (right) nuclei. Downwards : (1) observed spectrum, (2) reddening corrected, (3) the respective nearby face-on template with similar population content. The flux F_λ is normalized to 10 at 5870 Å.

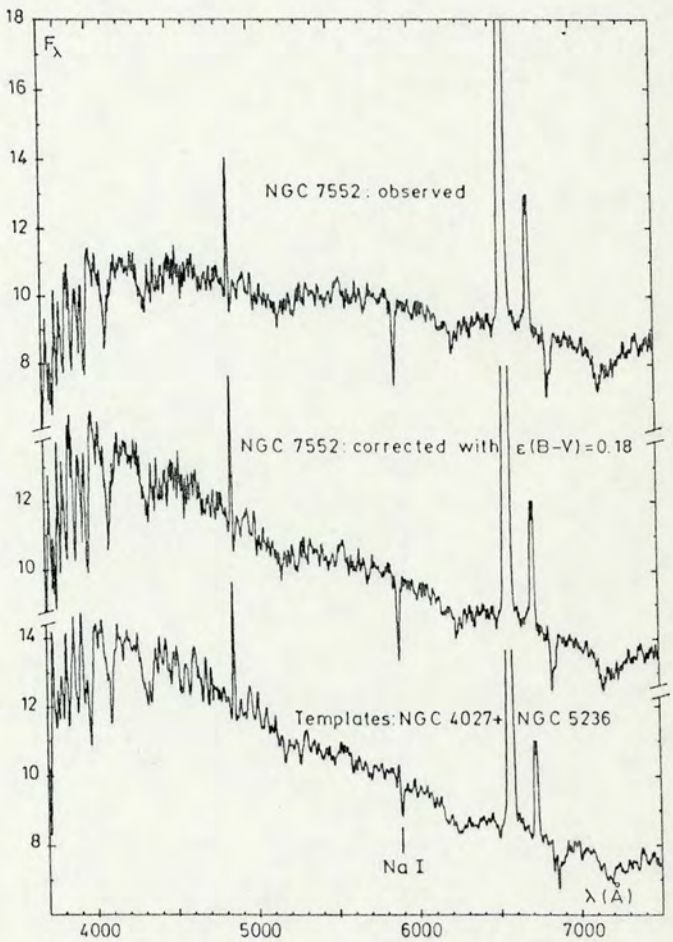

FIGURE 1(b).

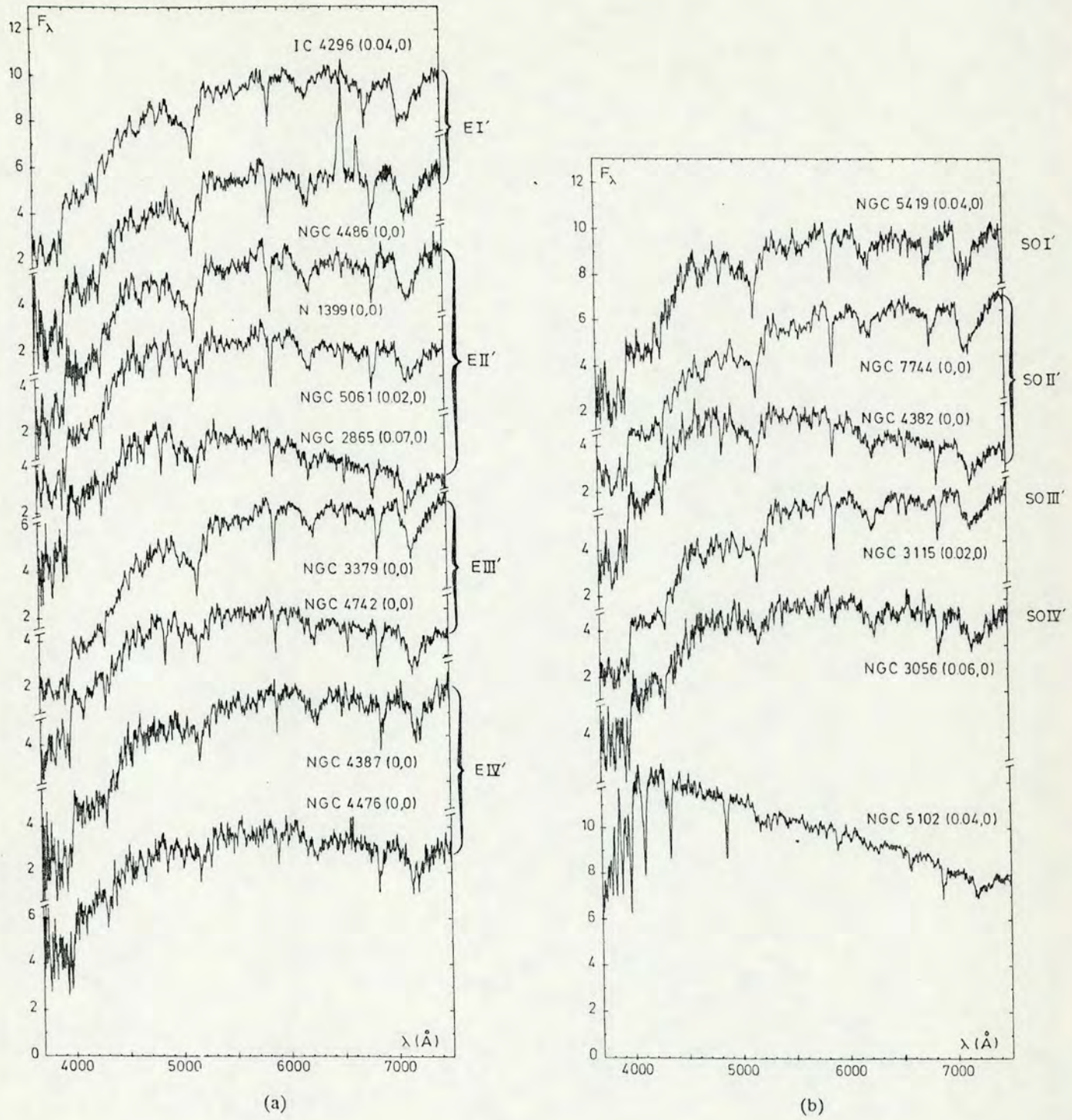

FIGURE 2. — Some typical and atypical spectra found in the luminosity *vs.* morphological type groups. (a) elliptical galaxies ; (b) S0 galaxies ; (c) spiral galaxies. Each galaxy is labelled with the extrinsic and intrinsic reddening corrections applied to the continuum. Normalization as in figure 1.

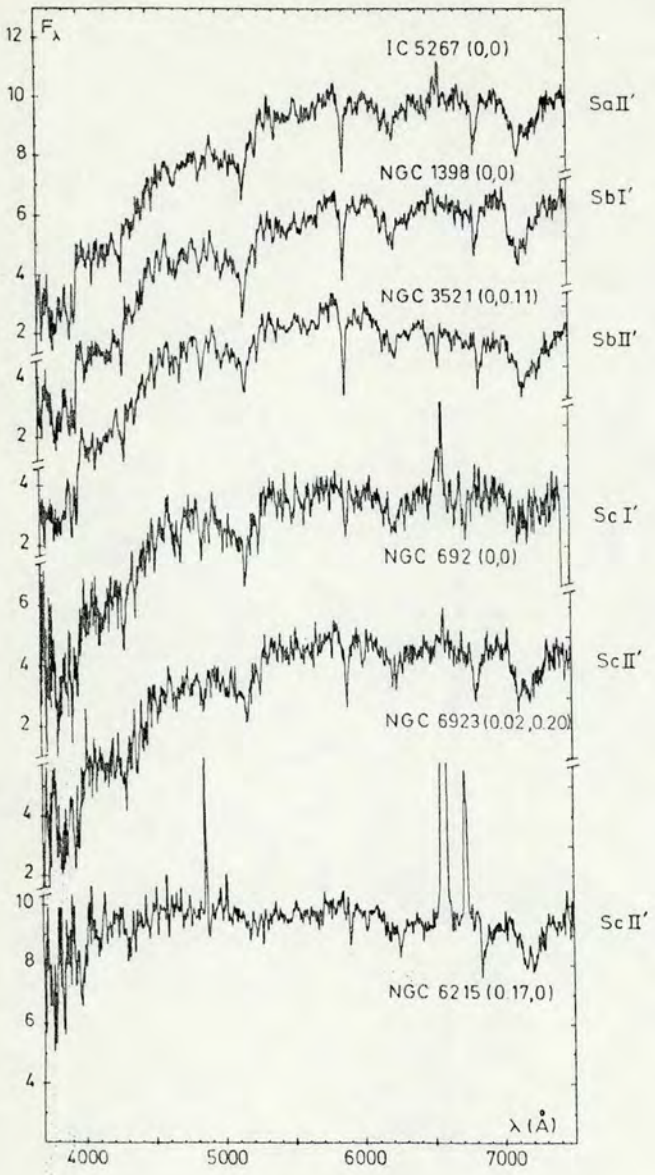

FIGURE 2(c).

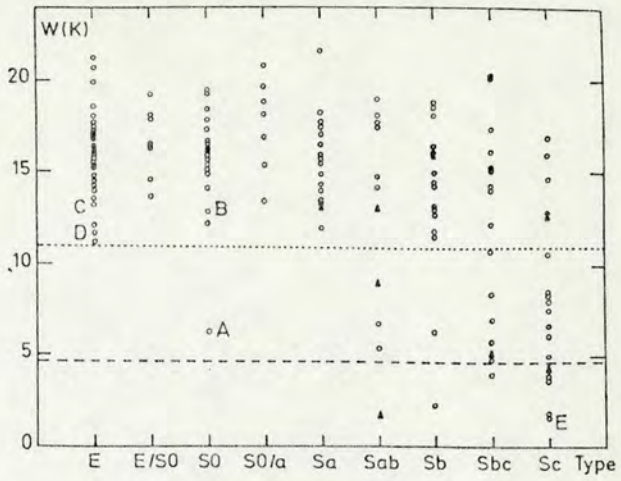

FIGURE 3(a).

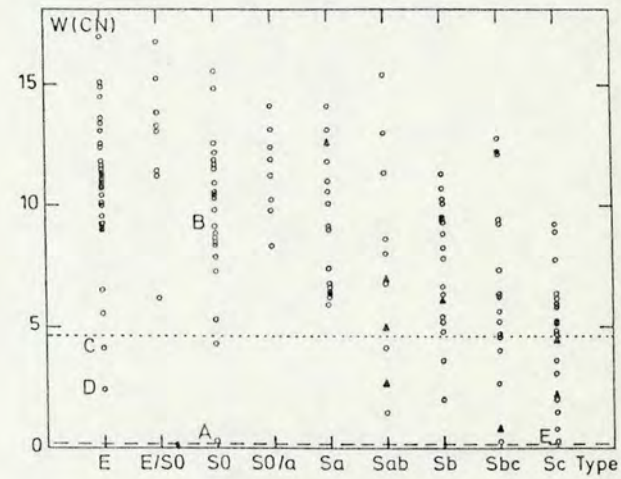

FIGURE 3(b).

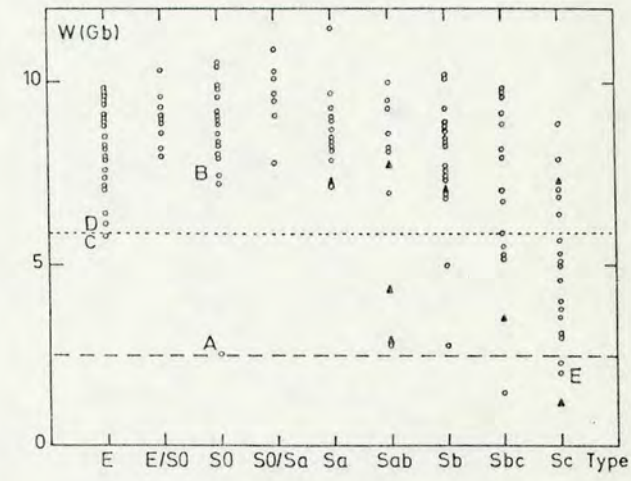

FIGURE 3(c).

FIGURE 3. — Equivalent widths in Å for the strongest metallic features as a function of morphological type (a) CaII K ; (b) CN λλ4150-4216 ; (c) *G*-band ; (d) MgI + MgH ; (e) TiO. Some galaxies which are discussed with more detail in the text are labelled : A = NGC 5102, young population component ; B = NGC 4382 and C = NGC 2865, intermediate age component ; D = NGC 4476, genuine metal poor ; E = NGC 5236, very blue nucleus in face-on Sc galaxy. Filled triangles represent Seyfert or Seyfert to linear transition objects. We recall in the figures, values for metal poor Galactic globular clusters, dotted line $[Z/Z_\odot] = -1$, dashed line $[Z/Z_\odot] = -2$.

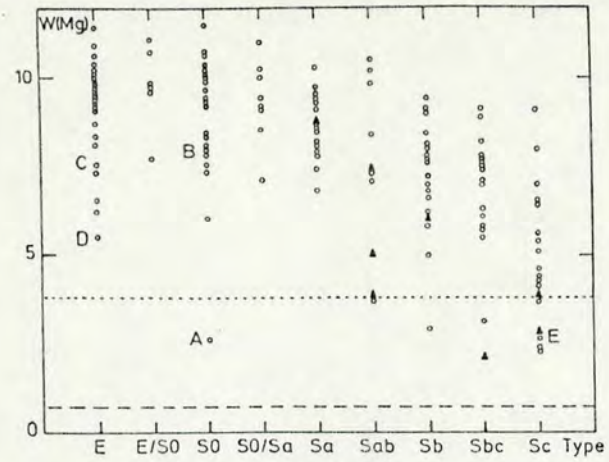

FIGURE 3(d).

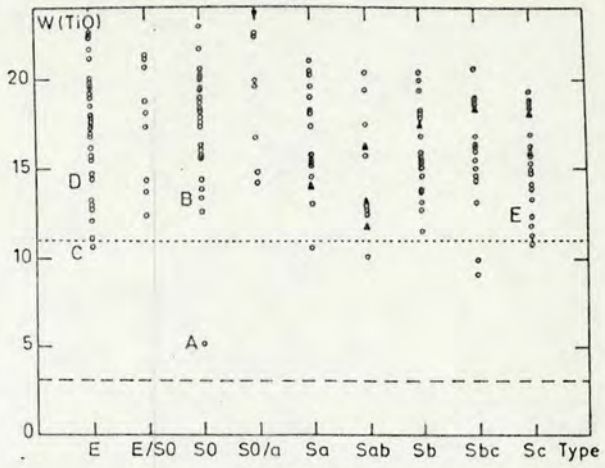

FIGURE 3(e).

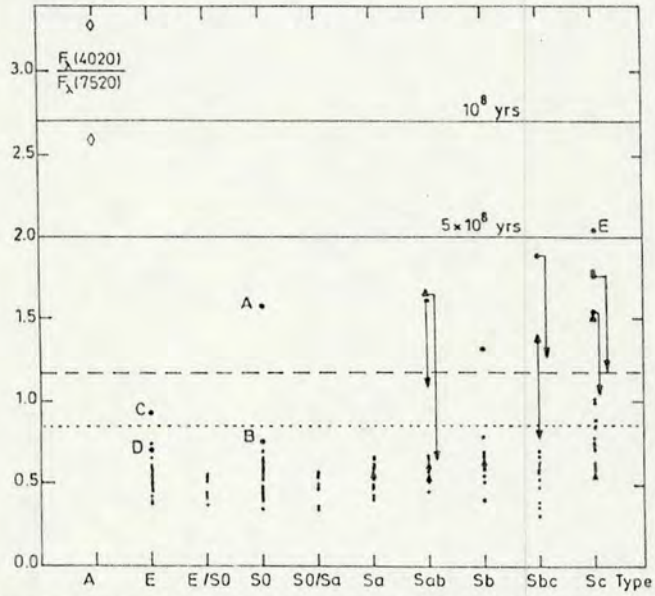

FIGURE 4. — Continuum slope expressed as the F_λ ratio C(λ4020)/C(λ7520). The values are corrected for external an internal reddening. Arrows indicate for the inclined blue spirals, the position of the object if not corrected for internal reddening. Notice the very blue continuum of the 2 amorphous galaxies (HII regions) on the upper left corner (diamonds). For the rest, same symbols as in figure 3. Continuous lines are young star clusters. We emphasize that the Globular cluster at $[Z/Z_\odot] = -2$ corresponds to the upper dashed line, as opposed to figure 3.

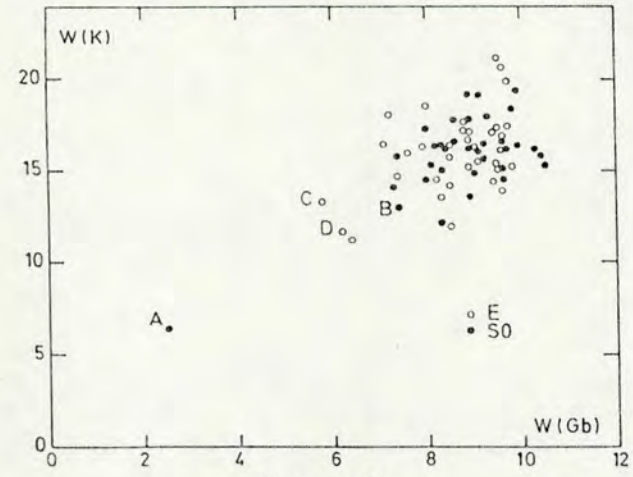

FIGURE 5(a).

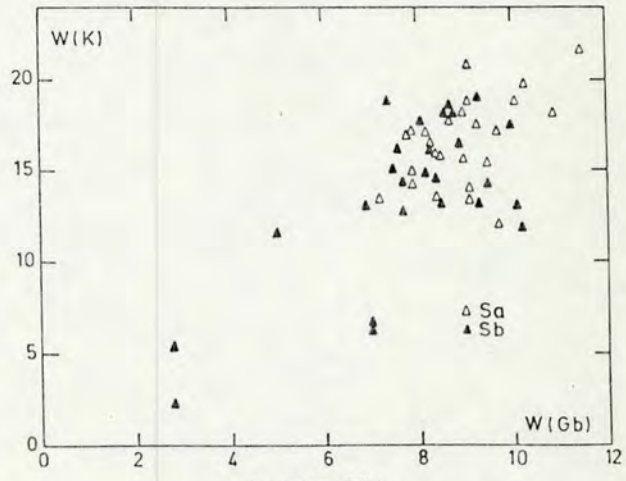

FIGURE 5(b).

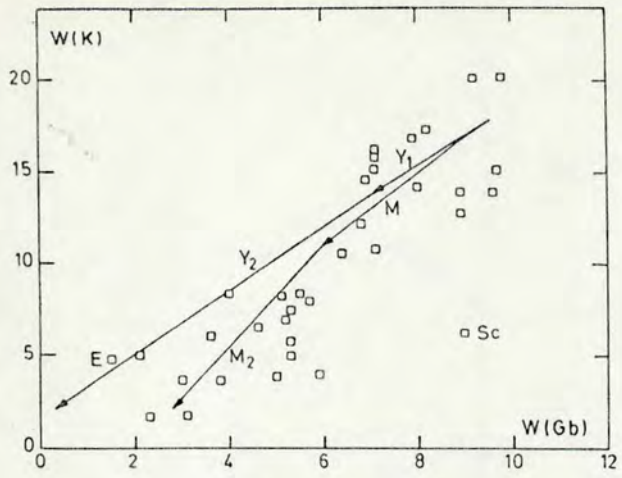

FIGURE 5(c).

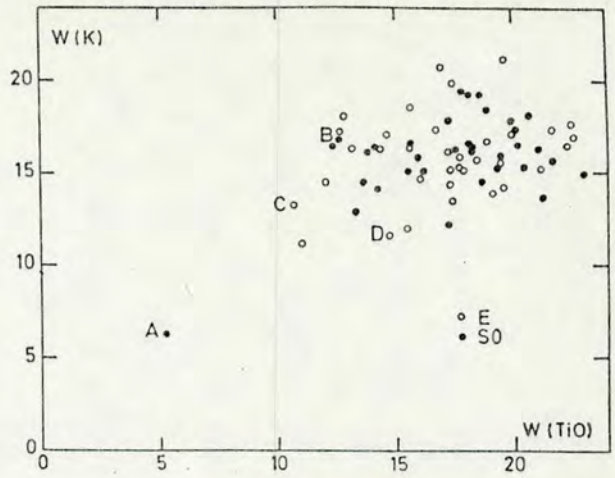

FIGURE 5(e).

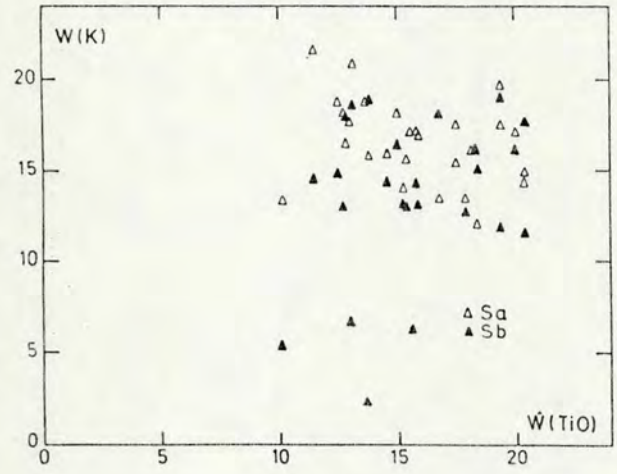

FIGURE 5(d).

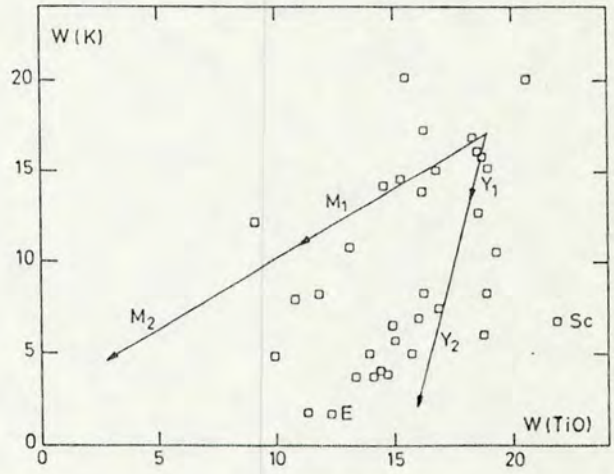

FIGURE 5(f).

FIGURE 5. — Figures 5(a) though 5(c) *W vs. W* for two metallic features in the blue (Ca II K and *G*-band), respectively for morphological types E + S0, Sa + Sb and Sc. *W* values are in Å.
Open circles : elliptical galaxies.
Filled circles : S0 galaxies.
Open triangles : Sa galaxies.
Filled triangles : Sb galaxies.
Black stars : Sc galaxies.
Figure 5(d) through 5(f), *W* for one metallic feature in the blue (CaII K) *vs.* another in the red (TiO). Arrows represent youth and metallicity vectors as described in section 6.1. Particularly, a comparison of the plots for the Sc sample (Figs. 5(c) and 5(f)) shows how the contamination from young age components mimics a metallicity sequence in diagrams involving only features in the blue.

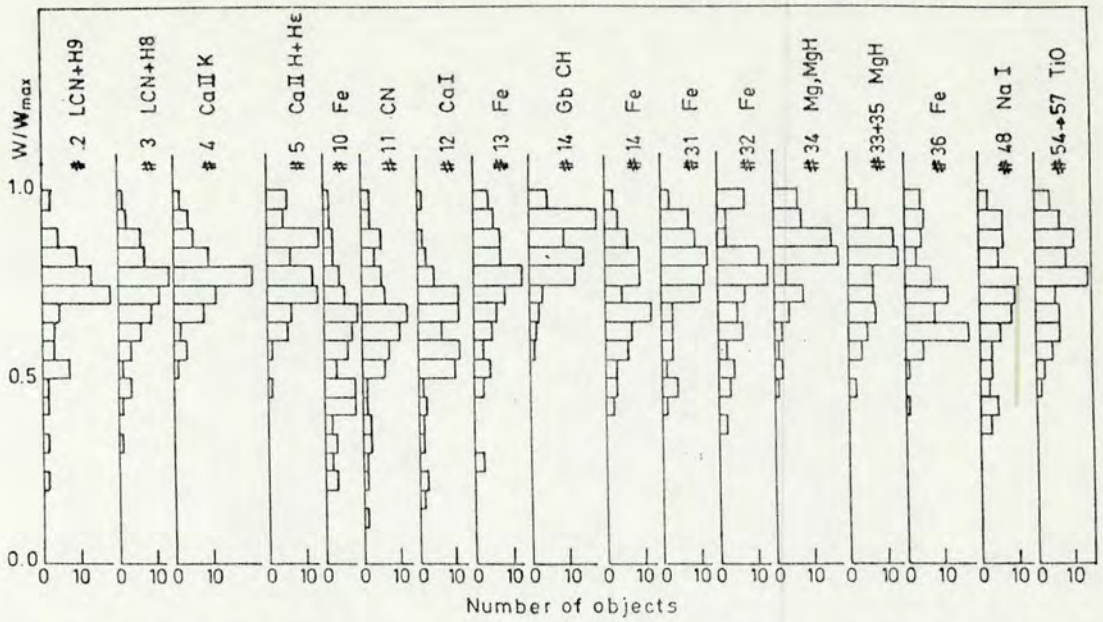

FIGURE 6. — *W* histograms for 17 metallic features in E and S0 galaxies (NGC 2865, 4382 and 5102 have been excluded, due to large age effects). Values are normalized to the maximum in each window. Notice the large dynamical range for CN # 11.

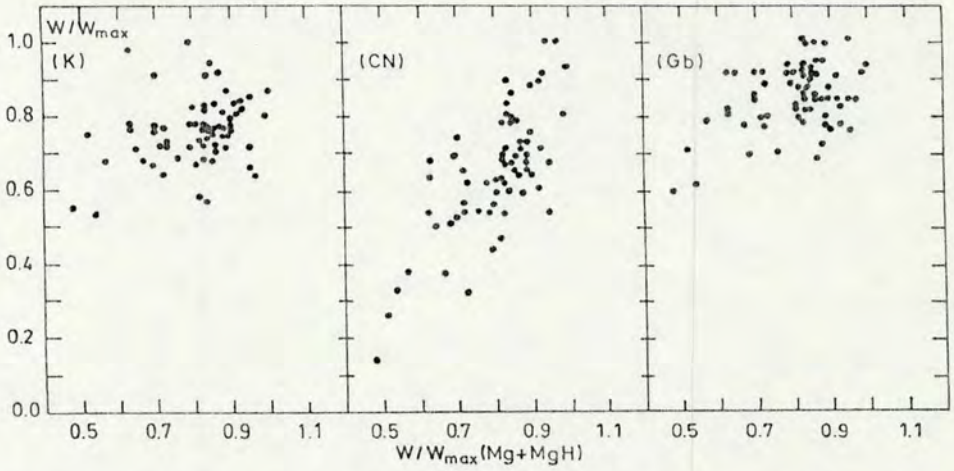

FIGURE 7. — For the subsample of galaxies in figure 6, we compare metallicity indicators. The large dynamical range of CN is confirmed.

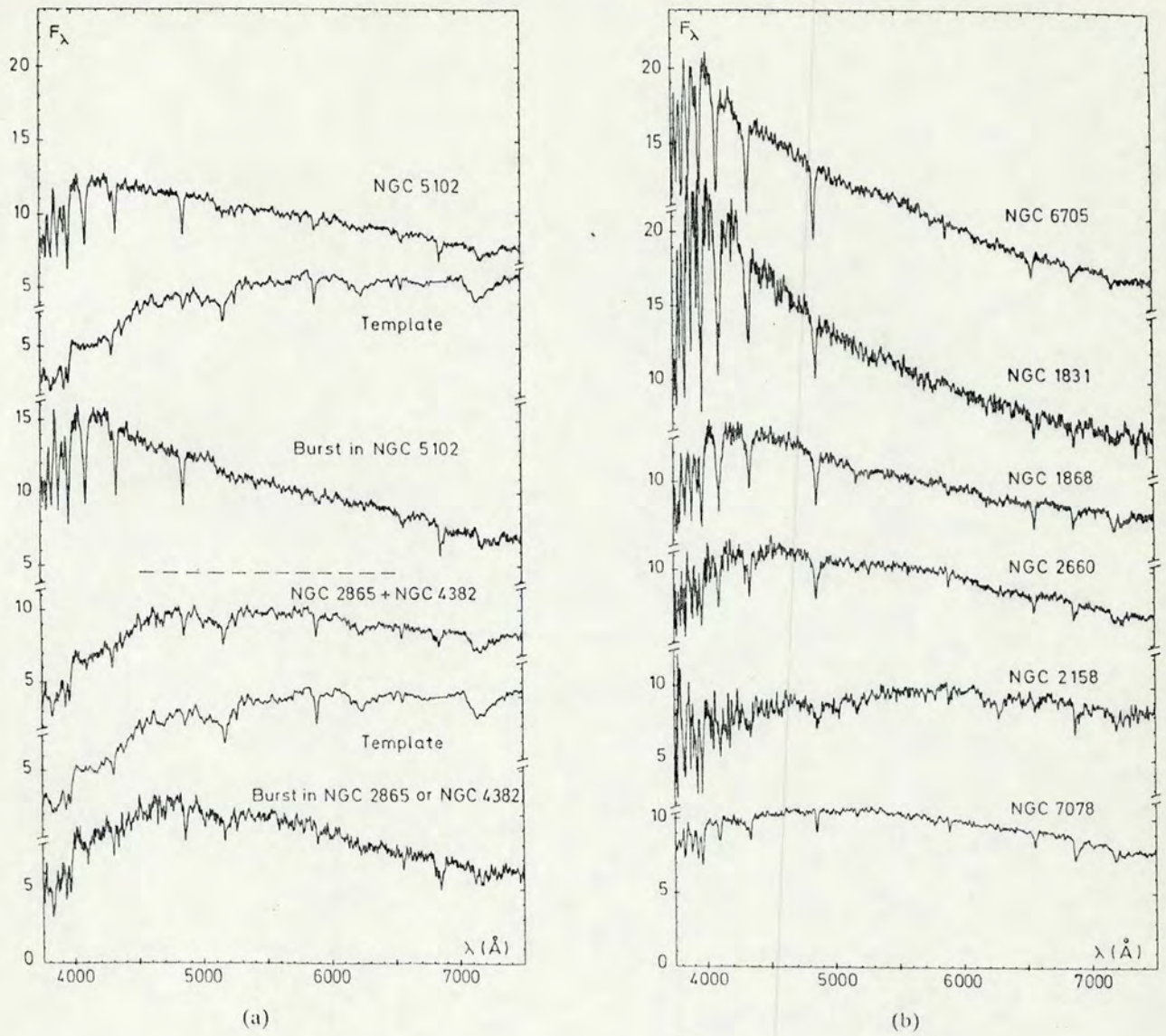

FIGURE 8. — Empirical synthesis for the blueish early type galaxies NGC 5102, NGC 4382 and 2865. (a) Observed spectra, templates and difference spectra. (b) Galactic and LMC star clusters with ages from 10^8 to 3×10^9 yr, as well as the metal poor globular cluster NGC 7078. Normalization as in figure 1. Difference spectra resemble young clusters rather than the old metal-poor one.

Astron. Astrophys. 181, 270–272 (1987)

ASTRONOMY AND ASTROPHYSICS

The metallicity versus luminosity relationship for early-type galaxies*

E. Bica and D. Alloin

Observatoire de Paris, Section de Meudon, F-92195 Meudon-Principal, France

Received October 7, 1986; accepted February 23, 1987

Summary. In the equivalent width (W) vs absolute magnitude (M_B) diagram corresponding to the best metallic features in the visible range, CN and Mg + MgH, field giant E and S0 galaxies are shifted towards weaker line-strengths with respect to galaxies belonging to the Virgo and Fornax clusters. We find evidence that this is a genuine stellar population effect. For part of the deviating galaxies it results from an aperture effect, galaxies at larger redshifts including more of the metal poor component outside their nucleus. For the rest, the shift is due to a variable content of intermediate age components in the range 4–10 Gyr, superimposed on the very old underlying population.

Key words: galaxies: evolution of – galaxies: stellar content of galaxies : elliptical – clusters of galaxies

1. Introduction

The strengthening of absorption lines and the reddening of colours in early-type galaxies when the absolute luminosity increases, is well established and, most probably, a result of metallicity differences. These correlations present however a considerable scatter, for which many explanations have been proposed, either in terms of colours or absolute magnitude dispersions (Faber, 1977; Sandage and Visvanathan, 1978). If related to population effects, this scatter among galaxies at a given luminosity, might result from a variable content of hot stars belonging to a young population rather than to the blue horizontal branch (Véron and Véron-Cetty, 1985). Another source of scattering might be an intrinsic dispersion in the star formation rate at fixed galactic mass (Arimoto and Yoshii, 1987). Space ultraviolet observations (e.g. Bertola et al., 1982) have revealed important colour differences among early-type galaxies which, extrapolated to longer wavelengths could explain the colour dispersion observed in the visible. Some early-type galaxies present an upturn of the flux shortwards of 2000 Å and hence, must contain a hot stellar component. This population could consist of recent residual star formation or blue horizontal branch stars. In the range 2600–3800 Å, giant early-type galaxies also show some relative flux scatter, possibly due to a variable content of intermediate age populations. In the particular case of elliptical galaxies, the scatter in the line strength vs absolute magnitude relation is correlated to that observed in a similar plot of the velocity dispersion vs absolute magnitude (Terlevich et al., 1981). This correlation of the scatters seems to be associated with the intrinsic axial ratio; it would also be a natural consequence of uncertainties in the absolute magnitude values such as those introduced by departures from a uniform Hubble flow.

2. Discussion

Recent spectral observations of a sample of 35 elliptical and 34 lenticular galaxies have been described in Bica and Alloin (1987). From this data set, we use the sum of the most sensitive metallic indices, namely equivalent widths W(CN 4150, 4214 Å) and W(Mg + MgH 5156, 5196 Å), to investigate the metallicity versus absolute magnitude M_B relationship in early-type galaxies. However, one should keep in mind that both indices are subject to dilution effects in a composite spectrum if intermediate or young age components are present. Dilution will be stronger for CN, although Mg + MgH might be considerably affected as well, according to our analysis of integrated star cluster spectra (Bica and Alloin, 1986). Thus, we also include in the present study the E and S0 galaxies which contain important contributions from intermediate (NGC 2865, 4382) and young (NGC 5102) age components (Bica and Alloin, 1987). Results are displayed in Fig. 1 where at first glance little correlation appears, while a colour-magnitude relationship exists, especially if one considers ultraviolet and infrared colours and early type galaxies as faint as −14 (e.g. Persson et al., 1979). As a matter of fact our sample consists mostly of luminous galaxies and some of the fainter ones ($-18.5 \leqq M_B \leqq -16.5$) are certainly atypical. Galaxies which depart most in the right part of the diagram are NGC 4486B, a tidally stripped object (Bica and Alloin, 1987), and NGC 1400 for which the M_B value is quite uncertain. This S0 galaxy, at $M_B = -17.9$, is red and strong-lined with little evidence for tidal stripping and it is probably more luminous than implied by its redshift. It is projected on a small southern group of galaxies, forming a close pair with the group member NGC 1407. The group itself presents a larger redshift with $\Delta V \simeq 700\,\mathrm{km\,s^{-1}}$ and if NGC 1400 belongs to it, then $M_B = -20.6$. In addition, the velocity dispersion in NGC 1400 is typical of massive galaxies (Kormendy and Illingworth, 1983). Prugniel et al. (1987) have studied the luminosity profile and the velocity dispersion in three M 87 dwarf companions which we have also observed. They find that the luminosity profile of NGC 4478 is severely truncated. Indeed, this galaxy lies at the right edge of the relation in Fig. 1a, suggesting that some tidal stripping may have affected it. Its

Send offprint requests to: D. Alloin

* Based upon observational data collected at the European Southern Observatory

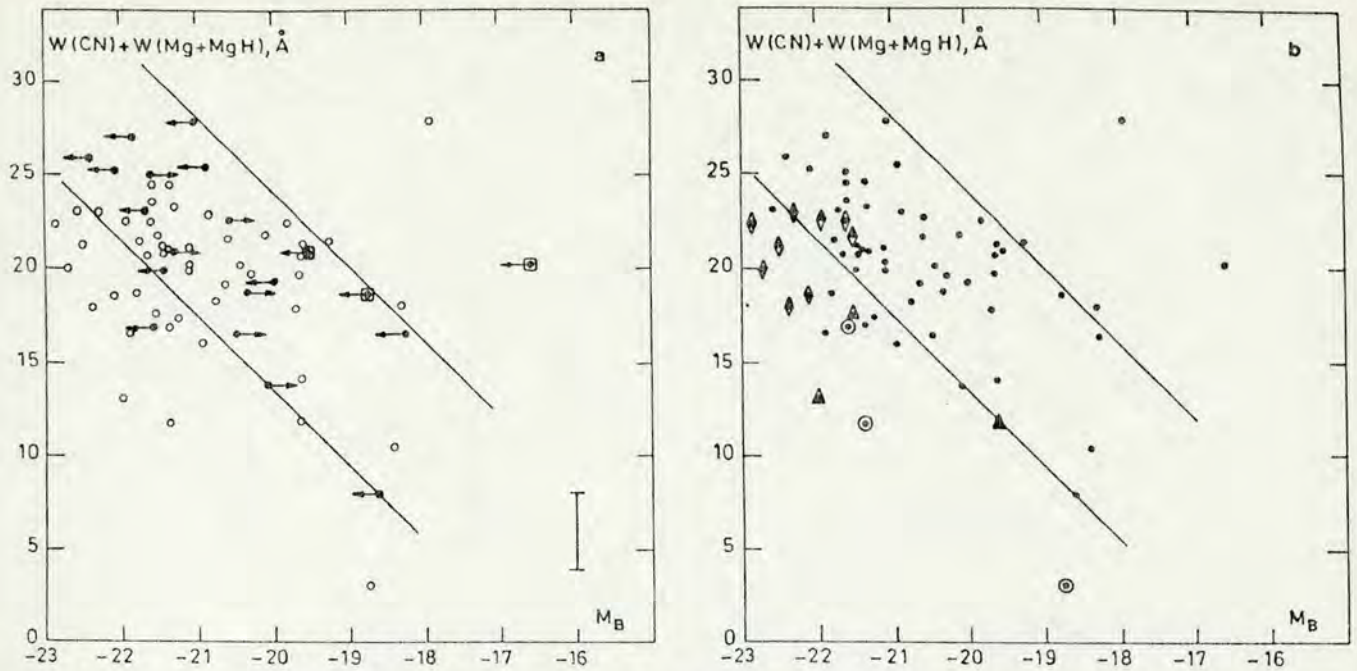

Fig. 1. **a** Best metallicity index, $W(CN) + W(Mg + MgH)$, as a function of absolute magnitude for early-type galaxies. Members of small groups and field galaxies are shown with open circles. Virgo and Fornax members are represented with black dots and the arrow attached to each point shows the effect of correcting for the Virgo-centric infall (Fornax galaxies correspond to arrows pointing to the right and Virgo galaxies to the left). Notice the systematic lowering of this index in the case of luminous field galaxies. The three points within squares indicate tidally stripped objects. The error-bar is provided in the lower right corner. Light continuous lines enclose 90% of the Virgo and Fornax members. **b** All points are shown again without discriminating between field and cluster galaxies. Points within diamonds indicate galaxies for which the projected slit was larger than 4 kpc^2; points within circles indicate galaxies in which age effects have been demonstrated in Bica and Alloin (1987); points within triangles are for galaxies in which age effects are suspected from their strong Hβ absorption. Therefore, the systematic effect just described (Fig. 1a) can be understood in terms of a metal-poor population around the nucleus or in terms of young nuclear stellar components. Galaxies discussed in the text are given with their (M_B; W) values: NGC 1400 (−17.94; 27.8), NGC 2865 (−21.37; 11.6), NGC 4382 (−21.60; 16.8), NGC 4387 (−18.75; 18.6), NGC 4476 (−18.62; 7.9), NGC 4478 (−19.55; 20.7), NGC 4486 (−22.08; 25.2), NGC 4486B (−16.59; 20.1), NGC 4649 (−21.87; 27.0), NGC 5018 (−21.99; 13.0), NGC 5061 (−21.54; 17.5), and NGC 5102 (−18.73; 2.9)

central velocity dispersion is moderate however (150 km s^{-1}). According to Fig. 1a, NGC 4486B should be a highly stripped object, a conclusion in agreement with its large central velocity dispersion (200 km s^{-1}) typical of massive galaxies. Its luminosity profile shows some truncation too, although not as much as in the case of NGC 4478. On the other hand NGC 4476 is definitely not a tidally stripped galaxy since its luminosity profile follows an $r^{1/4}$ law and its central velocity dispersion is small (132 km s^{-1}). It represents a genuine low metallicity, low luminosity elliptical galaxy with a spectrum similar to that of a globular cluster in the range $-1.0 \leqq [Z/Z_\odot] \leqq -0.5$ (Bica and Alloin, 1987). Another dwarf galaxy NGC 4387 falls at the edge of the relationship in Fig. 1a. This galaxy lies near the centre of the Virgo cluster and, because of its high surface brightness, is suspected to be a stripped object.

The scatter observed in the diagram for luminous galaxies is of the same order as that in the optical colours (Faber, 1977; Sandage and Visvanathan, 1978). The formal error-bar in W(CN, Mg + MgH) is ± 2.1 Å, suggesting that the scatter in Fig. 1a is intrinsic. As recalled in the introduction, it could be accounted for in many ways. However, if only Virgo and Fornax members are considered, a tighter correlation appears, especially when one disregards the tidally stripped galaxy (NGC 4486B) and the case of NGC 4382 for which age effects are obvious. Remaining scattered galaxies in this diagram are field objects or they belong to small groups. Figure 1a indicates that luminous field galaxies present with respect to giant cluster members, a systematic shift towards weaker line strengths.

Absolute magnitudes for our sample galaxies were derived assuming a uniform Hubble flow (Sandage and Tammann, 1981). More specifically, M_B values for Virgo and Fornax members were computed using the mean velocity of the corresponding cluster. The infall of the Local Group towards Virgo (Aaronson et al., 1981) changes the relative positions of Virgo and Fornax galaxies as indicated by arrows in Fig. 1a. Indeed correcting for this effect reduces slightly the scatter in the relationship based upon these two clusters. The distribution of Virgo plus Fornax members with respect to the rest of the sample remains essentially unchanged.

The effect of departures from the Hubble flow on the present sample taken as a whole does not seem to be responsible for the observed scatter either. Sandage and Tammann (1984) suggest that the 600 km s^{-1} infall of the Local Group with respect to the microwave background can be decomposed into a motion towards Virgo and another of Virgo towards the Hydra-Centaurus supercluster. Davies et al. (1986) think rather, that the local volume of the Universe, 120 Mpc accross, is moving with 600 km s^{-1} towards $l = 312°$ and $b = +6°$, with respect to the microwave background. Regardless of the motion direction and of which fraction of the local Universe takes part into these coherent motions, the inclusion of galaxies in their apex and antiapex would introduce at most, a scatter of $\pm$ 600 km s^{-1} in the observed radial velocities of a given galaxy sample. The mean recession velocity in

our sample is 2000 km s^{-1}, implying that departures from the Hubble flow amount to ± 0.6 magnitude in Fig. 1a. This is too small to account for the total scatter or for the systematic difference between field and cluster giant galaxies. We suggest instead that this difference is due to a stellar population effect.

3. Concluding remarks

Indeed, Larson et al. (1980) found a significant difference in the colour-magnitude diagram between field and cluster galaxies: this effect could be due to star formation in field galaxies which, because of their isolation, have kept gas for a longer time. Positions in Fig. 1b of the galaxies NGC 2865 and 4382 containing a 1 Gyr component (Bica and Alloin, 1987), together with NGC 5018 and 5061 showing strong Hβ absorptions with respect to the remaining redder giant galaxies (Bica and Alloin, 1987), suggest that the latter form a sequence with variable amounts of an additional intermediate age component in the range 4–10 Gyr. From our simple diagram however, we cannot exclude an interpretation of this effect in terms of a variable content of a low metallicity component. In fact, this seems to be the case for galaxies at large redshifts for which the aperture includes more contribution from the metal-poor zones outside the nucleus. This is particularly important for galaxies with $M_B < -22$, where all deviating points correspond to apertures larger than 4 kpc^2 (Fig. 1b). The age effect remains the best explanation in the region $-22 \leqq M_B \leqq -21$, where most of the galaxies are seen through slit surfaces similar to those of Virgo and Fornax galaxies, because they present W values between those of the cluster galaxies and of objects in which age effects have been clearly demonstrated.

We suspect that the shift in Fig. 1 is not due to a very recent star formation from residual gas if this is related to the ultraviolet upturn shortward of 2000 Å, because two of the most typical examples of the latter phenomenon, NGC 4649 and 4486 (Bertola et al., 1982) are Virgo giants at the top of our diagram. A better explanation to the shift is in terms of an intermediate age stellar component. The spectral differences observed among nearby massive E and S0 galaxies indicate also that the visible line indices or colours may be misleading as luminosity criteria for deriving distances of more distant galaxies, even after aperture effects have been taken into account.

Acknowledgements. We are gratefully indebted to Pr. B. Pagel for interesting suggestions. E.B. thanks the Brazilian Institution CNPq for a fellowship.

References

Aaronson, M., Dawe, J., Dickens, R., Mould, J., Murray, J.: 1981, *Monthly Notices Roy. Astron. Soc.* **195**, 1 P
Arimoto, N., Yoshii, Y.: 1987, *Astron. Astrophys.* **173**, 23
Bertola, F., Capaccioli, M., Oke, J.: 1982, *Astrophys. J.* **254**, 494
Bica, E., Alloin, D.: 1986, *Astron. Astrophys.* **162**, 21
Bica, E., Alloin, D.: 1987, *Astron. Astrophys. Suppl.* (in press)
Davies, R., Burstein, D., Dressler, A., Faber, S., Lynden-Bell, D., Terlevich, R., Wegner, G.: 1986, *Proc. IAU Symp.* No. **124** (to appear)
Faber, S.: 1977, in *Evolution of Galaxies and Stellar Populations*, eds. B. Tinsley, R. Larson, Yale University Observatory, New Haven, p. 157
Kormendy, J., Illingworth, G.: 1983, *Astrophys. J.* **265**, 632
Larson, R., Tinsley, B., Caldwell, C.: 1980, *Astrophys. J.* **237**, 692
Persson, S., Frogel, J., Aaronson, M.: 1979, *Astrophys. J. Suppl.* **39**, 61
Prugniel, P., Nieto, J.L., Simien, F.: 1987, *Astron. Astrophys.* **173**, 49
Sandage, A., Tammann, G.: 1981, *A Revised Shapley-Ames Catalogue of Bright Galaxies*, Carnegie Institution of Washington
Sandage, A., Tammann, G.: 1984, in *Large Scale Structure of the Universe, Cosmology and Fundamental Physics*, eds. G. Setti, L. Van Horn, CERN, Geneva, p. 127
Sandage, A., Visvanathan, N.: 1978, *Astrophys. J.* **225**, 742
Terlevich, R., Davies, R., Faber, S., Burstein, D.: 1981, *Monthly Notices Roy. Astron. Soc.* **196**, 381
Véron, P., Véron-Cetty, M. P.: 1985, *Astron. Astrophys.* **145**, 433

Astron. Astrophys. 186, 49–63 (1987)

ASTRONOMY
AND
ASTROPHYSICS

Near-infrared spectral properties of star clusters and galactic nuclei*

E. Bica and D. Alloin

Observatoire de Paris, Section de Meudon, F-92195 Meudon Principal Cedex, France

Received January 6, accepted February 23, 1987

Summary. We present CCD spectra with 12.5 Å resolution from 6300 to 9700 Å of 30 star clusters covering ranges 10^6 to $1.65\ 10^{10}$ yr in age, and -2.0 to 0.1 in metallicity, $[Z/Z_\odot]$. As well, 62 galactic nuclei have been observed in galaxies with morphological types E to Sc and intrinsic luminosities $-23.3 \leqq M_B \leqq -16.7$. For every object in the present sample, the visible spectrum has been discussed in earlier papers. We describe a powerful method for correcting CCD fringes in the near-infrared. We measure the near-infrared continuum distribution and the equivalent widths (W) of 13 absorption features. Analysis of the star cluster sample indicates that in the near-infrared spectral range, metallicity is the dominant parameter. Age produces second order effects of various types: (i) enhancement of molecular bands in certain phases of a blue cluster evolution by the accumulation of luminous red stars, (ii) contamination of metallic lines with Paschen absorption lines and, (iii) slight steepening of the continuum slope for young clusters. In view of population synthesis of galactic nuclei using the star clusters, we present grid predictions as a function of metallicity and age for 5 metallic features and for the continuum distribution. Spiral galaxies and luminous elliptical galaxies show similar strong-lined spectra suggesting that their metallicities in the central regions are comparable. Even very blue galaxies exhibit in the near-infrared spectra quite similar to those of more classical galaxies. Evidence is found however that a large flux contribution to this range is not from their old underlying population. Strong-lined globular clusters like NGC 6528 have integrated spectra comparable to those of massive galaxies. Consequently, they are of a great help in population synthesis work, whatever their precise metallicity value.

Key words: near-infrared spectra – star clusters – galactic nuclei

1. Introduction

As yet much effort has been devoted to the interpretation of near-infrared feature strengths in the spectra of galactic nuclei, in terms of the stellar types which contribute most to their integrated light (e.g. Spinrad and Taylor, 1971; Turnrose, 1976; Cohen, 1979; Faber and French, 1980; Jones et al., 1984; Carter et al., 1986). These studies also showed how the Ca II triplet (8498, 8542, 8662 Å), the Na I 8190 Å line and various molecular bands depend on gravity, temperature and metallicity of stars, the latter parameter being in general restricted to 0.5 dex around the solar value. We shall undertake a similar analysis for our sample of galactic nuclear spectra studying them in the light of stellar properties in a forthcoming paper.

The aim of the present work is, on the other hand, to analyze features in galactic nuclear spectra as a function of those observed in the integrated spectra of a sample of star clusters with known age, metallicity and reddening. This new approach is part of a population synthesis program over a wide spectral domain. The library of star cluster integrated spectra covers a large range in age and metallicity. This method offers the advantage over the one using stellar libraries, of being a two-parameter analysis (Bica and Alloin, 1986a, hereafter Paper I). The present approach constitutes in turn, an intermediate step towards a deeper insight into the stellar content itself of galactic nuclei since the HR diagrams of the star clusters are known from independent studies.

The observations are presented in Sect. 2. We describe also in this section, the CCD reduction procedure, in particular the removal of interference fringes and the correction of atmospheric absorption bands. In Sect. 3 we identify absorption features, we discuss criteria for continuum tracings and we define windows for equivalent width measurements W to be used in the synthesis. We study in Sect. 4 the star cluster properties as a function of age and metallicity. Results for galactic nuclei are examined in Sect. 5, as a function of morphological type and intrinsic luminosity of the parent galaxy. Conclusions of this work are given in Sect. 6. In Appendix A, we present grid predictions for equivalent widths (W) and continuum distribution of star clusters as a function of age and metallicity $[Z/Z_\odot]$, following the grid already obtained in the visible range (Bica and Alloin, 1986b, hereafter Paper II).

2. Observational data and reduction procedure

2.1. The sample

We observed 30 star clusters and 62 galactic nuclei for which a visible spectrum had already been obtained and discussed in Paper I and Papers III, IV (Bica and Alloin, 1987a, b). The present sample is a subset of the visible one, about a half; nevertheless, we still cover for star clusters the same ranges in age from 10^6 to $1.65\ 10^{10}$ yr and in metallicity $-2.0 \leqq [Z/Z_\odot] \leqq 0.1$, and, for galaxies the same ranges in intrinsic luminosity $-23.3 \leqq M_B \leqq -16.7$ and in morphological types from E to Sc. The star clusters are listed in Table 1 and the galaxies in Table 2, while their basic parameters have been compiled in Papers I and III respectively.

Send offprint requests to: D. Alloin

* Based upon observational data collected at the European Southern Observatory

Table 1. Col. (10), (12), and (16): The values correspond to a low continuum tracing with the aim of minimizing molecular contamination in the Ca II windows (Sect. 3). Symbol id. means that the measurement is identical to that in the preceeding column. Col (19)–(25): Continuum points, expressed in F_λ units, are corrected for reddening according to Sect. 3 and are normalized to the value at $\lambda = 5870$ Å

(1) NGC	(2) #b9 CaI FeI	(3) #80 Hα	(4) #66/7/8 TiO	(5) #71 TiO	(6) #72 CN	(7) #74 NaI	(8) #75/6 TiO TiI	(9) #77 CaII TiO	(10) #77 CaII	(11) #78 CaII TiO	(12) #78 CaII	(13) #79 P14 TiO	(14) NGC	(15) #80 CaII TiO	(16) #80 CaII	(17) #81 P12 FeI	(18) #83/84 TiO P11+10	(19) Cont 6630 5870	(20) Cont 6990 5870	(21) Cont 7520 5870	(22) Cont 8040 5870	(23) Cont 8408 5870	(24) Cont 8700 5870	(25) Cont 9100 5870
Large Magellanic Cloud Clusters													**Large Magellanic Cloud Clusters**											
1714	0	-1370	-103	-26	0	0	0	0	0	0	0	0	1714	-5	0	-11	-22	0.76	0.69	0.61	0.49	0.44	0.41	0.37
1783	0.4	2.9	18.3	5.5	2.5	1.3	4.5	2.5	id.	4.0	id.	1.0	1783	4.9	id.	1.6	8.8	0.93	0.91	0.86	0.81	0.76	0.76	0.75
1831	0.4	7.3	5.1	0.0	6.2	0.9	13.4	0.4	id.	4.8	id.	1.9	1831	6.1	id.	5.1	12.8	0.79	0.72	0.63	0.57	0.52	0.50	0.49
1847	0.7	1.8	11.9	2.9	5.1	2.7	9.0	2.8	id.	4.6	id.	1.4	1847	5.8	id.	3.2	13.1	0.80	0.73	0.67	0.61	0.58	0.61	0.56
1856	0.7	5.5	8.7	2.1	4.3	2.6	9.2	2.1	id.	4.1	id.	1.1	1856	4.3	id.	2.1	11.6	0.77	0.71	0.64	0.58	0.54	0.54	0.50
1866	1.1	3.8	25.8	15.0	12.4	0.9	10.3	4.3	3.1	5.5	4.6	3.9	1866	5.3	4.8	2.6	14.6	0.90	0.84	0.81	0.75	0.71	0.71	0.68
1868	0.4	5.2	4.6	2.1	4.2	1.3	7.7	1.9	id.	3.5	id.	1.3	1868	3.9	id.	1.9	10.1	0.91	0.83	0.76	0.70	0.66	0.65	0.61
1978	0.9	3.6	14.2	0.0	5.2	1.4	8.8	0.7	id.	3.1	id.	0.8	1978	2.9	id.	1.9	4.5	1.10	1.07	1.01	0.94	0.89	0.90	0.85
2004	2.5	0.0	34.8	3.6	6.4	1.8	11.1	3.2	2.3	6.1	5.4	1.7	2004	6.2	4.8	1.2	6.9	0.96	0.96	0.98	0.94	0.93	0.94	0.92
2157	0.3	2.6	8.1	1.4	2.2	1.6	7.5	1.5	id.	4.0	id.	1.2	2157	4.3	id.	1.4	9.6	0.88	0.79	0.71	0.63	0.59	0.58	0.54
2214	0.8	-3.3	15.4	0.9	5.4	0.3	3.8	1.6	id.	4.1	id.	1.2	2214	4.9	id.	0.9	16.2	0.89	0.81	0.73	0.65	0.61	0.61	0.58
Galactic Globular Clusters													**Galactic Globular Clusters**											
5024	0.3	2.7	0.0	0.5	0.6	0.3	2.2	0.7	id.	1.4	id.	0.1	5024	1.8	id.	0.7	3.5	0.92	0.86	0.81	0.77	0.73	0.71	0.69
5824	0.6	2.7	1.9	0.2	0.3	0.5	1.6	0.8	id.	1.9	id.	0.4	5824	2.0	id.	0.0	2.0	0.92	0.89	0.84	0.80	0.76	0.76	0.73
5927	1.5	2.6	26.8	8.2	6.9	1.7	11.9	4.6	3.1	5.8	4.5	4.3	5927	5.2	4.2	2.8	8.4	0.96	0.95	0.93	0.92	0.92	0.92	0.91
6093	0.2	2.6	2.4	1.2	1.2	1.8	3.9	1.2	id.	2.4	id.	1.1	6093	2.2	id.	0.4	3.7	0.95	0.91	0.86	0.82	0.79	0.79	0.77
6293	0.4	2.4	0.7	1.9	1.3	0.7	2.4	0.9	id.	1.4	id.	0.3	6293	2.0	id.	0.4	4.5	0.87	0.84	0.81	0.78	0.74	0.74	0.71
6316	0.8	1.8	11.7	4.7	3.4	2.2	10.2	2.5	id.	4.2	id.	1.8	6316	4.1	id.	1.1	3.7	0.94	0.94	0.94	0.93	0.92	0.92	0.89
6356	0.6	2.0	9.5	1.0	2.3	1.2	5.3	1.9	id.	3.5	id.	0.6	6356	3.6	id.	1.0	2.4	0.90	0.89	0.88	0.85	0.83	0.83	0.80
6388	0.6	1.7	13.8	2.6	2.5	1.6	8.6	3.0	id.	4.4	id.	2.4	6388	3.9	id.	1.7	3.6	0.97	0.95	0.91	0.90	0.90	0.89	0.88
6440	1.1	2.2	21.4	9.2	7.9	1.8	14.8	4.4	2.5	5.8	4.1	4.4	6440	5.5	3.9	2.7	6.7	1.07	1.10	1.13	1.16	1.18	1.20	1.21
6453	0.7	2.3	2.5	3.6	1.6	1.5	5.4	1.4	id.	2.5	id.	1.8	6453	3.0	id.	0.3	5.1	0.95	0.93	0.89	0.86	0.84	0.84	0.81
6528	2.1	2.7	38.6	14.5	12.4	2.3	18.2	5.7	3.3	7.4	5.4	5.9	6528	6.3	4.5	2.4	9.3	0.94	0.96	0.98	0.97	0.97	0.99	1.00
6624	1.2	2.5	26.0	9.9	7.9	1.9	12.6	3.9	2.6	5.4	4.3	3.3	6624	4.4	3.8	0.8	5.2	0.89	0.89	0.91	0.88	0.87	0.87	0.85
6638	0.4	1.8	6.3	1.0	1.3	1.1	4.7	1.6	id.	2.9	id.	0.3	6638	3.0	id.	0.1	1.9	0.91	0.89	0.89	0.86	0.84	0.84	0.80
6642	1.1	2.8	4.3	1.5	1.7	0.6	4.4	1.7	id.	2.6	id.	0.0	6642	3.0	id.	0.4	3.3	1.02	1.00	0.98	0.95	0.93	0.93	0.90
6652	0.3	2.4	2.7	0.3	1.3	1.4	4.2	1.7	id.	2.9	id.	0.5	6652	3.2	id.	0.7	4.9	0.88	0.86	0.81	0.77	0.74	0.74	0.70
6715	0.3	2.5	5.2	3.6	4.6	0.9	3.8	2.1	id.	3.8	id.	1.4	6715	3.1	id.	0.6	5.2	0.93	0.87	0.82	0.79	0.74	0.75	0.73
6864	0.4	2.4	1.7	1.0	1.7	0.6	2.6	1.6	id.	3.0	id.	0.8	6864	3.0	id.	1.1	2.6	0.96	0.90	0.84	0.80	0.76	0.74	0.71
Galactic Open Clusters													**Galactic Open Clusters**											
2660	0.5	3.9	17.1	6.0	4.3	1.7	8.2	1.6	id.	2.8	id.	2.0	2660	4.4	id.	3.3	10.6	0.82	0.78	0.72	0.66	0.63	0.62	0.61
6705	1.1	5.5	8.3	0.9	3.8	1.8	6.6	2.1	id.	3.7	id.	2.6	6705	4.5	id.	3.4	8.7	0.75	0.67	0.58	0.52	0.48	0.48	0.47

The observations were carried out from 1985 April 29 to May 3, with the 2.2 m telescope at ESO, La Silla. We used a CCD attached to the Boller and Chivens spectrograph with a 300 lines/mm grating in first order providing a dispersion 228 Å mm^{-1}, and an OG 590 filter so as to eliminate the second order contamination. The CCD array (RCA thinned, backside illuminated) consists of 512 pixels along the dispersion, by 320 pixels of which the central 120 were illuminated by the slit length. A 30 μm square pixel corresponds to 1".8 on the sky and 6 Å along the dispersion. The spectral resolution, as measured by the FWHM of helium-argon comparison lines is of 12.5 Å. In order to get a spectral resolution similar to that achieved in the visible range, we had to keep a 2".5 slit width, narrower than the 4" to 5" slit previously employed. This procedure did not introduce however, significant or systematic differences in the spectra of galactic nuclei, as demonstrated by the comparison of the 1000 Å overlap between the two domains. For each galaxy we summed the pixel rows perpendicular to the dispersion in order to match the slit lengths used for observations in the visible. These values (in arc sec) and the corresponding dimensions at the source can be found in Paper III.

The slit was generally set E–W, but for galaxies presenting a preferential axis, particular orientations were chosen in view of a future spatial analysis of some absorption features. For instance, in edge-on spirals and lenticulars, the slit length was set along the minor axis. Star clusters were scanned spatially in the dispersion direction and we summed pixel rows along the slit length in order to reproduce the areas which had been looked at in the visible data as specified in Paper I. For large clusters a separate frame for the sky was considered. Owing to the strong night sky emission lines in the near-infrared range, these cases were given special attention in order to ensure a satisfactory sky cancellation.

2.2. *Reduction procedure*

The reductions were carried out with the IHAP system at ESO Garching and Institut d'Astrophysique de Paris. The CCD reduction procedure consisted of:

(i) removal of the dark current bias;
(ii) flat-fielding;
(iii) object and sky compression to one dimension;
(iv) sky subtraction and wavelength calibration;
(v) correction for atmospheric extinction and flux calibration;
(vi) removal of atmospheric absorption bands.

Items (ii) and (vi) deserve a more detailed description.

The presence of fringes in near-infrared CCD spectra is a well known problem. Normally these fringes should be removed through a standard division by the flat field frame (FFF).

Table 2. Col. (1): An asterisk denotes IC galaxies. Col. (4): Correction for emission line contamination was applied to NGC 5643. Cols. (10), (12), and (16): The values correspond to a low continuum tracing with the aim of minimizing molecular contamination in the Ca II windows (Sect. 3). Symbol id. means that the measurement is identical to that in the preceeding column. Cols. (19)–(25): Continuum points, expressed in F_λ units, are corrected for reddening according to Sect. 3 and are normalized to the value at $\lambda = 5870$ Å

(1) NGC	(2) #59 CaI FeI	(3) #60 Mn	(4) #66/7/8 TiO	(5) #71 TiO	(6) #72 CN	(7) #74 NaI	(8) #75/6 TiO TiI	(9) #77 CaII TiO	(10) #77 CaII	(11) #78 CaII TiO	(12) #78 CaII	(13) #79 P14 TiO
	E I'		-22.7 < M < -22.0									
4296*	0.6	-0.8	26.9	7.1	7.6	2.1	10.7	4.3	3.0	5.4	4.3	2.9
3557	1.2	1.1	30.2	6.6	8.3	3.1	11.3	4.5	3.0	6.3	5.0	3.7
6776	0.5	-1.9	22.2	6.6	7.5	2.8	12.3	3.8	2.0	6.0	4.6	2.6
	E II'		-21.9 < M < -21.0									
5018	0.5	0.6	20.1	4.4	4.3	1.8	10.8	4.4	2.9	5.7	4.4	2.4
4936	0.7	-4.9	23.9	7.4	7.8	1.6	13.3	4.6	2.9	5.9	4.5	3.9
6758	1.2	-0.6	27.6	6.6	7.2	1.2	10.6	3.5	2.2	4.7	3.6	2.2
5061	1.3	1.7	27.0	5.6	5.5	2.2	12.5	4.4	2.7	5.7	4.3	3.3
4697	3.4	2.6	33.4	8.4	8.3	2.3	14.5	4.7	2.8	5.8	4.2	2.4
2865	1.2	2.5	19.8	4.6	7.0	2.3	9.9	3.5	2.6	5.3	4.5	2.6
7144	0.8	2.1	26.9	8.6	9.4	1.9	15.7	4.7	2.9	5.8	4.3	4.2
	E III'		-20.9 < M < -19.0									
7145	0.7	2.3	26.6	8.8	10.0	2.5	16.8	5.0	3.0	6.5	4.8	4.5
3904	1.1	2.3	27.0	9.1	9.5	2.1	15.2	4.4	2.7	6.1	4.7	4.2
2434	0.9	1.3	26.7	9.2	9.8	1.8	16.7	4.9	3.3	6.8	5.5	3.7
4742	1.1	2.7	23.0	6.2	6.6	1.7	14.2	4.7	2.7	5.7	4.1	3.8
4478	1.3	2.9	23.6	7.8	9.0	3.0	14.5	5.7	2.1	5.3	3.9	5.8
3818	1.7	1.8	27.1	7.5	7.0	2.3	11.6	4.7	2.8	5.3	3.6	3.3
	E IV'		-18.9 < M < -16.5									
4486B	1.5	2.1	25.7	7.4	8.7	1.6	11.8	4.2	3.0	5.5	4.6	4.9
	S0 I'		-22.3 < M < -22.0									
5419	1.5	1.8	29.6	7.4	7.5	1.7	11.9	4.1	2.6	4.9	3.6	2.7
	S0 II'		-21.9 < M < -21.0									
6868	1.0	-4.0	27.2	7.3	8.6	2.7	12.8	4.7	3.3	5.8	4.6	3.4
5266	1.6	-6.5	26.4	5.5	7.6	2.0	10.2	4.1	3.3	4.6	3.9	0.9
6861	1.2	-0.9	27.7	7.6	8.7	2.4	12.2	4.6	3.1	5.0	3.8	2.8
5923	1.7	2.2	28.5	7.8	9.1	2.4	12.0	4.7	3.0	6.1	4.7	3.7
4797*	1.4	1.6	26.7	7.0	8.9	2.5	11.8	4.8	3.4	5.9	4.6	3.2
4889*	0.8	-0.2	26.4	8.5	10.4	1.2	12.1	4.6	3.1	5.1	3.7	2.9
3585	1.6	2.1	29.0	7.6	9.5	2.1	12.1	5.1	3.7	5.8	4.6	3.7
	S0 III'		-20.9 < M < -19.0									
4976	0.9	2.2	25.6	8.4	9.8	2.2	16.3	4.5	2.6	6.5	4.9	4.1
7041	0.9	1.8	27.3	8.3	9.6	1.8	15.0	4.6	2.9	6.1	4.7	3.6
4958	0.6	-1.0	26.3	7.6	8.3	2.0	13.0	4.6	3.1	6.3	5.0	3.9
3115	1.3	2.2	30.7	10.2	12.9	2.3	17.4	5.1	3.2	6.8	5.3	5.6
4033	1.3	2.2	27.3	7.4	9.7	2.2	13.1	4.8	3.3	6.8	5.5	4.7
	S0 IV'		-18.9 < M < -18.4									
5102	0.6	1.9	12.4	1.3	3.6	1.7	5.8	2.5	id.	4.6	id.	1.6
3056	0.7	-2.8	16.4	6.2	5.6	1.5	11.2	3.5	2.3	5.2	4.2	1.5

(14) NGC	(15) #80 CaII TiO	(16) #80 CaII	(17) #81 P12 FeI	(18) #83/84 TiO P11+10	(19) Cont 6630	(20) Cont 6990	(21) Cont 7620	(22) Cont 8040	(23) Cont 8408	(24) Cont 8700	(25) Cont 9100
	E I'		-22.7 < M < -22.0								
4296*	3.9	3.0	2.3	6.2	1.00	0.99	1.02	1.02	1.02	1.02	1.05
3557	4.2	2.9	1.3	5.6	0.99	0.99	1.01	1.00	1.00	1.00	1.02
6776	5.7	4.4	4.6	6.2	0.98	0.94	0.95	0.93	0.92	0.92	0.92
	E II'		-21.9 < M < -21.0								
5018	4.9	3.6	2.5	3.9	1.00	0.99	0.99	0.97	0.97	0.98	0.99
4936	5.4	4.1	2.7	5.9	1.05	1.05	1.12	1.13	1.15	1.16	1.20
6758	3.6	2.8	1.7	5.5	0.98	0.96	0.98	0.97	0.97	0.97	0.98
5061	5.6	4.3	3.5	7.3	0.95	0.94	0.93	0.92	0.92	0.92	0.91
4697	5.9	4.3	3.5	6.6	0.97	0.99	1.00	1.01	1.02	1.03	1.04
2865	3.7	3.1	0.8	6.9	0.90	0.87	0.85	0.81	0.79	0.79	0.78
7144	6.1	4.9	3.0	8.0	1.01	0.99	1.01	0.99	0.99	0.99	0.99
	E III'		-20.9 < M < -19.0								
7145	6.2	4.8	2.8	9.7	0.99	0.98	1.00	0.99	0.99	0.99	0.98
3904	5.7	4.3	2.6	6.2	1.01	0.99	1.02	1.00	1.00	1.00	1.00
2434	5.3	4.2	1.4	13.5	1.04	1.05	1.11	1.12	1.14	1.15	1.17
4742	6.3	4.9	4.5	9.3	0.94	0.91	0.89	0.87	0.87	0.86	0.85
4478	5.5	4.6	3.3	8.4	0.95	0.95	1.01	1.02	1.02	1.02	1.01
3818	4.4	3.0	3.8	4.8	0.97	0.98	0.99	1.00	1.00	1.00	1.00
	E IV'		-18.9 < M < -16.5								
4486B	3.6	2.8	1.8	5.6	0.96	0.97	1.01	1.00	1.00	1.00	0.98
	S0 I'		-22.3 < M < -22.0								
5419	4.1	2.8	2.8	10.5	1.01	0.99	1.03	1.01	1.01	1.02	1.04
	S0 II'		-21.9 < M < -21.0								
6868	4.2	3.4	2.1	7.3	1.03	1.03	1.06	1.06	1.07	1.07	1.10
5266	3.0	2.7	0.0	7.6	1.02	1.04	1.09	1.08	1.08	1.09	1.11
6861	4.0	3.2	1.8	5.3	1.06	1.06	1.09	1.09	1.09	1.09	1.11
5923	4.3	3.0	2.4	5.2	0.99	1.01	1.07	1.06	1.06	1.07	1.07
4797*	4.8	3.7	2.2	6.1	0.96	0.96	0.98	0.97	0.97	0.98	1.00
4889*	5.0	3.8	1.6	12.6	0.96	0.96	0.97	0.94	0.93	0.94	0.93
3585	4.5	3.4	2.6	4.9	0.97	0.97	1.02	0.99	0.99	1.00	0.99
	S0 III'		-20.9 < M < -19.0								
4976	5.6	4.1	2.9	7.6	0.99	0.97	0.99	0.97	0.97	0.97	0.98
7041	4.6	3.4	1.7	7.5	1.00	1.02	1.07	1.06	1.06	1.05	1.03
4958	4.9	3.7	2.3	3.7	0.94	0.94	0.96	0.95	0.95	0.96	0.96
3115	6.0	4.7	2.4	9.8	1.02	0.99	1.04	1.03	1.03	1.02	1.03
4033	5.4	4.2	2.1	7.9	0.97	0.96	0.97	0.95	0.95	0.94	0.94
	S0 IV'		-18.9 < M < -18.4								
5102	3.9	id.	1.5	7.1	0.92	0.86	0.81	0.76	0.72	0.72	0.69
3056	4.7	3.9	1.7	5.7	0.96	0.93	0.94	0.92	0.91	0.90	0.89

However this was not so in our spectra where we verified that the fringe systems in the FFF and in the scientific frame (SF) might present relative shifts up to 1.5 pixels along the dispersion, most probably as a result of flexures. Furthermore, the fringe intensities in the SF were around 10% stronger than in the FFF, although showing the same patterns. This effect, due to scattered light after the grating, has also been faced by Carter et al. (1986). In order to remove these two effects, we first separated through filtering, the interference fringe system from the flat-field higher and lower spatial frequencies. We emphasize the fact that, using at this stage a filtering procedure such as a median filter, avoids any spectral degradation to be applied to the SF. Then, on one side the "fringeless" FFF was used to correct the SF. On the other side, the frame containing only the fringe system was translated along the dispersion by the required shift and its intensity scaled so as to match the fringe system observed in the SF. This method proved to be quite powerful and allowed us to reduce fringe residuals in most of our spectra to a level comparable to the data noise (Fig. 1).

Because the near-infrared spectral range contains many atmospheric absorption bands (AAB), it is imperative to remove them carefully from star cluster and galactic spectra, by means of comparison with hot stars containing very few intrinsic absorption

Table 2 (continued)

Sa I'			-22.3 < M < -22.0									
5064	1.3	-2.3	24.9	6.4	6.8	2.2	9.1	4.1	2.6	5.4	4.3	1.9
Sa II'			-21.9 < M < -21.0									
2811	1.2	0.4	26.9	8.5	9.9	2.3	13.7	4.5	3.2	6.0	4.9	4.0
3358	0.7	-1.0	26.3	8.6	8.2	1.6	13.8	3.8	2.6	4.7	3.7	3.2
7049	1.2	-1.2	30.7	6.9	7.8	2.0	14.4	4.2	2.7	5.5	4.3	3.6
4767	1.0	1.8	27.7	6.6	7.0	2.0	11.4	4.6	3.5	5.9	5.0	2.8
7079	1.2	2.1	24.4	8.7	8.9	1.6	11.5	4.1	2.9	5.1	4.0	2.6
5101	0.7	-3.8	27.4	7.0	7.8	2.2	11.8	5.0	3.7	6.1	5.0	3.1
Sa III'			-20.9 < M < -19.8									
6942	1.3	-1.4	28.0	8.3	7.0	3.6	12.4	4.0	2.9	5.7	4.6	2.2
2781	1.4	0.5	25.0	6.4	7.9	1.8	11.7	4.8	3.3	5.6	4.4	2.3
4856	0.3	-2.1	24.4	7.6	7.8	1.7	11.8	4.4	2.7	5.6	4.2	3.2
6684	0.4	2.1	24.4	7.8	7.9	1.5	12.5	4.7	3.3	6.5	5.3	2.9
5121	1.1	1.2	24.6	7.5	8.0	1.9	12.0	4.7	3.4	6.3	5.2	2.1
Sb I'			-22.7 < M < -22.0									
3223	1.0	0.0	23.7	8.1	7.7	1.8	11.4	4.3	2.9	5.6	4.4	1.7
6782	0.0	-6.9	22.1	5.8	8.1	2.9	11.8	3.1	1.8	4.1	2.9	1.7
Sb II'			-21.9 < M < -21.0									
5612	0.3	-1.7	21.9	6.6	7.4	1.4	12.3	4.4	3.1	4.6	3.6	1.8
Sb III'			-20.9 < M < -20.3									
4462	1.6	0.7	27.0	9.8	8.6	1.7	17.6	5.0	2.7	6.4	4.6	3.2
3887	0.6	-9.6	18.8	4.5	8.5	2.4	12.2	4.0	2.9	5.9	5.0	3.7
Sc I'			-22.4 < M < -22.0									
6925	0.6	-0.6	24.1	6.5	8.1	2.1	13.2	4.2	2.8	5.9	4.8	3.9
7329	1.6	-0.8	27.0	6.3	7.0	1.9	11.2	3.4	2.3	5.0	4.1	2.6
Sc II'			-21.9 < M < -21.0									
6744	0.5	-1.1	24.9	8.2	7.1	1.4	11.7	4.3	3.3	6.5	5.6	2.6
6699	0.0	-8.6	16.0	8.5	5.4	1.7	13.4	4.0	2.5	4.4	3.1	2.6
6923	0.6	-2.0	23.2	6.5	7.9	1.6	14.7	4.3	2.6	6.0	4.6	4.5
3054	1.9	0.7	23.8	7.6	9.9	2.1	9.6	4.1	2.6	5.5	4.3	1.7
2997	0.7	-45.0	22.3	9.1	9.2	1.2	14.9	4.4	3.2	5.9	4.9	2.4
2442	0.8	-12.3	22.4	6.7	6.9	2.5	14.4	4.2	2.5	6.3	4.8	3.7
5236	0.4	-78.0	20.8	7.8	5.6	1.2	14.0	4.7	3.1	5.4	4.1	1.6
Sc III'			-20.9 < M < -20.9									
4981	1.6	-13.1	22.4	8.7	7.2	3.5	15.9	4.9	3.0	6.1	4.4	4.1
Seyferts			-21.3 < M < -21.2									
6300	-0.4	-14.0	18.8	6.6	7.3	2.6	12.5	4.5	3.3	6.7	5.8	2.1
5643	-3.5	-76.2	12.3	3.4	5.5	2.4	11.9	3.6	2.5	5.8	4.9	1.7
Amorphous			M = -18.3									
5253	0	-901	-99	-21	0	0	0	0	0	0	0	-2

Sa I'			-22.3 < M < -22.0					
5064	4.4	3.8	1.8	8.3	0.94	0.95	0.95	0.91	0.91	0.90	0.89
Sa II'			-21.9 < M < -21.0					
2811	4.9	4.1	2.2	7.8	0.95	0.93	0.95	0.92	0.91	0.91	0.91
3358	4.8	4.1	1.9	9.6	0.95	0.95	0.96	0.94	0.93	0.93	0.93
7049	4.8	3.8	2.3	7.8	1.03	1.06	1.08	1.07	1.06	1.06	1.04
4767	4.3	3.4	1.7	6.6	1.01	0.99	1.01	1.00	0.99	0.99	1.01
7079	4.3	3.3	1.2	12.8	1.02	1.00	1.03	0.99	0.98	0.98	0.99
5101	4.5	3.6	1.6	7.9	1.01	1.00	1.03	1.03	1.03	1.04	1.06
Sa III'			-20.9 < M < -19.8					
6942	4.8	3.7	2.5	8.8	0.95	0.95	0.95	0.90	0.89	0.88	0.86
2781	4.1	3.3	2.2	8.2	0.96	0.97	0.98	0.94	0.93	0.93	0.91
4856	4.6	3.3	2.6	5.3	0.99	0.98	1.00	1.00	1.00	1.00	0.99
6684	5.0	3.9	1.7	7.9	0.92	0.90	0.92	0.89	0.89	0.88	0.87
5121	4.5	3.6	0.7	5.3	1.04	1.00	1.00	0.98	0.97	0.96	0.96
Sb I'			-22.7 < M < -22.0					
3223	4.1	3.0	1.6	7.1	0.94	0.93	0.93	0.91	0.90	0.89	0.89
6782	5.0	3.8	3.3	7.9	0.97	0.97	0.97	0.95	0.95	0.95	0.95
Sb II'			-21.9 < M < -21.0					
5612	3.6	3.4	1.3	16.5	0.96	0.94	0.91	0.87	0.85	0.84	0.84
Sb III'			-20.9 < M < -20.3					
4462	4.7	3.2	2.1	10.8	0.96	0.96	0.97	0.95	0.94	0.94	0.94
3887	4.5	3.6	1.5	9.3	0.99	0.99	1.00	1.00	1.00	0.99	1.01
Sc I'			-22.4 < M < -22.0					
6925	5.4	4.3	2.2	6.7	0.95	0.93	0.94	0.92	0.92	0.92	0.92
7329	4.7	4.0	3.0	9.8	0.99	0.99	0.99	0.95	0.93	0.92	0.91
Sc II'			-21.9 < M < -21.0					
6744	4.5	3.9	1.4	10.7	1.00	0.99	1.00	0.98	0.97	0.97	0.96
6699	5.7	4.5	4.2	8.2	0.97	0.95	0.94	0.93	0.93	0.93	0.94
6923	6.3	5.1	2.8	7.3	0.96	0.95	0.96	0.95	0.96	0.96	0.97
3054	3.8	2.9	2.7	7.5	0.96	0.98	1.01	0.98	0.96	0.94	0.92
2997	5.4	4.5	1.0	10.4	0.96	0.97	0.97	0.94	0.94	0.93	0.93
2442	5.0	3.8	2.3	5.2	1.10	1.14	1.20	1.23	1.28	1.32	1.35
5236	5.4	4.3	1.8	4.9	0.84	0.79	0.72	0.66	0.64	0.63	0.61
Sc III'			-20.9 < M < -20.9					
4981	4.8	3.2	3.3	2.3	1.07	1.08	1.08	1.09	1.10	1.11	1.11
Seyferts			-21.3 < M < -21.2					
6300	4.8	4.3	1.6	6.9	0.97	0.96	0.95	0.92	0.91	0.91	0.92
5643	4.1	3.5	0.6	-1.5	1.04	1.03	1.03	1.03	1.02	1.02	1.02
Amorphous			M = -18.3					
5253	-2	0	-8	-87	0.83	0.78	0.72	0.66	0.61	0.57	0.52

lines. For this purpose, we observed the standard stars LTT 3218, 6248, and 7987, which are hot white dwarfs usually considered for flux calibration in the near-infrared (Baldwin and Stone, 1984). The star LTT 6248 is somewhat cooler than the other two and exhibits detectable Ca II triplet which was straightforwardly removed. These three stars showing an Hα absorption line, the corresponding spectral range was set to unity in the atmospheric correction files, owing to the absence of AAB around. We also verified that Paschen lines were negligible in the stellar spectra. Ideally, for each cluster or galactic nucleus, a hot star should be observed simultaneously and at the same airmass, if we wish to achieve a perfect AAB cancellation. In practice, we observed a standard star at the beginning, middle and end of each night. Comparison of the AAB strengths in these stars revealed that the atmospheric absorption remained stable within each of the 5 nights. We have displayed in Fig. 2 an example of the normalized atmospheric correction file derived from the three stars within a given night, as well as the spectra for one of the stars before and after this correction was applied. We also recall the main AAB in our spectral range. Standard stars were observed at small airmasses and so were most of the galaxies and Galactic star clusters. In contrast, LMC clusters were often observed at larger

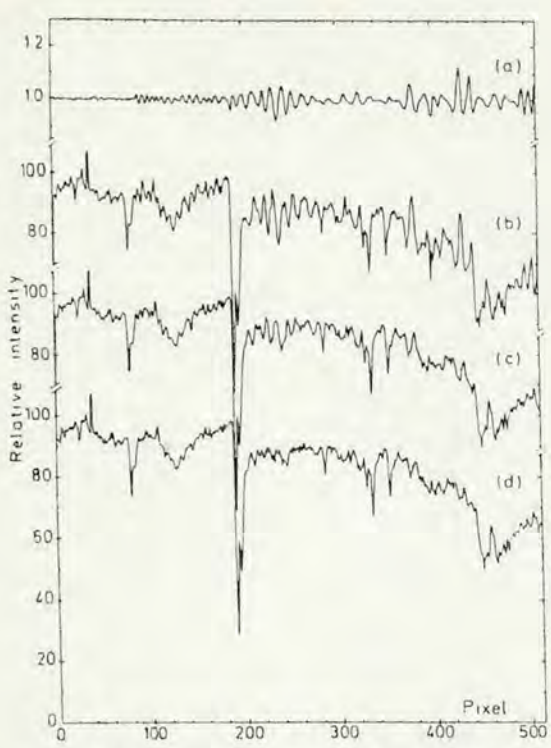

Fig. 1. The fringe correction, (a) the fringe system isolated from the flat field, (b) galaxy corrected by the fringeless flat field, (c) simple division of the spectrum in (b) by the fringe system in (a) showing that fringe residuals remain, (d) the spectrum in (b) divided by the fringe system (a) after shifting the latter by the required pixel number and matching the small fringe amplitude difference. The fringe residuals are then essentially indistinguishable from the noise

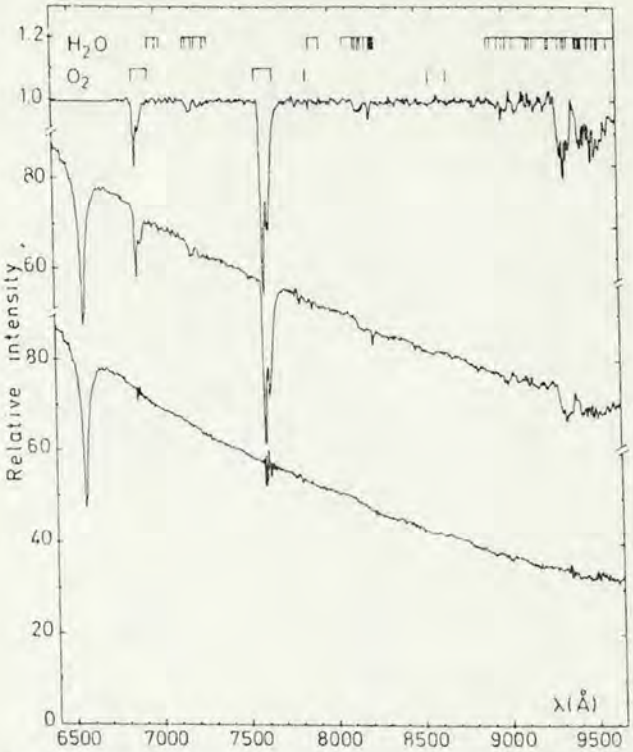

Fig. 2. The atmospheric correction, (a) correction file derived from 3 standard stars in one of the nights, (b) a standard star spectrum affected by atmospheric absorptions, (c) the corrected spectrum

airmasses, AM ~ 2. In order to cancel at best the stronger atmospheric absorptions seen at such large airmasses, we determined for each object a constant percentual level p% to be subtracted from the normalized atmospheric correction file, using the strongest O_2 and H_2O AAB as a control for residuals. The simultaneous cancellation of molecular oxygen and water vapor absorption strengths indicates that they follow the same linear dependence on airmass for AM ≤ 2, described as p% = 20.3 (AM-1). The precision of atmospheric absorption corrections is estimated from the rms residuals measured in the corresponding windows for the hot standard stars. The strongest features, O_2 in windows No. 67 and No. 70A and H_2O in No. 87 provide values of respectively 5%, 6%, and 12%. For weaker atmospheric features, residuals are difficult to estimate since they become smaller than the measurement precision. A precision level of 10% for the corrections, together with the mean value $W \sim 1.7$ Å for H_2O contamination in the Na I 8190 Å window of hot standard stars indicate that the expected residuals for galaxies and clusters amount to 0.17 Å, thus are smaller than the 0.25 Å precision inferred for the measurements in this window.

3. Measurements

The star cluster spectra were corrected for Galactic reddening using the values compiled in Paper I. Galactic nuclei were corrected for (i) the Galactic reddening described by a cosecant law with absorption free polar caps and (ii) the intrinsic reddening due to inclined discs according to the template method described in Paper III and to the values given therein. Galactic nuclear spectra were then corrected for redshift with the velocities provided in Paper III. We confirm from our near-infrared data that NGC 6942 has a velocity $V = 3200$ km s^{-1} as derived previously (Paper III), the value in Sandage and Tammann (1981) being incorrect. The fully corrected continuum points, expressed in F_λ units and normalized to that at 5870 Å by means of the overlapping region for each spectrum are presented in Tables 1 and 2, respectively for star clusters and galaxies. In all figures in this study, the continuum distribution corresponds to reddening corrected spectra.

In view of defining windows for W measurements of well-known features, and of providing identifications for weaker ones, we generated high signal to noise mean spectra for typical red strong-lined and blue populations. These are shown in Fig. 3a and b respectively. The red spectrum is a mean of 22 redshift corrected early type galaxies which are free from emission lines. The fact that the originally observed spectra correspond to different galaxy velocities ensures that all rest frame sources of uncertainties, namely residuals from night sky emission, atmospheric absorption and fringes, average out and thus every weak feature in Fig. 3a is real. This may not be the case in Fig. 3b where the blue spectrum consists of a mixture of young LMC clusters, the Galactic open cluster NGC 6705 and the blue lenticular NGC 5102. However, the Paschen series is clearly seen up to P18. We provide

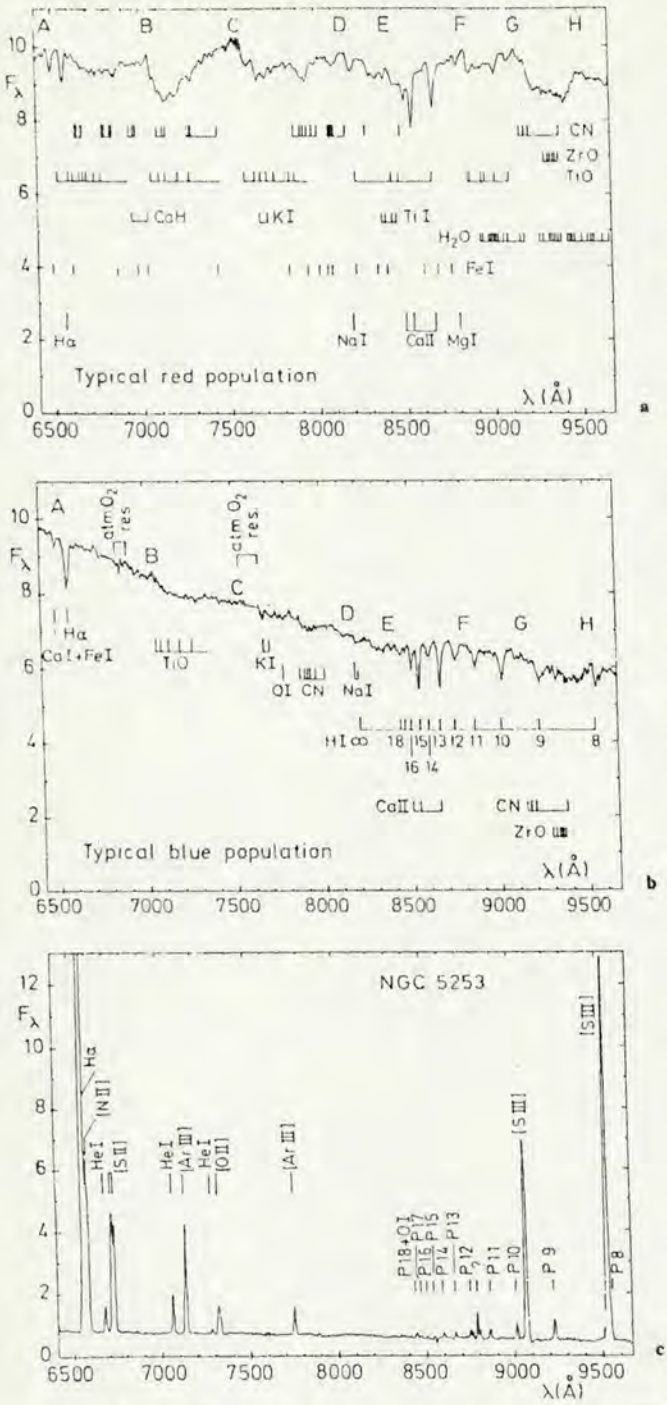

Fig. 3a–c. High signal-to-noise spectra for feature identifications, **a** mean of 22 red strong-lined early type galaxies, **b** typical blue population built up from Magellanic Cloud and Galactic blue clusters, as well as from the blue S0 galaxy NGC 5102, **c** the emission line galaxy NGC 5253

in Fig. 3c one example of an emission line galaxy (NGC 5253) in order to show which windows might be seriously affected by emission in such objects.

The parameters of and main contributors to the absorption line windows are listed in Table 3. These windows have been defined from the star cluster sample and are a continuation of the listing initiated in the visible range (Paper I). In Fig. 3a, we have shown the adopted criteria for continuum tracings. Points A, C, F, and G are very possibly true continuum points. Points B and D are certainly depressed by molecular and/or line absorption but still represent local maxima and were selected in order not to rely on a few points only. Measurements of the strong absorption CN, ZrO from 9130 to 9490 Å, are unfortunately very dependent on point H which is affected by molecular absorption and furthermore is subject to border effects in some of the spectra. Thus we do not use this feature. We provide in Tables 1 and 2 the equivalent widths W for a selection of 13 features. Line EF matches an alternative tracing which is intended to minimize molecular absorption in the Ca II infrared triplet windows. It corresponds to the local continuum defined for stellar spectra by Jones et al. (1984). Point E departs from the DF line more particularly in the case of strong-lined galaxies and very metal rich globular clusters. Whenever differences arise between the feature equivalent widths outlined by the two different tracings, we provide in Tables 1 and 2 the two corresponding values. Line identifications and continuum points displayed in Fig. 3a are most important for the selection of spectral ranges in future analysis of high dispersion spectra. Absorptions being present almost everywhere in the near-infrared, some doubt raises about the usual definition of molecular band indices with respect to flux side bands. Indeed absorptions may quite often be very important in the so-called continuum side bands, changing the desired strength measurement of a feature into that of a ratio between two features. In particular, such indices may hide important metallicity dependences.

In order to test the consistency of our IDS and CCD data sets, we have compared the results obtained for a window in the overlapping region, Hα (Fig. 4). This demonstrates that the measurements from the two data sets are in good agreement, whether Hα appears in absorption or in emission and this conclusion holds true for more than 3 decades.

In the case of star cluster spectra, a further check should be made about the consistency of the spatial coverage for any cluster belonging to the two data sets. To achieve this, the use of a molecular band is more appropriate than that of Hα, since molecular absorptions are quite strong in bright giant stars and hence would reveal any sensible difference in the spatial sampling. However, the strong TiO λλ 7050, 7464 in the overlapping region could not be used in the case of the IDS data set, because the spectra were not corrected for atmospheric absorption. We decided to use instead the same molecule TiO, seen in its λλ 6156, 6386 band with the IDS and in its λλ 7050, 7464 band with the CCD, these two bands being expected to vary together in first order (Fig. 5). The scatter observed for star clusters is not larger than that for galactic nuclei which certainly are not subject to any sampling effect. In conclusion, we are fairly confident that using two different devices, IDS and CCD, did not affect much the homogeneity of our data set.

4. Star cluster properties as a function of age and metallicity

The main properties of star cluster spectra in the near-infrared can be seen in Fig. 6a and b which present respectively a metallicity sequence for Galactic Globular Clusters (GGC) and an age sequence for young and intermediate age Magellanic Cloud Clusters (MCC). Two major conclusions arise from these figures: (i) the strength of molecular bands increases drastically in metal rich GGC, and (ii), in the MCC age sequence, a continuum slope

Table 3. Definition of the windows from the star cluster sample

Window	$\Delta\lambda$ (Å)	$\bar{W}/\Delta\lambda$ [1]	Absorbers
No. 59	6474–6540	0.01	Ca I; Fe I; Ba II; CN; l.c.m. [2]
60	6540–6586	0.06	Hγ; TiO; Fe I
61	6586–6670	0.01	TiO; Fe I; CN
62	6670–6736	0.02	TiO; Ca I; Fe I
63	6736–6858	0.02	TiO; CN; Fe I; CaH
64	6858–6934	0.01	Atm O_2 res.; CN; CaH
65	6934–7050	0.01	CaH; CN; Fe I; l.c.m.
66	7050–7158	0.03	TiO; CN; Ca I; Fe I; He I; Ni I
67	7158–7274		TiO; Atm. H_2O res.
68	7274–7464		TiO; CN; Fe I; VO
69	7464–7580	0.00	CaH; Fe I; l.c.m.
70 A	7580–7640	−0.01	Atm. O_2 res.; TiO; l.c.m.
70 B	7640–7704	0.03	TiO; K I; Atm. O_2 res.
71	7704–7852	0.02	TiO; Fe I; O I
72	7852–8040	0.02	CN; VO; Fe I
73	8040–8160	0.01	CN; Fe I; l.c.m.
74	8160–8234	0.02	Na I; Fe I; TiO; H I; Atm H_2O res.
75	8234–8408	0.03	TiO; Ti I; Fe I; CN; H I
76	8408–8476		TiO; Ti I; H I(P17, 18)
77	8476–8520	0.05	Ca II; TiO; H I(P16); Fe I; CN
78	8520–8564	0.09	Ca II; TiO; H I(P15); VO
79	8564–8640	0.02	TiO; H I(P14); VO
80	8640–8700	0.07	Ca II; H I(P13); TiO; VO; Fe I
81	8700–8786	0.02	H I(P12); Fe I; CN; ZrO
82	8786–8844	0.01	Mg I; Fe I; l.c.m.
83	8844–8940	0.03	H I(P11); TiO
84	8940–9066		H I(P12); TiO; Fe I
85	9066–9130	0.03	TiO; l.c.m.
86	9130–9270	0.03	CN; H I(P9)
87	9270–9490	0.05	ZrO; H_2O [3]; CN; Atm. H_2O res
88	9490–9600	0.02	H I(P8); H_2O; Atm. H_2O res; l.c.m

Notes to Table 3:

[1] $\bar{W}/\Delta\lambda$ for metallic features appears to be systematically lower than in the study of the visible data refering to a larger sample. Although the present infrared cluster sample still covers the entire metallicity range specified in Paper I, as a mean the clusters selected for the infrared study have a lower metal content and this explains the lowering of $\bar{W}/\Delta\lambda$

[2] l.c.m. = local continuum maximum

[3] We estimate that in this window, intrinsic H_2O absorption may contribute significantly since other H_2O bands are detected at longer wavelengths in stars and galaxies (Aaronson et al., 1978)

effect due to the blue stellar content is still detectable in the near-infrared range, as also revealed by the presence of the Paschen series in these spectra. However, this spectral range is obviously very sensitive to the flux contribution from low temperature stars. This can be seen more particularly at some short phases in the evolution of a young star cluster, when an accumulation of red evolved stars occurs, e.g. red supergiants at $t \sim 10^7$ yr (NGC 2004) and asymptotic giant branch (AGB) stars with massive progenitors at $t \sim 10^8$ yr (NGC 1866). The reality of the latter case, where AGB stars are expected to contribute significantly to the integrated flux for a short period of time in a blue cluster, is predicted theoretically (Renzini and Buzzoni, 1985; Chiosi et al., 1985) and is observed in the LMC cluster NGC 1866 besides evidences that the same effect is present in some Galactic open clusters (Paper I).

In the following analysis we adopt for NGC 1866 a value $[Z/Z_\odot] = -0.5 \pm 0.4$. The metallicity value $[Z/Z_\odot] = -1.2$ from Richtler and Nelles (1983) which was used in Paper I, is not compatible with the strong TiO bands observed in the present spectrum, nor with the metallicity expected for a blue LMC cluster under the chemical evolution scenario of the LMC, even if one takes into account the intrinsic metallicity dispersion observed for H II regions and red clusters (Bica et al., 1986). Also, Becker and Mathews (1983) deduced an almost solar metallicity by means of synthetic HR diagram fitting in this cluster.

We show in Figs. 7a, 7b and 7c respectively, the behaviour of metallic lines W(Na I 8190 Å), W(Ca II 8542 Å), and W(Ca II 8662 Å) as a function of metallicity. The relations are essentially single-valued, regardless the cluster age. Such a behaviour was expected from the trend already observed in the visible range

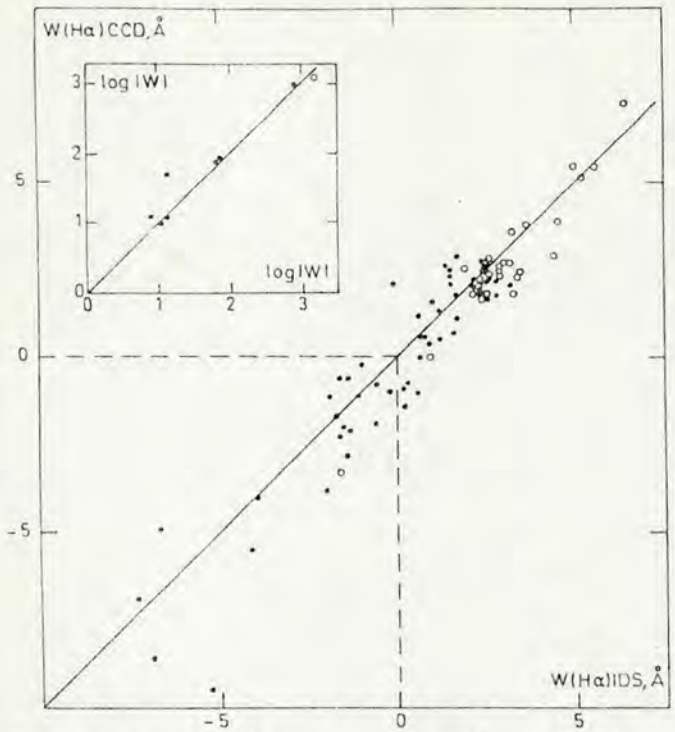

Fig. 4. Comparison of $W(H\alpha)$ measurements derived from the IDS (abscissa) and CCD (ordinate) data sets. Open circles represent star clusters and H II regions, and black dots galactic nuclei. Negative values of W correspond to an $H\alpha$ line in emission and the very large emission lines are shown in a log-log inset in the upper left corner of the diagram

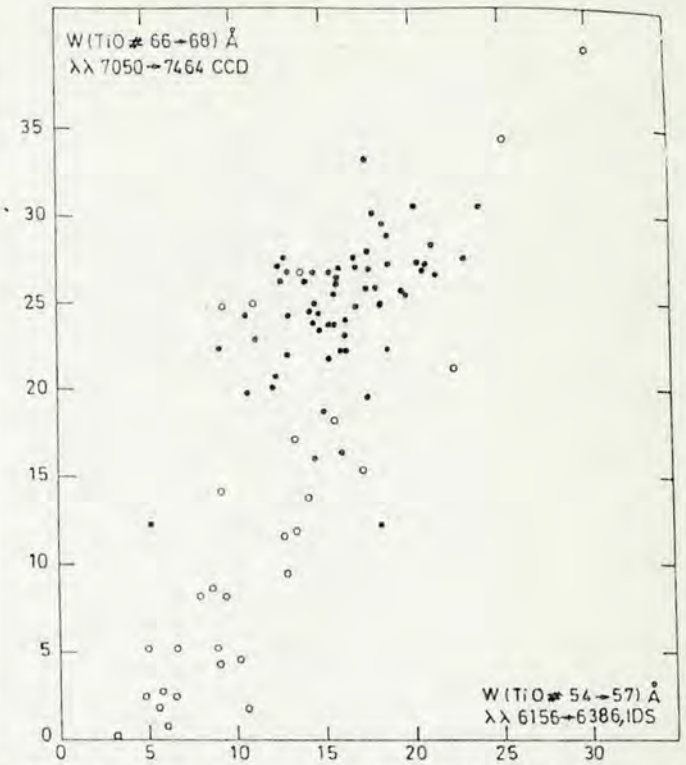

Fig. 5. Comparison of the strengths of two TiO bands showing that the observed scatter for star clusters (circles) is not larger than that for galactic nuclei (dots). This indicates that no major difference occured in the spatial coverage of the clusters, between the IDS and CCD observations

(Paper I) where isochrones in the W vs Z plane tended to merge at longer wavelengths, as a result of a decreasing dilution effect from the blue main sequence stars. Sources of scatter in Figs. 7a through 7c are various. In the Na I window the errors are relatively larger owing to the weakness of this feature. In the Ca II windows, contamination by TiO and Paschen lines are rather to be incriminated: TiO may reinforce the metallicity dependence while Paschen lines introduce a systematic increase for blue clusters whatever their metallicity is. TiO contamination is most important in the Ca II 8542 Å window and the Paschen absorption will affect more the Ca II 8662 Å window.

In first order, the windows dominated by molecular absorption share the same characteristic, e.g. TiO $\lambda\lambda$ 7050, 7464 for which the mean W value increases steadily with Z (Fig. 8a). But the scatter of points is larger than that observed for windows related to metal atomic lines. A comparison with Fig. 5 also demonstrates that the scatter is larger than that expected from observational errors and it is thus intrinsic. In particular it arises mostly from blue clusters rich in red evolved stars like NGC 2004 and NGC 1866. These clusters have stronger TiO bands than GGC of comparable metallicity, while other young clusters which are deficient in this red evolved population tend to show weaker TiO than GGC.

The reason why, in integrated spectra, molecular bands behave with Z in a more complex way than atomic metal lines do, is certainly related to the fact that atomic lines can be formed throughout a wide range of stellar temperatures from early M up to F types which constitute the bulk of the flux emission from 6000 to 10 000 Å for clusters of all ages. On the other hand, molecular bands arise essentially from cool stars, and the flux contribution from these cool stars to the integrated light of a cluster strongly depends on the cluster age. Thus, as shown in Fig. 8b, abrupt changes in the equivalent width of molecular bands occur at the red supergiant ($t \sim 10^7$ yr) and at the AGB ($t \sim 10^8$ yr) phases. These rapid red phases are accompanied by a flattening of the near-infrared continuum slope as displayed in Fig. 8c (see also Fig. 6b). The behaviour of molecular bands also differs from that of atomic lines in the sense that they preferentially exhibit a non-linear dependence on Z. This effect is present in the CN and TiO windows (e.g. Fig. 8a), particularly for the GGC sample where age effects are absent: for $[Z/Z_\odot] < -1.0$ molecular absorptions are almost null while they become prominent at a metallicity around solar. On the contrary, metal atomic lines (e.g. Fig. 7a) exhibit a steady regular increase with Z. The increase rate may, however, change from one line to the other. Taking as a reference the W value at $[Z/Z_\odot] = -1.0$, for an increase in metallicity by a factor 10, W(Na I λ 8190) increases by around 66%, W(Ca II λ 8542 + TiO) by 62% and W(Ca II λ 8542), corrected for TiO, by 55% (column 12 in Table 1). An intermediate behaviour between metallic lines and molecular bands is observed for windows in which both kinds of absorptions contribute equally. This can be seen in Fig. 9a and b the first one corresponding to windows

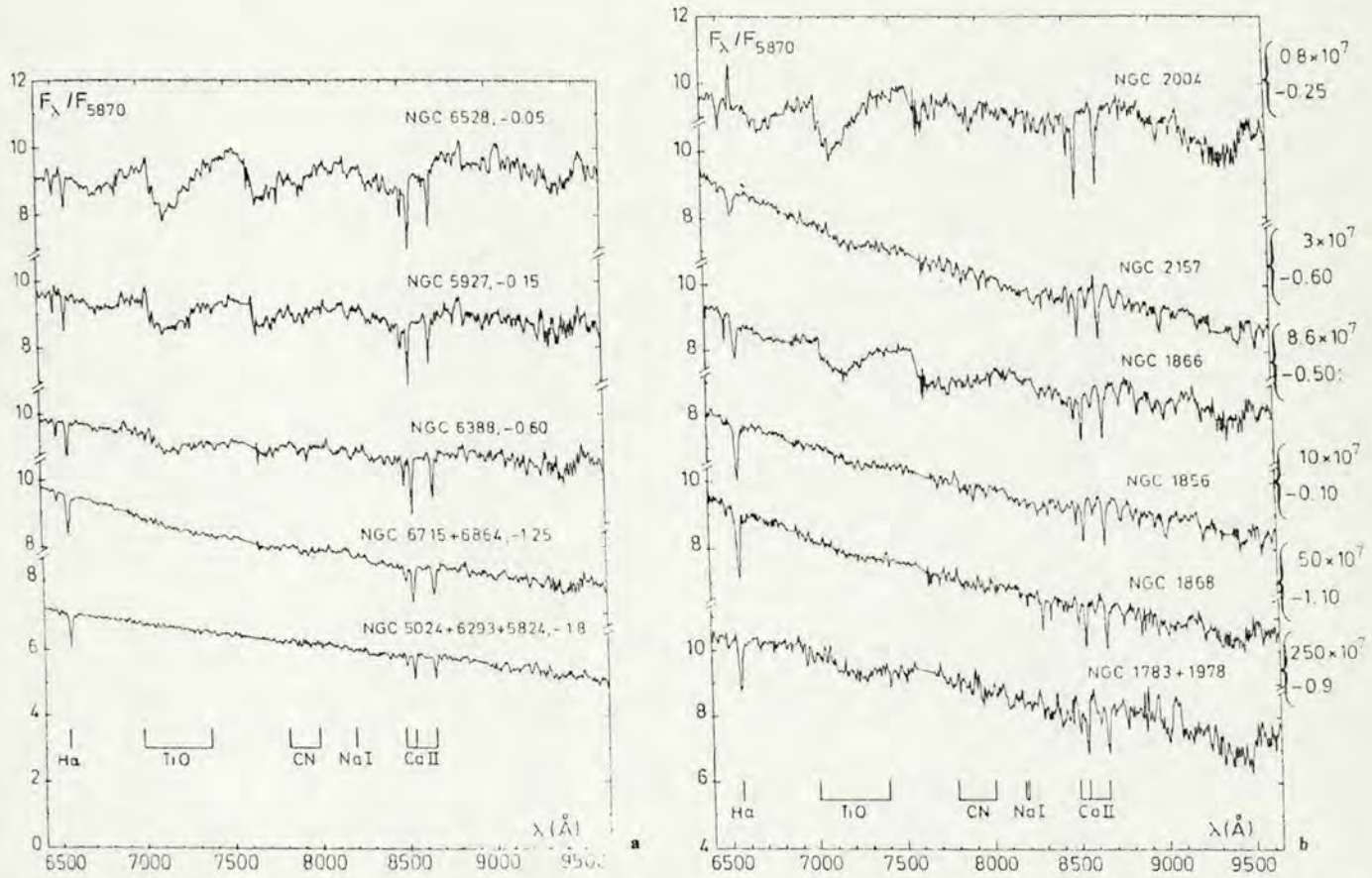

Fig. 6. **a** Downward metallicity sequence for Galactic globular clusters showing the increase of Ca II, Na I and molecular bands with $[Z/Z_{\odot}]$. **b** Age sequence for young clusters; the age and metallicity are provided in the right part of the figure. Ages around 10^7 yr and 10^8 yr are dominated by red evolved stars, as traced out by strong TiO molecular bands

Nos. 75 + 76 where the TiO absorption is significantly enhanced by Ti I and Fe I lines, and the second one corresponding to the smallest Ca II triplet line which is blend with a strong TiO molecular absorption.

Finally, we have displayed in Figs. 10a and 10b, the joined windows Nos. 83 + 84 which, in red clusters correspond to TiO absorption and in blue clusters are dominated by Paschen lines P10 and P11. In this case we face metallicity (Fig. 10a) and age (Fig. 10b) effects of comparable importance. Regarding the Ca II triplet, indeed weak Paschen lines may contribute to the window; but then, the metallic feature remains predominant even in blue clusters where, from the intensities of P17, P14, and P12 (Fig. 3a), we estimate that P16, P15, and P13 correspond to 45%, 36% and 45% of the absorption respectively in the Ca II λ 8498, λ 8542, and λ 8662 windows.

As in Paper I, we present on the right part of Figs. 7 through 10, the corresponding histograms for spheroidal (E, S0) and spiral (Sa, Sb, Sc) galaxies. Such a comparison is necessary in view of population synthesis to be performed and presented in a forthcoming paper. In the near-infrared very metal rich globular clusters like NGC 6440 and 6528 exhibit metallic features comparable to the strongest-lined galaxies. For example NGC 6528 presents molecular bands even stronger than in any galaxy (compare Figs. 6a and 11, also). In the visible range (Paper I) these two clusters, together with NGC 6553, also showed W for metallic features comparable to those observed in the strongest-lined galactic nuclei, with the exception of windows corresponding to Mg I + MgH and its surrounding. At that time, we adopted thus the conservative conclusion that 50% of the luminous galaxies could be described by the cluster library without any extrapolation in the W vs metallicity plane. The spectra of galaxies should not necessarily be identical to those of very metal-rich globular clusters since the latter are expected to be single generation objects while galactic nuclei might cover a certain range in metallicity and age. However, systematic differences in the mean metallicity or age do not explain why some metallic features are slightly stronger and others slightly weaker among different objects. Several explanations could be raised, such as abundance anomalies for a few elements, line saturation effects or differences in the initial mass function (IMF). Another interpretation could simply be variations in the number of luminous stars in which particular features are strong. Globular clusters are star-rich but the number of luminous stars they contain is finite and subject to fluctuations. Thus, the near-infrared molecular band excess in NGC 6528 with respect to galaxies and to the otherwise similar globular cluster NGC 6440, could result from a slightly enhanced population of

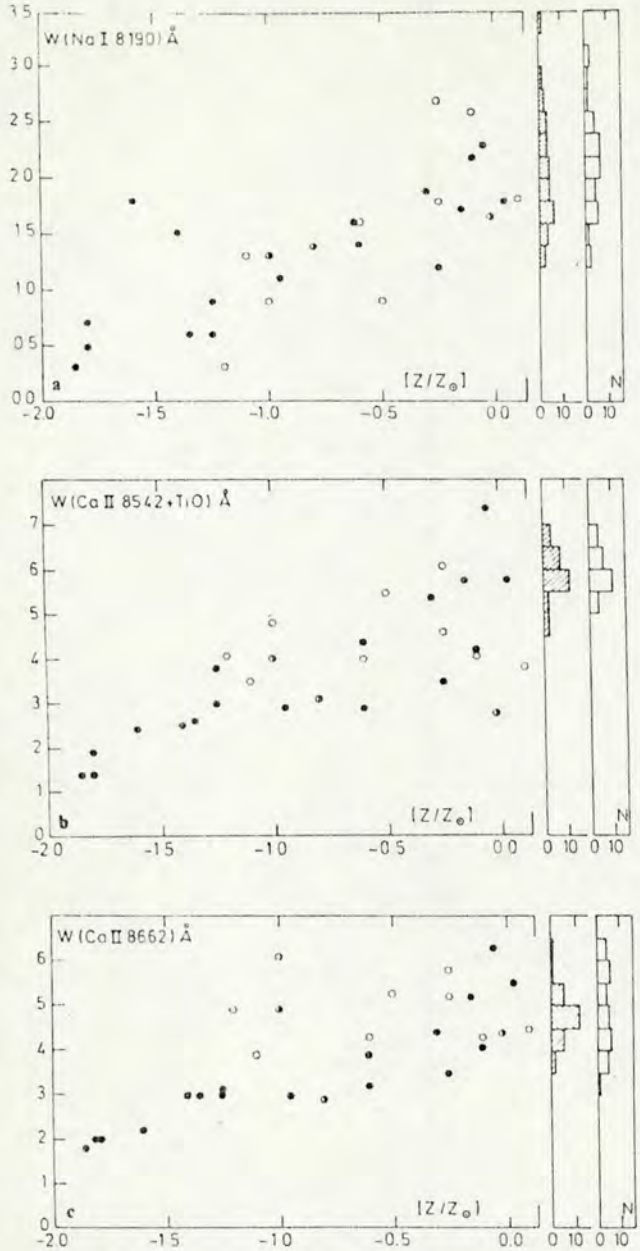

Fig. 7a–c. Metallic line windows as a function of metallicity. Filled circles are Galactic globular clusters, semi-empty and empty circles represent respectively intermediate age and young clusters. The relations are age-independent. On the right side we show histograms for spiral galaxies (hatched) and E + S0 galaxies respectively

bright M giant stars in which those features are very strong. Conversely, the weaker Mg I + MgH absorption in very metal rich globular clusters with respect to galaxies might be assigned to an excess, in the former, of K giants where this feature is weaker than in dwarfs (Spinrad, 1962). For the future population synthesis, it is thus, important to minimize fluctuation effects in the star cluster library, by interpolating the mean properties as a function of metallicity and age. Criteria for the interpolations were established in Paper I. The grid predictions for the near-infrared

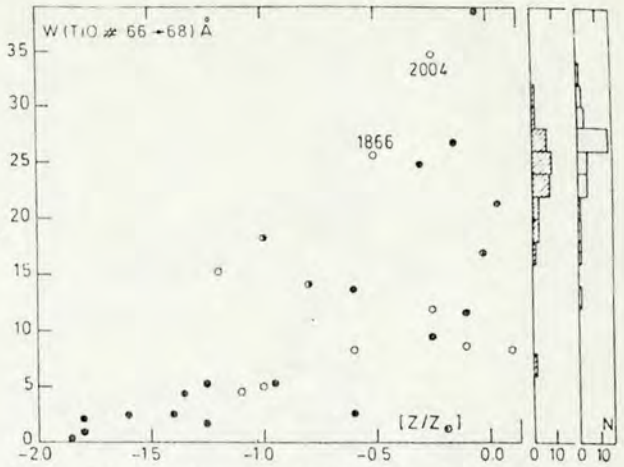

Fig. 8a. Behaviour of a strong molecular band as a function of metallicity; same symbols as in Fig. 7; for large metal content, some young clusters tend to lie below the globular clusters, of equal metallicity, while others (labelled) containing luminous red stars, tend to lie above.

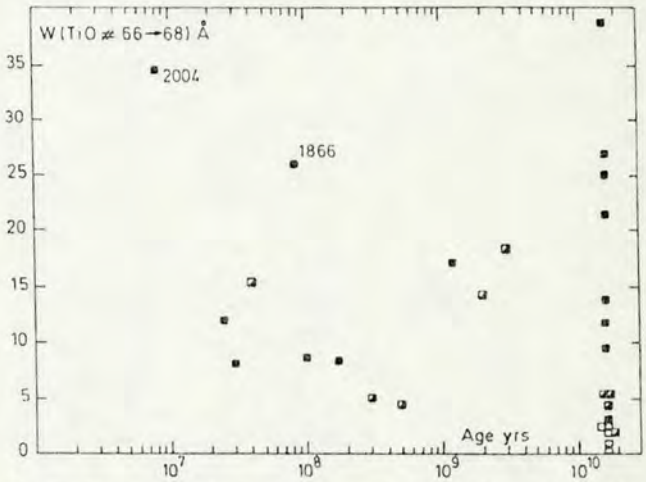

Fig. 8b. The same molecular band as a function of age. Young clusters in the red phases (10^7 and 10^8 yr old) show prominent molecular absorption. Filled squares correspond to $[Z/Z_\odot] > -0.7$ semi-empty ones to $-1.4 < [Z/Z_\odot] < -0.7$ and empty ones to $[Z/Z_\odot] < -1.4$

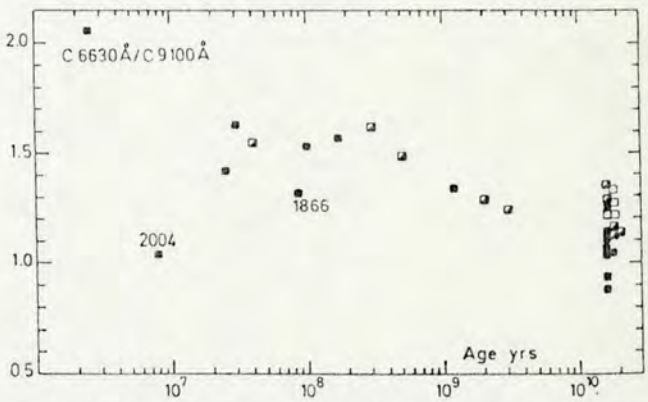

Fig. 8c. The near-infrared continuum slope as a function of age. Symbols as in Fig. 8b. Young clusters in the red phases have a flatter continuum than other young clusters. For comparison, we also show the H II region NGC 1714 in the upper left corner

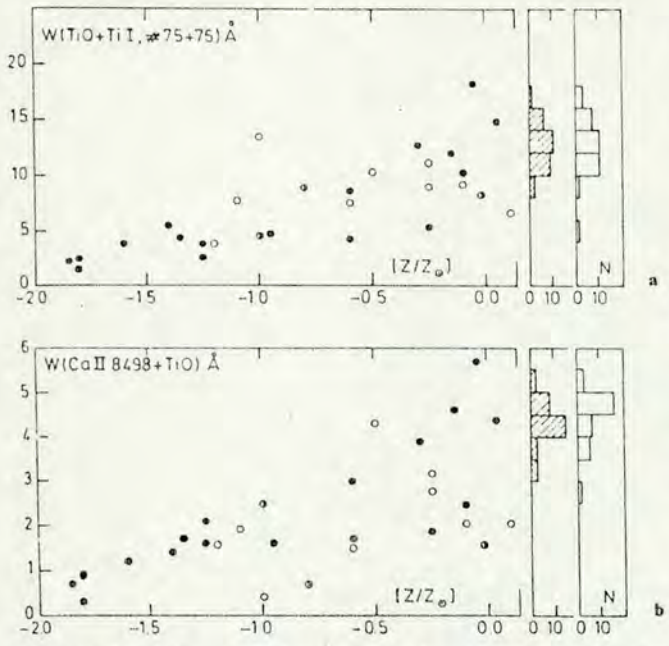

Fig. 9a and b. Windows in which molecular bands and metallic lines contribute with a comparable weight to the total absorption; their behaviour with Z is intermediate between those in Figs. 7 and 8a. Same symbols as in Fig. 7

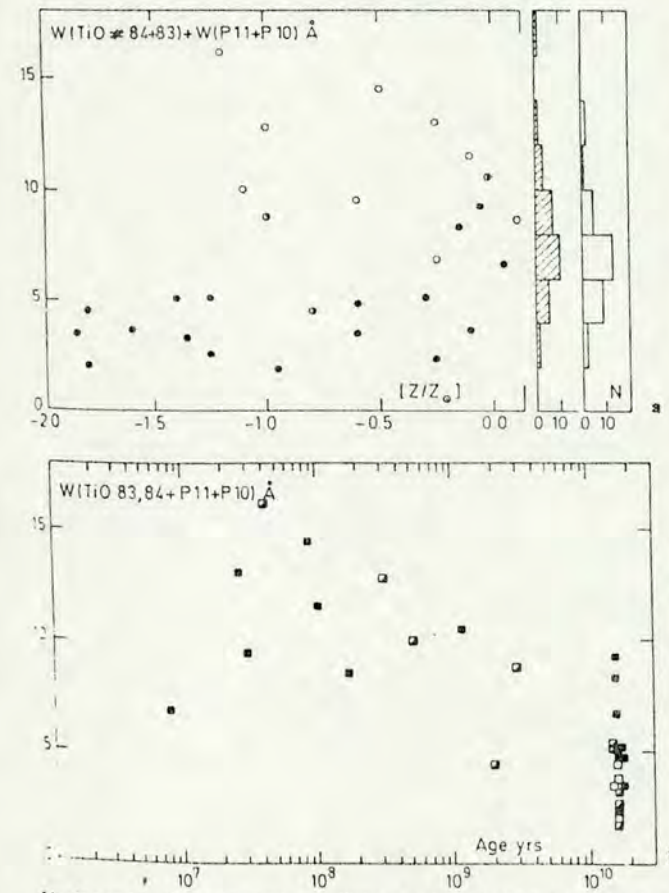

Fig. 10a and b. Behaviour with metallicity **a** and age **b** of a window dominated by molecular absorption in old clusters and Paschen lines in young ones. Symbols are respectively as in Figs. 7 and 8b

range are given in Appendix A, following the same format as that initially used for its visible counterpart (Paper II).

Early spectroscopic studies had included the very metal rich GGC NGC 6440, 6528 and 6553. In particular, Morgan (1960) pointed out the similarity of their spectrum with that of the nucleus in M 31. Unfortunately, recent works comparing GGC to galaxy nuclei used, as metal rich clusters, NGC 6637 (M 69) and NGC 6356 which are not as suitable (e.g. Faber, 1973; Aaronson et al., 1978; Frogel et al., 1978; Burstein et al., 1984). The integrated spectra and colours of the latter clusters are indeed like those of NGC 6388 (Fig. 6a) and thus, weak-lined with respect to massive galaxy nuclear spectra. Consequently, a consensus was established suggesting that GGC were not useful for population comparisons with galaxy nuclei, unless large extrapolations in metallicity were made for the cluster properties. This extrapolation problem was further exacerbated by the different metallicity scales proposed in the last 10 years based on 47 Tuc (NGC 104) and M 71 (NGC 6838): different techniques led to metallicities ranging from solar to $[Z/Z_\odot] = -1.2$. Integrated properties of 47 Tuc and M 71 are also similar to those of NGC 6388, and hence their spectrum is weak-lined with respect to those observed in massive galaxy nuclei. Presently, the best $[Z/Z_\odot]$ values for 47 Tuc and M 71 range from -0.6 to -0.8 (Zinn and West, 1984; Gratton et al., 1986) and the metallicities we adopted in Paper I are from a calibration where 47 Tuc has $[Z/Z_\odot] = -0.7$. The cluster NGC 5927 (Fig. 6a) is 0.6 dex more metal-rich than 47 Tuc, on the basis of spectroscopic analysis of red giants (Cohen, 1983). However, values for the metal content in NGC 6440, 6528, and 6553 still rely on extrapolations and it would be interesting to derive them directly from individual member stars. Inspection of the integrated spectrum of NGC 6528 (Fig. 6a) and its locus in Figs. 7 and 8a, suggest that a value $[Z/Z_\odot]$ as large as $+0.3$ might be possible. Nevertheless we emphasize the fact that the GGC vs galaxy nuclei problem is solved by the present observations and those presented in Papers I and II: *the spectra of very strong-lined GGC are comparable to those of massive galaxies*, whatever their precise metallicity value. We also point out that the synthesis approach we have undertaken is little dependent on the adopted age and metallicity calibrations for the clusters. It relies rather upon the properties observed directly on the cluster spectra.

5. Spectral properties of galactic nuclei in the near-infrared

We have displayed in Fig. 11 examples of galactic spectra for different morphological type, luminosity groups. The spectra look similar, whatever the group, dominated by strong metallic features. Even extreme cases in the visible range like the blue objects NGC 5102 and 5236 do not show spectra much different than for the rest of the galaxy sample in this range. However it should be noticed that in the near-infrared we are not necessarily looking at the underlying old population of these two blue nuclei. Indeed we observe that the near-infrared flux in young star clusters is always a significant fraction of the visible one (Table 1). The burst of star formation 4 10^8 yr old in NGC 5102 (Paper III) and responsible for 70% of the light at 5870 Å, still dominates at 9100 Å with a 57% contribution. Information about the burst duration can also be derived as follows. The deep Hα absorption in the star clusters NGC 1831 and 1868 (Fig. 6b and Table 1) which have the same age as the burst in NGC 5102 (Paper III), indicates that Hα is just filled in by emission in the latter. This evidence, together with weak [N II] and [S II] line emission (Fig. 11) indicate that we are still observing a residual star formation

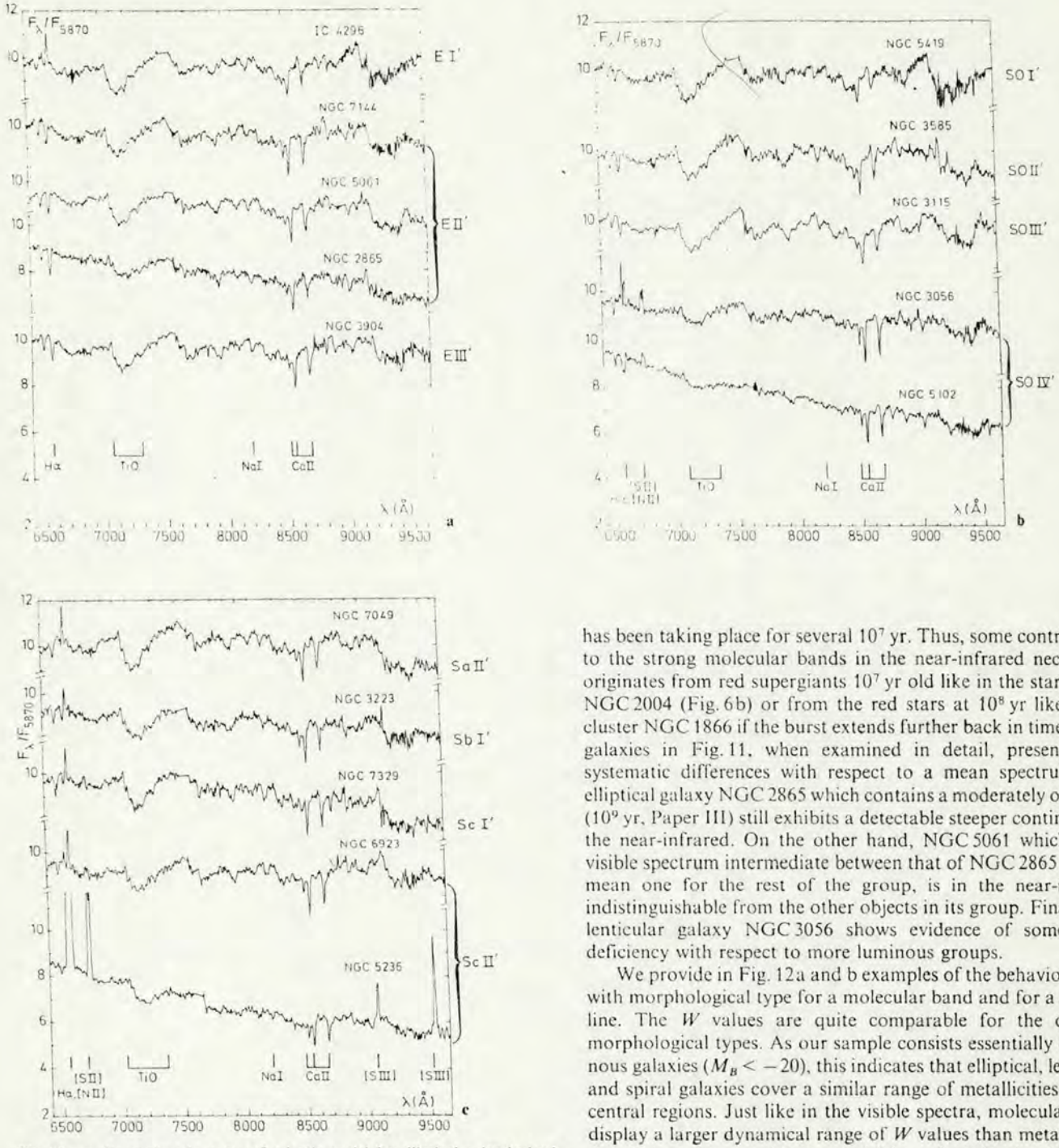

Fig. 11a–c. Examples of spectra of galactic nuclei for elliptical **a**, lenticular **b** and spiral **c** galaxies. Luminosity classes I', II', III', and IV' are according to Table 2 and were defined in Paper III

related to the strong burst initiated 4 10^8 yr ago. A detailed synthesis will possibly give more information about how the burst behaved in the meantime. The emission line spectrum of NGC 5236 originates at least in part, from H II regions. The continuum distribution as well as the Balmer lines higher than Hδ which appear in absorption (Paper III) suggest that star formation has been taking place for several 10^7 yr. Thus, some contribution to the strong molecular bands in the near-infrared necessarily originates from red supergiants 10^7 yr old like in the star cluster NGC 2004 (Fig. 6b) or from the red stars at 10^8 yr like in the cluster NGC 1866 if the burst extends further back in time. Other galaxies in Fig. 11, when examined in detail, present small systematic differences with respect to a mean spectrum. The elliptical galaxy NGC 2865 which contains a moderately old burst (10^9 yr, Paper III) still exhibits a detectable steeper continuum in the near-infrared. On the other hand, NGC 5061 which has a visible spectrum intermediate between that of NGC 2865 and the mean one for the rest of the group, is in the near-infrared indistinguishable from the other objects in its group. Finally, the lenticular galaxy NGC 3056 shows evidence of some metal deficiency with respect to more luminous groups.

We provide in Fig. 12a and b examples of the behaviour of W with morphological type for a molecular band and for a metallic line. The W values are quite comparable for the different morphological types. As our sample consists essentially of luminous galaxies ($M_B < -20$), this indicates that elliptical, lenticular and spiral galaxies cover a similar range of metallicities in their central regions. Just like in the visible spectra, molecular bands display a larger dynamical range of W values than metallic lines do. This reflects a better sensitivity of molecular bands to metallicity, according to star cluster results (Sect. 4). Indeed, the mean metallicity of a massive galaxy is expected to fall in the range where molecular bands grow non-linearly with Z (Sect. 4). The larger dynamical range of molecular bands can also be seen in Figs. 13a and 13b where we have plotted respectively W(TiO $\lambda\lambda$ 7050, 7464) vs W(CN $\lambda\lambda$ 7852, 8040), and W(Na I λ 8190) vs W(Ca II λ 8542).

In Figs. 14a and 14b, the behaviour of W(Ca II λ 8542) and W(TiO $\lambda\lambda$ 7050, 7464) as a function of absolute magnitude M_B of the galaxy, is demonstrated. No dependence of the Ca II triplet line with luminosity is observed, possibly a result of the smaller

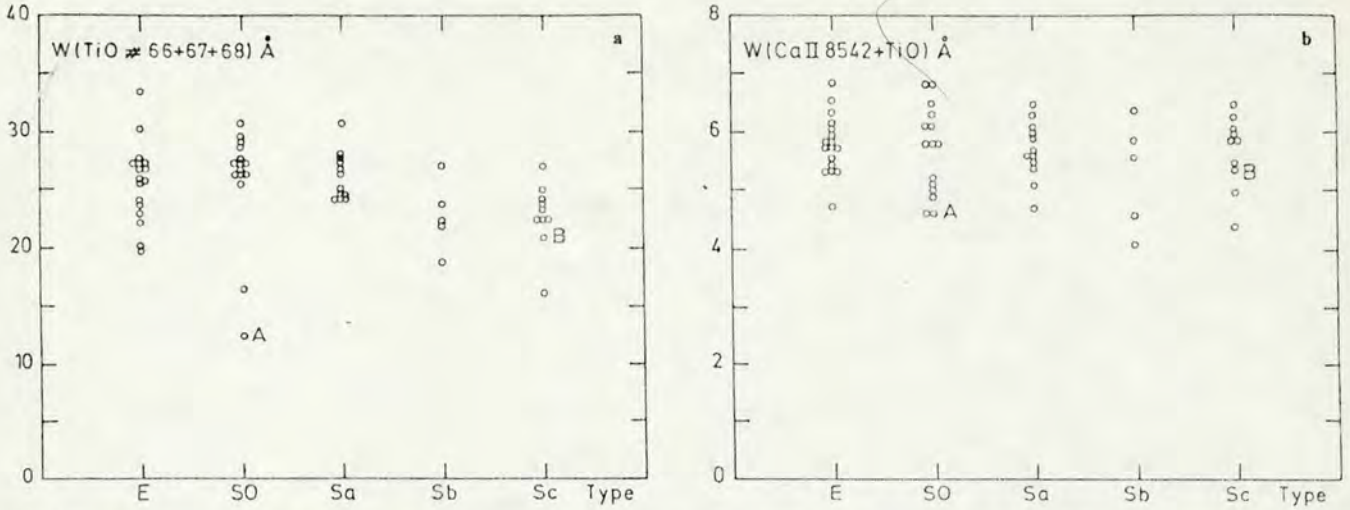

Fig. 12a and b. Behaviour of a molecular band **a**, a metallic line **b**, with different morphological types. Points labelled A and B correspond respectively to the blue galaxies NGC 5102 and 5236

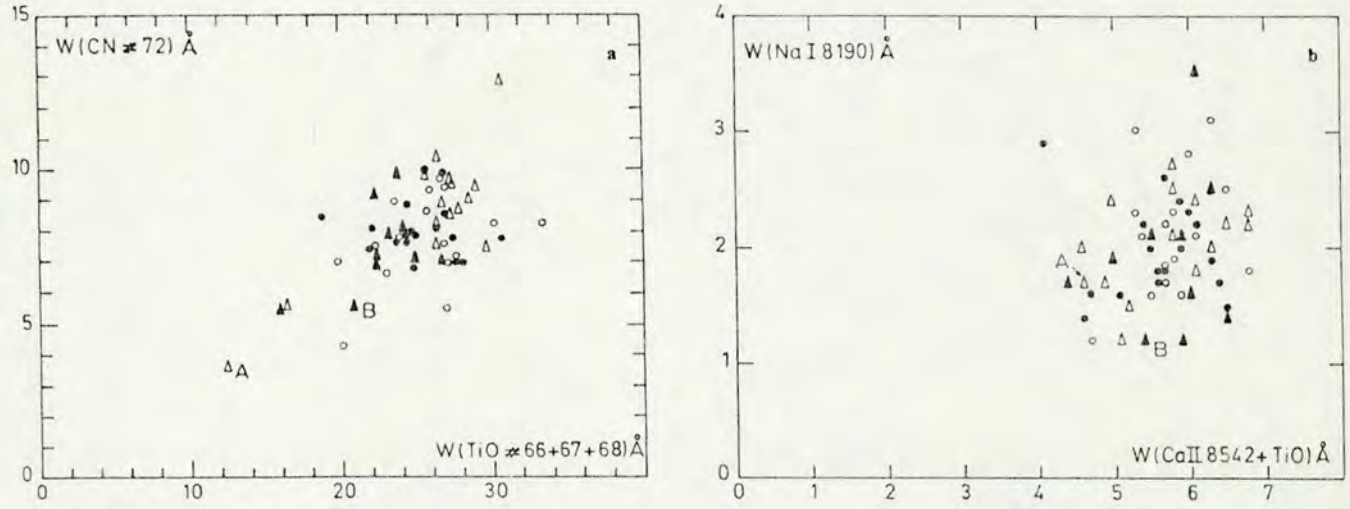

Fig. 13a and b. Comparison, of respectively two molecular bands and two metallic lines. Molecular bands present a larger dynamical range of values. Open circles: elliptical galaxies; open triangles: lenticular galaxies; filled circles: Sa and Sb types; filled triangles Sc galaxies

sensitivity of this feature to metallicity. If metallicity effects are present they should be more important for TiO as suggested in Fig. 14b. Only 3 galaxies in our sample have $M_B > -19$ and they are all E or S0 galaxies. One, NGC 4486B, is comparable to its massive counterparts, in terms of W values. This object is the companion of a giant elliptical in the Virgo cluster and thus is possibly tidally stripped (Paper IV and references therein). There is evidence that NGC 3056 is indeed metal deficient with respect to more massive galaxies. Unfortunately, we did not observe in the near-infrared NGC 4476, which in the visible range appeared as a genuine metal-poor galaxy. Because of its position in the metallic feature distributions, NGC 5102 is probably metal deficient. Its weak TiO however may also result from the burst age in this galaxy, 4 10^8 yr corresponding to fewer red stars. Indeed, red evolved stars are expected to contribute substantially at two peak values which are 10^7 and 10^8 yr, just prior to the burst age in NGC 5102. Spiral galaxies in Figs. 14a and 14b behave like the E and S0 galaxies. This suggests that small bulges in spiral galaxies have a metal content comparable to that in early type galaxies, the total absolute luminosities of the galaxies being the same.

6. Conclusions

Main conclusions of the present work are as follows:

1. We present near-infrared CCD spectra with 12.5 Å resolution for 30 star clusters having known ages, metallicities and reddenings. We also observed a sample of 62 nuclei in galaxies of all morphological types. A special attention is given to removal of fringes in this wavelength range.

2. We measure the continuum distribution and the equivalent widths of 13 absorption features for star cluster and galactic nuclei.

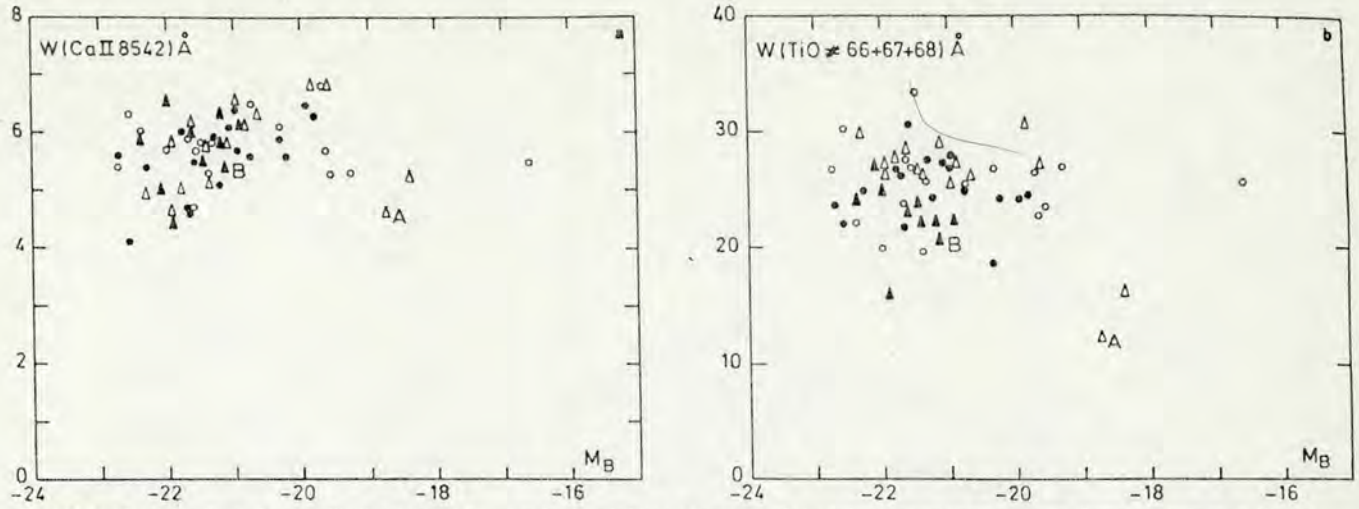

Fig. 14a and b. Behaviour of a metallic line (**a**) and a molecular band (**b**) as a function of the galactic absolute magnitude. Same symbols as in Fig. 13

3. Analysis of the star cluster sample shows that in the near-infrared, metallicity is the dominant parameter. Metallic lines present single-valued linear relationship with the metal content while molecular bands tend to depart from linearity at large metallicities. Age effects in blue clusters disturb the relationship for molecular bands.

4. Age produces second order effects of various types: (i) at some particular stages in the evolution of a blue cluster, molecular bands are quite strong owing to the accumulation of luminous red stars, (ii) absorption Paschen lines contaminate some of the metallic windows and, (iii) the continuum slope steepens slightly for young ages.

5. In view of population synthesis of galactic nuclei, we present star cluster grid predictions as a function of age and metallicity for 5 metallic windows and the continuum distribution.

6. Strong-lined globular clusters like NGC 6528 have integrated spectra comparable to those of massive galaxies. Consequently, they are important tools for population synthesis, regardless of their precise metallicity.

7. Strong-lined spectra are observed in the central regions of both spiral galaxies and luminous elliptical galaxies, suggesting a comparable metal content.

8. Even very blue galaxies exhibit, in the near-infrared, spectra quite similar to those observed for the rest of the galaxy sample. However, evidence is found that a large contribution to this range is not from their old underlying population.

Appendix A

We provide the grid predictions as a function of star cluster age and metallicity for a selection of 5 absorption features and 7 continuum points from Table 1 (Tables A1, A2, A3). We have excluded a number of features for various reasons:

a) molecular windows with strong CN and TiO, owing to a complex behaviour we could not fully model because of our restricted number of data points.

b) CaI + FeI, No. 59, which is rather weak and moreover contaminated in emission line galaxies,

Table A1. For Galactic globular clusters, mean relative continuum points at different wavelengths, as a function of metallicity

	C6630/C5870	C6990/C5870	C7520/C5870	C8040/C5870	C8408/C5870	C8700/C5870	C9100/C5870
$[Z/Z_\odot]$							
0.6	0.97±0.05	0.99±0.05	1.01±0.06	1.01±0.07	1.03±0.08	1.04±0.08	1.03±0.09
0.0	0.95±0.05	0.95±0.05	0.96±0.06	0.96±0.07	0.96±0.08	0.96±0.08	0.95±0.09
-0.5	0.95±0.05	0.94±0.05	0.93±0.06	0.91±0.07	0.90±0.08	0.90±0.08	0.88±0.09
-1.0	0.94±0.05	0.91±0.05	0.89±0.06	0.86±0.07	0.84±0.08	0.84±0.08	0.82±0.09
-1.5	0.93±0.05	0.89±0.05	0.86±0.06	0.81±0.07	0.78±0.08	0.78±0.08	0.76±0.09
-2.0	0.92±0.05	0.87±0.05	0.81±0.06	0.77±0.07	0.72±0.08	0.71±0.08	0.68±0.09

Table A2. For intermediate and young clusters, mean relative continuum points at different wavelengths, as a function of age

	C6630/C5870	C6990/C5870	C7520/C5870	C8040/C5870	C8408/C5870	C8700/C5870	C9100/C5870
age							
5 E9	0.96±0.07	0.94±0.08	0.92±0.09	0.88±0.10	0.87±0.11	0.87±0.12	0.85±0.13
E9	0.92±0.05	0.85±0.05	0.81±0.07	0.74±0.07	0.70±0.08	0.70±0.08	0.67±0.08
5 E8	0.87±0.04	0.80±0.04	0.72±0.05	0.65±0.05	0.61±0.06	0.60±0.06	0.57±0.07
E8	0.81±0.05	0.74±0.05	0.67±0.06	0.61±0.07	0.59±0.07	0.58±0.08	0.54±0.08
5 E7	0.84±0.05	0.77±0.05	0.73±0.06	0.64±0.06	0.60±0.07	0.61±0.08	0.57±0.09
E7	0.87±0.11	0.80±0.13	0.77±0.15	0.68±0.17	0.65±0.19	0.68±0.21	0.64±0.25

Table A3. Mean equivalent widths of five metallic features as a function of metallicity. Being age effects in these windows essentially negligible, the values are valid for clusters of all ages

	W(#74) NaI	W(#75/6) TiO+TiI	W(#77) CaII 8498 TiO+P16	W(#78) CaII 8542 TiO+P15	W(#80) CaII 8662 P13+TiO
$[Z/Z_\odot]$					
0.6	2.5±0.4	16.0±2.9	5.0±1.1	6.8±1.0	8.0±0.9
0.0	2.0±0.4	12.3±2.9	3.9±1.1	5.5±1.0	6.0±0.9
-0.5	1.6±0.4	9.3±2.9	3.0±1.1	4.5±1.0	4.2±0.9
-1.0	1.2±0.4	6.3±2.9	2.2±1.1	3.4±1.0	3.3±0.9
-1.5	0.9±0.4	3.2±2.9	1.3±1.1	2.3±1.0	2.5±0.9
-2.0	0.5±0.4	0.2±2.9	0.4±1.1	1.2±1.0	1.6±0.9

c) Hα, No. 60, which was already studied in Papers I and II,

d) P14, No. 79 and P12, No. 81, which, in blue clusters are indicators of the Paschen contamination in the Ca II windows, and, in red clusters and galaxies are rather dominated by molecular absorption,

e) TiO, No. 83 and No. 84, where age and metallicity effects are of an equal weight (Fig. 10) as a result of the presence of P11 and P10 in blue clusters. Contamination from [S III] may be important in emission line galaxies.

The dispersion attached to each value represents the rms differences between W observed in the cluster sample and the grid predictions for 3 age groups: (i) young clusters, (ii) intermediate age clusters and (iii) globular clusters. For blue clusters in particular, where W of molecular bands vary abruptly along the red phases (Sect. 4), these dispersions are large. Although there are strong observational and theoretical evidences that the red phases in blue clusters are real, we do not take them here as age criteria, i.e., using W of strong molecular bands to distinguish populations in small intervals around 10^7 yr and 10^8 yr from those outside these age domains. But, indeed, we believe that a *larger* sample of clusters would allow to derive the exact duration of these phases and their dependence on metallicity. This, in turn, would provide important criteria for determining the age and duration of starbursts in blue galaxies, complementary to the best age discriminator, namely the continuum distribution (Paper I).

Acknowledgements. We are gratefully indebted to the ESO staff at La Silla and Garching, to the Paris Institute of Astrophysics and to the staff at the Computer Centre in Paris/Meudon Observatory, especially the group who developed the new command system eVe. We thank Dr. H. Spinrad and Dr. G. Cayrel for interesting comments. E.B. thanks the Brazilian Institution CNPq for a fellowship.

References

Aaronson, M., Frogel, J., Persson, S.: 1978, *Astrophys. J.* **220**, 442
Baldwin, J., Stone, R.: 1984, *Monthly Notices Roy. Astron. Soc.* **206**, 241
Becker, S., Mathews, G.: 1983, *Astrophys. J.* **270**, 155
Bica, E., Alloin, D.: 1986a, *Astron. Astrophys.* **162**, 21 (Paper I)
Bica, E., Alloin, D.: 1986b, *Astron. Astrophys. Suppl.* **66**, 171 (Paper II)
Bica, E., Alloin, D.: 1987a, *Astron. Astrophys. Suppl.* **70**, 281 (Paper III)
Bica, E., Alloin, D.: 1987b, *Astron. Astrophys.* **181**, 270 (Paper IV)
Bica, E., Dottori, D., Pastoriza, M.: 1986, *Astron. Astrophys.* **156**, 261
Burstein, D., Faber, S., Gaskell, C., Krumm, N.: 1984, *Astrophys. J.* **287**, 586
Carter, D., Visvanathan, N., Pickles, A.: 1986, *Astrophys. J.* **311**, 637
Chiosi, C., Bertelli, G., Bressan, A., Nasi, E., Pigatto, L.: 1985, in *Starforming Dwarf Galaxies*, eds. D. Kunth, T. Thuan, J. Van, Editions Frontières, p. 449
Cohen, J.: 1979, *Astrophys. J.* **228**, 405
Cohen, J.: 1983, *Astrophys. J.* **270**, 654
Faber, S.: 1973, *Astrophys. J.* **179**, 731
Faber, S., French, H.: 1980, *Astrophys. J.* **235**, 405
Frogel, J., Persson, S., Aaronson, M., Mathews, K.: 1978, *Astrophys. J.* **220**, 75
Gratton, R., Quarta, M., Ortolani, S.: 1986, *Astron. Astrophys.* **169**, 208
Jones, J., Alloin, D., Jones, B.: 1984, *Astrophys. J.* **283**, 457
Morgan, W.: 1960, *Astron. J.* **64**, 432
Renzini, A., Buzzoni, A.: 1985, in *Spectral Evolution of Galaxies*, eds. C. Chiosi, A. Renzini, Reidel, Dordrecht, p. 195
Richtler, T., Nelles, B.: 1983, *Astron. Astrophys.* **119**, 75
Sandage, A., Tammann, G.: 1981, *A revised Shapley – Ames Catalogue of Bright Galaxies*, Carnegie Institute of Washington
Spinrad, H.: 1962, *Astrophys. J.* **135**, 715
Spinrad, H., Taylor, B.: 1971, *Astrophys. J. Suppl.* **22**, 445
Turnrose, B.: 1976, *Astrophys. J.* **210**, 33
Zinn, R., West, M.: 1984, *Astrophys. J. Suppl.* **55**, 45

Population Synthesis in Galaxy Nuclei using a Library of Star Clusters*

E. Bica[1)]

OBSERVATOIRE DE PARIS/MEUDON

ASTRONOMY AND ASTROPHYSICS, in press
October, 1987

PUBLICADO EM A&A. (1988), 195, 76

*Based upon observational data collected at the European Southern Observatory

---

Thesaurus code : 07.07.1 ; 07.22.1.;

Main Journal, Section 1 (Extragalactic Astronomy)

1) New adress: Instituto de Física , UFRGS
Av. Bento Gonçalves, 9500
Porto Alegre, RS, 90000
BRAZIL

SUMMARY :

Population syntheses for normal nuclei in E/SO and spiral galaxies are derived using a library of star clusters. This method allows to determine the chemical enrichment and to date successive generations of star formation. Thus it is more than a simple population synthesis, providing for the first time a direct estimate of the chemical evolution in these nuclei. For the E/SO groups following the normal metallicity vs luminosity relationship, the last generation of stars in the nucleus has reached a metallicity 4 times solar for $M_B = -22$ and 0.5 to 0.3 solar for $M_B = -18$. The bulk of the population is older than 10 Gyr but these galaxies have formed stars at least until look-back times of $\simeq$ 5 Gyr. Some metallicity dispersion is detected within the nuclei : in the most metal rich group, around 10% of the optical flux arises from populations with metallicities lower than solar. For the relatively less numerous bluer E/SO groups, younger age components are present, which we have been able to isolate and date. The red spiral groups also form a metallicity sequence which is related to the bulge luminosity, spanning metallicities from a factor 4 solar to solar. Finally, the groups of bluer spiral nuclei contain younger age components superimposed on an older population, which has reached at least the solar metallicity. The relative importance of the star formation bursts with respect to the older population is derived : in the bluest group, with NGC 5236 as a prototype, the population younger than 3×10^8 yr amounts to 87% of the flux at 4000 Å and 57% at 9000Å. The present method constitutes a powerful tool for the interpretation of composite spectra and will certainly have many applications in the study of large redshift galaxies.

I - INTRODUCTION

Previous studies of population synthesis in galaxies have been performed with libraries of stellar spectra and, in some cases, with libraries containing a mixture of stars and globular clusters (Pagel and Edmunds, 1981 ; Pickles, 1985 and references therein). We have undertaken a different approach using a base of *star cluster integrated spectra* only. A synthesis using stars requires the knowledge of T,g,Z and of the slope of the Initial Mass Funtion (IMF). The latter parameter is implicit in real cluster spectra. Clearly, the advantage of the present method is to be a two parameter analysis : age and metallicity (Bica and Alloin, 1986a, hereafter BA86a).

We have obtained visible and near-infrared spectra for a large sample of star clusters and galaxy nuclei at 12 Å resolution, respectively with the ESO telescopes 1.52m using the Image Dissector Scanner and 2.2m using a CCD. The visible cluster spectra are discussed in BA86a while those of galaxy nuclei are presented in Bica and Alloin (1987a, hereafter BA87a). The near-infrared results are given in Bica and Alloin, 1987b, hereafter BA87b). The sample clusters had a-priori known age, metallicity $[Z/Z_\odot]$ and reddening. Thus it has been possible to study the equivalent widths (W) and continuum distribution in the integrated spectra as a function of age and $[Z/Z_\odot]$ (BA86a). Then a grid of star cluster properties was interpolated at suitable steps in age and $[Z/Z_\odot]$ and the results were given in Bica and Alloin 1986b (hereafter BA86b) and BA87b, respectively for the visible and near-infrared ranges.

An important result of this analysis is that the equivalent widths W of metallic lines in the near-infrared are simple functions of $[Z/Z_\odot]$, while those in the blue are sensitive to age, in addition to metallicity, owing to

the dilution effect of blue luminous stars in young clusters. The spectra of star clusters and galaxy nuclei had been previously corrected for foreground reddening. The internal reddening arising from inclination effects in spiral galaxies was straightforwardly removed using the method developed in BA87a. We have also shown that the NaI5890Å.doublet is not suitable for population synthesis, owing to its interstellar gas contribution, which may dominate the stellar one in the case of inclined spiral galaxies (Bica and Alloin, 1986c, hereafter BA86c).

The present paper deals with the synthesis results. In section II we group the galaxy spectra showing similar properties. In section III we present details of the synthesis method and the computations. In section IV we discuss the synthesis results for our 15 types of galaxy spectra. Section V provides comments on the synthesis for individual groups. Finally, the concluding remarks of this work are given in section VI.

II – THE SPECTRAL GROUPS

Initially we intended to obtain a mean galaxy spectrum for each box determined by morphological type vs luminosity class. Nevertheless it soon became clear that every box contained atypical spectra and particularly that late type spiral galaxies were forming a highly heterogeneous class, for which no prototype could be assigned (BA87a). Thus we have first grouped spectra sharing the same properties within error bars and in a second step made the further separations according to morphological type or luminosity class. However, we have analyzed E/S0 and spiral galaxies separately. The galaxies in each group are given in Table 1 and values of W and continuum distribution for the various groups are shown in Table 3. The descriptions of the different

kinds of spectra, in BA87a, have delineated the present groups. We obtained nine groups for early-type galaxies (Table 1). They are shown in Figure 1, in terms of the best metallicity indicator and of the total magnitude M_B. The latter relationship has been discussed in detail in Bica and Alloin (1987c, hereafter BA87c). Groups E1 to E4 correspond to galaxies which follow the normal metallicity vs luminosity relationship, being dominated by a very old stellar population. Groups E5 to E8 mostly show age effects, as discussed in Section IV. The shapes of the boxes in Figure 1 are rather irregular : they reflect the fact that the consideration of only two metallic lines is in general insufficient to determine all spectral properties. This is illustrated particularly by a comparison of E3 and E7 which have similar W(CN) and W(MgI) but differ considerably in terms of W(Hβ) and other Balmer lines, as well as in terms of continuum distribution (Table 3 and figures 4 and 8). Thus we have also taken into account the latter important spectral properties in the definition of our groups. Group E9 corresponds mostly to galaxies with an evidence of tidal stripping (BA87c and references therein). However, spectroscopically it is indistinguishable from group E2, which indicates that the star formation took place quite early, before the stripping. Owing to their similar properties we synthesize only the group E2. Group E2 is also spectroscopically very similar to the more luminous E5, but we have decided to keep them apart because there is no evidence that E2 are simply stripped E5 galaxies. Rather, E5 might have been very strong lined like E1 and the spectral similarity with E2 should arise from an additional population component which dilutes the metallic lines. E3 and E6 are, perhaps, a more clear example of this effect : at similar metal indicator value (Figure 1), the more luminous group E6 presents a systematic increase of Balmer absorption lines (Table 3). The component which enhances the Balmer lines could also be responsible for the dilution of metallic lines, which

otherwise should be much stronger in such massive galaxies. We emphasize however that the objective of the spectral groups and the subsequent syntheses is not to explore such marginal differences between neighbouring groups. These should be regarded, rather, as the limits for the application of the method.

The selected groups of spiral galaxies are shown as a function of morphological type and luminosity class in Table 2. Notice how the red groups S1 to S4 migrate *simultaneously* towards lower luminosities *and* later morphological types. This is indeed a metallicity sequence spanning a factor 4 in metallicity (section IV), which is associated with the bulge size of the galaxies. On average, the nuclear properties of a giant Sc are similar to those of a dwarf Sa. Note that galaxies in the most metal poor groups S3 and S4 are strong-lined, very different from metal-poor globular clusters (BA87a). Groups S5 to S7 are subject to various age effects (Section V). The position of these galaxies in the grids of Table 2 gives information on the nature of the older underlying population.

Within each E or S group a small dispersion in spectral properties exists and, in some cases, we have possibly sacrified information for the sake of a better signal to noise ratio. However the quantitative criterium used in the definition of the groups makes the present classification a more detailed and precise version of the early blue-violet spectral types of galaxies (Humason et al. 1956). The extreme groups S1 and S7 correspond respectively to the K and A spectral types. We point out that the ranking order E1-9 and S1-7 are simple designations not necessarily intended to represent sequences whatsoever. However, the synthesis results (sections IV and V) indicate that E1 to E4 and S1 to S3 form, basically, sequences of decreasing average metallicity at constant (mostly old) age population content. On the other hand S4 to S7 form a sequence of increasing young age population content at nearly constant average

metallicity.

Prior to averaging the spectra, it was necessary to apply a supplementary reddening correction to some particular galaxies, in addition to that arising from foreground sources or spiral inclination effects (Section I). Evidence is found, as noted in Table 1, that for most of these galaxies, the extinction arises from an atypical amount of dust in the nuclear region, but for others at low Galactic latitudes, it possibly arises from uncertainties in the previous foreground reddening correction.

We call attention to the fact that some E and S groups are essentially indistinguishable from a purely spectroscopic viewpoint (Table 3) : in particular the strong-lined E1 group is similar to S1 and E2 to S2. Thus the star formation history of these nuclei must have been very similar, in spite of the fact that the global galaxies differ considerably in appearance. Nevertheless the spiral groups which present clear young age population components (S5 to S7 cf. sections IV and V) are spectroscopically very different from the E7 and E8 groups, for which age effects are the strongest among early-type galaxies. This suggests, at least for the present sample, that whenever star formation has occured in the nuclei after the initial collapse, it has been different in spirals and ellipticals.

III - PRINCIPLE OF THE METHOD AND COMPUTATIONS

We have used for the computations strong metallic features over a *wide spectral range*. Metallic lines provide constraints on the metal content ; but they also constitute a powerful age discriminator owing to their W wavelength dependence, which arises from dilution by blue stars in young star clusters (BA86a). We use K CaII 3933Å, CN 4200Å, the G band of CH 4301Å,

MgI+MgH 5175Å and CaII 8542, 8662Å. These are strong features measured with a good precision, they are not disturbed by emission lines and have a comprehensively-modeled behaviour as a function of the cluster age and metallicity (BA 86b, 87b). The NaI 5890Å line is strong as well, but the interstellar contamination precludes its use for population synthesis (BA 86c). Red TiO bands are not used owing to their complex behaviour in young clusters containing luminous red stars ; this behaviour has to be further studied (BA 86a, 87b) before we can model it. However, we use the TiO bands to check the output of the computations, since the resulting template galaxy spectrum, built from a combination of star cluster spectra, must reproduce them as well. The Balmer lines can be used only when they are free of emission contributions : Hα, as a rule, is emission contaminated, even when seen in absorption. In the latter case however, Hβ can be safely employed and so on for Hγ and Hδ. For the spiral groups S5 to S7, all Balmer lines are contaminated, so the computations in these cases rely exclusively on metallic features.

Previous population syntheses have used, in general, minimization procedures which looked for the best solution, starting from a plausible initial guess. The problem in these computations has always been to test the uniqueness of the solution. This has been very difficult, if not impossible altogether, owing to the fact that many parameters can be modified in a synthesis using stellar libraries.

Using a fast computer and having only two parameters, age and metallicity, it has been possible to test an extremely large number of star cluster combinations, and thus to be more confident about the uniqueness of the solution we found. Two chemical evolution arguments constrain the space in the $[Z/Z_O]$vs age plane where the solution is searched for. First, galaxy nuclei correspond to small volumes where it is plausible to assume that the gas

is chemically homogeneous at any time, so that the solution must describe a path in the diagram. Second, the metallicity cannot decrease for younger generations. Thus in a first phase, the method consists of testing all possible combinations at 10% step of 8 points (clusters) which form a path (chemical evolution) in the age versus $[Z/Z_O]$ plane. We point out that it is not possible to have time information for ages older than ~ 8 Gyr. We assume in this work that the chemical enrichment in the nuclei has taken place quite early. Thus in practice an initial path of 8 star clusters in the $[Z/Z_O]$vs age diagram is distributed along two sequences : (i) a metallicity sequence from $[Z/Z_O] = -2$ to $[Z/Z_O]_{MAX}$ at fixed very old age and (ii) an age sequence down to 10^6 yr at constant $[Z/Z_O]_{MAX}$ (see Tables 4 and 5). Typically we test 5 paths which reach up respectively $[Z/Z_O]_{MAX} = +0.6$; $+0.3$; 0 ; -0.5 and -1. We emphasize that the objective is not simply to determine the maximum metallicity reached up by the nucleus, but rather to determine the relative contributions of the different types of clusters along the path. In spite of the fact that it is assumed that all the chemical enrichment has taken place in the old age bin, the relative contributions of the components of differing metallicity in this bin, still tell us about the chemical evolution (e.g. Hartwick, 1976). The points along the path are taken from the grid of cluster properties which was interpolated at suitable steps in age and metallicity (BA 86b, 87b). The program selects the solutions which reproduce the galaxy W values within the error bars. Typically these error bars are windows amounting to 10% of a given galaxy W value. We recall that for 8 points (clusters) at 10% step, 19448 combinations have a sum of individual contributions totalling 100%. The result consists of 5-20 solutions which form a highly degenerate family in the sense that a cluster contribution in the set of solutions in general does not vary by an amount larger than the 10% step. The ratio between the number of solutions

found with respect to the total number of tested combinations in the 5 paths provides an estimate of the uniqueness of the result. We find that a typical family of solutions corresponds to 1 part among 10 000 possibilities.

A second phase consists of exploring at a 5% step, a restricted space of combinations centred on the family of solutions found during the first phase. This time we use a larger number of points (clusters) in the grid path and we obtain a larger number of degenerate solutions. This allows to make statistics on the individual cluster contributions. Thus a small star cluster contribution of 1% in tables 4 and 5 means that on average one solution presents a 5% contribution and in four others it results null. In the second phase the solutions remain essentially the same, but the finer star cluster step then employed quite often provides improvements in the sense of an astrophysically more plausible solution such as more smoothly increasing contributions towards high metallicities in the old age bin.

Another way of estimating the uniqueness of the solution and the relevance of the small number contributions in tables 4 and 5 is to compare the outcome for groups with similar input spectra and to analyze the path obtained and the corresponding contributions of the three main components :(i) old metal rich ; (ii) old metal poor and (iii) young component. We conclude that the relevance of differences in synthesis results between e.g. E5 and E2 are marginal, whereas e.g. between E6 and E3 are significant. In fact for part of the E groups the family of solutions is distributed between two metallicity paths and we have adopted the one where other E groups with similar luminosity occured. Thus E5 was placed in a path reaching the same metallicity as E1, and E6 was matched to E2 in order to compare the resulting models assuming equal upper metallicity. On the other hand differences between non-neighbouring groups like e.g. E1 and E3 are fully significant. We also conclude that the

contributions become relevant at the 10% level ; however the small numbers accessed statiscally should not be disregarded. Although higher precision is always desirable, we do not think it will considerably improve the situation. Rather, it is the addition of information in other spectral regions like the near-ultraviolet that will help to constrain more the models. In the present work if only the visible range were available not much information would have been extracted from the data because we have verified that the near-infrared CaII lines have been fundamental for separating the competing contributions from old metal poor and young components.

It is important to note that no constraints are imposed on the continuum distribution. Instead the resulting continuum when compared to that of its respective real galaxy group is used to determine the nuclear reddening.

IV - RESULTS AND DISCUSSION

The mean observed W values for each galaxy group are given in Table 3 together with those for the computed templates. A set of observed and calculated continuum points are also shown, from which we derived a nuclear reddening $E(B-V) \simeq 0.04$ affecting most groups. We emphasize that the W computations straightfowardly give this kind of solution for the continuum distribution. The fact that we obtain neither solutions with an awkward continuum distribution nor solutions demanding a negative reddening correction is evidence that the library of clusters and the spectral range spanned by our observations have considerably constrained the synthesis problem. We interpret the resulting $E(B-V) \simeq 0.04$ as a global extinction present in the bulge of many galaxies. A doubt could remain whether this extinction arose from an underestimation of the reddening in our Galaxy, since

we have used foreground corrections according to Sandage and Tammann (1981), who predict very low Galactic reddening. However Sparks et al. (1987) find independent evidence favouring this low reddening model, using Balmer-line flux ratios in HII galaxies. We have also compared the cosec law values adopted in this paper with the values from Burstein and Heiles (1984), which are based on HI column densities and galaxy counts. Nearly 75% of the present sample are high Galactic latitude galaxies and both methods predict $E(B-V) < 0.04$ with essentially no zero-point systematic difference. For the rest of the sample Burstein and Heiles' method predicts on average slightly stronger reddening values. Thus in the groups of Table 1 a large systematic difference arising from foreground reddening corrections is not probable. Consequently we conclude that our excess of reddening $E(B-V) \simeq 0.04$ arises indeed from a small amount of dust present in the interstellar medium of central regions of all galaxies, even in the absence of obvious evidence of recent star formation. We also call attention to the fact that we have not applied internal reddening corrections to our library of star clusters. Thus the computations make use of blue cluster and HII region continua affected by the extinctions which are inherent to star forming regions. This procedure is justified because in the case of a galaxy nucleus with regions of recent star formation, the associated dust will certainly be localized within these regions, not necessarily affecting much the surrounding older populations.

We present in Tables 4 and 5, respectively for the E/SO and spiral groups, the resulting percentage contributions at $\lambda = 5870\AA$ of the grid points (clusters) of different ages and metallicities. It can be seen that the present method is more than a simple population synthesis, providing for the first time a direct estimate of the chemical evolution of these nuclei. The fact that solutions exist for at least one of the paths in Section III supports

the validity of the assumption that for all groups the chemical enrichment has taken place very early. We can definetely exclude paths in the $[Z/Z_O]$ vs age diagram linking a metal poor population directly to a metal rich one younger than 1 Gyr, because these two types of population are too blue, and even our bluest nuclei demand at least some contribution from a red population. We cannot exclude however the possibility that in some groups a metallicity increase of 0.5 has occurred in between the most metal rich globular-like population and that at 5 Gyr. Some enrichment is also possible for ages smaller than 1 Gyr, but this effect would be very hard to detect from the stellar population only, because the integrated spectrum becomes little sensitive to metallicity, particularly for $\lambda < 6000\AA$, owing to the dilution effects of blue stars. For some groups in Tables 4 and 5, the maximum metallicity is certainly intermediate between two $[Z/Z_O]$ values in the grid, because the family of solutions is distributed in two different paths. Thus groups E2 and S2 have possibly reached $[Z/Z_O] = 0.4$, groups E3 and S4 $[Z/Z_O] = 0.1$ and group E4 $[Z/Z_O] = -0.3$. A detailed comparison of the nuclear flux contributions at $5870\AA$ (Tables 4 and 5) with chemical evolution models would require transforming them into mass contributions, as well as taking into account slit projection effects which integrate along the line of sight outer metal poor shells. In the present paper we only point out that the computations indicate a dispersion in metallicity for the observed nuclei (Tables 4 and 5).

We illustrate in Figures 2 to 16, for each galaxy group, the real mean galaxy spectrum corrected for the nuclear reddening derived in Table 3 as well as the template galaxy with its decomposition in terms of cluster contributions. We also give the residual spectrum (galaxy - template) which brings forth the galaxy emission lines as well. Figures 2 to 16 allow to compare the average emission lines in normal galaxies with the respective underlying

population. Most of the galaxies in our sample have very weak or otherwise undetected emission lines. Thus, the mean emission line spectrum for each group corresponds to a phenomenon on a smaller scale than that occuring in typical LINERS (e.g. Keel, 1983). A detailed analysis of the spectrum for each group as well as that of individual strong LINERS, will be presented in a forthcoming paper. In the present work we have excluded 10 galaxies from our initial sample of 164 objects (BA87a). These are two HII region nuclei for which the absorption line population is essentially absent and 8 Seyfert or Seyfert-like objects for which a non-thermal continuum contribution is certainly important. For modelling the groups in Table 1 a featureless HII region continuum was considered which was derived from the mean of several extragalactic HII region observations (BA 86a, 87a, 87b). In the computations this component acts only as a dilution agent of metallic features. In the particular case of groups with LINER characteristics this contribution results null and we do not think that an additional non-thermal continuum is detectable, unless it is much steeper than an HII region continuum. This should be further checked with spectra in the near-ultraviolet range.

The star cluster groups used in the decomposition of Figures 2 to 16 are averages of spectra from BA 86a and BA 87b. The mean metallicities of the five globular cluster groups are $[Z/Z_\odot] = -1.9, -1.5, -1.0, -0.4$ and $+0.05$. The latter group consists of the strong-lined inner bulge globular clusters (IBGC), NGC 6440, 6528 and 6553. Note that we have used $E(B-V) = 1.25$ for NGC 6440 , the value adopted in BA 86a being slightly underestimated. For the intermediate and young age groups we have used averages of Galactic disc and LMC clusters, for the sake of a better S/N. This is a reasonable choice because metallicity effects on an integrated spectrum become increasingly smaller towards younger ages. Nevertheless we have excluded the SMC clusters from

these means.

We emphasize that Figures 2 to 16 are simply a visualization of the results, using the nearest available clusters, whilst the contributions in Tables 4 and 5 were computed as described in Section III, using a detailed grid of cluster properties at suitable steps in age and metallicity. This grid contains a straightforward extrapolation of the cluster properties to $[Z/Z_\odot] = 0.6$ (BA 86b, BA 87b). Particularly, the E1 galaxy group computations have required the use of grid points at $[Z/Z_\odot] = +0.6$. For its visualization in Figure 2b we have replaced the 66% contribution of the super metal-rich globular cluster (SMRGC) at $[Z/Z_\odot] = 0.6$ by the observed IBGC group. The strongest residuals in Figure 2c correspond to the Swan bands with heads at 4737Å and 5165Å. The latter region also contains MgH, but the fact that the (1,0)C_2 4737Å head is clearly identified, implies that a non-negligible amount of absorption from 5000 to 5165Å is due to the stronger (0,0) C_2 head. Indeed, synthetic spectra of stellar types which are expected to dominate the flux in this spectral range predict in many cases C_2 contributions which are stronger than those of MgH (Barbuy, 1987). The remaining features cancel out quite well, particularly the near-infrared TiO bands. Thus C_2 is very sensitive to an increase in the global metal content from solar to $[Z/Z_\odot] = +0.6$. This strong metallic dependence might be associated with the diatomic nature of the molecule. The C_2 residuals decrease for the galaxy groups which reach $[Z/Z_\odot] = +0.3$ or solar metallicity (e.g. Figures 3 and 4). Carbon stars do not seem to be responsible for the C_2 residuals, because these stars are very weak in the blue. A suitable number of such stars to explain the C_2 residuals would produce far too much flux in the near-infrared range.

In the strong-lined E and SO galaxy nuclei significant NaID residuals also remain. These residuals are possibly associated with an interstellar gas

component (BA 86c). The existence of gas, at least in ionized form, is indicated by the emission lines (e.g. Figure 2). In addition, dust is detected on CCD images for ~ 25% of elliptical galaxies (Sparks et al. 1985). This dust could also be responsible for the nuclear reddening $E(B-V) \simeq 0.04$ derived in the present synthesis (Table 3). In the case of the spiral galaxies, NaID residuals also show up. But then, they arise at least in part from gas in the disc, because the sample contains many very inclined spiral galaxies (BA 86c).

The spectrum of a SMRGC at $[Z/Z_\odot] = +0.6$ can be empirically derived by subtracting from the galaxy group E1, all other cluster contributions (Table 4a), as well as the emission line residuals (Figure 2). This predicted spectrum is compared in Figure 17 to the observed group IBGC and to the one at $[Z/Z_\odot] = -0.4$. We recall that the object with weakest lines in the latter group is NGC 104(47TUC). Thus, this Figure shows that the present synthesis was made possible because we have observed the IBGC NGC 6440, 6528 and 6553, which have metallic feature almost similar to those in giant galaxies, while star clusters usually called metal-rich in the literature, like 47TUC, NGC 6637(M69), NGC 6838(M71) and NGC 6356, would clearly not be suitable. The predicted SMRGC at $[Z/Z_\odot] = +0.6$ will be important for comparisons with synthetic spectra or with clusters in the very center of M31. It could also be injected in spectral synthesis models. Indeed its use in other galaxy groups such as S1, which also requires grid points at $[Z/Z_\odot] = +0.6$, would obviously eliminate the C_2 residuals.

The present synthesis method relies on the assumption that the IMF within a galaxy nucleus can be reproduced from a combination of the IMF within individual star clusters. There are several sources of uncertainty, such as possible dependences of the IMF on the metallicity and on the kinematics of the initial gas cloud, as well as changes in the luminosity function of the

resulting stellar system, as a consequence of dynamical evolution. However, the fact that we obtain satisfactory synthesis results favours the validity of our assumption. Indeed the shape of the IMF in the high mass range, taken over scales $\geq$ 1 Kpc appears to be universal, with no compelling evidence for any systematic slope variations depending on metallicity, galactocentric distance or galaxy morphology (Scalo, 1986). On the other hand there is evidence that in its low-mass end, the IMF presents a trend with metallicity, as indicated by the main sequence luminosity function of globular clusters from CCD observations (Mc Clure et al. 1986). This dependence is implicitly taken into account in our synthesis, since we use real clusters spanning a wide range of metallicities. Another important question is a possible spatial dependence of the IMF, arising from the initial physical conditions in central regions of galaxies, such as the gas kinematics and a large gas density in a strong gravitational potential. Even star formation in such an environment has possibly been taken into account in our synthesis, because, according to the computations, the dominant type of population in most nuclei, resembles that of the very metal-rich globular clusters NGC 6440, 6528 and 6553. These *are inner bulge objects* which have been formed in such extreme physical conditions. A more difficult problem to solve is the possible effect of the internal dynamical relaxation of star clusters with the subsequent evaporation of low mass stars by tidal effects. However, the main sequence luminosity functions at least in the observed intervals, indicate that the loss of low mass stars occurs only in small clusters (Mc Clure et al. 1986). This effect is minimized in our sample because we have observed the richest clusters in the Galaxy and Magellanic Clouds (BA 86a). The dynamical evolution of galaxy nuclei would be an additional complication. Nevertheless, the satisfactory synthesis results obtained with our method which does not make an explicit use of the IMF, suggest

that in past stellar synthesis, the importance of the slope of the IMF has been, perhaps, overestimated with respect to more interesting parameters like age and metallicity.

Finally we emphasize that the present synthesis method is little dependent on the adopted age and metallicity calibrations for the star clusters. It rather relies upon the properties directly observed in the cluster spectra. Thus, if revisions of the cluster ages and metallicities eventually occur in the future, the proportions of different types of clusters derived in the synthesis will not be affected, only their assigned age and metallicity would have to be modified. It should be stressed that there is still some uncertainty in the high metallicity end of the calibration and that metal abundance determinations of individual stars in the very strong-lined globular clusters NGC 6440, 6528 and 6553 are of great interest.

V - COMMENTS ON THE SYNTHESIS FOR EACH GROUP

Groups E1 to E4 follow the metallicity vs luminosity relationship (Section II). The results in Tables 4a to 4d together with Figure 1 indicate that the last generation of stars has reached $[Z/Z_\odot] \simeq +0.6$ at $M_B = -22$ to $[Z/Z_\odot] = -0.3$ or -0.5 at $M_B \simeq -18$. The bulk of the population is older than 10 Gyr.

No age has been assigned to the last column of the grids in Tables 4 and 5 ; we simply call it GC (globular cluster) because the properties of the integrated spectra remain essentially constant for $t \geq 10$ Gyr. However the cluster properties around 5 Gyr are significantly different (Bica, Alloin 86b). The present computations indicate that for the E1 to E4 groups this intermediate age population amounts to ~ 10% in the optical spectrum (Figures

2 to 5). No significant contributions from young populations ($T \leq 5 \times 10^8$ yr) are detected from the optical data only. Old metal-poor contributions are present even in the strong-lined E1 group ; then the lower than solar metallicity population amounts to 10% in the optical flux (Figure 2). For the group E3 the $[Z/Z_\odot] < 0$ population amounts to 30%. Finally, for the group E4, the whole population is metal-poor.

An extension of the present method to the ultraviolet range, has demonstrated that the UV rising branch in giant elliptical galaxies arises from on-going star formation at a small rate rather than from metal poor populations (Bica and Alloin, 1987d). The contribution of this very young component has a minor effect in the optical, where at $\lambda = 5870$Å, it is less than 2%.

The group E5 contains two types of nuclei (BA87c) : firstly, more distant galaxies which may differ from the strong-lined E1 galaxies due to an aperture effect bringing a larger contribution from metal-poor components outside the nucleus ; secondly, in galaxies for which the slit corresponds to the same volume as that observed for E1, the spectral difference with respect to E1 could arise from an age effect. However the differences between the two E5 subgroups are only marginal, so it is their mean which we have synthesized. The results suggest a slight enhancement of the intermediate age and of the metal-poor components with respect to those in the E1 group (Table 4e, Figure 6).

Groups E6 and E7 are less constrained in terms of computations. A significant contribution from intermediate age populations is required, particularly for the E7 group (Table 4g, Figure 8) ; but some metal-poor population excess shows up too, with respect to the groups E1 and E2. Basically two mechanisms are possible : either a major star formation event which has

evolved into an intermediate age population or a merging with a metal-poor galaxy such as those in group E4, or both. In order to clarify this point, high S/N observations of individual galaxies in these groups are required, together with the extension of the present method to the near-ultraviolet. However the presence of an intermediate age population in group E7 is conclusive and further evidence is given by the empirical synthesis in BA87a. There are also difficulties in the visualisation of the results because our intermediate age groups, which are made of Galactic disc and LMC clusters are weak-lined with respect to the expected appearance of SMR intermediate age populations in giant E/SO galaxies.

Group E8 which corresponds to the particular case of the low luminosity SO galaxy NGC5102, shows a very strong age effect (Table 4h, Figure 9). There are two methods to compute such strong age effects : i) using clusters of various ages and metallicities, as described in section III and ii) computing the excess population with respect to an underlying red galaxy, which is included together with intermediate and young age clusters in the model. The latter method relies on the assumption that a star burst has occurred indeed. For NGC 5102 both methods lead to the same result. The computations also indicate that the metallicity in NGC 5102 has only reached a sub-solar level, in agreement with its low luminosity. This case represents a major star forming event on top of an underlying population like in group E4. The bulk of the star burst was formed between the ages 3 to 5 x 10^8 yr. The fact that this burst is rather old is also suggested by a small HII region continuum contribution and by the residual weak emission lines (Figures 9b and 9c).

The reddest spiral spectra, in groups S1 to S4, are very similar to the red E groups. Groups S1 to S4 migrate diagonally in the morphological type vs luminosity class diagram (Table 2). The computations indicate that the maximum

metallicity has reached values a factor 4 solar (S1) to solar (S4). Their distribution in Table 2 thus implies that the maximum metallicity is related to the bulge luminosity. Note that the most metal poor groups S3 and S4 are strong-lined, very different from metal poor globular clusters (BA 87a). Groups S1 to S3 do not require a significant contribution from young components, but the small bulges in group S4 are systematically coupled with a small amount of recent star formation (Table 5d and Figure 13). This is certainly due to the availability of gas but also to the fact that even a weak star forming event will show up easily with respect to the older population in the small nuclei of low luminosity Sc galaxies.

In the S4 group, all galaxies have their Hβ absorption line contaminated by emission. However, some of them have a pure absorption at Hγ and Hδ. So we have used only the latter Balmer lines in the computations. In the groups S5 to S7, Balmer lines down to Hδ are emission contaminated, thus the computations rely on metallic features only. The fact that we find a unique family of solutions confirms the powerful use of metallic features, when considered over a wide spectral range, as an age discriminator. An additional test is provided by comparing the computations for the S4 group, with and without Hγ and Hδ being taken into account, the solution remains the same.

From Figures 13 to 16, it is possible to estimate directly the relative contribution of younger components at any wavelength. For the bluest group, S7, the population younger than 3 x 10^8 yr represents 87% of the flux at 4000Å.and 57% at 9000Å. This will be an important constraint on the contribution of red supergiants with respect to other red stars in the synthesis using stellar libraries.

For the group S6 no spectrum was taken for $\lambda > 8000$Å. However from 6000 to 8000Å, the spectrum in group S6 perfectly matches that observed for group

S5. Thus we have used in the computations for group S6, the values of W(CaII)8542, 8662Å obtained from the spectrum representative of group S5. Indeed group S6 seems to differ from group S5 only by the presence of a more important young age component (Figures 14 and 15).

As for group E8, the S5 to S7 groups have been computed with and without an input underlying red galaxy, and the results are essentially the same. The underlying red populations from groups S3 and S4 provide the best results, as expected from the distribution observed for groups S5 to S7 in Table 2. This indicates that the blue spirals have reached at least the solar metallicity.

The HII region continuum contribution increases steadily from group S4 to group S7, in agreement with the strengthening of the emission lines. Indeed, groups S5 to S7 include many nuclei which have been spatially resolved into HII regions such as NGC 2903, 2997, 3351, 4303, 4321, 5236, 5248 and 7552 (Sersic and Pastoriza, 1965 ; Pastoriza, 1975). The contributions of the nuclear HII regions in Table 5 should be regarded as preliminary, because a precise determination requires observations in the near-ultraviolet , where it is more conspicuous. However, we can discuss their average properties, using group S7, where the HII contribution is the strongest. Adding the featureless HII region continuum (Figure 16b) with the residuals containing the emission lines (Figure 16c), we derive W(Hβ) = 52Å, I([OIII] (4959 + 5007)) / I(Hβ) = 0.6 and I(Hα) / I(Hβ) = 4.2. It is known that W(Hβ) and the ratio ([OIII]) / I(Hβ) are good age indicators (Dottori and Bica, 1981 ; Copetti et al. 1986). The observed values in our case imply that the average age of the nuclear HII regions is 4.5 − 6 10^6 yr. The observed ratio I(Hα) / I(Hβ) suggests an internal reddening E(B-V) = 0.35. As already pointed out, this high reddening is inherent to star forming regions and does not necessarily apply to the surrounding older populations.

A quantitative comparison of the present results with previous syntheses is difficult because we derive star cluster contributions of various ages and metallicities while previous results were expressed in terms of stellar group contributions of various spectral types and luminosity classes. However, it is gratifying that, at least qualitatively, both approaches agree well in most of their predictions. The synthesis by O'Connell (1976) indicates that in giant elliptical galaxies the bulk of the stars were formed 8 to 11 Gyr ago, with some residual star formation until 4 Gyr ago. This is in fair agreement with our results for this galaxy group. Pickles (1985) derived turnoff ages of 6 to 10 Gyr for elliptical galaxies of all luminosities. We also find evidence that the E/S0 galaxies in the whole luminosity range have formed stars to look back times of 5 Gyr, but the present method indicates in addition that the rate of star formation must have decreased by a factor 10 sometime between 10 and 5 Gyr. According to the present study, the maximum metallicity reached at a given E/S0 luminosity is in good agreement with Pickles' results for the Fornax elliptical galaxies, considering that he derives mean metallicities. A dispersion of metallicity, as we have detected in E/S0 nuclei, is also predicted by evolutionary synthesis methods (Arimoto and Yoshü, 1987), at least for the total galaxy. The presence of a metal poor component in the nucleus is expected from simple models of galactic chemical enrichment and is also detected by the spectral index method of Rose (1985). However, as pointed out in Section IV, a detailed comparison of the metal poor contributions in Table 4 with chemical evolution models requires model predictions for the metallicity distribution in galaxy shells, as well as the consideration of slit projection effects.

Our detection of different amounts of younger age components for the spiral groups is in agreement with the synthesis results from Turnrose (1976).

Also his internal reddening estimates for spiral galaxies, in the range E(B-V) 0.10 to 0.40, are basically compatible with ours. The way we decompose the internal reddening in terms of (i) inclination effects, (ii) global nuclear and bulge absorption and (iii) absorption inherent to star forming regions, has however given more insight into this problem.

We conclude that synthesis methods based on stellar libraries and the present method are complementary. Both techniques should be further developed and applied to the study of particular objects. Of fundamental importance will also be the application of stellar library methods to the integrated spectra of star clusters, particularly with the help of synthetic spectra for metallicity entries which are difficult to observe.

VI - CONCLUDING REMARKS

A new population synthesis method has been developed which makes use exclusively of a library of star clusters. The method has allowed to date successive stellar generations and to determine the chemical enrichment in E/SO and spiral galaxies. It has provided a direct estimate of the chemical evolution in these nuclei.

The method will have important applications for distant galaxies. A larger volume can be observed for distant early type galaxies, thus giving information on the global chemical evolution. Also it will be interesting to explore the disc contributions in spirals. For very large redshift galaxies, the method can be used to study galaxies in early evolutionary stages, which are becoming accessible with modern detectors and large telescopes.

An extension to the ultraviolet range will help to determine more precisely the contributions from hot populations. A preliminary study in this

direction is presented in Bica and Alloin (1987d).

Finally, the grid of star cluster properties can be refined with a larger number of cluster observations, particularly for young and intermediate age objects in the Magellanic Clouds, Galactic disc and in M31. Also of great help will be the use of synthetic spectra.

The present method is complementary to those using a library of stellar spectra. Further development of both techniques will certainly clarify many aspects in the interpretation of integrated spectra.

ACKNOWLEDGMENTS

It is a pleasure to thank my thesis supervisor Dr. D. ALLOIN for many stimulating discussions and invaluable advice. I am also thankful to Dr. B. Pagel and Dr. D. Burstein for interesting remarks. I am gratefully indebted to the ESO staff at La Silla and Garching and to the Paris / Meudon Observatory staff, especially at the Computer Centre the group who developed the command system eVe. I thank the Brazilian Institution CNPq for a fellowship.

References

Arimoto, N., Yoshii, Y., 1987, Astron. Astrophys. 173, 23.

Barbuy, B., 1987, in preparation.

Bica, E., Alloin, D., 1986a, Astron. Astrophys., 162, 21.

Bica, E., Alloin, D., 1986b, Astron. Astrophys. Suppl. Ser., 66,171.

Bica, E., Alloin, D., 1986c, Astron. Astrophys., 166, 83.

Bica, E., Alloin, D., 1987a, Astron. Astrophys. Suppl. Ser., 70, 281.

Bica, E., Alloin, D., 1987b, Astron. Astrophys., in press.

Bica, E., Alloin, D., 1987c, Astron. Astrophys., 181, 270.

Bica, E., Alloin, D., 1987d, subm. to Astron. Astrophys.

Burstein, D., Heiles, C., 1984, Astrophys. J. Suppl. Ser., 54, 33.

Copetti, M., Pastoriza, M., Dottori, H., 1986, Astron. Astrophys., 156, 111.

Dottori, H., Bica, E., 1981, Astron. Astrophys., 102, 245.

Hartwick, F., 1976, Astrophys. J., 209, 418.

Humason, M., Mayall, N., Sandage, A., 1956, Astron. J., 61, 97.

Keel, W., 1983, Astrophys. J., 269, 466.

McClure, R., VandenBerg, D., Smith, G., Fahlman, G., Richer, H., Hesser, J., Harris, W., Stetson, P., Bell, R., 1986, Astrophys. J., 307, L49.

O'Connell, R., 1976, Astrophys.J., 206, 370.

Pagel, B., Edmunds, M., 1981, Ann. Rev. Astron. Astrophys., 19, 77.

Pastoriza, M., 1975, Astrophys. Space. Sci., 33, 173.

Pickles, A., 1985, Astrophys. J., 296, 340.

Rose, J., 1985, Astron.J., 90, 1927.

Sandage, A., Tammann, G., 1981, A revised Shapley-Ames Catalogue of Bright Galaxies, Carnegie Institution of Washington.

Scalo, J., 1986, in Luminous Stars and Associations in Galaxies, ed. C. de Loore et al., p. 451.

Sersic, J., Pastoriza, M., 1965, P.A.S.P., 77, 287.

Sparks, W., Wall, J., Thorne, D., Jorden, P., van Breda, I., Rudd, P., Jorgensen, H., 1985, M.N.R.A.S., 217, 87.

Sparks, W., Ellis, R., McMahon, R., Terlevich, R., Melnick, J., 1987, 225, 769.

Turnrose, B., 1976, Astrophys.J., 210, 33

Table and Figure Captions.

Table 1 : The galaxy groups.

Table 2 : The distribution of the spiral groups as a function of morphological types and absolute magnitude.

Table 3 : Observed and computed properties and determination of the nuclear reddening.

Table 4 : Percentage contributions at $\lambda = 5870\AA$: the chemical evolution for the E/SO groups..

Table 5 : Percentage contributions at $\lambda = 5870\AA$: the chemical evolution for spiral groups.

Figure 1 : Distribution of the E/SO groups in a metal indicator vs absolute magnitude diagram.

Figures 2 to 16 : (a) the observed group spectrum ; (b) the template built from cluster spectra and its decomposition into individual clusters of differing age and metallicity ; (c) residuals and galaxy emission lines. The identifications of the main lines and molecular bands are given in Figures 2 and 16, repectively for typical red and blue populations. The star cluster groups used for the decomposition in (b) are as follows. Globular clusters : G1($[Z/Z_\odot] > 0$) ; G2($[Z/Z_\odot] = -0.4$) ; G3($[Z/Z_\odot] = -1.0$) ; G4($[Z/Z_\odot] = -1.5$) ; G5($[Z/Z_\odot] = -1.9$). Intermediate age : I1 (10^9 yr) ; I2(5 10^9 yr). Young clusters : Y1(10^7 yr) ; Y2(5 10^7 yr) ; Y3(10^8 yr) ; Y4(5 10^8 yr). HII region : H.

Figure 17 : a) the predicted spectrum for a globular cluster at $[Z/Z_\odot] = +0.6$; b) and c) observed globular clusters at respectively $[Z/Z_\odot] = +0.05$ and -0.4.

Table 1

Group	Prototype	Other Galaxies
E1	NGC4472	NGC1399,NGC3557,NGC3923,NGC4406,NGC4486,NGC4552,NGC4621 NGC4649,NGC5090,NGC7144,IC1459
E2	NGC3115	NGC1339,NGC1379,NGC1387,NGC1411,NGC1537,NGC1574,NGC1596 *NGC2434,NGC3379,NGC3818,NGC3904,NGC4435,NGC4478,NGC4958 NGC7041,NGC7145
E3	NGC4033	NGC1381,NGC1427,NGC4976
E4	NGC4476	NGC3056
E5	NGC6861	NGC584,NGC1201,NGC1395,NGC1404,NGC1553,NGC1600,NGC3585 NGC4374,NGC4697,*NGC4936,*NGC5266,NGC5419,NGC6758,NGC6776 NGC7507,NGC7744,*NGC6868,IC4296,IC4329,IC4797,IC4889 IC5105
E6	NGC5061	NGC5018
E7	NGC2865	NGC4742,NGC4382
E8	NGC5102	
E9	NGC4486B	NGC1366,NGC1400,NGC4387,NGC4479
S1	NGC7049	NGC524,NGC1380,NGC1398,NGC1533,NGC4594,NGC4767,NGC7329 NGC7410
S2	NGC1350	NGC488,NGC1316,NGC1371,NGC1543,NGC1617,NGC4548,NGC4856 *NGC5101,NGC5746,IC5267
S3	NGC3521	NGC289,NGC692,NGC779,NGC1232,NGC1302,NGC1425,NGC1512 NGC2781,NGC2811,NGC3054,NGC3223,NGC3358,NGC3368,NGC3623 NGC4192,NGC4438,NGC4440,NGC4462,NGC4501,NGC4579,NGC5064 NGC5612,NGC6684,NGC6744,NGC6923,NGC6925,NGC6942,NGC7079 NGC7184
S4	NGC3887	NGC772,NGC908,NGC1353,NGC1637,*NGC2442,NGC3627,NGC4254 *NGC4981,NGC5121,NGC5156,NGC7083,NGC7205,NGC7421
S5	NGC2997	NGC3351,NGC4038,NGC4321,NGC4536,NGC5248,NGC6699,NGC6782 NGC7392
S6	NGC4303	NGC1084,NGC4039,NGC6215,IC5325
S7	NGC5236	*NGC986,NGC2903,NGC4027,NGC4535,NGC4569,NGC7552

Note to Table 1

* In addition to the previous corrections of foreground and spiral inclination reddening (RA86c,87a,87c),it was necessary to apply supplementary corrections for the following galaxies:
  - NGC2434(E(B-V)=0.11): E galaxy at low Galactic latitude. The cosec law value was certainly underestimated.
  - NGC2442(0.29): dust possibly associated with nucleus.Perhaps more inclined than suggested by the axial ratio,which is uncertain owing to assymetric arms. No reddening correction due to inclination was previously applied. Also low Galactic latitude.
  - NGC986(0.17) and NGC4981(0.17): possibly internal reddening associated with nucleus.
  - NGC5101(0.07): possibly nuclear internal reddening; strong liner in nearly face-on SBa.
  - NGC4936(0.16) and NGC6868(0.09): possibly nuclear internal reddening; strong liners in early-type galaxies.
  - NGC5266(0.15): Early-type galaxy with dust lane along the minor axis.Also low Galactic latitude.

Table 2

Spectral Group S1 :

	Sa	Sb	Sc
M<-22	1	2	1
-22<M<-21	4	-	-
M>-21	1	-	-

Spectral Group S2 :

	Sa	Sb	Sc
M<-22	1	2	-
-22<M<-21	3	1	-
M>-21	4	-	-

Spectral Group S3 :

	Sa	Sb	Sc
M<-22	1	2	3
-22<M<-21	5	8	5
M>-21	4	2	-

Spectral Group S4 :

	Sa	Sb	Sc
M<-22	-	2	1
-22<M<-21	-	2	3
M>-21	1	1	4

Spectral Group S5 :

	Sa	Sb	Sc
M<-22	-	1	1
-22<M<-21	-	-	6
M>-21	-	1	-

Spectral Group S6 :

	Sa	Sb	Sc
M<-22	-	-	-
-22<M<-21	-	-	3
M>-21	-	-	2

Spectral Group S7 :

	Sa	Sb	Sc
M<-22	-	1	-
-22<M<-21	-	1	4
M>-21	-	-	1

Table 3

GROUP	W(K) 8933	W(CN) 4200	W(G) 4301	W(HgI) 5175	W(CaII) 8542	W(CaII) 8662	H_β 4861	H_γ 4340	H_δ 4102	Cont 4020	Cont 4570	Cont 7520	Cont 8700	E(B-V) nucl.
E1	16.8	14.5	9.3	10.8	6.1	4.9	3.4	4.8	5.7	.48	.81	.99	1.02	.04
Temp.	18.7	15.0	10.3	9.2	6.4	5.7	3.8	5.1	4.8	.49	.76	.98	.99	
E2	17.2	10.9	9.2	9.5	6.2	5.3	3.6	5.1	4.9	.53	.82	1.00	1.01	.05
Temp.	17.8	13.3	9.7	8.3	5.7	5.3	3.7	5.0	5.8	.53	.78	.97	.97	
E3	15.3	7.3	8.6	7.7	6.6	5.5	3.4	3.8	2.0	.57	.85	.98	.96	.01
Temp.	14.9	9.4	8.2	6.3	5.0	4.6	3.6	4.9	4.4	.60	.81	.94	.92	
E4	13.7	3.4	6.8	6.3	5.2	4.7	ec	4.6	3.8	.61	.88	.92	.90	.05
Temp.	12.0	5.7	6.5	5.5	4.4	3.9	3.7	4.6	4.6	.65	.84	.92	.89	
E5	15.8	10.6	8.7	9.6	5.4	4.5	3.4	4.0	3.8	.50	.81	1.00	.99	.05
Temp.	17.9	14.1	9.9	8.9	6.2	5.6	3.5	5.2	5.2	.54	.79	.97	.97	
E6	14.0	7.9	8.3	7.4	5.7	5.3	4.4	4.9	3.9	.56	.86	.98	.95	.05
Temp.	15.5	10.9	8.5	7.2	5.3	4.9	4.1	5.3	5.1	.65	.84	.93	.91	
E7	12.5	6.2	6.5	7.2	5.5	5.0	4.7	4.9	5.6	.67	.95	.86	.83	.01
Temp.	13.5	9.5	7.4	6.6	5.3	4.9	4.9	6.1	6.8	.76	.91	.90	.86	
E8	6.4	0.3	2.5	2.6	4.6	3.9	ec	6.6	9.2	1.21	1.19	.79	.72	.04
Temp.	6.5	2.2	3.2	3.3	4.4	4.0	6.5	7.3	9.5	1.34	1.26	.77	.67	
S1	19.0	13.0	10.0	9.8	5.6	4.6	3.6	5.6	5.3	.47	.76	1.03	1.03	.05
Temp.	18.6	14.7	10.2	9.0	6.3	5.6	3.7	5.1	4.6	.50	.77	.98	.99	
S2	16.4	10.4	8.8	9.2	5.9	4.6	3.7	3.9	4.1	.50	.79	1.00	1.02	.05
Temp.	17.2	12.8	9.5	8.0	5.6	5.2	3.8	5.1	4.7	.55	.79	.96	.96	
S3	15.5	8.5	8.5	7.9	5.7	4.6	3.8	4.4	3.1	.56	.85	.95	.92	.02
Temp.	15.3	10.8	8.5	7.1	5.3	4.9	3.9	5.2	4.9	.61	.82	.94	.92	
S4	13.1	6.2	7.3	6.3	6.2	4.7	4.2	5.4	4.2	.59	.80	1.02	.98	.04
Temp.	13.3	9.0	7.5	6.3	5.2	4.7	4.0	5.3	5.1	.68	.86	.93	.90	
S5	6.4	4.6	5.5	6.2	4.8	5.4	ec	ec	ec	.67	.87	.98	.94	.07
Temp.	9.9	6.6	5.9	5.2	4.7	4.3	3.6	4.7	4.5	.80	.91	.91	.87	
S6	5.5	3.9	4.6	3.7	_	_	ec	ec	ec	.86	.95	.95	-	.06
Temp.	8.1	5.5	4.9	4.8	4.7	4.3	3.8	4.9	4.9	.94	.99	.89	.84	
S7	3.5	2.4	2.2	3.3	5.4	5.4	ec	ec	ec	1.34	1.27	.76	.63	.01
Temp.	4.5	3.0	2.1	3.2	4.8	4.4	5.4	6.5	7.2	1.53	1.31	.78	.68	

Note to Table 3

Table 4a

GROUP E1:

		Age(yrs)						
		RHII	E7	5E7	E8	5E8	E9	5E9	Glob.
	+0.6						3	8	66
	+0.3								9
	0								5
[Z/Z$_\odot$]	-0.5								3
	-1.0								3
	-1.5								2
	-2.0								1

Table 4b

GROUP E2:

		Age(yrs)						
		RHII	E7	5E7	E8	5E8	E9	5E9	Glob.
	+0.6								
	+0.3							11	74
	0								6
[Z/Z$_\odot$]	-0.5								4
	-1.0								3
	-1.5								1
	-2.0								1

Table 4c

GROUP E3:

		Age(yrs)						
		RHII	E7	5E7	E8	5E8	E9	5E9	Glob.
	+0.6								
	+0.3								
	0							5	64
[Z/Z$_\odot$]	-0.5								14
	-1.0								11
	-1.5								4
	-2.0								2

Table 4d

GROUP E4:

		Age(yrs)						
		RHII	E7	5E7	E8	5E8	E9	5E9	Glob.
	+0.6								
	+0.3								
	0								
[Z/Z$_\odot$]	-0.5						2	4	55
	-1.0								25
	-1.5								11
	-2.0								3

Table 4e

GROUP E5:

		Age(yrs)						
		RHII	E7	5E7	E8	5E8	E9	5E9	Glob.
	+0.6						3	14	50
	+0.3								14
	0								6
[Z/Z$_\odot$]	-0.5								4
	-1.0								4
	-1.5								3
	-2.0								2

Table 4f

GROUP E6:

		Age(yrs)						
		RHII	E7	5E7	E8	5E8	E9	5E9	Glob.
	+0.6								
	+0.3						7	17	40
	0								10
[Z/Z$_\odot$]	-0.5								9
	-1.0								7
	-1.5								6
	-2.0								4

Table 4g

GROUP E7:

		Age(yrs)						
		RHII	E7	5E7	E8	5E8	E9	5E9	Glob.
	+0.6								
	+0.3				3	5	18	5	33
	0								10
[Z/Z$_\odot$]	-0.5								8
	-1.0								7
	-1.5								6

Table 4h

GROUP E8:

		Age(yrs)						
		RHII	E7	5E7	E8	5E8	E9	5E9	Glob.
	+0.6								
	+0.3								
	0								
[Z/Z$_\odot$]	-0.5	2	7	6	5	56	2	1	11
	-1.0								6
	-1.5								5

Table 5a

GROUP S1:

[Z/Z⊙] \ Age(yrs)	RHII	E7	5E7	E8	5E8	E9	5E9	Glob.
+0.6						1	11	55
+0.3								14
0								9
-0.5								4
-1.0								3
-1.5								2
-2.0								1

Table 5b

GROUP S2:

[Z/Z⊙] \ Age(yrs)	RHII	E7	5E7	E8	5E8	E9	5E9	Glob.
+0.6								
+0.3						2	10	60
0								7
-0.5								5
-1.0								3
-1.5								2
-2.0								2

Table 5c

GROUP S3:

[Z/Z⊙] \ Age(yrs)	RHII	E7	5E7	E8	5E8	E9	5E9	Glob.
+0.6								
+0.3						6	8	51
0								9
-0.5								8
-1.0								7
-1.5								6
-2.0								5

Table 5d

GROUP S4:

[Z/Z⊙] \ Age(yrs)	RHII	E7	5E7	E8	5E8	E9	5E9	Glob.
+0.6								
+0.3								
0	1	1	1	2	1	3	9	65
-0.5								7
-1.0								5
-1.5								3
-2.0								2

Table 5e

GROUP S5:

[Z/Z⊙] \ Age(yrs)	RHII	E7	5E7	E8	5E8	E9	5E9	Glob.
+0.6								
+0.3								
0	6	2	2	2	1	2	4	51
-0.5								12
-1.0								7
-1.5								6
-2.0								5

Table 5f

GROUP S6:

[Z/Z⊙] \ Age(yrs)	RHII	E7	5E7	E8	5E8	E9	5E9	Glob.
+0.6								
+0.3								
0	9	3	5	5	2	2	4	45
-0.5								11
-1.0								6
-1.5								5
-2.0								3

Table 5g

GROUP S7:

[Z/Z⊙] \ Age(yrs)	RHII	E7	5E7	E8	5E8	E9	5E9	Glob.
+0.6								
+0.3								
0	12	10	11	32	7	2	3	17
-0.5								2
-1.0								2
-1.5								1
-2.0								1

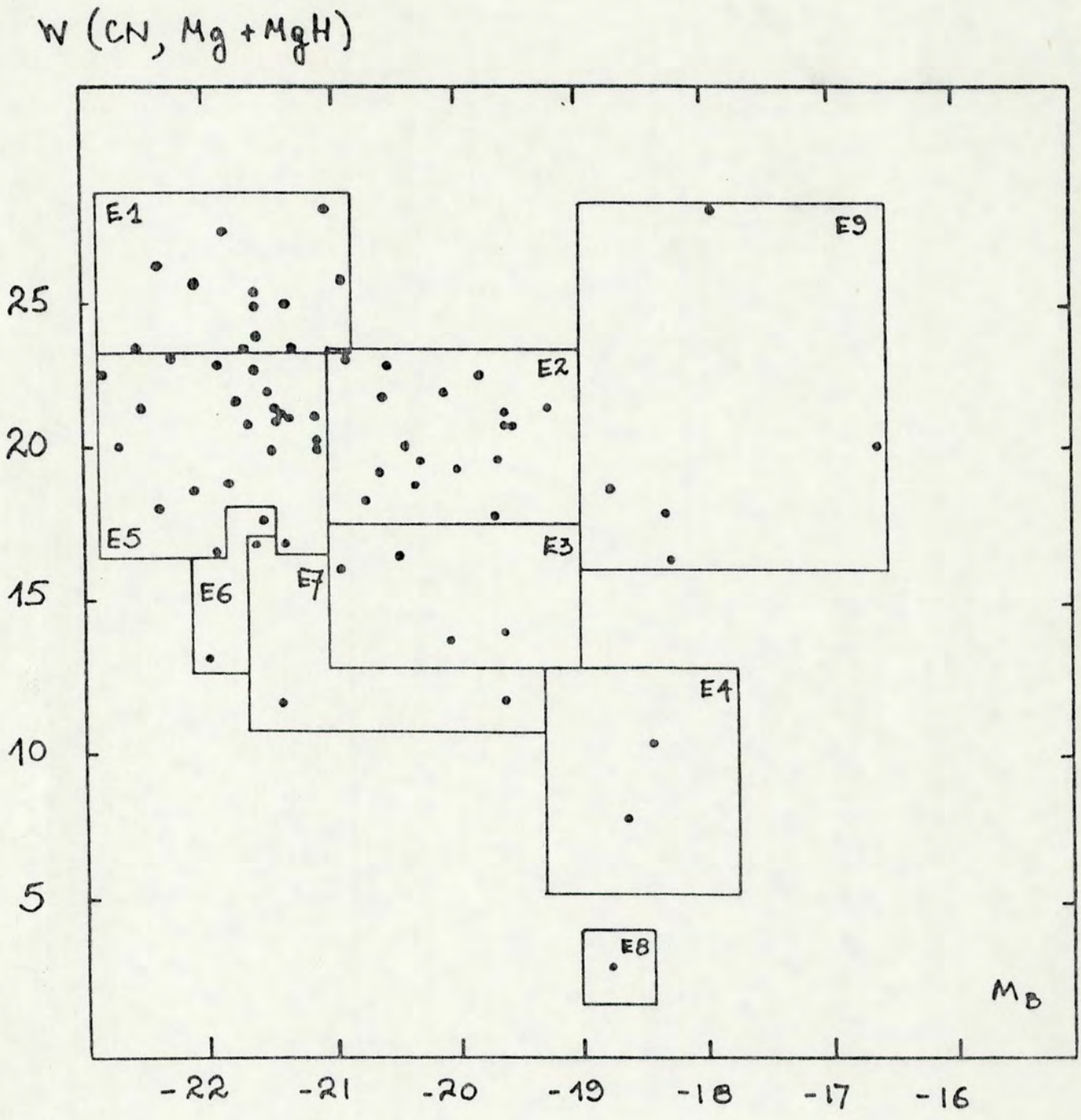
W (CN, Mg + MgH)
E1
E9
E2
E5
E3
E6
E7
E4
E8
25
20
15
10
5
-22
-21
-20
-19
-18
-17
-16
M_B

FIG.1

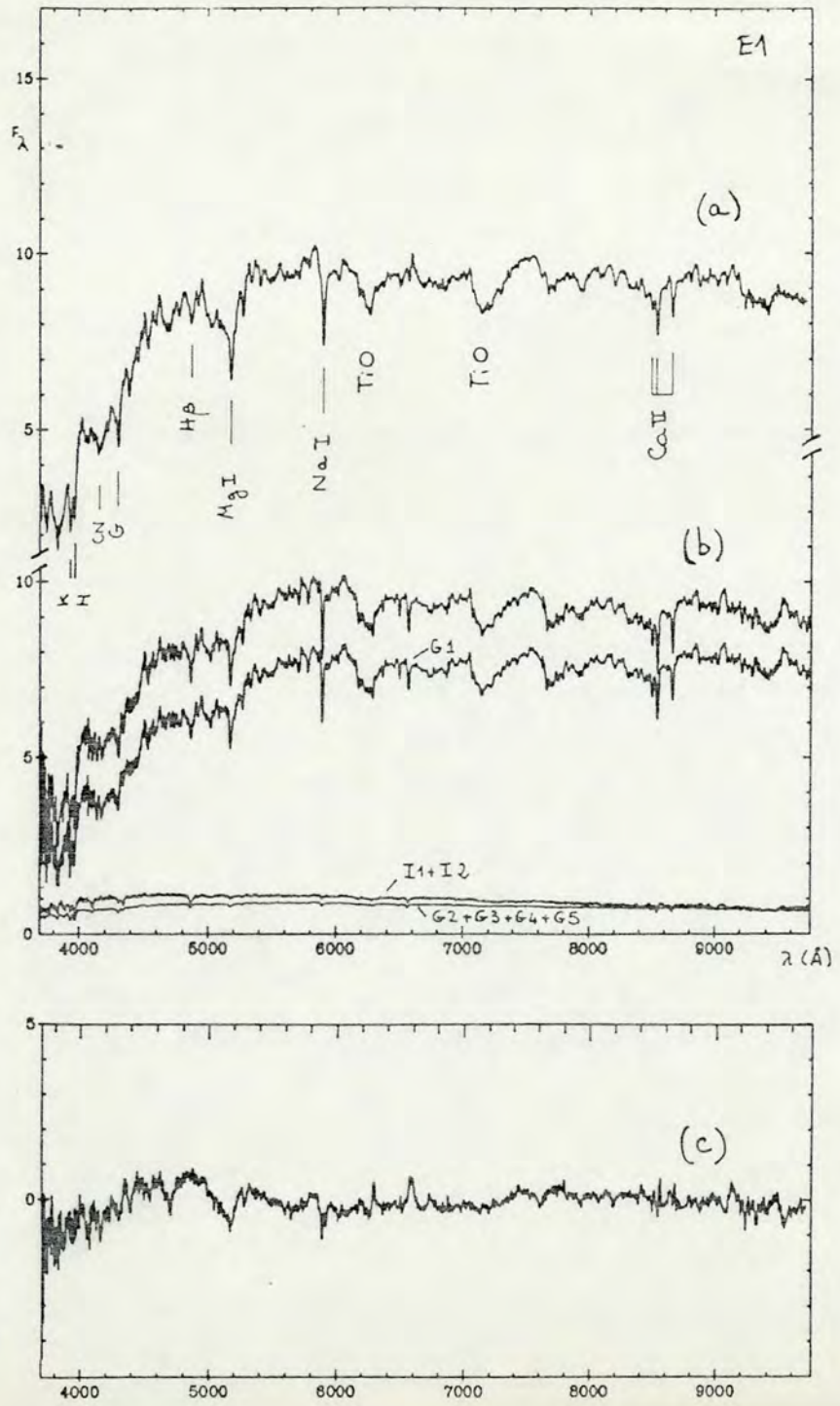
E1
(a)
(b)
(c)
F_λ
K H
3G
Hβ
MgI
NaI
TiO
TiO
CaII
G1
I1+I2
G2+G3+G4+G5
λ (Å)

FIG.2

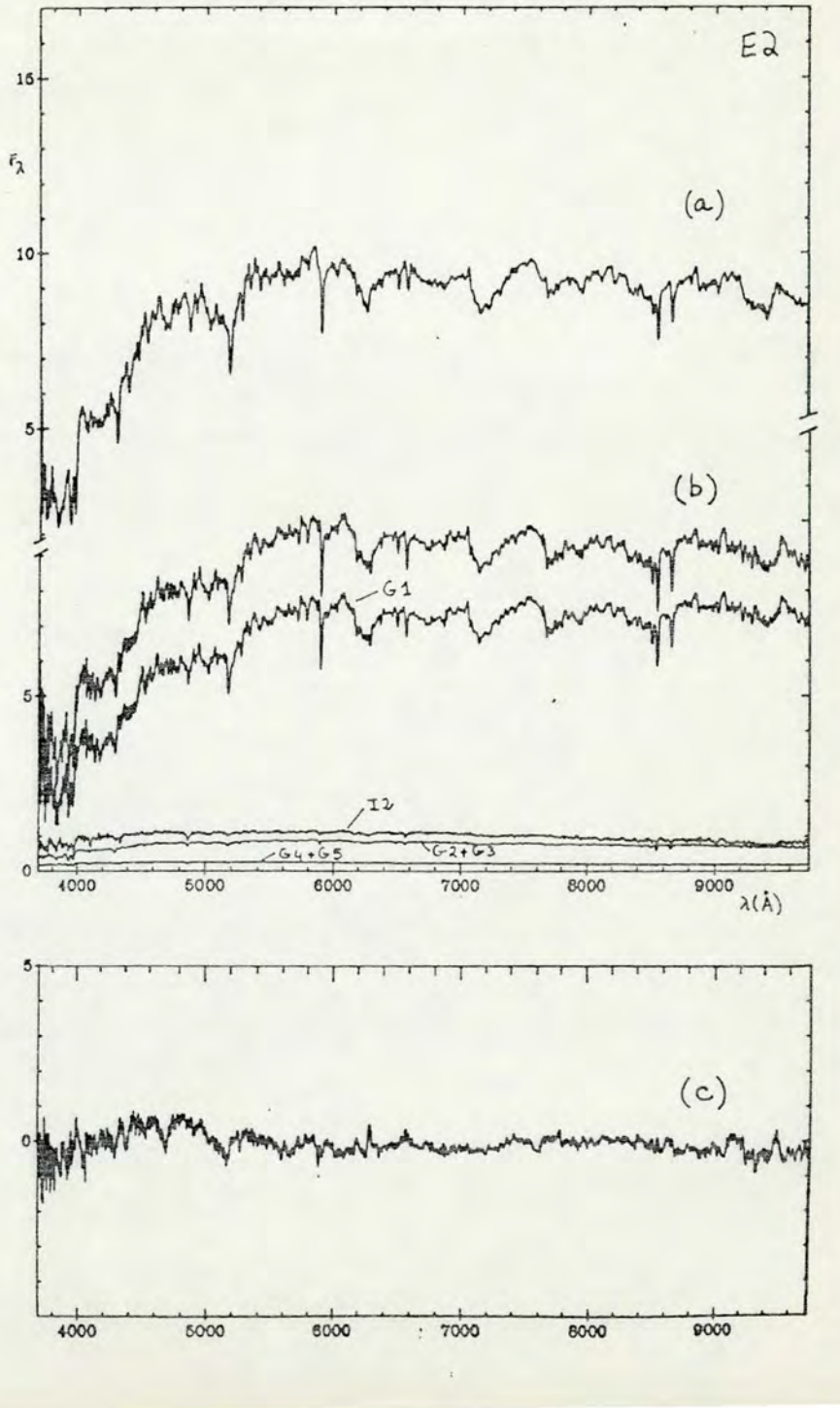
E2
(a)
(b)
(c)
F_λ
G1
I2
G4+G5
G2+G3
λ(Å)

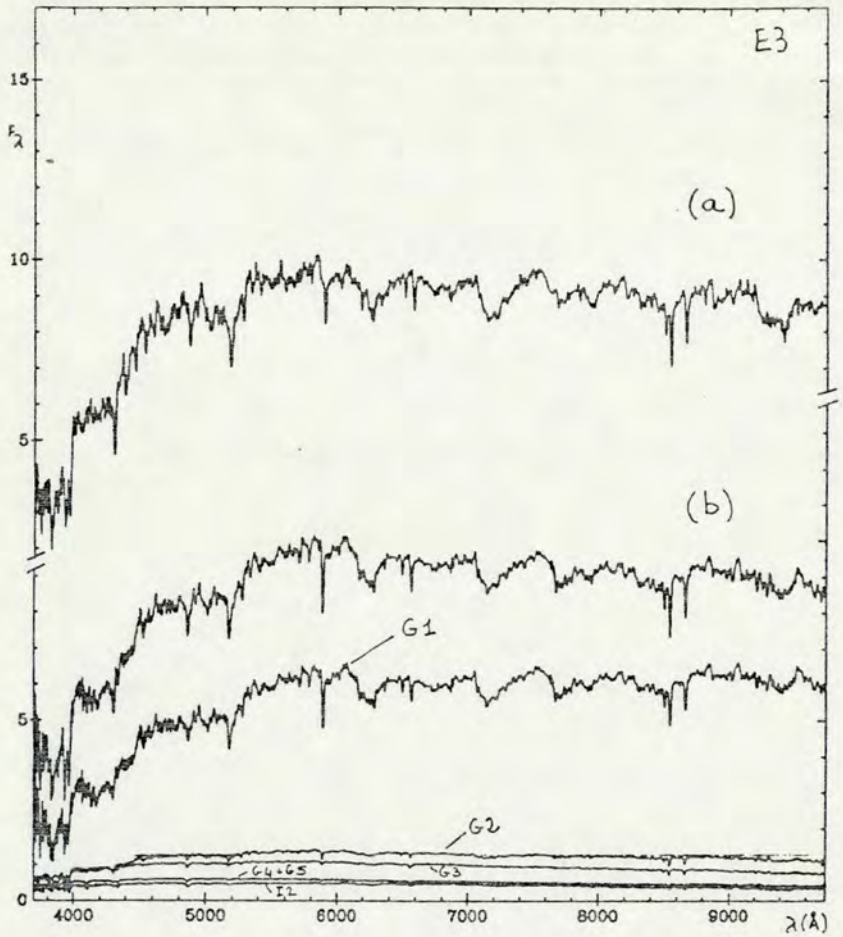
E3
(a)
(b)
G1
G2
G4+G5
G3
I2
F_λ
λ(Å)

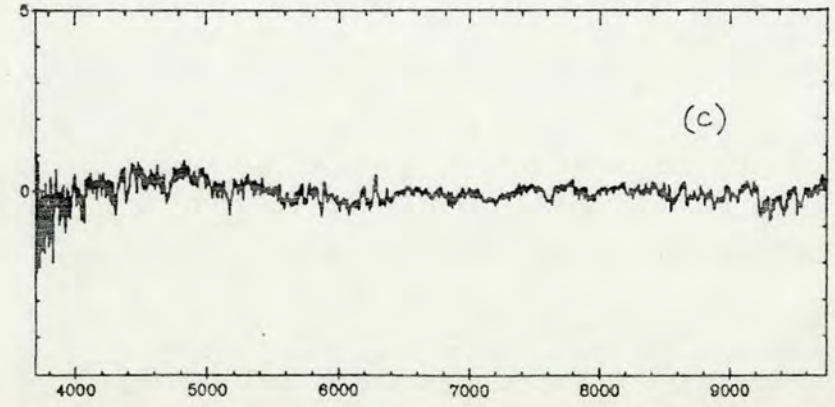
(c)

FIG.4

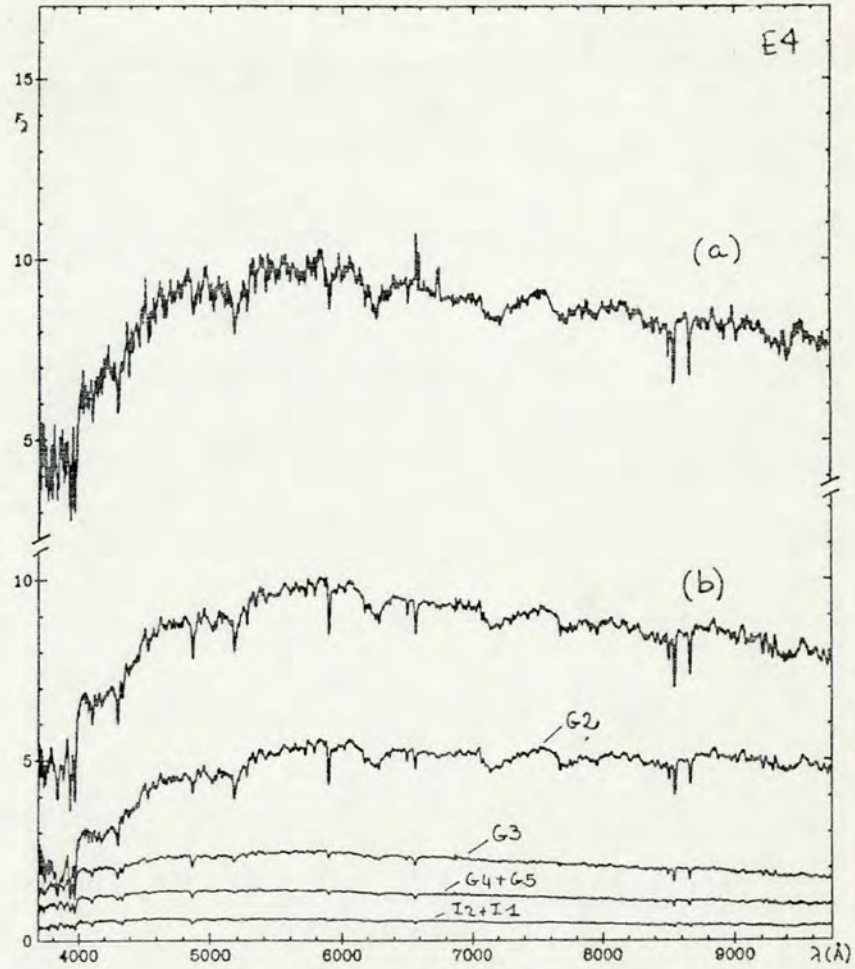
E4
(a)
(b)
G2
G3
G4+G5
I2+I1
F_λ
λ(Å)

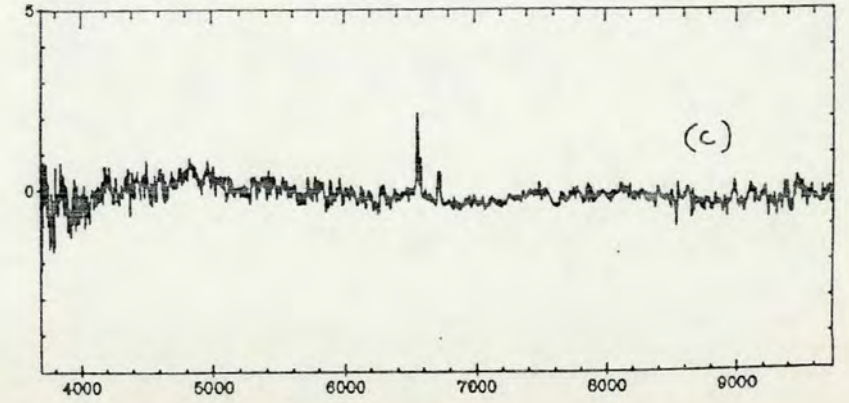
(c)

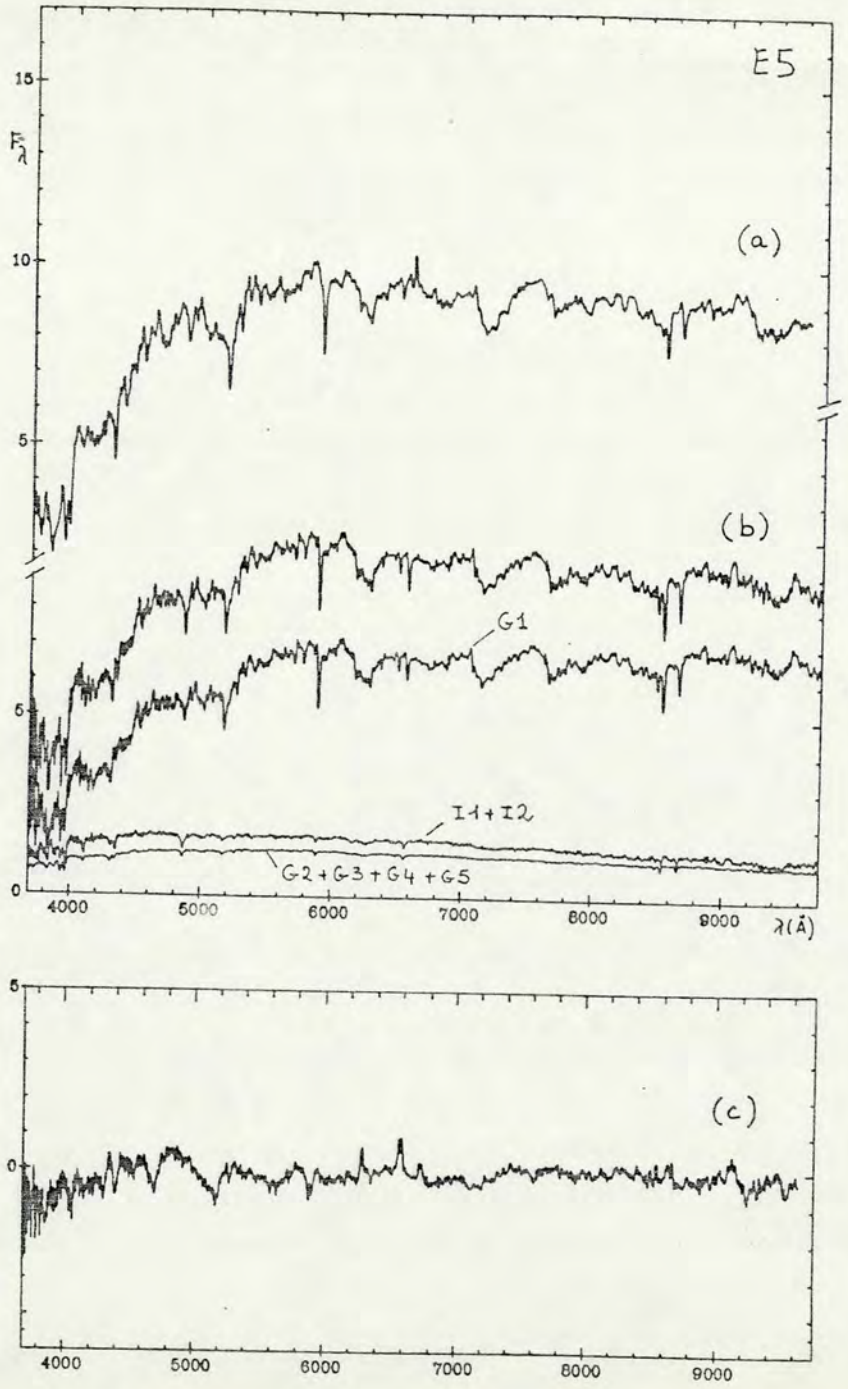

FIG.6

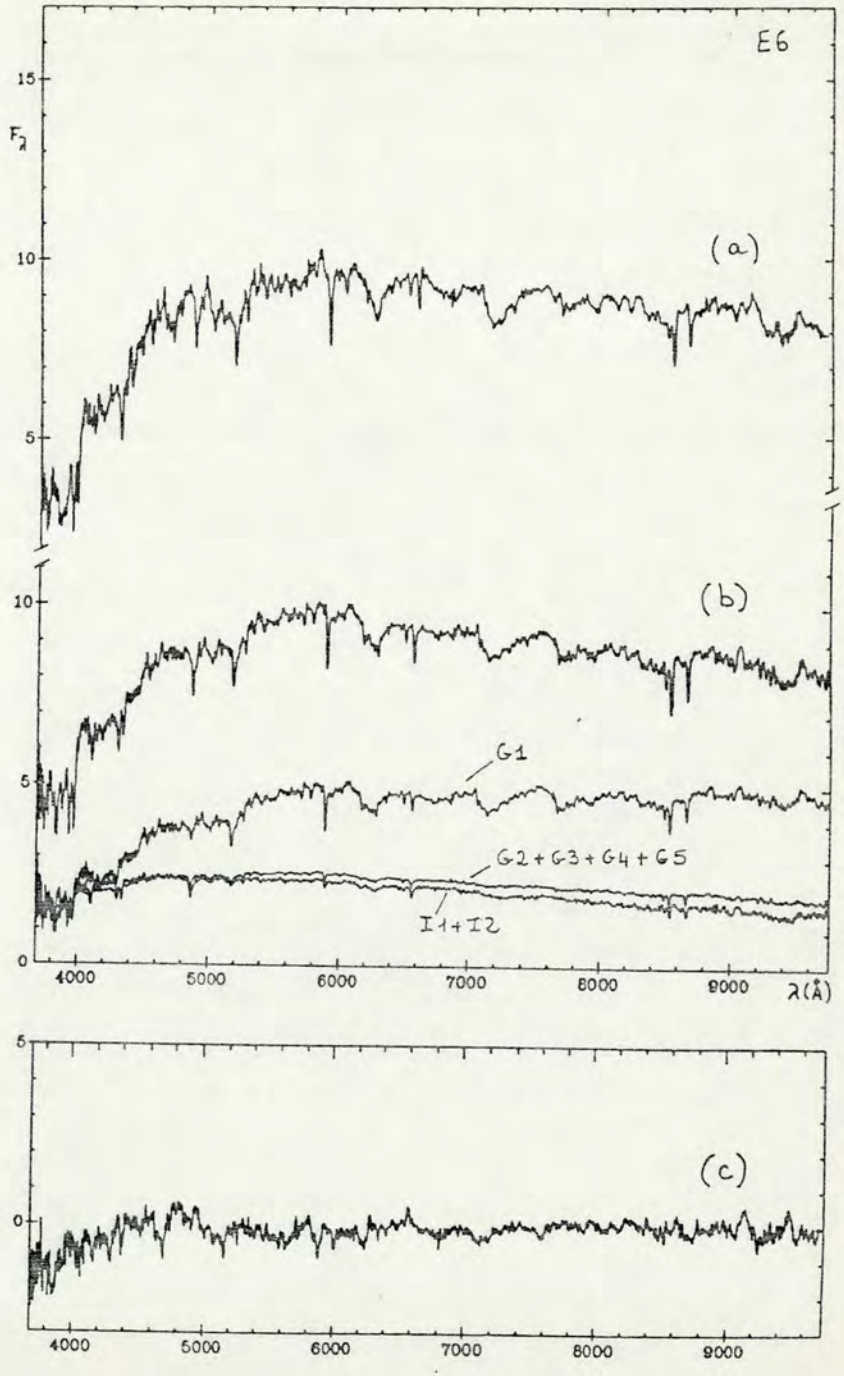

FIG.7

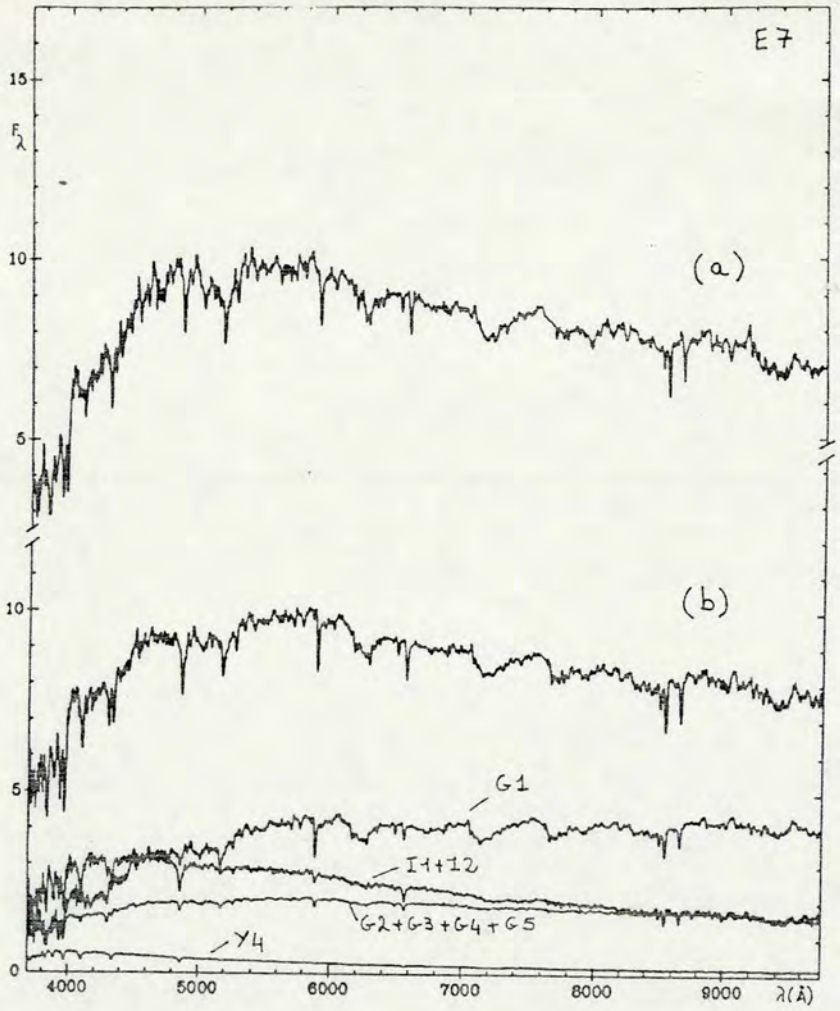
E7
15
F_λ
10
5
(a)
(b)
10
5
G1
I1+I2
G2+G3+G4+G5
Y4
0
4000
5000
6000
7000
8000
9000
λ(Å)

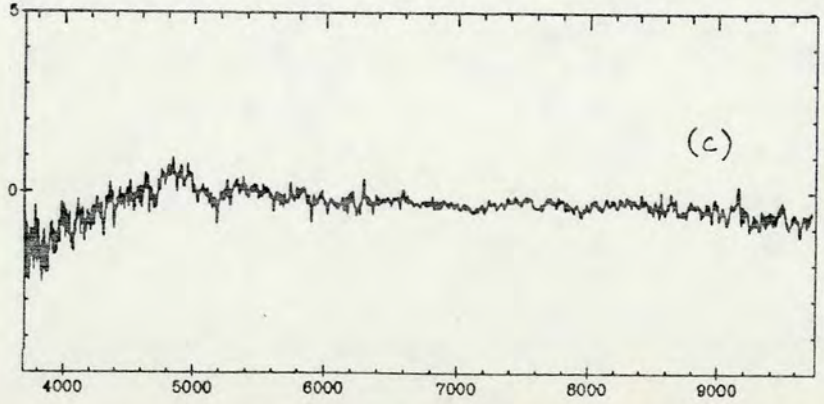
5
(c)
0
4000
5000
6000
7000
8000
9000

FIG.8

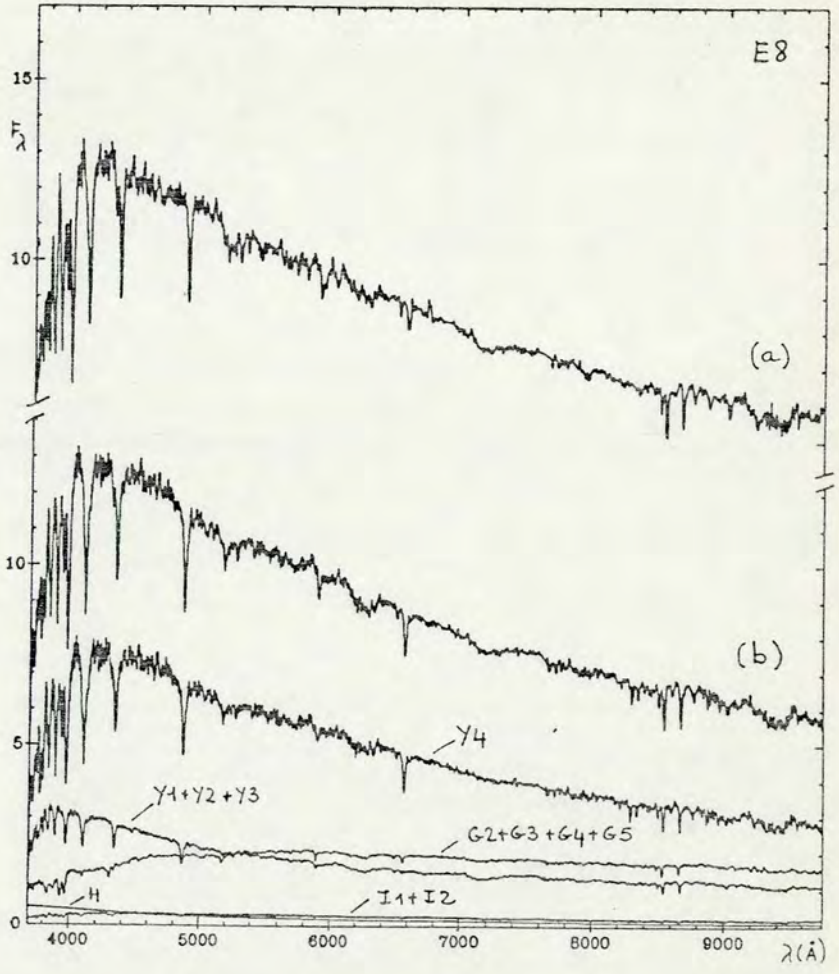
E8
15
F_λ
10
(a)
10
(b)
5
Y4
Y1+Y2+Y3
G2+G3+G4+G5
H
I1+I2
0
4000
5000
6000
7000
8000
9000
λ(Å)

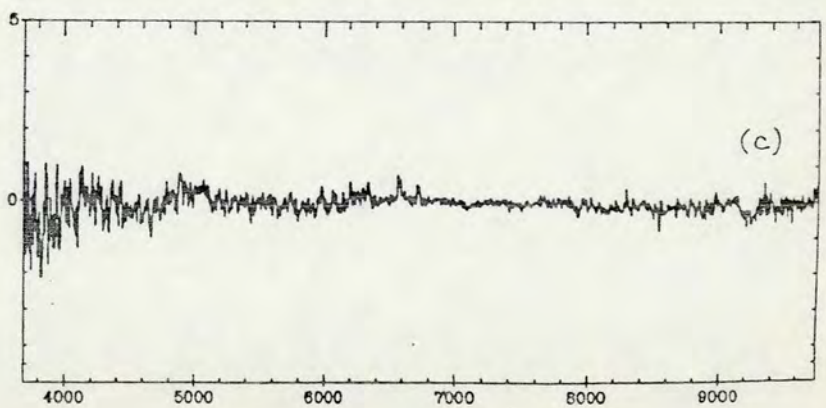
5
(c)
0
4000
5000
6000
7000
8000
9000

FIG

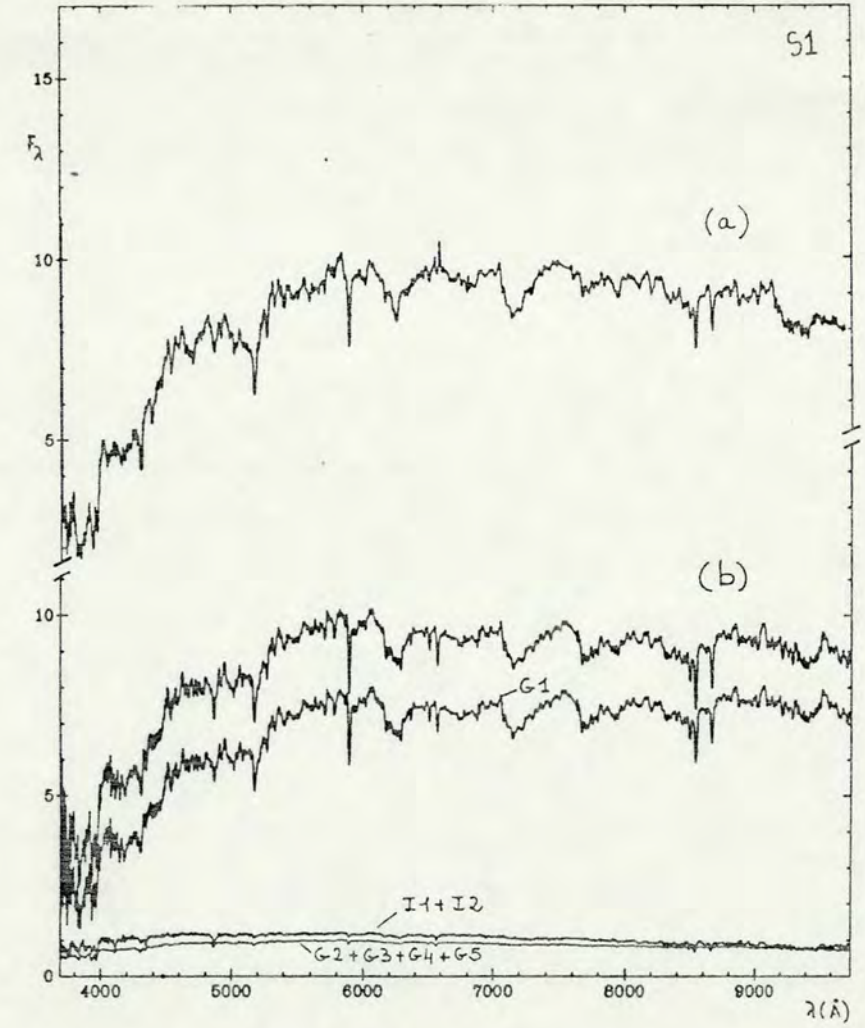
S1
F_λ
(a)
(b)
G1
I1+I2
G2+G3+G4+G5
λ(Å)

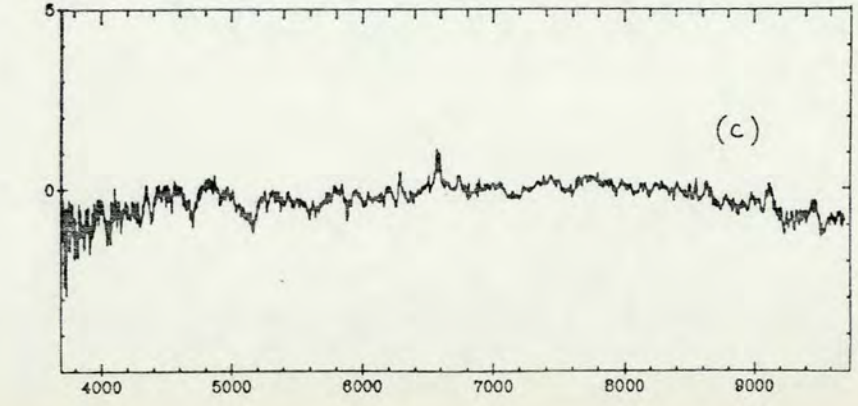
(c)

FIG. 10

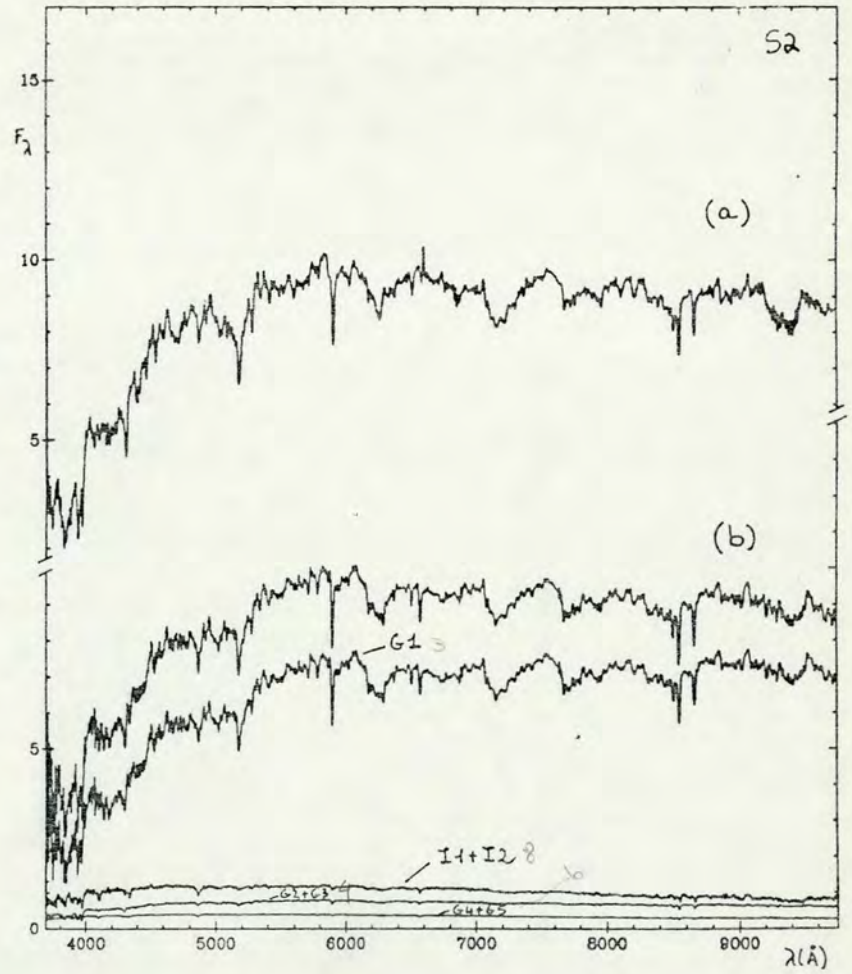
S2
F_λ
(a)
(b)
G1
I1+I2
G2+G3
G4+G5
λ(Å)

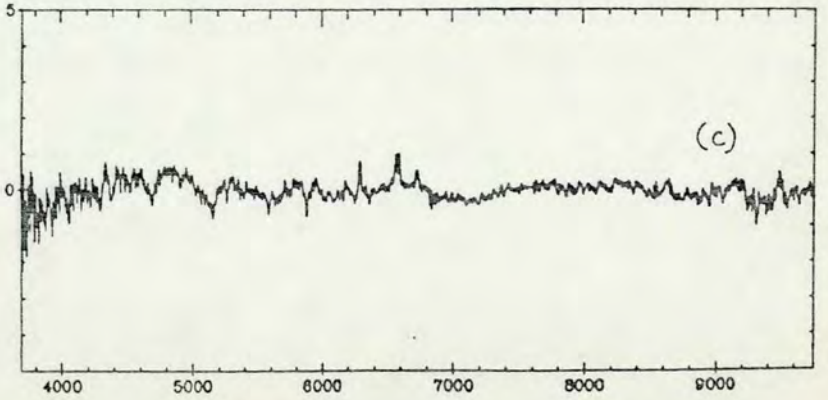
(c)

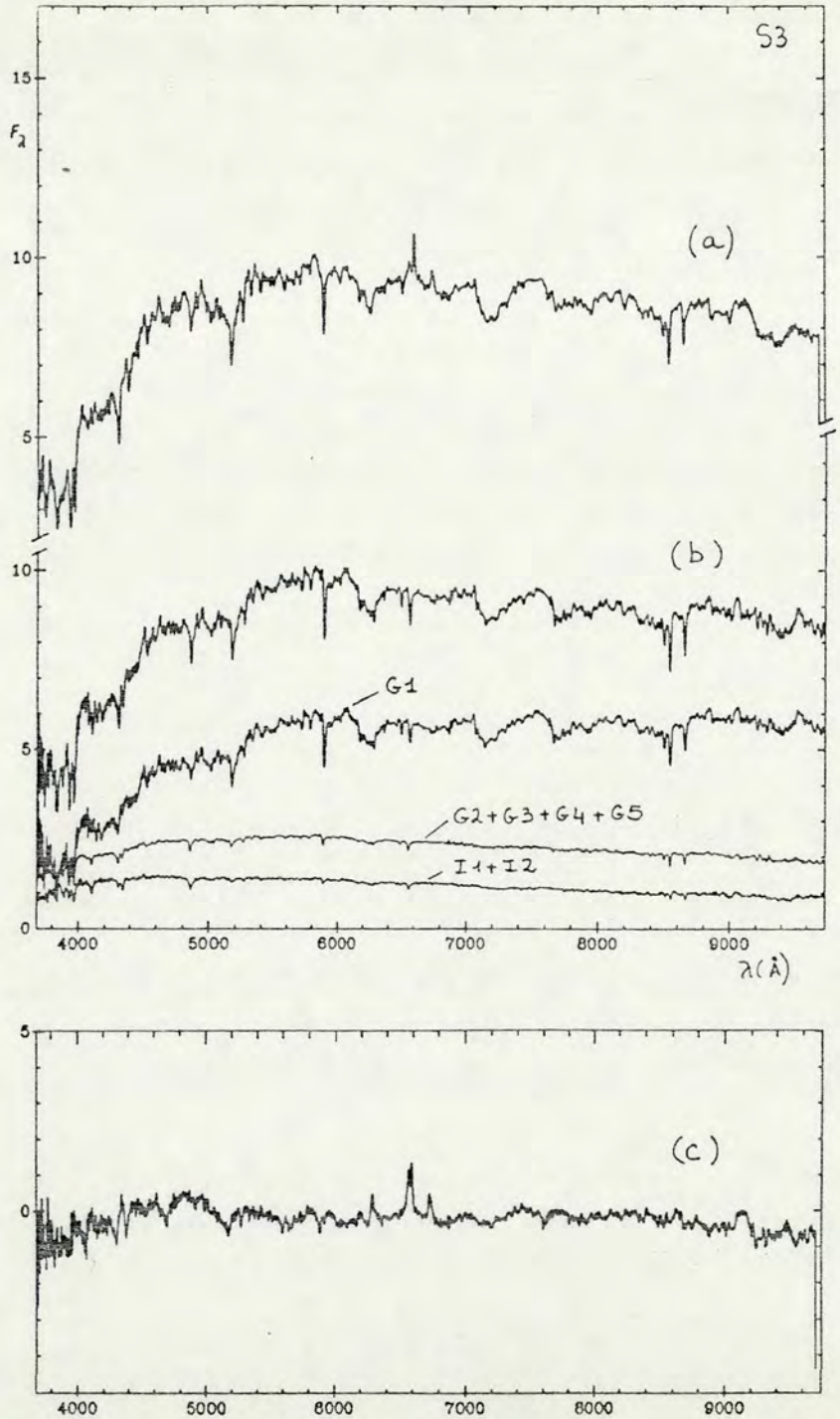
S3
F_λ
(a)
(b)
G1
G2+G3+G4+G5
I1+I2
(c)
λ(Å)

FIG.12

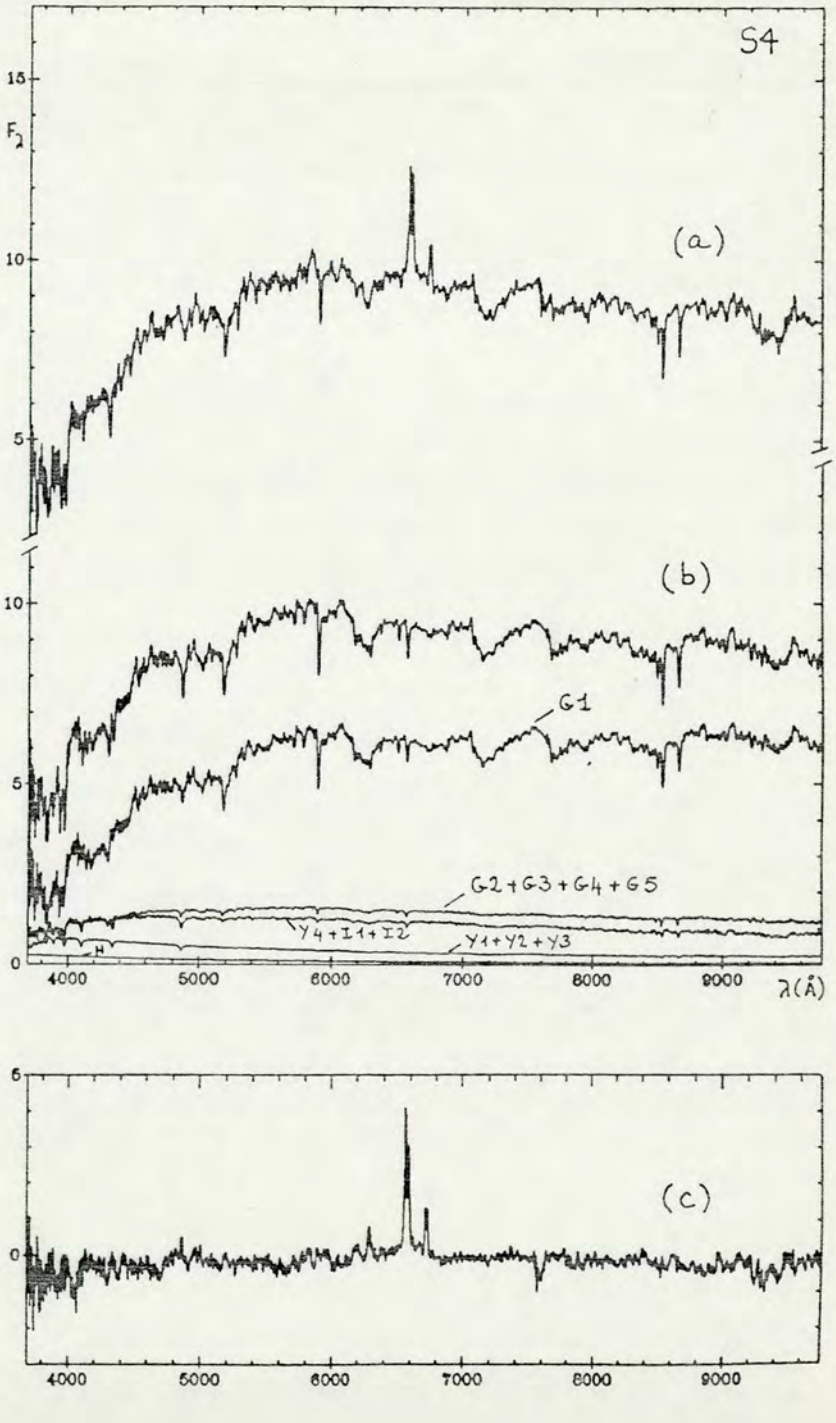
S4
F_λ
(a)
(b)
G1
G2+G3+G4+G5
Y4+I1+I2
Y1+Y2+Y3
H
(c)
λ(Å)

FIG.13

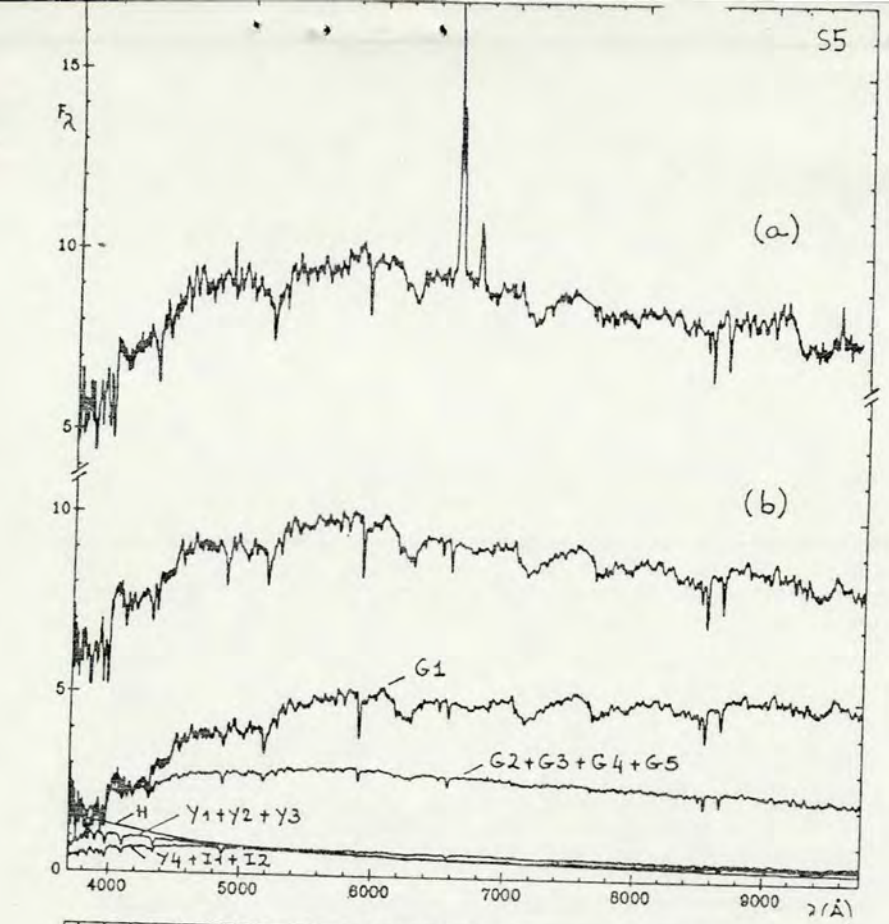
S5
F_λ
(a)
(b)
G1
G2+G3+G4+G5
H
Y1+Y2+Y3
Y4+I1+I2
λ(Å)

FIG.14

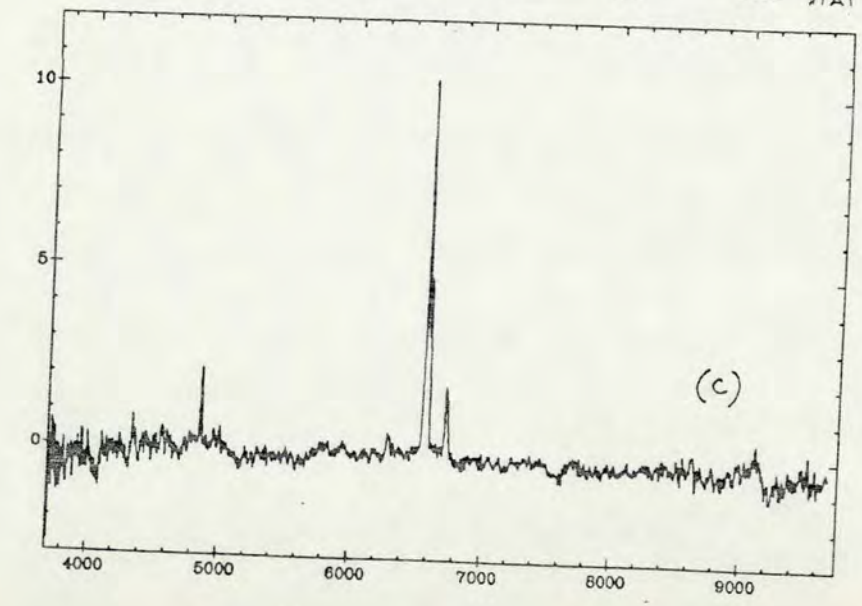
(c)

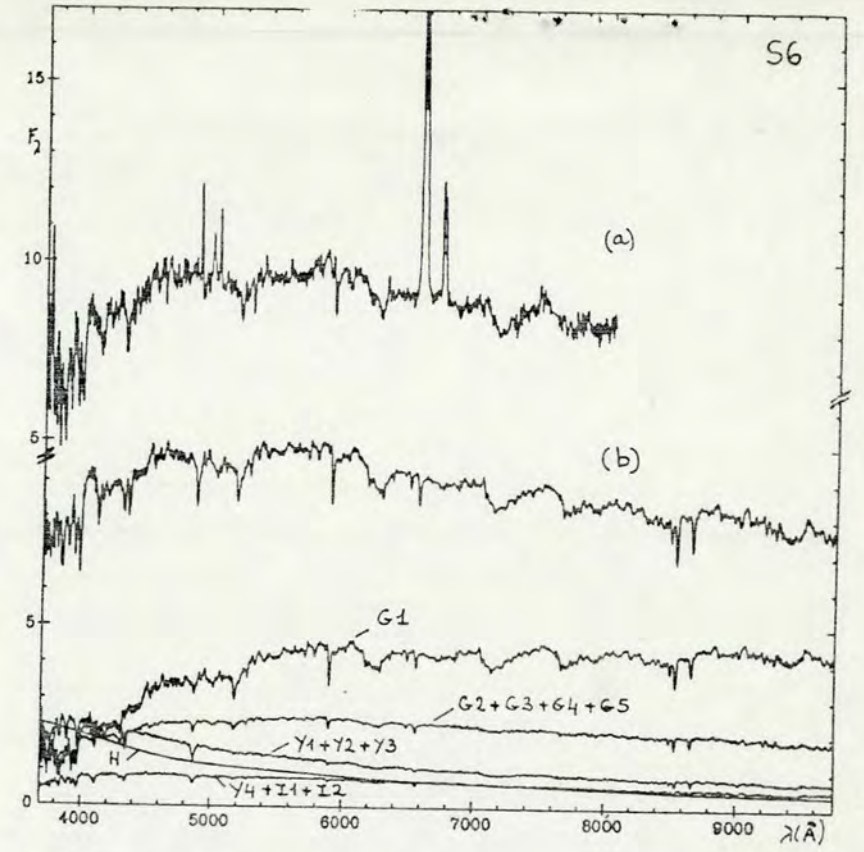
S6
F_λ
(a)
(b)
G1
G2+G3+G4+G5
H
Y1+Y2+Y3
Y4+I1+I2
λ(Å)

FIG.15

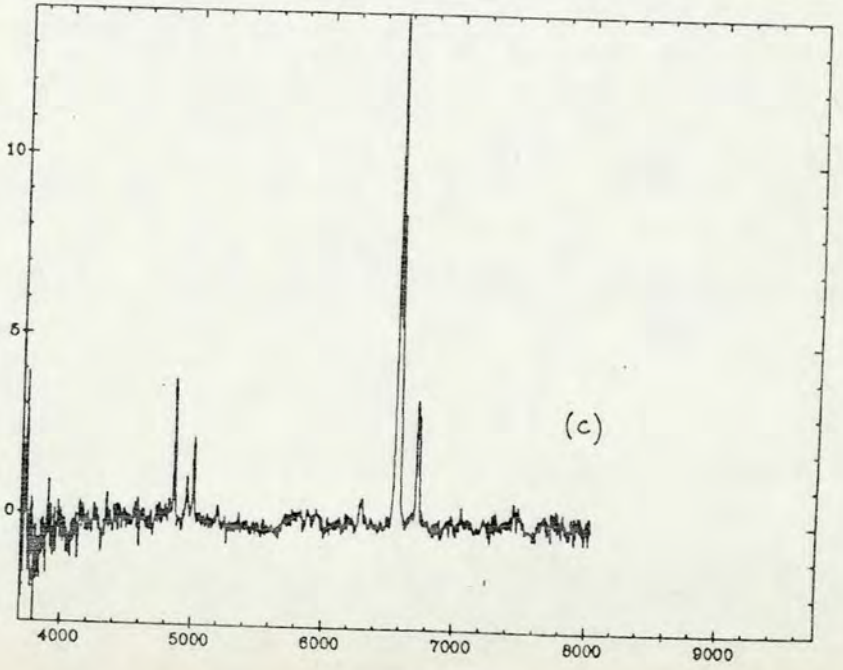
(c)

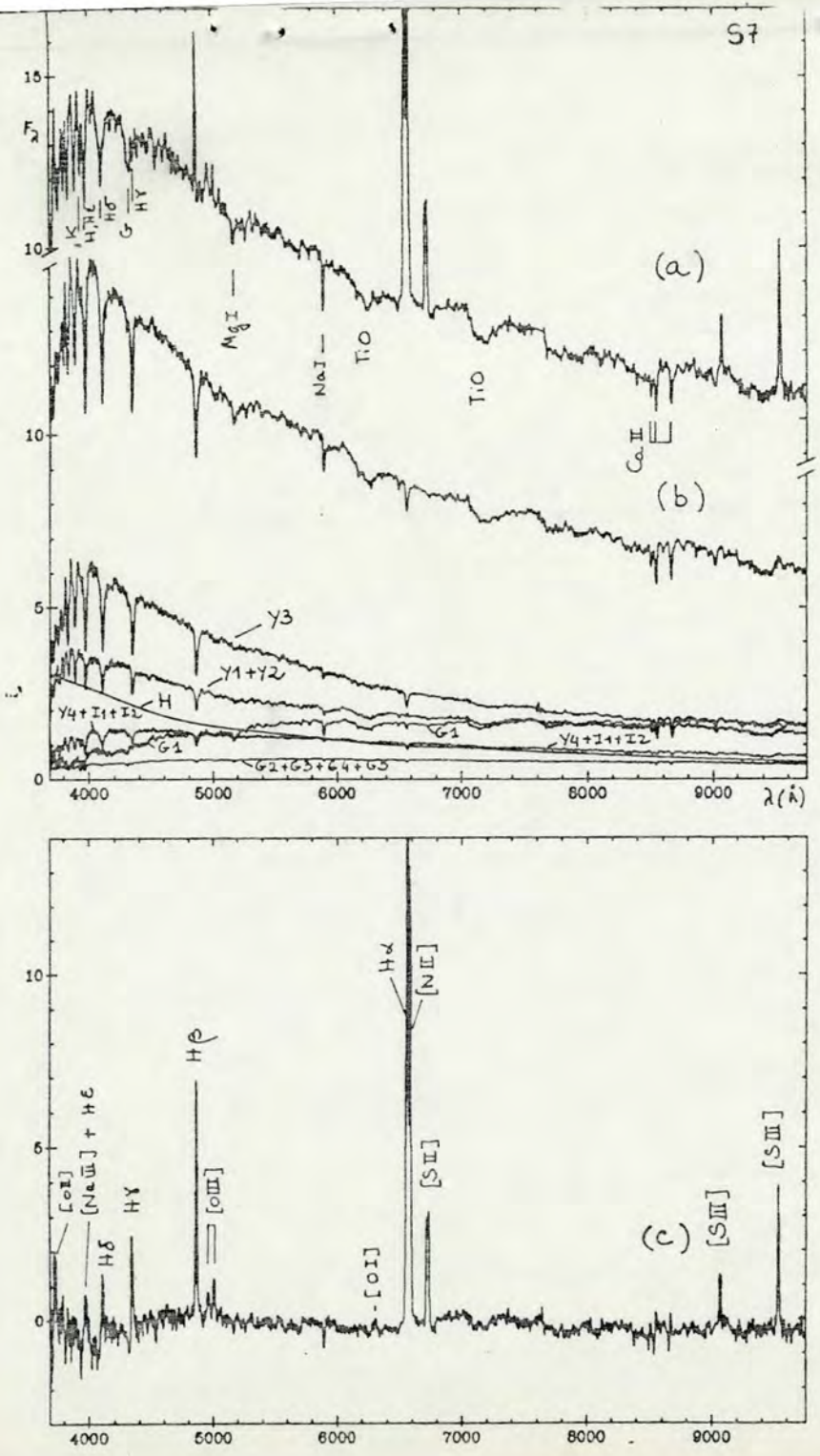

FIG.16

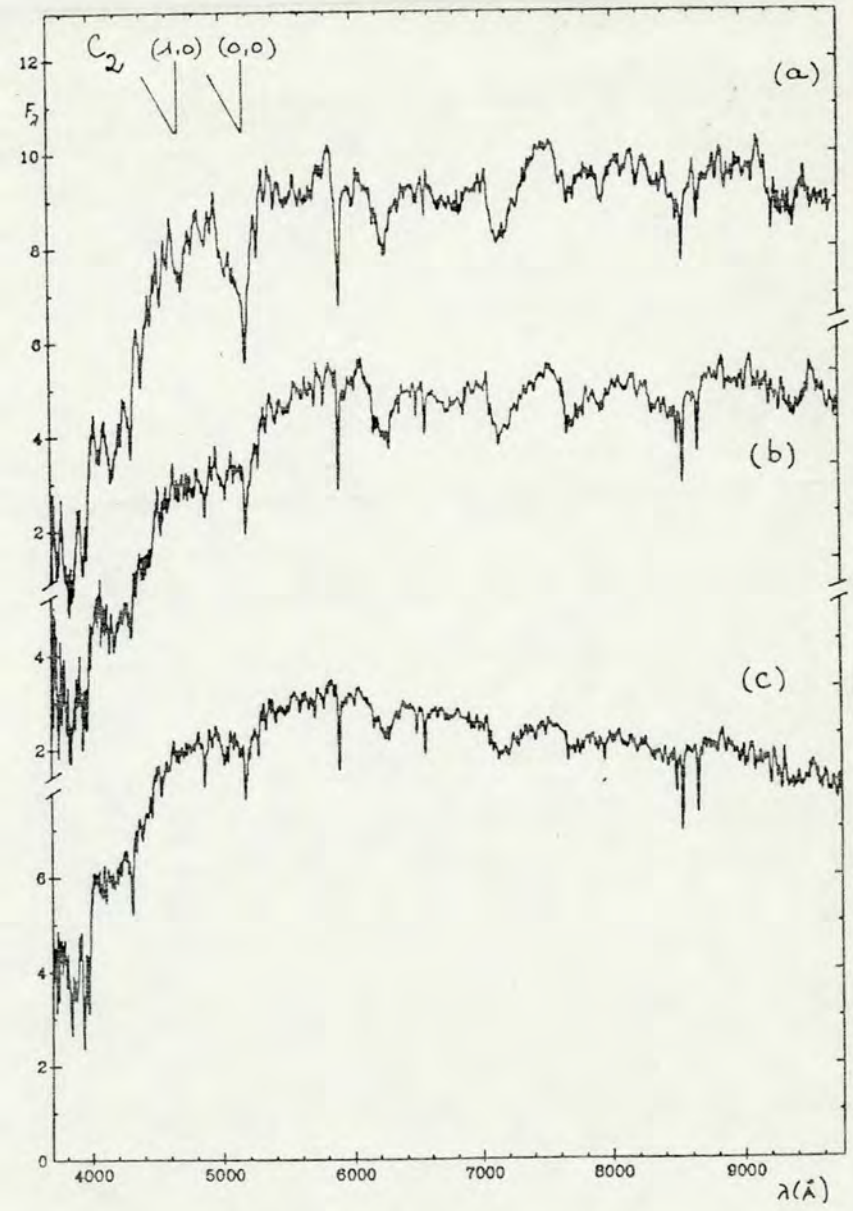

(a) artificial Glob. $[Z/Z_\odot] = +0.6$
(b) observed Glob. $[Z/Z_\odot] = 0/+0.1$
(c) observed Glob. $[Z/Z_\odot] = -0.4$

Fig. 17

CONSTRAINTS PROVIDED BY STAR CLUSTER SPECTRA ON THE NATURE OF THE UV TURN-UP IN GIANT ELLIPTICAL GALAXIES*

E. Bica**, D. Alloin[1])

1) Observatoire de Paris, Section de Meudon
92195 Meudon Principal Cedex, France

ASTRONOMY AND ASTROPHYSICS, IN PRESS
September, 1987

PUBLICADO EM A&A, 1988, 192, 98

*Based upon observational data collected at the European Southern Observatory

---

Thesaurus code : 21.01.1 ; 07.06.1 ; 07.18.1 ; 07.22.1 ; 19.37.1.

Main Journal : Section 1 (extragalactic astronomy)

** New adress: Instituto de Fisica, UFRGS. Av. Bento Gonçalves 9500
Porto Alegre, RS, 90000, BRAZIL

SUMMARY

We have linked available ultraviolet observations to the visible and near infrared spectra of some objects from our star cluster and galaxy nucleus samples. We have analyzed the nature of the UV turn-up in giant elliptical galaxies (gE) in the light of our recent population synthesis results which are based upon a library of star cluster integrated spectra in the visible and near infrared. We also investigate how star clusters can provide information on the frequency of occurence of particular types of stars with respect to the associated populations of a given age and metallicity. We definitely exclude the possibility that the UV turn-up in gE is caused by blue horizontal branch (BHB) stars associated with metal-poor components : even if they were a major contributor to the optical spectrum, their UV turn-up would be unable to account for that observed in gE, simply because it is not steep enough. Furthermore, our previous visible-near infrared synthesis has shown that only 10% of the flux originates from low metallicity components. On the contrary we find strong evidence that this UV turn-up is a result of on-going star formation in gE nuclei. Indeed, young blue clusters and/or HII region spectra match the UV turn-up quite well, without affecting much the optical range where their contribution is less than 2% at 5870 Å. Another possibility would be that the UV turn-up in gE is caused by post AGB stars from metal-rich components : data presently available about their frequency of occurence in metal-rich Galactic clusters, as well as about that of planetary nebulae in the bulge of M31 do not favour this interpretation however.

I. INTRODUCTION

So far, the nature of the UV turn-up in giant elliptical galaxies (gE) has not been definitely established (see for a review, Bertola, 1986). Basically, two types of hot stellar components have been proposed to explain this UV rising branch : luminous main sequence stars recently formed, or, blue horizontal branch stars from a metal-poor population. In addition, a few peculiar types of UV-bright stars may provide some contribution to the UV rising branch, such as accreting white dwarfs or post asymptotic giant branch (AGB) stars in the phase of planetary nebula nucleus (Nesci and Perola, 1985 ; Bertola, 1986). The fact that it is not possible to discriminate among all these possibilities reveals that synthesis methods based on stellar libraries are highly unconstrained, but also, that the wavelength range then considered might be too small.

We have recently developed a method for population synthesis in galaxies using a library of star cluster integrated spectra over the visible and near infrared ranges (Bica and Alloin, 1986, 1987a ; Bica, 1987). Only two free parameters are considered, age and metallicity, the initial mass function (IMF) being implicit in the observed star cluster spectra. Also some advanced stages of stellar evolution, which are still difficult to model theoretically, are naturally taken into account in real star cluster spectra with Nature's right proportions. This has considerably constrained the synthesis problem and has led to interesting results about the population content and the chemical evolution of different types of galaxy nuclei (Bica, 1987). In the present paper we study more particularly the nature of the UV turn-up which is observed in massive elliptical galaxies, in the light of our synthesis method. We have also investigated how star clusters can bring information about the frequency of occurence of certain types of stars in the

- globular cluster UV data are from OAO and ANS (de Boer, 1985) and were used together with IUE observations providing complementary information for $\lambda < 1550$ Å (Dupree et al., 1979 ; Caloi et al., 1981, 1984, 1985). Reddening was taken into account like in the case of NGC 6093. The optical spectra are the averaged globular cluster groups for various metallicites (Bica, 1987) : group G5 ($[Z/Z_\odot] = -1.9$), group G3 ($[Z/Z_\odot] = -1.1$) ; group G2 ($[Z/Z_\odot] = -0.4$) and group G1 ($[Z/Z_\odot] = +0.05$). The connections are shown in Figure 2 and deserve the following comments :

(i) the very metal-poor group G5, for which we have used UV data of NGC 5024, 6341, 6397, 6779, 7078 and 7099, is quite uniform in terms of its SED. As pointed out by de Boer (1985) clusters in this metallicity range have, on average, a weaker UV flux than the G4 group at $[Z/Z_\odot] \simeq -1.6$ represented by NGC 6093 in Figure 1.

(ii) group G3 exhibits a wide range of UV SED. This is caused by the well-known second parameter problem for horizontal branch (HB) morphology (e.g. Zinn, 1980). These effects are minor in the visible and near infrared ranges, which allowed us to define this group only in terms of $[Z/Z_\odot]$ in our previous papers. In the UV range however, the effect is important : a blue HB cluster like NGC 6402 presents a SED like that of NGC 6093 (Figure 1c) whereas a red HB cluster like NGC 362 shows a weak UV flux typical of more metal-rich globular clusters. For the sake of simplicity we have adopted the UV SED of NGC 6715 to represent the group : it is intermediate between those of NGC 6402 and NGC 362, as expected from its HB morphology which has equal proportions of blue and red stars (Zinn, 1980). However, the existence of this additional degree of freedom in the UV, for group G3, does not affect our subsequent conclusions. Indeed, we shall also consider the possibility that *all* subsolar groups (G2 through G5) present a UV bright flux like in NGC 6093

(iii) the ANS and OAO clusters for group G2 are NGC 104 (47 Tuc), NGC 6356, 6388, 6624 and 6637. These are clusters usually called metal-rich in the literature, although their visible and near infrared spectra are clearly weak-lined with respect to gE (Bica and Alloin, 1986, 1987a). As far as we are aware only NGC 6624 has a published IUE spectrum ; it shows a small far UV-excess which arises from a single non-extended source, possibly the UV counterpart of an X-ray source (Dupree et al., 1979), but it could as well be a post-AGB star. Observations of 47 Tuc are also reported in that paper : its SED resembles that of NGC 6624 for the long wavelength camera and there is no detectable flux shortward of 1900 Å. Therefore, the small UV turn-up adopted for G2 in Figure 2 arises from NGC 6624 only.

(iv) group G1 corresponds to the strong-lined Galactic globular clusters NGC 6440, 6528 and 6553 which have played a major role in the previous visible, near infrared population synthesis because they present metallic features comparable to those of gE nuclei (Bica, 1987). Unfortunately no UV observations are available for these clusters and so, we have linked group G1 to the UV SED of group G2. This tentative substitution by a less metallic group must be reminded because line blanketing in the UV will therefore be underestimated : this will seriously limit any attempt of a *quantitative* synthesis for gE nuclei in the UV (Section III).

Finally we have also linked the intermediate age groups I1 and I2 (Bica, 1987) to the UV SED of the LMC clusters NGC 1987 and NGC 1978 + NGC 1806 respectively (Cassatella et al., 1987). The results are displayed in Figure 3. Owing to the lack of data in the range 3200-3700 Å, it was necessary to interpolate the spectra, as for NGC 2004. The visible, near infrared spectra for I1 are from the Galactic open cluster (GOC) NGC 2660 at an age $\simeq 1.2 \times 10^9$yr, and for I2 are from the GOC NGC 2158 and the LMC clusters

1987a). As pointed out in the empirical synthesis for the elliptical galaxies NGC 4382 and 2865 (Bica and Alloin, 1987b), these clusters should be metal-deficient with respect to an eventual intermediate age component in gE nuclei. In the quantitative synthesis (Bica, 1987), this drawback was avoided in the computations by using a complete grid of star cluster properties for all ages and metallicities. However, for the visualisation of the results, the weak blanketing of the substituted cluster spectra is troublesome and should also be kept in mind while looking at representations in the UV range (Section III).

III. DISCUSSION

We recall in Table 1, the optical population synthesis results for the E1 group, in terms of the relative flux contributions at λ 5870 Å (Bica, 1987). The method gives information about the nuclear chemical evolution : 80% of the light at 5870 Å arises from a population similar to that of very metal-rich inner bulge globular clusters in group G1 with $[Z/Z_{\odot}] \geq 0$ (Section III), 9% comes from moderately rich and metal-poor old populations ($[Z/Z_{\odot} < 0$) while the remaining 11% of the flux is from metal-rich intermediate age populations (1 to 7 Gyr). No significant contribution from young ages (less than 1 Gyr) is detected using the optical range only. These results, including the UV range, are displayed in terms of a template and its decomposition (Figure 4(b)) and compared to NGC 4649 (Figure 4(a)). The residual (galaxy-template) is shown in Figure 4(c). The positive residual from 1250 to 2400 Å corresponds to the UV turn-up, while the negative residual from 2500 to 4000 Å can be assigned to the deficient blanketing in the available clusters. Therefore, it is not possible to perform a quantitative synthesis in the UV range with the data presently available for

star clusters. However, in spite of this blanketing problem, we can study qualitatively the nature of the UV turn-up a a function of star cluster spectra, assuming that it can arise from recent star formation and from a metal-poor or metal-rich old stellar population.

In Figure 5, we see that the young star cluster provides a good fit to the UV turn-up without introducing any significant change in the long wavelength range because its flux contribution at 5870 Å is 1.6% only. The problem of the small missing flux in the UV rising branch could easily be solved by adding a slightly younger cluster (HII region). The flux between 2500 and 4000 Å could be matched if intermediate age and old star clusters with strong blanketing were available.

It is obvious from Figure 6 that the metal-poor globular cluster NGC 6093 cannot reproduce the gE UV rising branch because the minimum in the cluster spectrum at 2000-3000 Å is not deep enough, or, conversely, the UV rise in the cluster SED is not steep enough. Furthermore, the strongest possible contribution in the UV using NGC 6093 (Figure 6(b)), produces an optical flux which is incompatible with the population synthesis in Table 1 inferred from the optical spectrum (3700-10000 Å). It is a factor 7 to 8 stronger than the predicted contribution from metal-poor populations similar to NGC 6093 at $[Z/Z_{\odot}] \simeq -1.6$ (Figure 6(d)) : remember that all the UV-bright globular clusters have metallicities, $-1.8 < [Z/Z_{\odot}] < -1.2$, (Van Albada et al., 1981 ; de Boer, 1985). We also see that the strongest possible contribution of NGC 6093 in the UV (Figure 6(b)) is a factor two stronger than the total contribution of populations with $[Z/Z_{\odot}] < 0$ (Figure 6(c)). We emphasize that in this sum is included our average globular cluster group, centered at $[Z/Z_{\odot}] = -0.4$ (G2), with clusters like NGC 104 (47 Tuc), NGC 6637 (M 69) and NGC 6624 which are among the most metal-rich ones observed with IUE, ANS or OAO and are UV-weak (Figure 2). We thus conclude

that blue horizontal branch stars associated with metal-poor populations, even in an extreme case such as the cluster NGC 6093, cannot account for the UV turn-up in gE nuclei. In the case of previous synthesis with libraries of stellar spectra, the contribution of blue HB stars was certainly overestimated because the wavelength range considered was too small when only the ultraviolet domain was used. When both the ultraviolet and optical ranges were taken into account, the HB stars were treated as a supplementary group in addition to metal-rich types. In fact, the HB contribution is tied to the associated metal-poor giants, which, as a rule, have been neglected and, consequently, quite arbitrary numbers of blue HB stars were allowed in the synthesis. Thus the frequency of occurence of UV-bright stars with respect to the associated populations is a strong astrophysical constraint.

We compare in Figure 7 NGC 4649 to the very metal-rich group G1 representing the total contribution of globular cluster populations with $[Z/Z_{\odot}] \geq 0$ in Table 1. The small UV turn-up corresponds to the SED of NGC 6624 which in fact belongs to the less metal-rich group G2 (Section II). Assuming that this small turn-up is due to a post-AGB, 7 such stars per metal-rich globular cluster are required to reproduce the UV turn-up in gE nuclei (or 5 such stars only if the intermediate age and metal-poor components in Table 1 are taken into account). Considering the typical absolute magnitude for a globular cluster, $M_v = -9$ (Van den Bergh, 1969), and assuming that the typical nuclear region of a gE has $M_v = -19$, a total number of 10^4 post-AGB stars would be necessary to match the UV turn-up in a gE. An interesting test for this hypothesis would be to observe with IUE the very strong-lined Galactic globular clusters : NGC 6528 would be the best target because it is not as reddened as NGC 6440 and it is more compact than NGC 6553.

The fact that we deal with small numbers of post-AGB stars in a given cluster, suggests that a better approach might be to look for other indicators

of advanced stages of stellar evolution in *large cluster samples*. The frequency of occurence of planetary nebulae in star clusters might give a hint on the probability of having post-AGB stars in different populations. Among 1065 GOC (Alter et al., 1970), only NGC 2437 and 2818 contain planetary nebulae (O'Dell, 1963 ; Webster, 1976). Among 125 Galactic globular clusters (Alter et al., 1970) only the metal-poor cluster NGC 7078 has a planetary nebula (Webster, 1976). For the 1146 clusters in the two main catalogues of LMC clusters (Hodge and Sexton, 1966), only the intermediate age cluster NGC 1852 contains so far an identified planetary nebula (Webster, 1976). In the SMC finally, for 134 clusters (Hodge and Wright, 1974) only NGC 330 shows a planetary nebula which is certainly a projected object or else is another type of emission line star because of the very young age of this cluster (Webster, 1976). Thus, planetary nebulae appear to be very rare objects per population unit as defined from an entire set of star clusters. This observational evidence does not favour the hypothesis of post-AGB stars for explaining the UV turn-up in gE. It should be reminded however that most of these clusters have a solar or subsolar metallicity while it might be that a large metallicity somehow enhances the occurence of post-AGB stars. A test is provided by the comparison of the far UV IUE spectra and of the counts of planetary nebulae in the bulge of M31 and in its dwarf elliptical companion M32. After correction for losses in planetary nebula counts, it is found N_{PN} (M31 bulge)/N_{PN}(M32) = 775/34 = 23 (Ford and Jenner, 1975 ; Ford and Jacoby, 1978). The luminosity ratio in B light of the bulge of M31 to the total for M32 is 53 (Cowley et al., 1982). Thus, the more metal rich bulge of M31 is a factor 2 more deficient than M32 in planetary nebulae per blue luminosity unit. On the other hand, M31 is known to have a UV turn-up similar to those of gE, whilst M32 is UV weak (Welch, 1982 ; Bertola, 1986). This result also argues against the possibility that post-AGB stars in the phase of planetary nebula nucleus

are responsible for the UV turn-up. Last, planetary nebulae themselves might not be direct indicators of the frequency of occurence of post-AGB stars in general, if the ejection of the outer envelope is a metallicity dependent phenomenon.

IV. CONCLUSIONS

We conclude that horizontal branch stars associated with metal-poor components cannot explain the UV turn-up in gE. Post-AGB stars associated with metal-rich components might explain it, although available observational results do not favor this interpretation. Our analysis rather suggests that on-going star formation is responsible for the UV turn-up in giant elliptical galaxies. Although the number of elliptical galaxies observed in the UV is small, massive ones systematically exhibit a UV rising branch (Bertola, 1986). This evidence implies that a positive rate of present star formation in luminous elliptical galaxies, although small, is a common phenomenon and should be representative of the star formation rate over the past few Gyr. We suspect that the result of these frequent small bursts of star formation (or continuous star formation at a low level) is the existence of intermediate age components (Table 1).

It is also important to note that NGC 2004 is a young cluster with an important red supergiant component, as can be derived from its strong TiO bands in the near infrared (Bica and Alloin, 1987a). It is interesting that the resulting red supergiant population from on-going star formation in elliptical galaxies will be negligible in the near-infrared with respect to older populations (Figure 5(a)).

Finally, we also emphasize that it is not necessary to invoke extreme

values for the slope or upper and lower mass limits of the initial mass function in order to account for the UV turn-up : an ordinary star formation event, like those from which star clusters are born, explains it quite well.

We are presently extending our library of optical spectra - star clusters and galaxy nuclei - to the near UV range, using coated CCD detectors. These observations will allow to link more precisely clusters and galaxies with IUE data and will allow to use absorption line information at shorter wavelengths providing thus an invaluable tool for performing a quantitative synthesis from 1000 to 10000 Å.

Acknowledgements : We thank Dr. Burstein as well as an anonymous referee for interesting suggestions. E.B. thanks the Brazilian Institution CNPq for a fellowship.

REFERENCES

Alter, G., Balázs, B., Ruprecht, J., 1970, Akadémiai Kiado - Budapest.

Barbaro, G., Olivi, F., 1986, in "Spectral Evolution of Galaxies", ed. C. Chiosi and A. Renzini, Reidel, p.283.

Bertola, F., Capaccioli, M., Holm, A., Oke, J., 1982, Astrophys. J. 237, L65.

Bertola, F., Capaccioli, M., Oke, J., 1982, Astrophys. J. 254, 494.

Bertola, F., 1986, in "Spectral Evolution of Galaxies", ed. C. Chiosi and A. Renzini, A., Reidel, p.363.

Bica, E., Alloin, D., 1986, Astron. Astrophys. 162, 21.

Bica, E., Alloin, D., 1987a, Astron. Astrophys., in press.

Bica, E., Alloin, D., 1987b, Astron. Astrophys. Suppl., 70,281

Bica, E., 1987, Astron. Astrophys., in press

Cassatella, A., Barbero, J., Geyer, E., 1987, Astrophys. J. Suppl. 64, 83.

Caloi, V., Castellani, V., Galluccio, D., Wamsteker, W., 1984, Astron. Astrophys. 138, 485.

Caloi, V., Cassatela, A., Castellani, V., Machetto, F., Melnick, J., 1981, Astron. Astrophys. 103, 386.

Caloi, V., Castellani, V., Tarenghi, M., 1985, Astron. Astrophys. 145, 286.

Cohen, J., Rich, R., Persson, S., 1984, Astrophys. J. 285, 595.

Cowley, A., Crampton, D., Mc Clure, R., 1982, Astrophys. J. 263, 1.

de Boer, K., 1985, Astron. Astrophys. 142, 321.

Duprée, A. et al., 1979, Astrophys. J. 230, L89.

Ford, H., Jenner, D., 1975, Astrophys. J. 202, 365.

Ford, H., Jacoby, G., 1978, Astrophys. J. 219, 437.

Hodge, P., Sexton, J., 1966, Astron. J. 71, 363.

Hodge, P., Wright, F., 1974, Astron. J. 79, 858.

O'Dell, C., 1963, P.A.S.P. 75, 370.

Oke, J., Bertola, F., Capaccioli, M., 1981, Astrophys. J. 243, 453.

Savage, B., Mathis, J., 1979, Ann. Rev. Astron. Ap. 17, 73.

Van Albada, T., de Boer, K., Dickens, R., 1981, Mon. Not. R.A.S. 195, 591.

Van den Bergh, S., 1969, Astrophys. J. 171, 145.

Webster, B., 1976, P.A.S.P. 88, 669.

Welch, G., 1982, Astrophys. J. 259, 77.

Zinn, R., 1980, Astrophys. J. 241, 602.